CRANFIELD INSTITUTE OF TECHNOLOGY

SCHOOL OF INDUSTRIAL AND MANUFACTURING SCIENCE

PhD Thesis

Academic Years 1987-91

M DOWNING

A New Powder Encapsulation Method And Its Implications On Densification By Hot Isostatic Pressing

Supervisor: D J STEPHENSON

April 1993

This thesis is submitted in fulfilment of the requirements for the degree of Doctor of Philosophy

ABSTRACT

Hot isostatic pressing is now an accepted material processing technique for the consolidation of metal powders to near-net-shape components. This thesis examines the use of coatings as in-situ envelopes to overcome the problems associated with traditional containerisation of powder. The application of metallic coatings by physical vapour deposition, involving resistive and electron beam evaporation and ion plating, onto green powder metal compacts has been studied as a potential method for encapsulating powder metal products prior to hot isostatic pressing. The coating structures are discussed in terms of processing conditions and surface roughness influence. The most promising approach is a combined sinter-hot isostatic pressing cycle, which utilises the formation of a transient liquid phase to defect-heal the coating during the sinter cycle prior to the application of pressure. The influence of particle size distribution on densification has also been studied. This included both monosized and bimodal powders. The results of this study has been incorporated into a modified Ashby model computer program and it is shown that the model results in a shift of the dominance of the mechanism fields and gives good correlation between the predicted and measured values of density.

ACKNOWLEDGEMENTS

My thanks for this thesis must go out to my supervisor, Dr D Stephenson, for his patience, to Mrs C Kimpton, Mr J Hedge, Mr T Pryor and Mr D Timpson for their technical support throughout, to Mr M Brook for his help with computer programming, and everyone who chided and encouraged me.

CONTENTS

LIST OF FIGURES

LIST OF TABLES

1

INTRODUCTION

1. Hot Isostatic Pressing and Powder Metallurgy

Following the recent progress in powder metallurgy (PM) the hot isostatic pressing (HIP) process has attracted much attention as a forming and sintering technology.

Originally developed by Battelle to produce Zircalloy-clad nuclear fuel elements by diffusion bonding in the late 50's the area of application of HIP has widened considerably to include a variety of powder consolidation and defect healing operations. The history and development of HIP has been well documented in several reviews.[1-3]

The HIP process uses gas as a pressure transmitting medium to compact and/or bond material(s) under elevated temperatures. PM products via the HIP process offer the potential of producing homogeneous, isotropic, segregation-free, non-porous finished articles. The achievement of fully dense products is significant in applications where residual porosity cannot be tolerated because of its adverse effect on key properties such as:[4] (i) surface finish, (ii) corrosion resistance, (iii) ultimate tensile strength, (iv) fatigue strength, (v) impact strength, (vi) yield strength and (vii) elongation. The inherent nature of the HIP process minimises problems often encountered in conventional sintering processes (e.g. wettability, sintering activity or volatile component evaporation).

Powder metal parts have the potential of production to near-net-shape (NNS) with minimal or no machining or other subsequent metal forming processes. The advantages of a PM production route include:[5] (i) a reduction in manpower hours to complete and finish parts (compared to conventional processing), (ii) a reduction in energy requirements and shorter delivery times (owing to a reduction of processing steps compared to conventional techniques) and (iii) improved mechanical and physical properties attributed to elimination of metallurgical macrosegregation. The HIP process also offers the capability to fabricate non-equilibrium structures[6] that would prove difficult to produce via conventional routes (e.g. in aerospace applications).[7-9]

PM has a growing diversity and is advancing into new markets[10,11] as well as consolidating its hold in markets such as aerospace. A comprehensive study has been documented by Gorham[12] outlining PM technology (including the use of HIP) and forecasting demand (based largely on information obtained from PM end users). The global market for PM parts is projected to grow from $5 to $6 billion in 1987 to between $15 and $18 billion by the year 2000. The HIP process is discussed as a consolidation process combined with sintering, as a post-sintering process and as a NNS process.

Current applications of HIP technology in metal PM processing include:[13] net-shapes

in nickel-based superalloys for aircraft engine turbine disks and shafts, nickel-based PM forging and rolling preforms, and nickel-based PM integral pump and turbine impeller wheels; titanium alloy PM billets, forging preforms, and shapes; tool steel billets, large die blocks, and composite structures; net-shapes in PM beryllium, niobium alloys, and other refractory metals; and dispersion- and fibre-strengthened PM aluminium alloys. The HIP of PM components has been previously reviewed by the author.[14]

There is a need for small intricate near-net-shape components produced via powder metallurgy, but present canning technology limits design to simple shapes and introduces stress variations throughout the component due to can geometry. The aim of this present work is to investigate the influence of the can and of the powder distribution on the densification behaviour and relate this to modelling predictions. The Ashby model, and a modified program to take account of the powder distribution, will be considered. To overcome the limitations of the present canning process route for near-net-shapes the use of coatings as in-situ envelopes will be investigated. By combining the use of coatings with the knowledge of the densification behaviour of powder distributions it is believed a better prediction of the net shape can be achieved.

3

LITERATURE REVIEW

1. The Status of Hot Isostatic Pressing

Recent advances in hot isostatic pressing (HIP) equipment have contributed to the rapid development of the powder metallurgy (PM) industry and vice versa. Three important recent advances in the field of HIP include:[15] (i) high-temperature equipment (up to 2600 °C), (ii) sinter/HIP systems for the manufacture of cemented carbide and engineering ceramics and (iii) systems for oxygen-containing atmospheres to treat unstable oxide ceramics. There are also HIP units capable of pressures up to 1000 MPa in operation.

The HIP unit installed at C.I.T.[16] (see figure 1) is typical of research units, offering temperatures up to 2000 °C and pressures from soft vacuum to 200 MPa. The pressure transmitting medium can be argon and/or nitrogen. Different systems may contain varying HIP furnace styles[3] and/or be manufactured in other materials (e.g. platinum for use in oxygen furnaces). Graphite furnace elements (either bulk or fibre reinforced), operating in the temperature range of 400-2200 °C, have advantages owing to its excellent strength and high-temperature dimensional stability. The work-zone within the furnace is the primary limitation on the possible part size to be HIP'ed.

HIP has been extensively used, for example, in the defect healing and regeneration of castings,[17-19] in the processing of steels,[20] of composites,[21] of Astroloy,[22,23] of nickel aluminides,[24,25] of superalloys[26] and refractory metals[27] amongst others in the metal powder field.

The pressure/temperature/time relationship for the HIP cycle is dependent on the material(s) and microstructure/mechanical properties desired. These are primarily determined by the magnitude and sequence of pressure and temperature application[13] as shown in figure 2, although variations are possible with staged heating and cooling operations. A type I cycle initialises cold pressurization with the later increase in gas temperature resulting in a pressure rise. This cycle is particularly useful for control of large net shapes in sheet metal encapsulation. Type II cycle involves application of the process temperature prior to any substantial pressurization. This process cycle is used for glass-encapsulated powder to prevent container damage. The type III cycle involves the application of full working pressure prior to heating. There is a tendency for enhanced recrystallization of the powder particles (through low temperature plastic deformation) with this cycle. The type IV cycle is effectively an accelerated type I cycle, producing a reduced process time.

2. Powder Atomisation

Powder metallurgy (PM) offers an attractive method of fabricating high performance components owing to the inherent high quality (e.g. in terms of level of impurities,

degree of homogeneity, microstructure etc.) of the (pre-alloyed) metal powder. The most important properties of an atomised powder include[28] average particle size, particle size distribution (PSD), particle shape, chemical composition and microstructure. The engineering properties of the powder/part (apparent density, flowability, green strength, compressibility, sintering rate, forgeability and toughness) will be determined by the fundamental properties of the atomised powder.

The preferred mode of metal powder production is atomisation in which molten metal is broken into small droplets to solidify as particles. Atomisation processes include[28,29] water- and gas-atomisation (where the liquid stream is broken up by high pressure water or gas jets), centrifugal atomisation (where centrifugal force is used), vacuum or soluble gas atomisation (where atomisation is carried out in a vacuum) and ultrasonic atomisation (where ultrasonic energy is utilised). Schematics of the atomisation of metal powders[30] are shown in figure 3.

Atomisation of the melt is important owing to the droplet cooling rates, which can be as high as 10^6 °C/sec.[31] This allows the powder particle to retain high-temperature crystal structures. These powders are termed rapidly solidified (RS) powders.

The vacuum induction melting (VIM) furnace is considered to be the superalloy and specialist metal industry's work-horse for many years to come.[32] The melting stage is very important owing to the influence of melt temperature and mass transfer rate on the subsequent particle size distribution (PSD) of the powder produced by the processing route.

Water- and gas-atomisation processes account for the bulk of atomised metal powder production. In general water-atomised powders are irregular in shape with relatively high surface oxygen contents whilst gas-atomised powders are more spherical in shape and can have lower oxygen contents. A schematic of water- and gas-atomisation processes[30] is shown in figure 4.

The fundamental properties of the atomised metal powder are determined by many processing parameters including metal flow rates, nozzle design, atomising medium pressure (usually argon or nitrogen), collection chamber design,[32] cooling rate and droplet collisions[33] amongst others. The powders produced by water- and gas-atomisation have microstructural characteristics ranging from amorphous to fine crystalline and dendritic.

The rotating electrode process (REP), developed by Nuclear Materials, Inc., produces spherical powder particles through the break-up of the melt by centrifugal forces[34] (see figure 5). The powder shape produced depends on the mechanisms of droplet formation[29] but this method tends to a narrow spread of particle sizes.

The non-melting permanent cathode may be a simple tungsten-tipped device (REP) or a transferred arc plasma torch (PREP). Melting is usually conducted under helium

or argon. The rotation rate of the electrode is controlled to produce the desired range of PSD, also determined by such parameters as surface tension of the droplets and the trajectory aerodynamics.[34] The REP/PREP process is particularly suited to the production of powders where no liquid/container contact is desirable (e.g. titanium alloys) and to produce highly spheroidised, fully-dense powders with a tight PSD.

Vacuum, or soluble gas, atomisation was developed by Homogeneous Metals, Inc., based on the principle that a molten metal supersaturated with gas under pressure will cause liquid metal to be atomised when the gas expands and comes out of solution if suddenly exposed to vacuum[35] (see figure 6). This process produces an inherently clean powder, that is essentially spherical and with a PSD dependent on process modifications. The powders usually exhibit cellular or microcrystalline structures.

Spherical powders, which are not suited for cold pressing processes due to their particle surface topography, tend to be used in specialised applications where consolidation is achieved via hot isostatic pressing[34] such as for titanium alloys and nickel-based superalloys, where near-net-shape production is favoured.

3. Processing Metal Powder Compacts

3.1 Powder Characteristics

The processing parameters for metal powder compaction are directly affected by the fundamental properties of the metal powder. The apparent density of a powder is affected by the particle shape[36] (see figure 7) as well as particle size distribution (PSD), surface area and roughness of particles and particle arrangement.

Array	Density, %	Coordination No.
Simple cubic	52	6
Body-centred cubic	68	8
Face-centred cubic	74	12
Hex. close packed	74	12

Table 1. Regular Arrays Under Loose Packing Conditions.[37]

With equally sized spherical particles a number of regular arrays under loose packing conditions can be found[37] (see table 1). When a loose powder is mechanically agitated (i.e. by tapping or vibration) the short-term lowering in friction results in particle packing and leads to a higher density. Spherical powders lend to a greater tap density than irregular shape particles,[38] leading to less particle rearrangement upon consolidation and lower compact shrinkage rates.

3.2 Metal Powder Compressibility

The compressibility of a metal powder can be influenced by:[39] (i) inherent hardness of the metal, (ii) particle shape, (iii) internal porosity, (iv) PSD, (v) presence of non-metallics, (vi) lubricants and (vii) alloying elements. The 'green' (i.e. non-sintered) strength of such compacted powders, resulting mainly from mechanical interlocking of irregularities on the particle surface, is higher for irregularly shaped particles.

The compressibility and apparent (green) density are used to estimate the efficiency of a compacting process. It has been shown[40] that the capabilities for a powder for uniform densification during pressing may be fully characterised by means of a slide coefficient. However, the compressibility coefficient for metallic powders can only be assumed constant for a narrow range of density variations within the compact due to grain deformation above the proportional elastic limit.

3.3 Consolidation of Metal Powders

The compacting process can be defined in terms of three fundamental parameters:[41] the slide coefficient, the compactability (compressibility) coefficient and the cohesiveness. With knowledge of these parameters the local pressure and density variations within a specific powder compact geometry can be determined.

Powders can be compacted by the application of an external force either by[36] the pressing of powders in rigid dies, isostatic pressing in flexible envelopes, roll compaction into sheet or strip, or extrusion.

For the compaction of loose powder pressed in rigid dies or isostatically three stages have been postulated.[42] These are : (i) powder particles are initially restacked or rearranged leading to partial elimination of bridging between the particles, (ii) the particles undergo elastic and plastic deformation and (iii) the particles brittle fracture to form a smaller aggregate. It has been found[43] that for spherical powders deformation and sliding occur concurrently from the onset of compaction. Sliding of the particles stops at approximately 80% of theoretical density. Plastic flow was found to act in the deformation around particle contacts and in the filling of cavities through local extrusion.

The standard approach to the cold-compaction of metal powders is to add an organic binder which can be evaporated off prior to (or during) sintering. The choice of binder is very important as these agents can contribute to gas and carbon contamination during sintering.

3.4 The Pressure-Density Relationship

As the applied pressure is increased the density of the resultant powder compact will decrease. The relationship between the nominal pressure applied to a die and the

average density of the powder compact produced can be expressed empirically for low pressures as[44]

$$\ln P = -AV + B$$

where P is the applied pressure, V is the relative powder volume, and A and B are constants. However, the equation is only valid for certain powders and over a very narrow pressure range, and the equation is no longer valid at high pressures.

A theoretical basis for the relationship (based on fundamental principles) was developed later, and can be expressed as[45]

$$P = \frac{1}{K}\left[\ln \frac{1}{1 - D} + B\right]$$

where P is the applied pressure, D is the relative density of the compact, and K and B are constants. This has been shown to apply reasonably well to a number of powders over a broad pressure range.

It has been shown[46] that the compaction of metal powders by isostatic pressing leads to a higher density than by rigid dies. The isostatic pressing of powders[46,47] has shown two linear relationships of ln(1/1-D) versus P that occur for low- and high-pressure ranges.

3.5 Density Distribution in Powder Compacts

For powders compacted in a rigid die the distribution of pressure throughout the compact, and hence the resultant density distribution, is uneven. With isostatic compaction a uniform density throughout the powder compact can be assumed.

Work has shown[48] that pores within a powder compact are eliminated by size class with increasing pressure i.e. the pore size classes tend to decrease with increasing pressure.

Variations in density of single- and double-level rigid die compaction are shown schematically[37] in figure 8. The subsequent density distribution resulting from the compaction of metal powders is a result of the powders tending to flow only in the direction of the applied pressure. Friction between the die wall and the powder can be reduced with the addition of a lubricant. The density of the pressed compact at a given pressure is directly affected by the ratio of the area of the compact on which the pressure is applied to the area of particle and side wall contact.[49]

A typical density distribution of a powder compact subjected to pressure from only one direction[50] is shown in figure 9. Density will be highest where relative motion between the particles is at a maximum. This non-uniform distribution of applied stress

results in a stress distribution throughout the compact (and hence a density distribution), leading to anisotropic compaction in the subsequent processing.

A powder with a PSD will tend to a higher packing density than a monosized powder and hence reduces the subsequent density distribution upon compaction by promoting increased particle movement and deformation. Bimodal powders can also be used to increase the packing density. It has been found[51] that neither the material density or a difference in size from one material to another significantly affects the ultimate packing density, but the size and shape of the can did influence the type and density of the powder packing. The use of bimodal powders to increase the packing density relies on the smaller particles fitting into the interstitial spaces between the larger particles. Work on the packing of binary mixtures of atomised steel powder[52] has shown the optimum size ratio between the large and small particles to be 6.

The green strength of compacts results mainly from the mechanical interlocking of the particle surface irregularities. Hence, irregular shaped particles will tend to produce compacts with the highest green strengths, whilst spherical particles, by virtue of low surface contact areas and a low surface-to-volume ratio, produce compacts with low mechanical strength.

4. Powder Metallurgy Processing

With the growth of processing techniques for powder metallurgy (PM), aimed mainly at near-net-shape (NNS) production routes, (see figure 10), it is now possible to obtain metal powder parts with controllable microstructures and properties to suit the operating conditions, depending on the processing route.

As well as hot isostatic pressing (HIP) processes reviewed later (containerised and containerless) there are several techniques developed to take advantage of the unique properties of PM.

The Conform process[53] is an extrusion technique that depends on the heat-generating friction between the powder material and a rotating wheel, as together they move towards a fixed abutment and extrusion die. As a result of the temperature rise the metal powder flows through the die aperture and pressure welds to form a dense and homogenous extrusion. Due to the inherent low operating temperature and the high mechanical deformation which takes place the Conform process is ideally suited to rapidly solidified (RS) powders.

The Ceracon process[54] is a quasi-isostatic method of consolidation that uses carbonaceous particulate matter as a pressure transmitting medium. (The manufacturing steps are illustrated in figure 11). Upon grain pressurisation the preform experiences both axial and lateral components of force. The consolidation times are of the order of seconds but dwell time under load can be controlled to ensure densification with minimal microstructural changes. The Ceracon process is

particularly important when dealing with metastable microstructures such as those produced by RS. The part geometry also has great flexibility.

The Dynamic (or Explosion) Compaction process[55,56] has the capability of retaining RS microstructures as the heat generated within the powder upon consolidation promotes interparticle bonding whilst minimising bulk deformation. However, a subsequent HIP cycle is required owing to the low bonding strength.

5. Encapsulation Techniques for Metal Powder

A suitable encapsulation technique must be employed to ensure the pressure transmitting medium in the hot isostatic pressing (HIP) cycle (i.e. the gas) is isolated from the metal powder. Thus, the main process steps for a metal powder part consist of:[57] (i) capsule design and manufacture, (ii) filling and welding of the capsule, (iii) the HIP cycle and (iv) decapsulation and finishing. Figure 12 presents the basic process flowchart for production of various sized encapsulated (and unencapsulated) PM parts.[13]

The most commonly used 'can' is a preformed metal container which will be of similar shape to the desired finished article.[58] Mild steel or stainless steel are the usual materials for metallic containers, formed by metal spinning or superplastic sheet forming to the desired container design. Allowance in the design must be made for shrinkage during the HIP process and for degassing of the container. Any residual gas in the container can lead to incomplete densification and can, upon subsequent elevated temperatures, lead to thermally induced porosity within the compact. The container must be removed from the compact by mechanical or chemical means. However, this technique will clearly influence the densification process of the powder metal by virtue of the container and the welding seam.[59-62] The packing density of the powder is required for the design of the container used to produce near-net-shape parts to model the elastic/plastic collapse of the container. A metallic capsule processed by electroforming has also been proposed for difficult shape aspects.[58]

Ceramic/glass moulds allow for the HIP of complex shapes using powder metallurgy (PM).[29] Glass encapsulation, where the glass container is formed by casting and firing a slurry of ground glass prior to filling, degassing, and sealing, is usually limited to the use of ceramic parts/composites.[63,64] Ceramic containers can support a large mass of metal powder at elevated temperatures and hence do not lead to shape distortions. For ceramic containers a porous ceramic shell filled with powder is itself encapsulated by a sealed metal container which transmits the autoclave gas pressure. Glass containers will tend to spall from the compact upon cooling owing to differences in thermal expansion coefficients. Ceramic containers are generally inert to interactions with the powder.

Metal encapsulation is the most widely used method for experimental and production routes for HIP'ed parts, but is generally limited to simple shapes. Ceramic moulds

are used when complex precision net shapes are required, although longer cycle times are necessary for degassing.

The principal disadvantages of containerised HIP are:[65] (i) the lack of a suitable container material for use over broad temperature and compositional ranges, (ii) the cost of containerising (and then decontainerising), (iii) the difficulty of producing low cost small complex containers, (iv) the throughput can be as much as 50-90% higher for containerless parts than for containerised green parts or powders and (v) the difficulty of assuring the containers are completely leak tight.

6. Containerless Hot Isostatic Pressing

The containerless hot isostatic pressing (HIP) of powder metallurgy (PM) parts can be said to consist of three main processes, namely pressureless/pressure assisted sintering (PAS), injection moulding (IM) and sinter/HIP.

Consolidation in the presence of a liquid phase is utilised in pressureless and PAS processes. Pressureless sintering[66,67] uses capillary forces to drive the liquid phase into particle necks and small pores. The subsequent HIP cycle can either be performed on encapsulated or unencapsulated systems depending on the type of remaining porosity and/or the material composition. In the PAS process[4,67,68] the pressure cycle is typically at least an order of magnitude less than that employed in HIP, applied at a temperature near to, or at, the sintering temperature. PAS relies on the initial sintering step to form closed porosity with the pressure assisted step collapsing the isolated pores. A subsequent forming treatment is not necessary.

The advantages of the PAS process can be summarised as:[4] (i) consistently producing fully dense parts, (ii) mechanical properties that compare favourably with competing manufacturing processes, (iii) shorter cycle times than conventional sintering, (iv) superior dimensional control, (v) a reduction in excessive sintering additives, (vi) sintering gases or inert gases can be used and (vii) when used with IM metal powders it permits the use of coarser, lower cost powders.

For the IM process[69-71] the metal powder is firstly mixed with the binder to form the injection paste (so called green mixture). After moulding the part undergoes debinding[72] (usually of the order of 4-6 hours but this can take a week depending on part geometry) followed by sintering and HIP (see figure 13). It may also be possible to exploit a combination of IM with reactive HIP.[69]

Sinter/HIP is the processing technique that combines the advantages of vacuum-protective gas processing and HIP.[73] In the sinter/HIP process[74,75] the material is sintered to a condition of closed porosity using conventional techniques and then densified under the application of pressure (usually an order of magnitude less than a conventional HIP cycle).

The sinter/HIP cycle (see, for example, figure 14) is designed to be performed in the same workzone. Thus, it not only eliminates the need for the full HIP processing route but reduces production costs. This process should not be confused with the presinter + HIP compaction process[76] which operates in two distinct stages and requires containerisation for the HIP cycle.

Vacuum plasma spraying (VPS) is a recent addition to processing routes which can be classed as producing samples for containerless HIP. In the VPS process a substrate with a closed porosity coating can be given a subsequent HIP cycle (see later).

Although containerless HIP does require an 'independent' sintering step as opposed to containerised HIP[65] it does remove the disadvantages associated with containerisation.

By the use of nonagglomerating, fine powders, compacted to high green density and vacuum sintered, the possibility of producing parts suitable for containerless HIP'ing is increased. Surface sealing methods for small parts at present are difficult, expensive and largely experimental.[13]

7. Fundamentals of Metal Powder Densification

Although compaction provides the basic shape to the metal powder component the green state properties need to be improved via sintering to initiate interparticle welds through the provision of thermal energy.

Packed metal powders will coalesce as necks grow at particle contacts when subjected to temperatures in excess of approximately half the absolute melting temperature (i.e. a sintering process). The motion of an atom into the neck region is favourable as it reduces the net surface energy of the particle by decreasing the total surface energy. For metal powders the mechanisms of sintering are usually[77] diffusion processes with surface, grain boundary or lattice paths i.e. thermally activated mechanisms. The types of material transport[78] are illustrated in figure 15. It should be noted that while volume and surface diffusion cause spheroidisation of pores within the compact, grain-boundary and volume diffusion (i.e. bulk transport mechanisms) are responsible for shrinkage of the compact.

As sintering proceeds[77] (see figure 15) the pore structure changes from open and fully interconnected to a smoother, interconnected, cylindrical structure. Interfacial energy is the driving force at this point. Pore motion and isolation can occur. Grain growth and pore isolation reduce the sintering rate and are therefore not desirable. The cylindrical pore structure becomes unstable at approximately 8% porosity and collapses into spherical pores. The kinetics of the final stage are very slow.

The stresses caused by surface tension or capillary forces are related to the curvature of the surface according to Laplace's equation

$$\sigma = \gamma(-1/\rho + 1/x)$$

where σ is the stress acting on the neck, γ is the surface tension, ρ is the radius of curvature at the neck and x is the neck radius.

These stresses have been applied to the two-sphere model in solid-state sintering (see figure 16) where surface tension forces cause the transportation of material to the neck surface by volume diffusion, by grain boundary diffusion or by surface diffusion.

Pure nickel (and nickel alloyed with aluminium) has been investigated[79] to determine the neck radius as a function of time during sintering of spherical powders.

The distribution of the initial particle size and spatial packing leads to a pore size distribution in the final stage. A powder compacted prior to sintering will have a lower porosity level and an increased dislocation population, resulting in less shrinkage and a faster initial sintering rate.

Changes to aid sintering	Disadvantages
decrease particle size	compaction difficulties
increase time	grain growth greater cost
increase temperature	greater shrinkage grain growth higher cost
increase compaction pressure	tool wear
use alloying additions	embrittlement segregation compaction difficulties

Table 2. Processing Effects on Properties.[77]

As well as changing processing parameters[77] (see table 2) sintering can be enhanced by four common approaches, namely:[78] (i) hot pressing, (ii) phase stabilisation, (iii) activated sintering and (iv) liquid phase sintering. Sintering with a liquid phase is only possible if two or more phases of different melting points are present, with either the liquid phase being present during the entire sintering cycle or the liquid being formed during heat-up but disappearing at the sintering temperature by interdiffusion. The application of an external stress will tend to promote grain and particle sliding by diffusional processes, generate excess vacancies and cause pore collapse, leading to

more rapid densification.

Upon the application of a hot isostatic pressing (HIP) cycle to a metal powder workpiece a number of mechanisms may contribute to the densification process[80] (see figure 17). These contributory mechanisms can include[81-91] plastic flow, power-law creep, Nabarro-Herring creep, grain boundary sliding in the particles and grain boundary and bulk diffusion in the particle contacts, amongst others. The dominant mechanism (i.e. that which contributes most to the total rate of densification) depends on the stress and temperature and on the physical and compositional properties of the metal powder.

The densification processes, together with the powder parameters (size, grain size, current geometry, bulk material properties, interface properties) and the processing parameters (pressure, temperature, time) need to be understood in terms of their interrelation to permit accurate modelling of the HIP processing of powder metallurgy (PM) parts.

8. Modelling of Hot Isostatic Pressing

The modelling of the hot isostatic pressing (HIP) of powder metallurgy (PM) materials can be an important tool in the manufacturing process. With accurate modelling the can design and/or the pressure and temperature profiles can be optimised for the HIP cycle. The model should also be able to take into account the PM powder characteristics and other production variables. Depending on the aims of the model it will take the form of simulation methods, empirical-theoretical methods or computation of micromechanical aspects.

As well as the body of work described later other models considered have included the empirical model[92] (taking into account stress relaxation), the consideration of compressibility of metal powders,[40,41] and the compaction parameters of porous materials.[93]

8.1 Near-Net-Shape Techniques

The HIP of metal powder using near-net-shape (NNS) techniques is a single process production route to achieve dense and homogeneous articles. To this end the ability to predict the deformation of a (containerised) powder compact will be of great benefit.

The work by Abouaf et al[59,94,95] has centred on finite element analysis using rate form constitutive equations of the elasto-viscoplastic type. The work explicitly involves pressure gradients and porosity variations. Using this method in the prediction of part deformation has shown close agreement between computed shape and that obtained experimentally. The density variations of the part were imagined to be primarily due to the non-homogeneous temperature field. As this method of modelling attempts to

simulate the ongoing deformation and movement of all the particles it requires long calculation times (e.g. about 20 hours on a DEC VAX 750).

The finite element method (FEM) approach has been used by other workers to simulate the HIP process on containerised metal powder.[96-102] These models also give good agreement to experimental data.

The work by Aren et al[60,103-105] has centred on the effect of a temperature gradient within the powder body (although stress variation is ignored) and the resulting densification front. This study provides models that predict the shape change of containerised powder, albeit of simple design.

8.2 Theoretical-Empirical Modelling

A model not based on the FEM approach used for the numerical modelling of the shrinkage of the containerised metal powder during HIP has been proposed by Fallman et al.[62] Using an experimental results database the local shrinkage is determined with allowance for relative powder density, capsule wall thickness, edge effects and container aspect ratio. The program can also be used in an 'inverse-HIP' mode i.e. to recommend the design of the container. The results obtained offer short calculation times together with very good agreement with experimental results.

The work by Bouvard et al[106-109] has been aimed both at the use of interrupted HIP tests to determine densification rates in relation to morphological/microstructural changes of the particles and using random variables for the parameters that determine deformation of interparticle contacts.

The interrupted test method was developed due to the lack of data necessary to validate theoretical models. The studies indicated the effect of particle size distribution (PSD) as well as the predominant deformation mechanisms. The model based on random variables agrees with available experimental results for monosized particles. It has been proposed to extend the model to include any PSD.

The modelling of polyphase materials has been investigated by Kaysser et al.[110-112] Single isolated particles are isothermally deformed to investigate the creep behaviour with the assumption that the material of the deformed zones distributes homogeneously on the free surface of the particles. Good agreement is obtained with experimental results. When compared with the HIP cycle parameters (pressure, temperature, time) predicted by the Ashby model (see later), the Ashby parameters are found to be too low.

The relationship between the deformation of single spheres and HIP samples has been investigated for several materials.[113,114] The results have again been compared to the Ashby model. A dilatometer was used during the HIP runs and the data points obtained used to modify the parameters. The use of the dilatometer also highlighted

the non-steady state conditions arising from the continuously decreasing pressure during the cycle. (The nickel-based superalloy AP1 has been investigated extensively[115-117] by these workers).

8.3 Ashby Model

The Ashby model is a micromechanical approach to modelling the densification of powder by the HIP process. The computer program HIP487[118] has been developed to combine and illustrate the previous work on deformation-mechanism maps.[81,82,85,86,89,90,119,120] The following description of the Ashby model is found in the relevant literature.[121]

The densification of the powder body is for convenience divided into three sequential stages. The first stage (Stage 0) is that of powder packing, dependent on particle shape, particle size distribution (PSD), initial pack density and surface and frictional forces preventing rearrangement.

The second stage (Stage 1) describes the early stages of densification, when the residual porosity is open. Necks grow at the contact points between particles, produced by transport mechanisms.

The final stage (Stage 2) describes the final densification, when the residual porosity is in the form of small holes produced by growth and impingement of necks.

The effects of the densification and the dominance of individual mechanisms can be modelled by consideration of the rate equations (explained in more detail later) given in table 3, together with the nomenclature.

It has been shown by Arzt[122] that the assumption of a random dense packing as a model for the initial particle structure allows a more precise prediction of the particle geometry during densification by plastic flow and creep.

In figure 18 a particle (shaded) is shown to contact a number Z of its neighbours in small contact areas a. As the densification process proceeds the contacts Z increase (from typically about 7) and the area of each contact grows, causing the local pressure on a neck to decrease.

The topology of the densification process is considered by imagining each particle to expand about its fixed centre point, provided the volume of material remains constant.

Analysis of this problem[122] results in a calculation to determine the effective pressure and its variation with the progress of densification. This is illustrated in figure 19 where it can be seen that the effective pressure falls towards the external pressure as the density approaches unity.

Stage 1	Stage 2
Initial compaction	
$D_i = \left\{\frac{(1-D_0)}{1.3\sigma_y} P + D_0^3\right\}^{1/3}$	$D_i = 1 - \exp\left\{-\left[\frac{3}{2}\frac{P}{\sigma_y}\right]\right\}$
Volume diffusion (pressure driven)	
$\dot{D} = 43\, C(1-D_0)\frac{D_v}{R^2}\frac{(P-P_o)\Omega}{kT}$	$\dot{D} = 270\,(1-D)^{1/2}\left[\frac{1-D}{6}\right]^{1/3} \times \frac{D_v}{R^2}\frac{(P-P_i)\Omega}{kT}$
Boundary diffusion (pressure driven)	
$\dot{D} = 43\, C^2\frac{\delta D_B}{R^3}\frac{(P-P_o)\Omega}{kT}$	$\dot{D} = 270\,(1-D)^{1/2}\frac{\delta D_B}{R^3} \times \frac{(P-P_i)\Omega}{kT}$
Power law creep	
$\dot{D} = \frac{3.1}{C^{1/2}} D_{crp} D\left\{\frac{C(P-P_0)}{3\sigma_0 D^2}\right\}^n$	$\dot{D} = 1.5 D_{crp} D(1-D)\left\{\frac{1.5}{n} \times \frac{(P-P_i)}{\sigma_0}\frac{1}{(1-(1-D)^{1/n})}\right\}^n$
where $D_v = D_{0v}\exp\left\{-\frac{Q_v}{RT}\right\}$	$\delta D_B = \delta D_{0B}\exp\left\{-\frac{Q_B}{RT}\right\}$
$D_{crp} = 10^{-6}\exp\left\{-\frac{Q_{crp}}{RT_m} \times\left[\frac{T_m}{T}-2\right]\right\}$	$C = \frac{1-D_0}{D-D_0}$ $P_i = \left[\frac{1-D_c}{1-D}\right]\frac{D}{D_c}P_o$

D	Relative density
D_0	Initial relative density
D_i	Relative density from plastic yielding
D_c	Relative density at which pores close
$\dot{D}$	Densification rate
δD_B	Boundary diffusion coefficient times boundary thickness
D_v	Volume diffusion coefficient times boundary thickness
k	Boltzmann's constant
P	External pressure
P_o	Outgassing pressure
R	Particle radius
T	Absolute temperature
T_m	Absolute melting temperature
σ_0, n	Creep parameters
Ω	Atomic or molecular volume
σ_y	Yield strength

Table 3. Equations for Densification Rate.[121]

Pore pressure is also taken into account in the model, as any internal pressure sealed into the compact will ultimately limit densification.

The mechanisms and kinetics of hot isostatic pressing (HIP) have been modelled for a single average powder particle radius using the mechanisms of yield, power-law creep, diffusional creep and diffusion. Owing to the inherent uniformity of stresses this approach must be understood before size distributions can be accounted for.

Ashby conveniently divides densification into three stages as porosity is isolated and spheroidised. As densification proceeds the centres of particles approach each other to meet and form new necks. This enlarges both the area and the number of contacts between particles so that the contact force per unit area (the effective pressure) diminishes. Ashby also considers this topology by imagining each particle to expand about its fixed centre point, provided the volume of material remains constant.

Analysis of the problem[122] shows that the mean number of contact neighbours, Ź, grows with relative density, D, by

$$Ź = 12D$$

and the average area of each contact grows by

$$\frac{á}{4\pi R^2} = \frac{1}{12}\frac{(D-D_o)}{(1-D_o)}$$

where á is the average contact area at a neck and R is the radius of the particle. The total contact area per particle, áŹ, determines the contact pressure and when normalised gives

$$\frac{áŹ}{4\pi R^2} = \frac{D(D-D_o)}{(1-D_o)}$$

The effective pressure, P_{eff}, acting across each neck is the external pressure, P, distributed over these contact areas thus

$$4\pi(R')^2P = ŹáP_{eff}$$

where R' represents the radius of the volume associated with each particle including void space, given by

$$R' = \frac{R}{D^{1/3}}$$

from which

$$\frac{P_{eff}}{P} = \frac{1-D_o}{D^{5/3}(D-D_o)}$$

It can be seen that as densification proceeds the effective pressure falls and eventually equals the applied pressure at full density.

To take into account incomplete outgassing of the compact, which will oppose densification, P is replaced by $P-P_i$ in the modelling where

$$P_i = P_o \frac{(1-D_c)D}{(1-D)D_c}$$

where P_o is the initial gas pressure in the contact and D_c is the relative density at which the pores close off.

Hence, the ultimate limiting density for a HIP cycle at pressure P is

$$D_{ult} = \frac{\frac{P}{P_o}\frac{(D_c)}{(1-D_c)}}{1+\frac{P}{P_o}\frac{(D_c)}{(1-D_c)}}$$

Arzt et al[81] correlated the effective pressure and densification in several rate laws depending on the operating mechanisms, namely: (i) deformation by diffusional creep at low stresses, (ii) deformation by power-law creep at higher stresses and (iii) deformation by time-independent plastic flow at stresses above the yield stress.

(i) Densification by Diffusion

Surface tension forces are important at low stresses and densification will occur by volume or grain boundary diffusion (Nabarro-Herring and Coble creep). Densification is a result of the transport of material from contact zones to the surface of a contact neck. The rate of densification, $\dot{D}$, during the initial stage is

$$\dot{D} = \frac{12D^2}{D_o a^3 g(D)} \frac{\delta D_b + rD_v}{kT} \Omega Z P_{eff}$$

where g(D) is a purely geometric term.

During the final stage the material is transported along the grain boundaries to the surface of the spherical voids situated at the grain boundary intersections. The rate of densification is then given by

$$\dot{D} = 54 \frac{\Omega\delta D_b}{kTa^3} \frac{1-(1-D)^{2/3}}{3(1-D)^{2/3} - (1+(1-D)^{2/3})\ln(1-D) - 3} P_{eff}$$

(ii) Densification by Power-Law Creep

Densification will be governed by a power-law creep rate with an increase of pressure, giving the rate of densification during the initial stage of

$$\dot{D} = 5.3(D^2D_o)^{1/3} \frac{x}{a} \epsilon_o \left[\frac{P_{eff}}{3\sigma_o}\right]^n$$

where ϵ_o and σ_o are power-law creep parameters.

During the final stage densification is determined by

$$\dot{D} = \frac{3}{2} \epsilon_o \frac{D(1-D)}{(1-(1-D)^{1/n})^n} \left[\frac{3}{2n} \frac{P_{eff}}{\sigma_o}\right]^n$$

(iii) Densification by time-independent Plastic Flow

Densification becomes time-independent when pressure becomes sufficiently high to cause plastic flow, with the contact areas growing until the yield stress, σ_y, is no longer exceeded. For the initial stage the onset of yielding can be defined by

$$P_o = \frac{3\sigma_y}{4\pi a^2} AZD$$

where the average area A of a contact is given by

$$AZ = a^2 \frac{D-D_o}{D} (160(D-D_o)^2 + 16)$$

with

$$Z = Z_o + C((D/D_o)^{1/3} - 1)$$

Plastic flow is unlikely to occur under normal hot isostatic pressing conditions during the final stage.

It should be noted that the implicit assumption in the Ashby model is that all the particles are the same size. A dispersion of particle sizes will increase the initial packing density. However, while some mechanisms, like power-law creep, do not depend on particle size, others (particularly those involving diffusion) are influenced by the particle size.

In an intimately-mixed dispersion of sizes a region which shrinks more quickly than its surroundings generates a local hydrostatic tension which tends to cancel the external pressure. From this, effective particle radii which are approximations to the

mean of the size distribution can be calculated for boundary-diffusion and lattice-diffusion controlled mechanisms.

Using the Ashby model it is possible to formulate preferred process conditions and refine the theoretical results using experimental data.

An attempt to combine the modelling of powder body shrinkage with that of the micromechanical approach has been investigated by Easterling et al.[123-125] The dependence of the rate of densification across a whole sample upon the rate of heat flow is illustrated along with other parameters. Due to the presence of a densification front it is proposed that residual stresses may occur.

8.3.1 The Ashby HIP487 Program

The program HIP487 was developed by Ashby from the models and rate-equations based on earlier work (see Ashby[117] and Helle et al[82] for summaries).

Field Name	Description of Densification Type
YIELD	Compaction by plastic yielding when the pressure is applied
V-DIFF1S	Surface-tension driven by volume diffusion from neck boundary, stage 1
B-DIFF1S	Surface-tension driven by boundary diffusion from neck boundary, stage 2
V-DIFF2S	Surface-tension driven by volume diffusion from neck boundary, stage 2
B-DIFF2S	Surface-tension driven by boundary diffusion from neck boundary, stage 2
V-DIFF1	Pressure-driven by volume diffusion from neck boundary, stage 1
B-DIFF1	Pressure-driven by boundary diffusion from neck boundary, stage 1
V-DIFF2	Pressure-driven by volume diffusion from neck boundary, stage 2
B-DIFF2	Pressure-driven by boundary diffusion from neck boundary, stage 2
PL-CRP1	Pressure-driven by power-law creep, stage 1
PL-CRP2	Pressure-driven by power-law creep, stage 2
NH-CRP1	Pressure-driven by volume and boundary diffusion from grain boundaries within the particle (Nabarro-Herring creep), stage 1
NH-CRP2	Pressure-driven by volume and boundary diffusion from grain boundaries within the particle (Nabarro-Herring creep), stage 2

Table 4. Description of the Densification Mechanism Fields in HIP487.[118]

Using the data files supplied (or creating a data file), which consist of material

parameters and process variables, the program constructs deformation mechanism maps for powder materials from the rate equations. A density-pressure or a density-temperature map is drawn which is divided into fields showing the range of dominance of a given mechanism. The field names and their description are given in table 4. The program will be discussed in detail later in relation to the modifications.

The Ashby model program, HIP487, has been rewritten by workers[126] from the event driven format to simulate, in time, the densification of a component during a HIP cycle given functions for temperature and pressure. Densification of the compact is measured in-situ and compared directly against theoretical models. This allows analysis between the experimental and theoretical data to assess incorrect parameter values or modelling phenomena. The study also considered the effects of 'cold starts' (i.e. starting the modelling from standard atmosphere temperature and pressure), canister shielding, low temperature creep, initial compact density and the effects of grain growth.

8.4 Bimodal Modelling

A random close packed (RCP) structure has no long range order and this ideal structure can be precluded from being established by, for example, clustering of particles so as to produce non-uniform density regions and 'satellites' associated with powder particles. As has now become obvious by the modelling work so far described a knowledge of powder distribution is essential for the modelling of densification mechanisms.

Nair et al[127] have produced analytical derivations of the ideal RCP structure so as to compare it to the monosized and bimodal distribution of particles. It was concluded that a RCP structure is approximated by powder particles compacted together in both size distributions.

Borofka et al[128] noted that the typical HIP parameters for the consolidation of superalloys correspond to nearly complete densification via relatively rapid plastic flow. The smaller particles were deformed to a much greater extent than the larger particles, resulting in relatively undeformed particle surfaces. Kissinger et al[129] reported that densification occurs predominately by athermal plastic deformation of the powder particles. The athermal plastic flow field is found to be larger for the bimodal case than for the monosized case. It was concluded that the smaller particles in a distribution suffer a higher degree of plastic deformation in comparison with the larger particles and that different sized particles do not, in general, deform by the same mechanism of densification.

The model proposed by Tien et al[130,131] considers the stress differences between particles in the bimodal case. This bimodal model follows the technique used by Ashby, and is only extrinsically bimodal by consideration of differing powder particle radii. Densification is modelled as the fictitious growth of spheres, and the

mechanisms of yield, power-law creep, superplasticity, diffusional creep and long-range diffusion are considered. The final stage of densification is modelled as the closure of a bimodal distribution of pores. The densification rate equations defined determine the dominant mechanism, the densification rate being summed up and integrated to predict densification kinetics.

The HIP maps produced display regime boundaries with two values - one for the smaller particles and one for the larger particles. As can be seen in figure 20 the split between the mechanism boundaries increases as the ratio of particle sizes increases.

The model fits experimental HIP data using high pressures quite well but at low pressures the fit improves if heat-up time is considered.

This bimodal model has been developed due to the difficulty in treating a full size distribution but on the basis of the results it is possible to generalise to the full size distribution. The authors proposed that intrinsic differences in a distribution of powder should be included in future work.

When the model predictions of Arzt et al[81] are compared with Nair and Tien[130] in the monosized case it can be observed that there is no substantial difference between the results. Somewhat smaller interparticle stresses are predicted by Arzt et al, which translates to a slightly smaller athermal plastic flow region. Figures 21 and 22 show the model differences for the monosized case.

For the bimodal particle case it can be shown by consideration of the average interparticle contact stresses that the value of this stress is larger on the smaller particles (see figure 23). The boundary between the athermal plastic flow and the power-law creep regions on the HIP densification mechanism map will be different for the two different sized particles (see figures 24 and 25).

It was concluded that the non-uniform stresses in the bimodal particle case result in an asymmetric pattern of plastic flow. The single boundary between athermal plastic flow and power-law creep regions for the monosized case converts to a band for the full size distribution of particles. The model generated can relate the thickness of the band to the particle size distribution.

The model proposed by Li et al[132-134] differs from that proposed by Tien et al in regards to the interparticle contact force. In this model all interparticle contacts are not subject to the same force but vary so as to produce a uniform rate of densification across the compact.

The model considers yielding and power-law creep as the possible densification mechanisms, and the expanding particle frame of reference as previously used to model the densification process. When predicting the consolidation maps using the rate equations obtained, the criterion that a single particle (or two in the bimodal

case) characterises the system, and that the consolidation takes place by contact deformation (not by particle rearrangement), must be met. The border between yielding dominance and power-law creep dominance is predicted using the consideration of the ratio of contacts yielding to the number of contacts. Hence, the border can have a pre-set definition. The model provides a good quantitative prediction of the consolidation behaviour of monosized and bimodal powder distributions[134] (see figure 26). It was also noted that the prediction of extra contacts developed reduced the predicted densification rate from that assumed earlier.[122]

The model also indicated that the addition of smaller particles into a larger particle system may alter consolidation mechanisms even in the absence of the effects associated with the initial packing density. It was proposed that diffusion could be incorporated into the same model framework.

Composite powder mixes have also been investigated[134] by treatment with the bimodal model (although only athermal plastic flow is considered as a mechanism).

8.5 Further Modelling Modifications

By noting that the predicted densification rates of a sphere of creeping material containing a single, centred void were significantly increased by small deviations of the load from purely hydrostatic compression it has been shown that deviatoric stresses have a strong effect on densification rates.[135] Can shielding has been proposed as a contributory factor leading to the appearance of deviatoric stresses. A strain rate potential has been proposed to model these effects.

Work has been done to model the macroscopic creep parameters of powders due to diffusional mass transport on the interparticle contacts (by specifying the macroscopic strain rate and computing the energy dissipated in mass transport and interparticle shear).[136] This creep law includes a term which drives sintering.

9. Coating Technology

The majority of engineering failures are surface orientated owing to severe working conditions. This is due mainly to stress levels being often highest at the surface and that the surface is subject to environmental factors. It has been recognised[137] that the conditions defining the surface material are often dissimilar to those required for the bulk material. If the surface of the bulk cannot be modified by surface treatments then there is a need for coating technology.

The range of coating methods presently available include:[137] (i) various spraying techniques, (ii) electroplating, (iii) chemical vapour deposition and (iv) physical vapour deposition. The many techniques in these categories are illustrated in figure 27.

The two most routinely used methods for applying overlay coatings to superalloys are physical vapour deposition (PVD) and plasma spraying.

A comparison of the various available surface engineering techniques can be seen in figure 28.[138] These techniques have been classified into generic groups, with the advanced technologies subdivided into gaseous, molten or semi-molten state processes (see figure 29) which are dominated by 'dry' methods. The chamber size of the gaseous state processes limits the size and complexity of the shape to be coated owing to the mean free path distance. The ability of the vapour phase processes to coat complex part geometries in relation to the mean free path is shown in figure 30.[138] Processes such as PVD (owing to the relatively hard vacuum and consequently the large mean free path) and thermal spraying (due to the requirement of part manipulation) are regarded as 'line-of-sight' processes.

Extensive use of glow discharge plasmas are used in the dry processes to overcome the problem with coating uniformity. Plasmas are ionised gas, produced and driven by an external power source. This power source can operate in a range of frequencies from direct current (DC) to 10 GHz depending on the technique used to create and sustain the plasma, as shown in figure 31.[138] Figure 31a illustrates electrodes across which a high voltage is applied in the discharge chamber. DC and radio frequency (RF) diodes are among the devices that use this form of plasma excitation. The application of an electric field can be used to break down the plasma and cause ionisation (see figure 31b). A plasma can also be created and sustained by the injection of large electron currents which, upon acceleration into the plasma, cause ionisation to form the plasma as in figure 31c. All of these processes rely on the ionisation of background gas atoms by fast, or primary electrons. A direct consequence of excitation is the subsequent emission of a proton, hence the characteristic glow.

9.1 Physical Vapour Deposition

Evaporation physical vapour deposition is the process whereby deposition is a result of the condensation of the evaporant, melted at high temperature in vacuum, onto a substrate. The equipment required and material suitability have been previously investigated.[139,140] A schematic evaporation PVD system is illustrated in figure 32.

Under high vacuum (say 10^{-4}-10^{-5} Pa) the mean free path of the evaporant material will usually exceed the dimensions of the chamber. Deposition of the evaporant is line of sight. The uniformity and edge coverage of the coating can be improved by back-filling the system with an inert gas (to say 1-10 Pa) to reduce the mean free path of the evaporant. This results in multiple collisions and 'bathes' the substrate in evaporant. Electron beam heating of the evaporant can also be used instead of a resistance source.

Coatings of very high purity can be deposited at low rates of typically 1 μm/min.,

with the ability to produce mono-crystalline, amorphous and epitaxial structures.

As with any coating technique the final coating structure and composition is determined by phenomena at the substrate.[140] Evaporation PVD can also be performed with a reactive atmosphere.

Sputtering PVD is an atomistic process with material ejected from the target due to the momentum exchange associated with the bombardment of energetic particles (i.e. ions generated usually by a glow discharge). The sputtering chamber is evacuated (to say 10^{-3}-10^{-5} Pa) before backfilling (to say 10-0.1 Pa) with a heavy inert gas (usually argon) with the electrical discharge operating at voltages of 0.5-5 kV.

Unlike the thermal process of evaporation, the coating material in sputtering is passed into the vapour stage by momentum exchange, making many materials coating candidates.

9.2 Ion Plating

In the ion plating (or plasma-assisted PVD) process deposition is a result of condensation of the evaporant material (anode) that has been heated and connected to a high potential with a positive charge, onto the substrate (cathode) during glow discharge. The electric field formed in the vacuum (say 10^{1}-10^{-4} Pa) between the anode and cathode causes a glow discharge and generates a plasma. Owing to gas collisions and charge exchange the cathode is bombarded by a wide spectrum of energetic ions and fast neutrals.

The equipment required and material suitability has been previously investigated,[137,139] and a simple ion plating layout[141] is illustrated in figure 33. The glow discharge can be used to sputter clean the substrate prior to deposition as well as to heat the substrate. With the inclusion of a hot filament electron beam gun, using a double chamber construction, it is possible to produce high deposition rates and with feed systems for the evaporant thick coatings are possible. Ion plating can deposit coatings out of line of sight of the evaporant. The morphology and composition of the coating is again dependent on substrate temperature and substrate bias. Radio frequency (RF) bias can also be used in the ion plating process as can reactive gas deposition.

9.3 Chemical Vapour Deposition

Chemical vapour deposition (CVD) is the process where the nucleation of a stable solid reaction product grows in a environment where a vapour phase chemical dissociation or chemical reaction occurs. Many CVD processes operate at or near atmospheric pressure and as such possess excellent coating uniformity properties. Full descriptions of the varied CVD systems and the resultant coating properties can be found in the literature (for example in that of Hocking et al[142] and Rickerby and

Matthews[138]).

9.4 Flame Spraying

The flame spraying method is based on the coating material being introduced into a gas flame and then sprayed as molten particles in a carrier gas onto the substrate. The melt material is sprayed onto the substrate in a plastic or semi-molten state at a speed of 50-100 m/s with a flame temperature of up to 3000 °C.[139]

The cleaned substrate is preheated prior to spray coating and is then post-treated to approach full densification, (porosity is up to 20%). The materials deposited and feasibility in flame spraying has been discussed elsewhere.[139]

Spray forming has been used without the aid of a gas flame for a high deposition rate process achieving the rapid solidification of liquid metal.[143,144] Although as-deposited properties can be similar to the wrought condition,[143] hot isostatic pressing (HIP) treatment and forging[143] or HIP treatment and hot rolling[144] can be subsequently used to improve properties.

9.5 Plasma (Arc) Spraying

In the plasma spraying process the melt material is introduced into a plasma arc and then sprayed onto the substrate. Powders are the most commonly used material, being injected into a high temperature plasma[145] (see figure 34). This process is capable of producing thick coatings (of the order of 10^{-2} m).

Work to date on atmospheric plasma spraying[146] (APS) of ceramic onto metal or vacuum plasma spraying[147] (VPS) of superalloys, involved the use of HIP as a post treatment for the coating. The samples coated by APS required encapsulation of the sample for the HIP cycle owing to the relatively high levels of porosity associated with the process. The HIP cycle would also lead to diffusion bonding between substrate and coating. A VPS process, applicable for example for the deposition of superalloy and coating for a turbine blade is illustrated in figure 35.

APS and/or VPS have also been applied to nickel aluminides,[148] molybdenum-containing powders,[149] yttria partially stabilised zirconia[150] and aluminium-lithium alloys[144] amongst others. For wear applications underwater plasma spraying[151] (UPS) has been used and Ti-Ni alloy coating has utilised low pressure plasma spraying[152] (LPPS).

10. Coating Structure

For this study the use of physical vapour deposition (PVD) overlay coatings (primarily evaporation) was considered. The deposition conditions greatly affect the nucleation process and hence the growth and structural characteristics of the coating.

Coatings and thin films, owing to the production of metastable states and non-equilibrium phases, often exhibit different microstructures and properties from the bulk material. The structure of the deposited overlay coating on green metal powder compacts has a major influence on their ability to maintain the desired pressure differential during the hot isostatic pressing (HIP) process.

10.1 Nucleation

In the evaporation process[153] the evaporant atoms impinging on the substrate form a loose bond (i.e. adatoms) with the substrate lattice due to transference of energy. These adatoms migrate until they are absorbed at low energy sites or desorbed. Growth and atomic rearrangement form the overlay coating.

The factors influencing the formation of coatings are:[142] (i) the substrate, (ii) the temperature of the substrate and the process, (iii) the deposition medium, (iv) the rate of arrival and mass transfer and (v) the compatibility of the coating/substrate system.

The substrate surface morphology has a major influence on the coating structure. The growth of open columnar structures is promoted from rough surfaces with each powder particle at the porous powder compact surface nucleating the growth of a new columnar grained structure within the coating. With adjacent grains impinging the resultant coating structure would be highly defective, caused by the shadowing effects of neighbouring nucleation sites. The cleanliness of the substrate will have a marked effect on the adherence of the coating.

The pattern and influence of substrate temperature and supersaturation on the resultant deposited structure are illustrated in figure 36.[154] Diffusion of the coating will be promoted by increasing the substrate temperature by increasing the adatom mobility. However, at low temperature, the coating structure will tend to columnar outgrowths from the nucleation sites with weak open boundaries. Using atomistic deposition processes to form thick coatings often results in the formation of a columnar morphology with low density.

Interfacial reactions, nucleation and growth are effected by the energy of the system[155] (e.g. evaporant energy, the presence of a plasma, backfilled pressure). With the introduction of a high gas pressure during deposition the mobility of the adatoms is hindered and columnar structures can result even with high temperatures. The interaction between chamber pressure and temperature on coating structures is discussed in the next section.

10.2 Prediction of Coating Structure

The coating structure can range from open columnar to fine equiaxed, dependent on the deposition conditions. These structural zones have been shown to depend on the ratio of deposition temperature, T, to the specific melting temperature, T_m, i.e T/T_m.

The Movchan-Demchishin zone classification[156] (see figure 37) proposed that the structure of the coating could be represented as a function of T/T_m in terms of three zones. For metals, zone 1 ($T/T_m < 0.3$) consists of tapered crystals with domed tops, separated by voided boundaries. Zone 2 ($0.3 < T/T_m < 0.45$) consists of columnar grains separated by distinct dense intercrystalline boundaries. Zone 3 ($0.45 < T/T_m < 1$) consists of equiaxed grains. The transition temperatures between these structural zones increase as the operating pressure increases.

The dependence of the coating structure on the argon pressure and substrate temperature was shown by Thornton[157] (see figure 38). Although this figure applies to sputtered coatings it can be applied to evaporated coatings at zero argon feed pressure. Coatings within the Zone 1 structure are often in tension, apparently because they are lower density with a wider than equilibrium interatomic spacing. Coatings of Zone T structure often exhibit high compression type internal stresses. At $T/T_m > 0.45$ dense columnar grains are formed as the adatom mobility is now sufficient to overcome the self-shadowing effects (from the tapered crystals) seen in Zone 1.

The structure of nickel films has been studied by Grovenor et al[158] and a mechanism for coating structure development based on the dual processes of grain growth and granular epitaxy has been proposed. It was proposed that the grain structure is determined fundamentally by the mobility of individual grain boundaries in the deposit (itself influenced by process variables). This model for the grain structure of films (see figure 39) can be applied to other materials.

It can be seen that increasing the growth temperature causes the film to densify, while increasing the pressure produces the opposite effect.

It has been proposed by Messier and Yehoda[159] that the properties of vapour deposited films can not be predicted fully from a knowledge of their deposition conditions. The coating structure can also be modified by the species mobility, deposition rate (possibly as a result of increased source radiation), contaminant partial pressures (due to the introduction of argon gas), apparatus geometry and coating thickness (with increased coating thickness the influence of the substrate diminishes).

10.3 Residual Stresses in the Coating

Residual stresses can arise in deposited coatings due to any thermal mismatch between the coating and the substrate or an intrinsic stress due to the accumulated effect of atomic forces generated during coating. Mechanisms such as impurity concentration, the gas pressure, deposition temperature and rate and the angle of incidence of coating flux, can all effect the development of stress.

It is common with the vapour state coating processes that the evaporant is deposited in an array, perpendicular to the surface, of close packed columns. Intrinsic tensile

stresses are generally developed in evaporated coatings, whilst compressive stresses are developed in ion bombardment techniques. It has been shown, for example with TiN coatings,[138] that X-ray diffraction analysis gives a lattice strain of 0.09% for chemical vapour deposition (CVD) and 0.23% for plasma assisted physical vapour deposition (PAPVD). This is due to the higher temperatures employed in CVD, resulting in large grain size and few defects, and the non-thermal equilibrium conditions of PAPVD, giving small grain size and having a high concentration of point defects and other lattice distortions.

11. Coatings as In-Situ Envelopes

The influence of nickel overlay coating thickness on the closure of surface porosity on phosphor bronze substrates has been reported in a recent publication by the author.[160] Nickel coatings were deposited onto presintered phosphor bronze powder by ion plating at high pressure. The coating initially grows with a columnar structure but densifies as the surface pores are bridged as the coating thickness increases. The relationship between pore closure and coating thickness was studied by measuring the mass flowrate of air through coated samples. Coating thicknesses of the order of five times the particle size are required to ensure pore closure (see figure 40) i.e. to produce a defect-free coating suitable to act as an in-situ envelope. It was also demonstrated that the use of ion plating, as opposed to electron beam evaporation, resulted in a fully dense coating owing to the reduced atom flux and higher atom surface mobilities.

A similar sinter-HIP processing approach as that used in this study (see later) to produce a coating/substrate system that will satisfy the requirement of an in situ envelope has been used previously.[161] A low melting point eutectic phase was formed between the coating and substrate and used to densify aluminium and aluminium substrates.

A previous study at Cranfield[162] investigated the closure of artificial porosity in steel by HIP. It was found that pores close to the surface tend to close first which could affect the integrity of a coating to act as an envelope during a HIP cycle i.e. the action of the applied pressure/temperature could tear the coating due to the uneven powder substrate.

By considering the pore and surrounding material as a thick walled cylinder then, if

$$\frac{r_0^2}{r_o^2 - r_i^2} \approx 1$$

where r_o is the cylinder radius and r_i is the pore radius, then dimpling is unlikely to occur i.e. the coating will remain viable as a envelope. This will be important when the coating is of like material to the powder substrate and can not defect-heal prior to the HIP cycle.

EXPERIMENTAL PROCEDURE

1. Areas of Study

This work has considered two specific areas of study: namely, the use of in-situ coatings as envelopes for powder compacts, prior to the use of a hot isostatic pressing (HIP) cycle, to satisfy the requirements of a canning method for intricate part geometry, together with a study of the use and accuracy of process modelling and its dependence on processing routes and powder characteristics.

The use of metallic overlay coatings (namely those produced by physical vapour deposition) to form in-situ envelopes has been studied through the dependence of absolute pressure, substrate temperature, coating thickness and coating structure. The substrate surface, through its dependence on the powder characteristics and processing route, has been investigated as to its influence on coating growth and these factors correlated with the performance of the coating as a pressure barrier during HIP/sinter-HIP.

Work has also been undertaken to improve present modelling, namely the Ashby deformation-mechanism maps, to incorporate powder size distributions. Experimental results (both from the author and literature) have been used to assess the accuracy of the model through powder size distributions, canning techniques and the dominant mechanism of densification.

2. Powder Morphology

Powder metallurgy (PM) is ideally suited for making high quality near-net-shapes (NNS) as the rapidly solidified powders have a fine uniform microstructure, a high tap density, and good flow characteristics. The efficient use of PM depends on the application of scientific understanding of complex solid state reactions with highly developed engineering capabilities.[163] The combination of hot isostatic pressing (HIP) and PM offers the potential of producing high quality finished articles.

The method of powder production leads to specific powder morphologies. This work has mainly investigated spherical atomised powders.

The principal metal powder chosen for this study was commercial purity nickel (Ni) owing to its well known material constants and its importance as a base metal for modern superalloys. The use of a pure metal powder also allows for easier interpretation of the modelling rate equations, and validation of the predicted densification rates.

All powders (except PY114L) are commercial purity nickel powders, all produced (except Ni123) by atomisation processes. The PY114L powder, produced by Tecphy, is a nickel-boron (1.4 at.%) powder. The Ni123 powder, produced by Inco Alloys

Ltd., was manufactured by the decomposition of nickel carbonyl. The APA2 powder was produced by Wiggins Alloys Ltd. and the Goodfellow powder by Goodfellow Metals.

In some of the studies involving the use of overlay coatings to form in-situ envelopes two nickel-based alloys (namely nickel-chrome and Astroloy, both produced by Wiggins Alloys Ltd.) were used. Owing to the limited availability of the alloy powders and the intention to study the behaviour of deformation mechanisms these modelling studies used the commercially pure nickel powders that were available.

2.1 Particle Size and Size Distribution

The most widely used method of particle size measurement in the powder metallurgy (PM) industry is by sieving. For the purpose of spherical particles, where particle diameter is generally used to characterise size, sieving can be used effectively for powder separation. (For irregular shaped particles the equivalent spherical particle diameter can be calculated). For this study, sieving was used for the purpose of separation of the commercially available powder into smaller particle size distributions (PSD) i.e. to obtain a range of powder sizes more akin to the monosized PSD's assumed in the models. All sieving was mechanically performed using nylon mesh sieves. Bimodal powders were produced by the addition of two powder sizes.

In order to obtain a direct measurement of the PSD of a specific powder a Cambridge 250MkIII Stereoscan scanning electron microscope (SEM) was used. This allowed for the diameter of a representative sample of powder particles to be measured directly using the graticule scale.

The SEM also allowed for the investigation of particle shape, surface topography, surface/internal structure and internal voids.

The particle size distribution (PSD) of each powder was obtained from scanning electron microscopy (SEM) investigations. A size population sample was measured and using probability statistics (through the computer program EGRAPH, produced by Great Basin Associates) the distribution type i.e. whether normal or log-normal, was calculated. The EGRAPH program allows the imposition of the Pearson Type III distribution on the (non-normal) distribution arising from the Wiebull probability statistics. The (log-) Pearson Type III distribution can be applied to the y data as a measure of the fit to a (log-) normal distribution, with zero skew representing a true (log-) normal distribution. All calculated size distributions quoted were obtained by this procedure.

In this study a single sized distribution is taken as a distribution possessing only one size fraction irrespective of the size range. This type of distribution is representative of monosized powders, although commercially available powders tend to possess narrow PSD's. A double sized distribution powder is taken as a powder possessing

two distinct powder size fractions. These are representative of bimodal powders and were produced by the mechanical mixing of two sizes together.

The SEM investigation of the powders, as well as providing particle size data and qualitative analysis of the particle surface texture, also allows for the measurement of the powder grain size. The powder was cold mounted, polished and etched (and carbon coated if required for contrast or electrical conductivity) and the grain boundary size was calculated from the line-intersection technique i.e. the number of grain boundaries to intersect a unit length.

2.2 Containerisation

The use of powder metallurgy compacts formed by containerised hot isostatic pressing (HIP) allows the opportunity to study the effect of particle size distribution (PSD) on densification. By investigation of the density attained and the possible densification mechanisms involved, the experimental results can be compared with the theoretical model.

The metal powder under investigation was containerised in a sealed metallic preform prior to HIP. The container design was of a simple cylindrical preform (of varying aspect ratios) with welded ends, manufactured from grade 316 stainless steel. The initial dimensions of the can were an internal tube diameter of 10 mm with a depth of 10 mm and a wall thickness of 1.5 mm. The container was progressively filled with powder (mechanically agitated to give a maximum tap density) until a predetermined volume was reached. This determined the initial packing density figure. The filled preform was then outgassed (to soft vacuum) via an integral evacuation tube (subsequently crimped and welded) prior to the HIP process. For some preform designs an additional welding procedure was needed prior to outgassing. Figure 41 shows the three main types of preform used.

Throughout these tests the process conditions were chosen through the Ashby HIP487 program.

The use of containerisation for powder metallurgy components requires post-HIP machining, to remove the can, and finishing. The diffusion of elemental species between the can and the powder was investigated using Astroloy powder contained within a stainless steel can.

To gain a data base of reliable results from such HIP tests (i.e. to limit the intrusion of the weld seams on the true internal densification of the powder) it was considered necessary to increase the overall length of the can. The central portion could then be analyzed with regard to porosity without effects from sample ends.

The use of hot-outgassing the container prior to sealing, to reduce the level of entrapped gas within the container, was also investigated. Any residual gas can inhibit

densification and contribute to impurity levels. Hot-outgassing involved holding the filled container at 300 °C whilst under soft vacuum for 15 minutes prior to sealing.

In order to create more pressure/temperature results at a constant pressure per HIP run it was decided to disable the bottom heater in the furnace. This produced a temperature gradient within the work zone, measured by the top and bottom thermocouples. By investigation of the inter-diffusion at the coating/nickel interface of a pack aluminised nickel rod the gradient was found to be linear.[164] The work zone, experiencing a temperature gradient at a constant pressure, would lead to a density distribution throughout the powder compact if the temperature range was appropriate. To take maximum advantage of the variation of this fundamental processing parameter, the can length was increased to 150 mm (the maximum the work zone could accommodate) and the wall thickness reduced to 1 mm (to limit can effects). The degree of the temperature gradient was dependent on the applied pressure.

3. Hot Isostatic Pressing

The equipment used for the hot isostatic pressing (HIP) process was the Superhipper (see figure 42) produced by VG Systems Ltd. This particular process module was capable of pressure variation from soft vacuum up to 200 MPa and temperatures up to 2000 °C. All HIP cycles utilised argon as the pressure transmitting medium and where necessary, for purposes of protecting the heating elements, the compacts were placed in a graphite or ceramic container. The graphite furnace consisted of a radial and a base heating element. The base element could be disabled to produce a temperature gradient within the heating zone.

The microprocessor controlled parameters of pressure, temperature and time enabled run cycles to consist of numerous stages. The most common form of cycle consisted of: taking the system down to soft vacuum; ramping up the pressure and temperature over a given time; operating the system at said pressure and temperature for a given time and; ramping down to soft vacuum and ambient temperature over a given time. The initial purging of the system was to remove any water vapour to limit carburization. The pressure transmitting gas, in this case argon, must be delivered at high purity levels to reduce contaminants. Variations such as altering the ramp rates (more specifically rapid cooling rates), lagging the pressure behind the temperature (particularly for large work-pieces) and including thermal and pressure 'spikes' in the cycle could also be used. For a sinter-HIP cycle the compact is sintered under soft vacuum prior to the application of pressure (not necessarily at the same temperature) without the need to remove the compact from the work-zone.

4. Coating Procedure

To investigate coatings as in-situ envelopes for HIP, the powder (as substrate) must possess a sufficiently high strength to permit coating by the chosen processing route.

A cold compaction process and subsequent sintering step was used.

4.1 Powder Compaction

Spherical powders do not lend well to cold compaction so a binder was introduced to allow greater particle rearrangement during the compaction process. The binder used was a 3% solution in distilled water of saturated poly-vinyl alcohol and poly-ethylene glycol in a 1:3 volume ratio. This was added to the powder in a 1:25 weight ratio of binder to powder.

Initially, the press was of a simple design to produce disc compacts (see figure 43). These were pressed at approximately 100 MPa with a dwell time of 10 s. Later studies to investigate the effectiveness of coatings required a more complex part geometry (see figure 44) producing a 'gear-wheel' type compact. Compaction was carried out on a Denison model T42C. These compacts were then air-dried in a desiccator prior to sintering.

The method of fixing applied to the compact depended on the coating route, and was either a wire through the compact, a rod welded onto the compact, or a jig.

4.2 Compact Sintering

The initial compacts were loose packed powder in an open container and sintered under vacuum at 1200 °C for 4 hours to provide green strength for handleability. Owing to diffusion bonding between the powder compact and the base, graphite paper was subsequently used as the base material. In some cases a nickel-chrome wire was also included into the container passing through the powder. This was subsequently used as a method of suspending the compact in the coating stage to obtain overall coating coverage.

The pressed compacts were sintering in an oxygen-reducing atmosphere of hydrogen or argon at temperatures of 800-1150 °C for 1-4 hours, depending on the compact structure required (i.e. the level of porosity). The use of sintering also allowed for the removal of the binder.

Powder compacts with a low level of internal porosity (but good handleability) were used for initial studies to assess coating structures as surface porosity was still high. Powder compacts with true interconnected porosity were used in later stages to assess the effectiveness of the coating system as an in-situ envelope, as the stresses developed throughout the compact during HIP would be greater.

4.3 Coating Systems

The coating systems of nickel (Ni) and copper (Cu) were chosen to provide in-situ envelopes by two distinct routes, namely the Ni coating providing a fully dense

barrier prior to a HIP cycle, and the Ni or Cu coating providing a barrier capable of defect-healing through a sinter-HIP cycle.

The deposition of coatings onto the powder metallurgy compact (i.e. the substrate) was undertaken using three different coating units depending on the evaporant and/or the type of coating structure required.

In the Edwards 19E2 PVD coating unit (see figure 45) the evaporant is melted by use of a resistance source. For the deposition of nickel onto the substrate a wire helical source was used, loaded with nickel staples. For the deposition of copper a dimpled foil source was loaded with copper wire. Both types of resistance source used were tungsten. The substrate was suspended above the evaporant at a distance of 15cm by use of a rod attachment or jig. The substrate was rotated to deposit on the opposite face. With the Edwards at a vacuum of 10^{-2} Pa the chamber could be back-filled with argon gas up to a pressure of 1-10 Pa. This was used to lower the mean free path of the vapour source to provide a high localised level of deposition onto the substrate (particularly onto the substrate edges). The deposition rate was dependent on the power input to the resistance source and the chamber pressure.

This coating unit was used to deposit a thin film/multi-film coating onto the substrate that could be act as an in-situ envelope either as-deposited in a HIP cycle or after sintering in a sinter-HIP cycle.

The Electrotech SL10-20 (see figure 46) is an electron beam physical vapour deposition (PVD) unit which was used in the initial studies of nickel deposition onto sintered compacts. The nickel evaporant source used was commercial purity pellets held in a crucible in a cooling jacket. Under vacuum the vapour generated by electron beam heating is deposited onto the substrate. As PVD is a line-of-sight process the distance of the substrate from the evaporant source will determine the deposition rate, as well as the power input generating superheat in the molten pool. The temperature of the substrate will also affect the structure of the coating. The compacts were held above the evaporant source using a wire attachment.

The Electrotech unit was operated under a vacuum of 10^{-2}-10^{-3} Pa at 7.5 kV beam voltage and 5 A beam current for 3 hours with the substrate at a distance of 15 cm from the evaporant. The substrate was then rotated to deposit onto the opposite face. Preliminary studies, using a glass slide (with a thermocouple attachment) as the substrate and subsequent 'Talystep' investigation of the coating produced, showed that such a configuration would produce a deposition rate in excess of 10 μm/hour and the substrate temperature would not exceed 200 °C. Plasma cleaning was also used in some cases (conditions of 800 V, 0.25 A glow discharge parameters for 15 mins.) to prepare the substrate surface prior to the deposition process.

The coatings produced were examined to determine subsequent possible processing routes i.e. to determine if a sinter-HIP process or HIP process only needed to be used

for component fabrication, depending on the coating structure.

The Cranfield Ion Plating System (see figure 47) allowed the use of PVD of a nickel source (a continuous rod held in a water cooled copper hearth) whilst the substrate was held within a plasma. Several low level porosity compacts were fitted with a rod (screwed into the compact and welded) to produce a 'lollipop' shape compact. This enabled these compacts to be held over the nickel evaporant source in the Cranfield ion-plating unit whilst immersed in a plasma. The operating conditions were a lower chamber pressure of 3.6×10^{-4} Pa, up to 6 kW radio frequency power and the electron beam gun at up to 10 kW power for 1.5 hours. To vary the substrate temperature the substrate could be positioned relative to the source (i.e. either directly over the source or to the side) and was measured using optical pyrometry.

This coating unit was used to deposit a thick coating that could fulfil the role as an in-situ envelope without any pre-treatment before the HIP process.

The evaporant source, when in the form of staples, pellets or wire, required a cleaning procedure to ensure low contamination levels. This involved ultra-sonic cleaning of the source in inhibited 1,1,1-tetrachloroethane as a degreaser and iso-propan-2-ol as a dehydrator.

4.4 Coating/Substrate Alloy System

For the study of a sinter-hot isostatic pressing processing route the coating/substrate alloy systems chosen were nickel overlay coating and copper overlay coating on nickel substrate.

A nickel overlay coating was chosen as this would provide the simplest system giving no mis-match problems in terms of thermal and mechanical properties. If a coating is to provide an in-situ envelope to be retained on the finished article it can be of the form of like material to the substrate or to form an alloy system on the article surface.

A copper overlay coating can produce a simple binary alloy system with a nickel substrate. The nickel-copper phase diagram[165] (see figure 48) indicates the continuous phase present in all possible alloys of nickel and copper at all temperatures from 500 °C to 1500 °C. The liquidus curve denotes the temperature at which freezing begins during cooling or at which melting is completed upon heating. The solidus curve indicates the temperature at which melting begins upon heating or at which freezing is completed upon cooling.

The variation of the diffusivity of copper for the copper-nickel system at 1052 °C has been shown by Darken and Gurry.[166] The continuous series of solid solutions exhibit a tenfold variation in diffusivity.

5. Metallurgical Techniques

The sample to be investigated would (normally) be cut up by an electrical discharge machine (EDM) prior to mounting in either Bakelite (for the containerised samples) or cold-mounting resin (for the coated samples). The sample would then be polished down to 0.25 μm using diamond paste and, if necessary, down to 0.1 μm using alumina powder.

For this study two main etchants were used, namely Vilella's reagent (distilled water 10 ml, nitric acid 38 ml and glacial acetic acid 100 ml) to highlight grain boundaries and Marble's reagent (cupric sulphate 10 g, hydrochloric acid 50 ml and distilled water 50 ml) to reveal structure.

Optical microscopy was then used to investigate the compact structure and/or the coating integrity.

The scanning electron microscope (SEM) was used when qualitative and quantitative analysis of the sample was needed. Using the Link 860 Series 2 hardware quantitative analysis was performed through the ZAF4 program. Digipoint analysis and elemental distribution maps were also performed. Whilst the containerised samples would be mounted in conductive Bakelite the cold-mounted samples required carbon-coating prior to SEM inspection.

6. Density Measurement

For the sintered powder metallurgy (PM) compacts prepared for subsequent coating processing an open porosity structure was required. With this interconnected porosity the compact could be outgassed whilst the overlay coating was deposited. With the containerised PM compacts prepared for subsequent hot isostatic pressing (HIP) the level of (usually closed) porosity indicates the effectiveness of the processing parameters and variables. Any porosity within the final product generally leads to a lowering of mechanical properties.

6.1 Archimedes Principle

The Archimedes principle can be used to measure the density of a test piece and can also lead to a measurement of the level of open porosity[167] by forcing water into the pores using capillary action when the sample is boiled in water. The typical procedure make this method particularly suited to test pieces containing high levels of porosity.

The accuracy of this method depends to a large extent on the size of the test piece (the smaller the piece the larger the level of errors possible when measuring the level of porosity). This method was primarily used for samples with a high level of porosity.

6.2 Image Analysis

For test pieces with only closed porosity the image analysis system was used to determine the level of porosity by way of investigation of polished sections.

Using the Mini-Magiscan/IAS25/IV25 image analysis system the level of porosity from a polished section can be obtained and statistically analyzed, through the GENIAS and RESULTS programs.[168] The principal stages in image analysis (see figure 50) can be considered as:[169] (i) image capture, (ii) segmentation, (iii) object detection, (iv) measuring and (v) analysis.

The measurements primarily used through GENIAS were field area (of the object) and detected area (taking account of porosity within the object). The object image was captured from an optical microscope stage via a video camera and was then quantised spatially (into pixels) and by energy content (into grey levels).

The apparent contrast must be kept constant (i.e. by suitable microscope iris settings) or this can lead to effects on the measurement of objects, particularly small particles. Similarly, the threshold setting in the segmentation of data must be set correctly to make the width of binary objects equal to the width of objects in the grey image.

The RESULTS program was used to analyse the field and object measurements from GENIAS using a statistical package.

Samples prepared for image analysis needed careful polishing to ensure no smearing or removal of pore edges.

The two methods of density measurement showed good correlation, particularly at high levels of porosity.

RESULTS AND DISCUSSION

1. Presentation of Results

It is convenient in this study to present firstly the common section involving the powder characteristics, followed by the analysis of the Ashby HIP487 program and the modified HIP792 program (together with relevant comparisons). The containerised hot isostatic pressing (HIP) trials will then be presented along with the corresponding HIP792 program map. The use of overlay coatings on powder compacts to form in-situ envelopes to overcome/limit the shortcomings of canning technology will then be presented.

2. Powder Characteristics

Table 5 shows the main types of powder used. The APA2 nickel powder was used both in its as-received state and as sieved fractions to produce bimodal distributions.

Powder	PSD (dia. μm)	Dist.	Dist. Type	Surface Details
APA2 (virgin)	up to 250 nominal	single	-	smooth spherical
APA2l (<N30 mesh)	3-22	single	normal	-
APA2m (N30-N56 mesh)	10-100	single	normal	-
APA2h (N56-N80 mesh)	20-120	single	normal	-
Ni123*	1-6	single	normal	satellite spherical
Ni123/ APA2m*	-	double 50:50 wt%	-	-
Ni123/ APA2h*	-	double 50:50 wt%	-	-
Goodfellow*	3-7	single	normal	smooth spherical
PY114L*	5-75	single	log-normal	smooth spherical

Table 5. Types and Characteristics of Powder Used.

Powders marked '*' are used later in containerisation trials.

The particle size distribution (PSD) is measured from SEM analysis. The powder distribution type is analysed statistically from SEM data.

Figures 51, 52 and 53 show several powders, both as-received and sieved, as SEM photographs illustrating powder surface and size characteristics and the calculated particle size distributions. As can be seen in figure 52 the PY114L powder has some inherent bimodal characteristics, but for this study will be discussed as a single distribution powder. A log-normal distribution assignation gives the best fit.

The Ashby model, as well as requiring the particle size, also uses the grain size in the rate equations. The grain size was measured by considering particles that approximate to the calculated mean size (see table 6).

Powder	Grain Size (μm)	PSD (dia. μm)
APA2m	8	10-100
APA2h	8	20-120
Ni123	1	1-6
Goodfellow	1	3-7
PY114L	1.5	5-75

Table 6. Grain Size Measurements from the SEM Investigations of Various Powder Types.

The grain size appeared constant irrespective of the individual particle size, with the smallest particles comprising of individual (or few) grains. It was also observed (see, for example, figure 54) that with the larger particles there was evidence of gas entrapment from the manufacturing route. Argon entrapment within the powder compact during processing has been shown to lead to the detriment of mechanical properties.[170]

As densification proceeds for a containerised metal powder compact any gas present will be trapped when the pores close off. The pressure from the gas will increase as the pore closes until it eventually equals the applied pressure and hence halts densification. Incomplete out-gassing will have a negligible effect on the level of densification (assuming the external pressure greatly exceeds the internal pressure). However, argon entrapment within components has been observed to lead to thermally induced porosity upon high temperature operation of the component.[171]

Prior particle boundaries (PPB) have been shown to lead to be detrimental to

mechanical properties.[172,173] These PPB's are the result of oxide contamination on the particle surface which inhibit diffusion. The process conditions can be altered towards deformation mechanisms to favour power-law creep in an attempt to break up the formation of PPB's.

3. Modifications to the Ashby Deformation-Mechanism Maps

The Ashby deformation-mechanism map program HIP487[118] constructs maps based on experimental data fitted to model-based rate-equations. The maps show time driven events against constant pressure or temperature with mechanism field boundaries showing the dominant mechanism (that which contributes most to the total rate of densification).

These maps were used in the design of experimental parameters for the hot isostatic pressing (HIP) process and as guidelines for the identification of the mechanism by which a powder component may densify.

The material property data used throughout this study for the modelling work is based on that compiled by Ashby.[118] The particle radius was taken as the mean obtained from the powder distribution and the grain size from metallographic observations. The packing density was that taken from metallographic observations for cold pressed compacts (using a high viscosity glue) or directly from the packing procedure for containerised powder (using the known mass).

3.1 The HIP792 Program

The Ashby model should only be used as a first approximation to the deformation mechanisms involved in a sinter or HIP cycle owing to inherent assumptions in the models and rate-equations. It was felt that one simple area where the model could be made more true to life is in the prediction of the effect of the particle size. The aim of the modifications to the HIP487 program (i.e. the HIP792 program) was to present the maps in a more easily read form and to study the effect of particle radius and size distribution on the rate of densification (i.e. the size dependence of the mechanisms).

An initial study into the incorporation of a bimodal size distribution is also presented.

Changes were made to the program in the areas of: (i) the graphics, (ii) the menu system, (iii) the operating system requirements, (iv) the inclusion of experimental data alongside the map data, (v) the particle size (creating a monosized distribution) and (vi) the inclusion of bimodal powders.

(i) Program Graphics

The original system of graph plotting was based on the IBM CGA standard which

only allowed resolutions of 320x200 pixels. The plotting sections of the program were reprogrammed to use the IBM EGA standard, giving a resolution of 640x350 pixels. The EGA standard was also utilised by the colour and line type of the boundaries, time contours and experimental data (see later for examples) to aid analysis of the plot.

The graphics can be downloaded onto a high quality printer using a screen-dump program, to aid analysis as well as presentation.

(ii) The Menu System

The menu system of the original program was not flexible enough to allow changes to be made without traversing the whole menu structure. A menu bar was formulated to allow the user to make more efficient use of the program and to speed up simulation. The menu structure now is as follows:-

File		
	Load	-load variable and parameter sets
	Save	-save variable and parameter sets
	Create	-create new variable and parameter sets
Print		-print variables and parameters
Edit		
	Exp Data	-edit experimental data
	Parameters	-edit parameters
	Variables	-edit variables
Plot		
	Pressure	-plot a pressure map
	Temperature	-plot a temperature map
	Normal	-normal distribution
	Log Normal	-log normal distribution

(iii) The Operating System

The program was designed to run on a 8086 PC fitted with an 8087 maths co-processor. The HIP792 program allows the user to operate the program without the need for a co-processor, which is no longer necessary as the processing speed of modern PC's has greatly increased. The inclusion of experimental data on the plot significantly increases the run time.

(iv) Experimental Data

A menu option was installed to allow the user to enter experimental data to a simulation. A least-squares method of curve fitting was used to calculate the curve drawn on the plot. The program allows the inclusion of up to six density data points along with the corresponding pressure/temperature data. Each experimental data point

allows for the plotting of error bars. The x-axis error bar should not be used on the density-pressure map as the scale is log.

(v) Creating a Particle Size Distribution (PSD)

The original Ashby model provides a good first approximation for monosized spherical powders as it contains the implicit assumption that the particles are all of the same size. Plasticity and creep mechanisms are not affected by a range of powder sizes but will be affected by the initial packing density. However, the PSD of a powder will affect the local hydrostatic pressure. Diffusion mechanisms are particle size dependent as local hydrostatic tensions are generated, tending to cancel the external pressure and hence slow the local sintering rate. Ashby[121] states that the different rate equations depend on the size of particles, leading to an effective radius for boundary and lattice diffusion. These effective radii can be calculated as:

$$\text{boundary diffusion } \acute{R}_{eff} = \sqrt[3]{\Sigma(f_i R_i^3)}$$

$$\text{lattice diffusion } \acute{R}_{eff} = \sqrt[2]{\Sigma(f_i R_i^2)}$$

where f_i is the (volume) fraction of particles of radius R_i.

A mixture of 50:50 weight percent of particles of size R and 2R gives an $\acute{R}_{eff}$ of 1.65R for boundary diffusion and 1.58R for volume diffusion. Hence, it is apparent from these effective radii that densification will tend to be preferentially dominated by the larger particles in a bimodal mixture.

Commercial powders are supplied by quoting the mesh size numbers i.e. if a powder has a quoted size distribution between two mesh sizes the tolerance of the particle size is such that only 5% weight is allowed to be both above the large mesh and below the small mesh. Thus, by specifying the minimum and maximum particle radii, and with the knowledge that most powders have a normal distribution, the PSD of the powder can be specified without further investigation.

Any anomalies with the PSD of the powder, either with spurious particles above or below the specified PSD, will result in localised density variations through variations in the local hydrostatic pressure. The inclusion of a PSD is aimed at improving the approximation of a single particle radius to represent the powder, and as such will inherently be more tolerant to variations in particle size.

The user enters the minimum and maximum particle radii of the PSD (see below) and chooses a normal or log-normal distribution. The range is then divided into a hundred elements and the mean radius and the effective radii are calculated. The effective radii are used in the rate equations for boundary and lattice diffusion with the mean size used by the plasticity and creep mechanisms.

(vi) The Inclusion of Bimodal Particle Distributions

As an initial investigation into modelling a bimodal distribution it was proposed that this distribution may simply be represented by a distribution calculated from the mean radius and effective radii from the bimodal components. The user enters the minimum and maximum radii for each of the bimodal components together with the weight percent ratio of the mix. (All these values must be input even for monosized distributions - by setting the weigh percent value to 100% for one of the distributions will effectively consider that distribution as monosized). The radii are then calculated separately. The effective radii produced for each size are then used again in the boundary and lattice diffusion effective radii equations with the mixture ratio used as f_i. These new effective radii are used in the boundary and lattice diffusion rate equations. The new mean radius is determined from the two means and the mixture ratio.

The weight percent value is a simple measure of the bimodal mixture ratio. This figure could obviously be used as a weighting function once experimental data has illustrated the densification dependence on the mixture ratios.

When a plot is requested the following procedure is performed to calculate the effective radii:-

* take normal/logarithmic of particle radius maximum/minimum
* calculate mean
* calculate standard deviation
* for each radii in range -
    * calculate the fraction of particles in the sample
    * calculate $\acute{R}_{eff}$ for boundary diffusion and lattice diffusion

An example of a session might be that the user selects the file menu, then the load menu, and is prompted for a file name. Once a data file has been selected (or created), the experimental data (including the particle sizes) will then be input together with any necessary alterations to the variables and parameters. The user can then print the data set if required and then select the plot option. The map type can then be selected, followed by the distribution type. Plots can be printed using a screen-dump program. The menu structure can be traversed as required.

The code listings for the various modifications (except purely cosmetic changes) can be found in appendix A.

3.2 The Significance of a Particle Size Distribution

The particle size distribution (PSD) will effect the densification behaviour not only by its influence on the packing density but also by setting new effective radii for the diffusional mechanisms. The diffusion coefficient, D, is related to temperature, T, by the expression

$$D = D_0 e^{(-E/RT)}$$

where D_0 is the pre-exponential term for the diffusion mechanism, E is the activation energy for the diffusion mechanism and R is the gas constant.

By consideration of the activation energies given in the parameter data set,[118] the dominance of the activation energies for volume, boundary and surface diffusion with temperature can be observed (figure 55). For these data the rates of reaction for volume diffusion and boundary diffusion cross at approximately 800 K. The surface diffusion rate is lower at all temperatures. Hence, below 800 K boundary diffusion dominates and above this temperature volume diffusion dominates, with surface diffusion having negligible effect. In the Ashby model the pre-exponential term and activation energy for surface diffusion are used only to calculate a redistribution factor. If the particle size is comparable to the internal grain size, in the early stages of densification surface diffusion will be dominant at low temperatures, with volume diffusion dominant at high temperatures. In the later stages boundary diffusion will dominate at low temperature, with volume diffusion still dominating at high temperatures. The move towards boundary diffusion from surface diffusion will be due to the increased contact areas between neighbouring particles, forming grain boundaries. If the grain size is considerably less than the particle size, then boundary diffusion within the particle will dominate as opposed to surface diffusion, as the characteristic of the system has now changed from a free surface model to a high angle grain boundary model. At high temperatures volume diffusion will dominate.

The dominance of surface diffusion is clearly limited, and as such the role of the PSD will be dependent on the relationship between the particle size and the grain boundary size. The PSD will become more important as the grain size approaches the particle size. As such the pre-exponential and activation energy for the diffusion mechanism will be dependent on the particle and grain size.

For a bimodal mix of powders, the smaller particles will tend to have an increased grain boundary area as well as an increased surface area. However, the model assumes the densification to be dominated by the larger particles, as suggested by the effective radii.

3.3 Comparison of Original HIP487 and HIP792 Programs

The base-line data used for all data sets are based on those compiled by Ashby.[118] These are generally from bulk property data and as such are not necessarily characteristic of the powder particle properties. The aim of this section is to demonstrate the usefulness of incorporating the particle size distribution (PSD) and distribution type into the existing model. The data set may or may not require 'tuning' to describe the material accurately, by such means as experimental observation.

Ashby[118] considered maps for copper and type 304 stainless steel. By plotting experimental data points on the relevant map the discrepancy between the time contour and the data and the dominant deformation mechanism can highlight the area of data set inaccuracy.

The data base for copper quoted by Ashby is shown plotted as a HIP487 map in figure 56, together with the relevant experimental data. The data set, i.e. the input parameters and input variables, are also shown. When the same data set is run through HIP792, both with a normal and a log-normal powder distribution, no appreciable difference is calculated (see figure 57). This can be attributed to the very narrow PSD of the copper powder and shows that, under these conditions, HIP792 predicts similar densification behaviour as HIP487. In this case the predicted times are too short but a better fit can be obtained by increasing the particle radius. Decreasing the volume diffusion pre-exponential was resisted as other experimental data (from a private communication to Ashby) suggested that the data set gave a satisfactory description of the system. The powder compact has failed to reach theoretical density as there is a limiting density which can be reached by pressureless sintering with entrapped gas within the pores.

The data for type 304 stainless steel[174] was used to highlight the development of deformation maps for more complex alloys. The HIP487 map with the experimental data is shown in figure 58. The corresponding HIP792 maps are shown in figure 59. It can be seen that by considering a powder distribution there is movement of the time contours, indicating that the dominance of the mechanism fields are altered. The assumption of a normal powder distribution gives lower predicted time contours for the experimental data, whereas the log-normal distribution more closely matches the HIP487 map. It was reported that the sintering rate was controlled by volume diffusion and, from the experimental data, the program predicted times are too low. By consideration of the rates of reaction for the diffusion mechanisms (figure 60) the dominant mechanism over the temperature range is volume diffusion. Ashby concluded that the experimental particle size data was incorrect as it assumes the mean particle size on the basis of volume average (i.e. the assumed radius is too large) and that boundary diffusion data (reliant on the particle size) is the least reliable of all the material parameters. To achieve agreement with both mechanism and rate, Ashby tailors the data file by reducing the contribution of boundary diffusion and the particle radius.

It can be seen that although the differences between the two programs is not always greatly appreciable the introduction of the powder PSD can result in a shifting of the dominant mechanism region and hence the calculated time contours. By consideration of the powder PSD a more realistic first approximation of the densification behaviour can be obtained.

4. Containerised Powder Compacts

The material chosen for the investigation was commercial purity nickel of various size fractions and PSD's.

The problem of diffusion bonding between the can and powder was investigated using a nickel superalloy contained in a stainless steel can, and processing at a typical manufacturing HIP cycle. Using spot analysis on the scanning electron microscope (see figure 61) it can be observed that there was diffusional transport of species across the powder/can interface (up to a depth of 60 μm). Some species, such as cobalt, follow the typical normal penetration curve seen across a Matano interface. Others, such as such as chrome, appear to follow the nonuniform distribution observed by Darken.[166] This diffusion could be disrupted by a suitable barrier between the powder and can, such as boron nitride. For the tests involving nickel powder there was no significant diffusion bonding between the powder and the can, and no extensive machining processes were needed.

4.1 The Influence of the Can Geometry

The effect of can deformation under a HIP cycle being strongly influenced by the container design (i.e. the inherent strength at the welding seams) was observed at HIP cycles of both high temperature (at 1250 °C and 85 MPa for 1 hour) and high pressure (at 200 MPa and 750 °C for 1 hour). Any modelling work should be aware of the influence of the canning design on the subsequent densification behaviour of the powder compact. The effect of the length of can was investigated to show the densification dependence on the proximity of a welding seam.

Tests were undertaken with HIP runs of 750 °C at 200 MPa for 60 minutes with the can lengths of 20 mm and 30 mm. As can be seen in figure 62, there is no significant microstructural difference, with the porosity level for both cans being 0.2-0.3 %. The can deformation however was more uniform over the central portion of the longer can and this design was used in all subsequent trials.

4.2 The Temperature and Pressure Dependence of Densification

Tests were performed to determine the effect of varying the temperature and pressure variables independently (with time held as a constant at 1 hour). The series of HIP cycles is shown in table 7.

Figure 63 shows the variation in density as a function of processing temperature, illustrating a near linear dependence over these conditions. The microstructural development is illustrated in figures 64(a)-(c), together with the grain growth as a function of temperature (see figure 64(d)). An increase in the processing temperature results in a decrease in porosity levels and a corresponding increase in grain size. At 400 °C there is still some evidence of powder particle boundaries but by 550 °C there

HIP run no.	Temp. °C	Press. MPa
84	400	150
90	450	150
92	475	150
93	550	150
85	750	30
86	750	50
87	750	60
88	750	70
89	750	90

Table 7. HIP Run Series for Varying Temperature or Pressure Parameters (using Ni123 Powder).

is considerable grain growth. The HIP792 map for these processing parameters is shown in figure 65. The experimental data fits the slope of the time contour (i.e. the densification rate) well, and to within approximately 100 °C. It calculates the dominant mechanisms to be either Nabarro-Herring creep (at the low temperatures) or final stage boundary diffusion (at the higher temperatures). These mechanisms can be supported by the observed microstructures.

In figure 66 the variation in density is shown as a function of pressure. The microstructure over the pressure range (see figures 67(a)-(c)) shows large grain growth development. The corresponding HIP792 map, see figure 68, whilst calculating the dominance of densification to be by diffusional mechanisms, is approximately an order of magnitude out in the predicted pressure from the experimental data.

It can be concluded that the HIP792 map for this system calculates the rate of densification and the dominant mechanism to close agreement with the experimental data when considering density as a function of temperature. However, the pressure map deviates somewhat from the experimental pressure but gives good agreement with the rate of densification.

4.3 The Effect of a Temperature Gradient

By establishing a temperature gradient within the work zone the number of temperature results at constant pressure can be increased. A long can design was compared with the existing design through a series of HIP runs (see table 8).

HIP run no.	Temp. °C	Press. MPa
166	750	200
170	750	150
208	1120	-0.1
185	1120	100
200	1120	1
207	1120	-0.1

Table 8. HIP Run Series (all 1 hour) to Determine the Effect of the Furnace Bottom Element Disablement.

There was very good agreement of the final compact density between the two can designs and with no substantial microstructural changes. The longer can also proved to be less prone to container failure and was used in all subsequent trials.

4.4 The Effect of a Particle Size Distribution

The long design cans were filled with the five main powders listed in table 4. A series of HIP runs was used to compare the experimental results of the single sized and double sized distribution powders to theoretical predictions (see table 9).

HIP run no.	Temp.Range °C	Press. MPa
281	710-740	30
282	740-780	40
283	390-465	150
284	295-340	150
288	1095-1100	20
290	390-450	200
295	1095-1100	10
303	290-335	200
356	730-830	30

Table 9. HIP Run Series using Single Sized and Double Sized Type Powders (all for 1 hour).

Figure 69 illustrates the deformation of the filled cans following the effects of a HIP cycle.

It was noticeable in the HIP runs that the can shape had a marked influence on the densification of the powder, with the welding seams providing a fulcrum around which the can deformed. This clearly leads to non-uniform shrinkage of the powder compact and can result in density distributions. It should be noted that the Ashby model has no facility to take account of canning effects and assumes no hinderance to the application of pressure and temperature. The can was also prone to occasional failure due to a fault in the welding seam.

4.4.1 Single Sized Distribution Powders

4.4.1.1 Ni123 Powder

Owing to the choice of temperature and pressure parameters to cover all powder sizes the Ni123 powder achieved full density (i.e. greater than 99% of theoretical density) in all the HIP runs. However, it can be observed that all the low pressure cycles (i.e. those at 100 MPa or less), irrespective of temperature, resulted in the experimental data to the right of the respective time contour (see, for example, figure 70) i.e. all demonstrating density levels as high as those theoretically predicted. The high pressure cycles, all at low temperatures, resulted in data to the left of the time contour (see, for example, figure 71) i.e. all demonstrating full density achieved earlier than that theoretically predicted.

For both the low and high conditions the retained microstructure was very fine (in the order of several microns) and homogeneous, showing low levels of grain growth. The original particle sites can not be distinguished in the matrix. The HIP792 program calculates the dominance of boundary diffusion from the neck region, consistent with low grain growth.

Although no conclusion can be drawn from the results for the low pressure cycles, other than the powder compacts are fully densified as can be expected, the high pressure cycles data points to a deviation from the theoretical results. By achieving full density before that theoretically predicted the data suggests either the data set is inaccurate and/or that processing parameters, such as heat-up time, need to be incorporated and/or the model is flawed. The container does not appear to have a significant effect on the powder densification in this system.

To simulate the effect of heat-up time on the final density the HIP792 program was run in increments of temperature and pressure, with the resulting density put back into the program as the starting density. Unfortunately, the program will not except starting densities in excess of 80% theoretical density but initial increments suggested little difference in the final time contour (see figure 72).

4.4.1.2 Goodfellow Powder

It can be observed that the data for HIP runs at low pressure (irrespective of temperature) are to the right of the time contour whilst the data for the high pressure cycles again show densities to the left of the time contour (see, for example, figures 73 and 74). This is consistent with the results for the Ni123 powder although the deviation from the predicted time contour is somewhat more pronounced. As a density range can be seen in both cases it would tend to suggest that the data set is incorrect or the principles of the model are flawed.

The microstructure was again fine and homogeneous for both low and high pressure cycles, exhibiting little grain growth although creep and diffusional mechanisms are calculated to be dominant.

4.4.1.3 PY114L Powder

The results for the PY114L powder are all for the low pressure cycles and the data used is for pure nickel. It can be seen that the experimental data shows good agreement with the theoretical time contour (figure 75). This would suggest that the data set and model are a good representation of the system but a wider selection of processing parameters is required to fully test the model.

Prior particle boundaries are still visible at these processing conditions, mirroring the calculated densification mechanism of Nabarro-Herring creep.

4.4.2 Double Sized Distribution Powders

4.4.2.1 Ni123/APA2m and Ni123/APA2h Powders

The problem of incorporating a bimodal distribution has been dealt with by the consideration of the constitutive parts. However, with powders of widely varying PSD's the problem of individual powder parameters, such as the grain size, become apparent. Figures 76 and 77 show typical HIP runs using cans filled with Ni123/APA2m and Ni123/APA2h bimodal powder respectively, with the grain size held at 1 μm (representative of the Ni123 powder) and 8 μm (representative of the APA2m/APA2h powder).

Taking the grain size as the lowest value gives a good fit to the predicted time contour at full density at low pressures. In the bimodal case there is no dependence on the processing parameters in the fit of the experimental data to the predicted time contour. However, there is insufficient range in the data to allow comparison with the rate (i.e. the slope of the contour) of densification. For all the HIP cycles the resultant experimental data for the larger grain size is invariably to the left of the theoretical time contour i.e. the data shows a higher obtained density. The limiting grain size would be expected to be the larger of the two, as suggested by the

densification dependence on the larger particle. This would suggest that the influence of a the smaller particle size in a bimodal mixture is greater than expected (assuming the data set is accurate).

It can also be seen that the choice of the grain size affects the calculated fields of dominance of the deformation mechanisms. The prior particle boundaries of the larger particles can still clearly be seen, suggesting little plastic deformation or power-law creep, but the interstitial smaller particles have undergone extensive deformation. Clearly the two size powders are not deforming by the same mechanisms.

By consideration of a high pressure HIP cycle (figure 78) the predicted time contour is now overestimating the time taken to reach full density in both grain size cases. The model clearly deviates from that experimentally obtained although the data distribution is representative of the rate of densification. This would suggest that high pressure cycles clearly influence the rate of densification for a bimodal mixture far greater than expected. This is probably due to the excessive 'squeezing' of the smaller particles between the larger ones upon the early stages of high pressure/temperature application. This will clearly lead to prior particle boundaries (PPB's) in the compact as the surfaces of the larger particles are relatively undeformed.

The deformation fields are again effected by the grain size.

5. PVD Coatings as In-Situ Envelopes

It has been shown that the modelling of containerised powder has many areas of possible error, from the role of the can itself to the basic assumptions of the model. To overcome the container effects and to present the powder with a less restricting environment during densification the use of coatings as in-situ envelopes was considered. These coatings could act as envelopes by either encasing the compact with a pore free coating (in effect a very thin walled can) or by self-healing the coating to alloy with the compact such that a pore free surface layer would be produced. This would offer the potential of a more uniform densification and hence a greater predictability of the final shape.

During this study the route of powder compact processing was dependent on the coating unit and the subsequent coating structure required.

5.1 Single Layer Evaporation Films

Sintered disc compacts of the nickel powder Ni123 were loaded in a jig into the Edwards coating unit to assess the performance of resistive PVD coatings as in-situ envelopes. Initial studies investigated the use of nickel (Ni) as the coating evaporant.

With 0.5 g of Ni loaded onto the resistive element the coating coverage on the compact surface was very low and of poor quality i.e. it did not provide an envelope.

To obtain a coating of higher structural integrity it was proposed to evaporate a thicker overlay coating. However, with 3 g of Ni loaded onto the resistive element the reactive nature of the Ni and W resulted in the premature failure of the element. The use of multi-layer deposition using a light evaporant loading was not considered feasible owing to the large level of consumables involved.

To investigate a thicker evaporation layer to seal the powder compact surface the Electrotech unit was used.

Initial studies concerning the production of sintered metal powder compacts involved the use of full particle size distributions i.e. virgin powder. The commercially pure Ni powder used was APA2, with a size distribution up to a quoted nominal 250 μm. The powder compacts would require porosity levels of approximately 10% to retain true open interconnected porosity whilst providing the compact with sufficient green strength for handleability.

The sintered powder compact retained a high degree of open porosity, attaining approximately 78-88% of theoretical density.

The Electrotech unit was used to produce a nickel coating structure of the porous columnar type preferentially grown on the particle surfaces, as shown in figure 79, with large defects over the surface porosity produced between neighbouring particles i.e. the powder surfaces offer favoured sites to the initial nucleation of the coating. Overall coverage showed little lateral growth of the coating, with shadowing effects on the growth morphology most pronounced on the side of the compact. The source facing surface generally received up to four times the deposition rate than the sides, which also suffered from oblique impingement of the evaporant. This type of coating structure is consistent with the zone 1 structure in the models[156,157] as regards deposition temperature/pressure. The introduction of the wire in the powder compact also led to a preferential site for coating structural weakness (figure 80) as the driving force during sintering tended to separate the compact from the wire. (To limit the influence of the wire on the coating integrity it is proposed that the wire diameter should be reduced).

The use of a plasma to ion clean the compacts prior to the coating process was not observed to influence the subsequent coating structure.

The influence of very rough surfaces is to promote the growth of open columnar structures. Each powder particle nucleates the growth of a new columnar grained structure within the coating. Where adjacent grains impinge, highly defective coatings may result, which would not fulfil the necessary requirements as an in-situ envelope for HIP. Hence, lateral growth of the coating should be encouraged. Unfortunately only one powder type was used and we can not quantify the influence of the powder size with the coating structure.

Clearly we have a process related problem involving the particle size and the coating coverage. The powder size has a marked effect on the growth of the coating, resulting in nucleation sites on individual particles producing a highly defective coating. The coating coverage must seal the powder compact or it will fail the requirement of an envelope. To overcome these problems the particle size distribution of the powder can be reduced to a finer and smaller fraction (to reduce surface defects by promoting a more continuous coating film formation) and to modify the coating structure such that the internal defect level would be reduced (by thicker films or multi-layer processes).

5.2 Single Layer Ion Plated Films

The 'lollipop' shape compact, using Ni123 powder, was used in the study of the deposition of Ni coatings in the Cranfield ion plating unit to promote a thick coating capable of overall coverage. This method of coating production also offered the opportunity to vary the substrate temperature, by varying the distance of the substrate from the source, and observing its dependence on the coating structure.

The compact coated with a substrate temperature of 400 °C resulted in a porous columnar structure with evidence of nucleation of the coating on individual powder particles (see figure 81a). The compact held at 650 °C however did produce a coating structure of high integrity of approximately 60 μm thickness and good edge coverage (see figure 81b). Overall coverage of the compacts was good with little variation in coating thickness. The higher deposition temperature has increased adatom mobility and encouraged lateral growth of the coating. The coating thickness on the 650 °C substrate was greater than that of the substrate held at 400 °C. Compacts were also produced with temperatures of 300 and 800 °C. Only one sample at each temperature was produced.

The powder compact coated at the higher temperature of 800 °C was assumed to possess a coating structure of higher integrity than that of the compact coated at 650 °C, consistent with the models[156,157] which indicate that higher substrate temperatures result in higher integrity coatings. Conversely, the coating deposited at a substrate temperature of 300 °C was assumed to possess a lower integrity than that at 400 °C. For a nickel compact with a nickel overlay coating the coating must possess no internal defects as the hot isostatic pressing (HIP) cycle will operate below the melting temperature of the metal. Hence, there is little opportunity for defect-healing of the coating prior to the onset of the HIP cycle.

The coated compacts (with the substrate held at 300 and 800 °C) were HIP'ed (on a bed of boron nitride powder to minimise interaction with the crucible) at 1200 °C at 110 MPa for 1 hour. It is expected that at these processing parameters full densification of the compact would be achieved. As can be seen (figure 82) the coating structure has failed to provide an effective envelope even at the higher deposition temperature. The compact at the lower deposition temperature may have permitted gas infusion prior to any defect-healing of the coating itself causing the

densification to slow/halt. For the higher temperature deposition compact it is suggested that the coating failure may emanate from the rod attachment process.

The use of a vacuum sintering step, in a sinter-HIP cycle, may be sufficient to heal a coating prior to the onset of the HIP cycle but would require the compact to be held at an elevated temperature for an unacceptable length of time. This would effect the inherently small grain size of the particles and hence alter the mechanical properties, and as such would be undesirable.

It is clear that to provide an effective envelope by means of an overlay coating has many process related problems. However, if the coating was able to self repair prior to the onset of the HIP cycle, such as in a sinter-HIP process, it would provide an effective pressure barrier.

5.3 A Sinter-HIP Process

A combined surface coating and sinter-HIP approach has the potential to overcome the defect limitations of the surface coating and permit reduced sinter-HIP cycle times. To provide an effective envelope for the subsequent HIP cycle the chosen surface coating material should produce a transient liquid phase during the vacuum sintering cycle to enable defect-healing of the coating. The nickel-copper (Ni-Cu) system was chosen to illustrate this process route as a continuous series of solid solutions is formed by this binary alloy system.

Initial tests, using the disc shaped compacts made from Ni123 powder, showed an evaporant loading (on a tungsten boat resistive element) of 0.5 g produced a very thin coating (in the order of 2-3 μm) that nucleated only on the particle surfaces (figure 83). 'Heavy' coatings, using 3 g of Cu wire on the resistive element, produced a porous columnar coating of the order of 15 μm (figure 84), with evidence of particle nucleation sites and shadowing effects. Edge coverage is very poor. The porous columnar structure of the coating is as expected at these processing conditions. To 'repair' the inherent defects in a coating of this nature it is necessary to either increase the amount of evaporant deposited or use multiple coating stages. A multi-coat procedure, with two runs per side, was then investigated. It is noticeable (figure 85) that the second coating has a better structural integrity than the underlying coating in direct contact with the powder compact surface. However, edge coverage was still poor, resulting from the line-of-sight nature of evaporation. As the resistive source could not accommodate any further increase of evaporant material a partial pressure of inert argon gas was introduced into the system to increase the overall coverage of the coating onto the substrate by reducing the mean-free path of the evaporant. Once the system was at the normal operating pressure the chamber was back-filled with argon gas up to a pressure of 1-10 Pa. The compact was again multi-coated to improve the integrity of the coating structure i.e. to defect-heal the columnar structure. With a two-coat stage (i.e. turning the compact face down to the evaporant source on four occasions) it can be seen that a coating of the order of 30 - 40 μm

capable of producing a near defect-free envelope was produced (see figure 86). The introduction of argon into the system has tended to 'bathe' the substrate in evaporant, rather than produce a line-of-sight deposition. It can be observed that the evaporant even succeeds in laying a thin coat on the face opposite to the evaporant source, at up to one fifth that of the surface facing the source. Overall coating coverage was consistent, with less variation in thickness from edge effects normally seen in resistive PVD coatings.

A more complex die configuration of the 'gear-wheel' design was then chosen to assess the dependence of the coating structure on the geometry of the compact. Using the same coating procedure it was found that the coating was still capable of producing a near defect-free envelope.

The Cu-coated Ni compact was tested for its ability to form an in-situ envelope by the sinter-HIP route as shown schematically in figure 87. The compact was first vacuum sintered (in boron-nitride powder to prevent unwanted reactions with the container) at 1150 °C for 1 hour to form a surface binary alloy and then the pressure cycle of 100 MPa for 2 hours was applied. The sintering step enabled the compact to defect-heal itself by forming an alloy whilst under vacuum (figure 88). It should be noted that the coating has recrystallised, driven by the stresses inherent in the coating. No significant dimensional change was observed. This part of the cycle need be only of sufficient duration to ensure that sufficient liquid phase is produced to repair any defects inherent in the coating and that effective evacuation of the compact occurs. Inward diffusion of copper is inhibited by the formation of a higher melting point Cu-Ni solid solution at the coating/powder compact interface. The diffusion of the elemental species during the sinter stage of the sinter-HIP process can be observed qualitatively via scanning electron microscopy (SEM) elemental maps and quantitatively by SEM digipoint analysis (figure 89). The subsequent application of the high pressure cycle was used to achieve full density of the compact as observed in figure 90. Dimensional change was relatively consistent over the compact, with a reduction of 13-17 % across the face and 10-12 % across the edge. After the full sinter-HIP cycle the copper penetration is limited to 60 - 80 μm (figure 91).

This system is ideally suited to the production of near-net-shape components, where subsequent machining and finishing operations can be minimised, with the resulting encapsulation forming an in-situ part of the component surface. As the envelope does not possess any inherent strong points (such as a welding seam on a metallic can) the densification should prove more uniform, with little shape deviation from the original compact.

The exact sinter-HIP cycle requires optimisation for any given coating/powder compact system.

6. Summary of Results and Discussion

6.1 Containerised Powder Modelling

The influence of the can geometry and the particle size distribution (PSD) have been investigated as to their effect on the modelling predictions of densification.

The can was seen to introduce stress variations throughout the powder compact due to the inherent strong points at the welding seams. To fully understand the densification behaviour of a powder body the Ashby model was employed. This program was extended to include a PSD to fully account for the contribution of the diffusional mechanisms that are size dependent. Good agreement was seen between the two models and between the modified model and experimental data. An initial investigation for the inclusion of a bimodal powder mixture has concluded that the model can not take account of the interaction of the powders due to the dominance of different densification systems for the different size fractions.

6.2 Coatings as In-Situ Envelopes

The use of a coating to act as an in-situ envelope will not introduce excessive stress variations on the powder compact as it effectively acts as a very thin walled can. The use of electron beam evaporation and ion plating has shown the potential of producing a defect-free in-situ envelope for the hot isostatic pressing (HIP) of powder components. However, the processing conditions must be optimised and the surface roughness effect on the coating structure investigated. The use of a resistive evaporation coating to produce an in-situ envelope by means of forming a transient liquid phase during a sinter-HIP cycle has proved successful. This process route led to the full densification of the powder compact, with the surface layer becoming an integral part of the component. Compact dimensional change was low and hence provides a route for near-net-shape production.

CONCLUSIONS

1. The Ashby model for powder densification by sinter or HIP has been extended to include a particle size distribution (PSD) and distribution type to provide a better approximation to true powder systems. Good agreement is found between the predicted densities and experimental data over several powders. The inclusion of a preliminary study into bimodal powders has suggested a larger dependence on the smaller size than expected for the densification rates due to different dominant mechanisms applying to the different size fractions.

2. Electron beam evaporation and ion plating offer the potential for the encapsulation of powder metal compacts prior to hot isostatic pressing (HIP). However, the process route is difficult and the deposition conditions require optimisation to ensure a defect-free coating.

3. The difficulties associated with the formation of a defect-free coating can be overcome by forming a transient liquid phase at the surface by the use of a sintering step to react the coating and surface layer. This sintering step can be incorporated into a sinter-HIP cycle. The surface layer can act as an integral part of the finished article. The choice of the coating/substrate system requires optimisation to reduce cycle times.

FUTURE WORK

The extended Ashby model program, HIP792, could be improved by the addition of a grain size distribution and by further experimental work to determine the effect of each of the constituent powders in a bimodal mixture. It would appear necessary to calculate the densification of the different size fractions separately, whilst taking into account the overall densification rate of both sizes. However, the model is essentially a first approximation to the densification of powder bodies and, as such, any modifications to the scope of the program should be chosen carefully.

It is suggested that the electron beam evaporation and ion plating systems are investigated further in terms of the required processing conditions for deposition of a defect-free envelope on powder metallurgy compacts and their relationship with the powder size. However, the formation of defect-free coatings on a powder compact surface will be difficult to achieve and the cost effectiveness of the process route may be inhibitive.

The coating/substrate system for use in a sinter-HIP cycle will require further optimisation to determine the optimum coating thickness, dependent on the compact surface topography, and to reduce the cycle time (particularly in the sintering step). Other potential systems can be investigated. This method provides the opportunity for the near-net-shape processing of complex parts.

REFERENCES

1. Hanes, H.D. Seifert, D.A. Watts, C.R.
Hot Isostatic Pressing.
Battelle Press (1979).

2. Hellman, P.
Review of HIP Development: HIP of Metals and Alloys, Technology and Applications Today.
Proc. of Int. Conf. on HIP (1987). pp 3-18.

3. James, P.J.
Isostatic Pressing Technology.
Applied Science Publishers Ltd (1983).

4. Andersen, I.F. Nyce, A.C.
Pressure Assisted High Temperature Sintering of Metal Alloys and Ceramics.
Advanced Sintering Technology. (1988). pp 47-65.

5. Kennedy, M.D.
Increased Use of Powder Metals in the 90's.
Industrial Heating (Apr. 1989). pp 50,61.

6. Wood, J.V.
Powder Metallurgy - Old Concepts and New Horizons.
Metals and Materials (Mar. 1987). pp 128-133.

7. Froes, F.H. Williams, J.C.
Titanium Alloys: Powder Metallurgy.
Encyclopedia of Materials Science and Engineering (1986). pp 5089-5094.

8. Hunt, M.
Out of This World Shapes with Powder Metallurgy.
ME (Nov. 1988). pp 29-32.

9. Price, P.E.
Hot Isostatic Pressing in the Aerospace Industry.
Metal Progress (Feb. 1982). pp 46-47.

10. Johnson, P.K.
P/M's Growing Diversity.
Proc. of 1989 PM Conf. and Exib. vol.1 (1989). pp 551-560.

11. White, D.G.
State of the P/M Industry in North America.

Proc. of 1989 PM Conf. and Exib. vol.1 (1989). pp 1-8.

12. 'Executive Summary'
The Global Powder Metallurgy Industry: Market Forecasts and Applications, Business Opportunities and Technology Assessments to 2000.
Gorham Advanced Materials Inst. (1990).

13. Price, P.E. Kohler, S.P.
Hot Isostatic Pressing of Metal Powders.
Metals Handbook 9th Edition vol.7: Powder Metallurgy (1984). pp 419-443.

14. Stephenson, D.J. Downing, M.
Hot Isostatic Pressing of PM and Cast Components.
Mat. at High Temp. vol.9, no.2, May 1991. pp 59-68.

15. Asari, A. Fujikawa, T. Ishii, T. Kofume, S.
Recent Progress in CIP and HIP Systems.
Proc. of IISS Symposium vol.2 (1987). pp 761-766.

16. 'Superhipper' literature.
V.G. Special Systems (1988).

17. Barice, W.J.
Hot Isostatic Pressing of Castings.
Proc. of Gorham HIP Conf. (1978). pp 1-9.

18. Busch, W.-B. Wortmann,
Influences of Regeneration Treatments on Creep Rupture Lifes of Turbine Blades.
Proc. of High Temp. Alloys: Their Exploitable Potential (1985). pp 337-346.

19. Widmer, R.
The Current Status and Future of Castings Densification Via HIP.
Proc. of Int. Conf. on HIP (1988). pp 3.1-3.8.

20. Eriksson, H. Friborg, S.
HIP Steels and Applications.
Proc. of Int. Conf. on HIP (1987). pp 255-257.

21. Ekbom, L. Elliasson, A. Bogegard, S.
Hot Isostatic Pressing of Tungsten-Nickel-Iron Composites.
Proc. of Int. Conf. on HIP (1987). pp 231-238.

22. Prakash, T.L. Chari, Y.N. Bhagiradha Rao, E.S. Thamburaj, R.
Microstructures and Mechanical Properties of Hot Isostatically Pressed Powder

Metallurgy Alloy APK-1.
Metall. Trans. A. (14A) (Apr. 1983). pp 733-742.

23. Somani, M.C. Bhagiradha Rao, E.S. Sarma, G.S. Sood, R.K.
Characterization and Evaluation of Hot Isostatically Pressed Low Carbon Astroloy Powder.
Trans. Indian Inst. Metals (39) (Oct. 1986). pp 435-444.

24. Wright, R.N. Flinn, J.E.
Microstructure and Properties of Hot Isostatically Pressed Nickel Aluminides.
Proc. of Int. Conf. on HIP (1987). pp 225-230.

25. Wright, R.N. Rabin, B.H. Kaibloe, J.R.
Consolidation of Ni_3Al Powders by Hot Isostatic Pressing.
Mater. Manuf. Process. (4(1)) (1989). pp 25-37.

26. Kissinger, R.D. Nair, S.V. Tien, J.K.
Hot Isostatic Consolidation of P/M Superalloys.
Mat. Res. Soc. Proc. vol.28. (1984). pp 157-162.

27. Kny, E. Danninger, H. Heim, G. Ostensson, M.
Effects of HIP on Heavy Metal Samples.
Proc. of 12th Int. Plansee Seminar vol.1 (1989). pp 869-882.

28. ASM Handbook Committee.
Atomisation.
Metals Handbook 9th Edition vol.7: Powder Metallurgy (1984). pp 25-51.

29. Lawley, A. Doherty, R.D.
Rapidly Solidified Powder Processes: Models and Mechanisms for Atomisation and Consolidation.
Rapidly Solidified Crystalline Alloys (1985). pp 71-91.

30. Klar, E. Fesko, J.W.
Gas and Water Atomisation.
Metals Handbook 9th Edition vol.7: Powder Metallurgy (1984). pp 25-39.

31. Lewis, C.F.
Shaping Up with Powder Metallurgy.
ME (Mar. 1986). pp 42-45.

32. Jonsson, S. Ertl, M. Hohmann, M.
Modern Production System for Inert Gas Atomisation.
Proc. of 1989 PM Conf. and Exib. vol.2 (1989). pp 68-80.

33. Klar, E. Fesko, J.
On the Particle Shape of Atomised Metal Powders.
Prog. Powder Metall. vol.37 (1981).

34. Roberts, P.R.
Rotating Electrode Process.
Metals Handbook 9th Edition vol.7: Powder Metallurgy (1984). pp 39-42.

35. Fox, C.W.
Vacuum Atomization.
Metals Handbook 9th Edition vol.7: Powder Metallurgy (1984). pp 43-45.

36. ASM Handbook Committee.
Apparent Density of Metal Powders.
Metals Handbook 9th Edition vol.7: Powder Metallurgy (1984). pp 272-275.

37. Lenel, F.V.
Mechanical Fundamentals of Consolidation.
Metals Handbook 9th Edition vol.7: Powder Metallurgy (1984). pp 296-307.

38. Soper, W.E.
Tap Density of Metal Powders.
Metals Handbook 9th Edition vol.7: Powder Metallurgy (1984). pp 276-277.

39. Davidson, J.E.
Compressibility of Metal Powders.
Metals Handbook 9th Edition vol.7: Powder Metallurgy (1984). pp 286-287.

40. Gasiorek, S. Korczak, K.Z. Kaminski, K.K.
Compressibility of Metal Powders.
Proc. of 1989 PM Conf. and Exib. vol.1 (1989). pp 53-62.

41. Korczak, K.Z. Gasiorek, S. Kaminski, K.K.
New Approach for Testing and Evaluation of Ceramic and Metallic Powder Compressibility.
Proc. of 1989 PM Conf. and Exib. vol.1 (1989). pp 75-84.

42. Seelig, P.R. Wulff, J.
The Pressing Operation in the Fabrication of Articles by Powder Metallurgy.
Trans. AIME vol.166 (1946). pp 492-500.

43. Fischmeister, H.F. Arzt, E. Olsson, L.R.
Particle Deformation and Sliding During Compaction of Spherical Powders: A Study by Quantitative Metallography.
Powder Metall. vol.21 (1978). pp 178-187.

44. Balshin, M.Yu.
Theory of Compacting.
Vestnik Metalloprom. vol.18 (1938). pp 137-147.

45. Heckel, R.W.
An Analysis of Powder Compaction Phenomena.
Trans. AIME vol.221 (1961). pp 1001-1008.

46. Morgan, V.T. Sands, R.L.
Isostatic Compacting of Metal Powders.
Metallurgical Reviews no.134 J. Met. May 1969 pp 85-88.

47. James, P.J.
Particle Deformation During Cold Isostatic Pressing of Metal Powders.
Powder Metall. vol.20 (1977). pp 199-204.

48. Bockstiegel, G.
The Porosity-Pressure Curve and its Relation to the Pore Size·Distribution in Iron Powder Compacts.
Mod. Devel. in Powder Metall. vol.1 Plenum Press (1966).

49. Squire, A.
Density Relationship of Iron Powder Compacts.
Trans. AIME vol.171 (1947).

50. Kuczynski, G.C. Zaplatinsky, I.
Density Distribution in Metal Powder Compacts.
Trans. AIME vol.206 (1956). p 215.

51. McGeary, R.K.
Mechanical Packing of Spherical Particles.
J. Am. Ceram. Soc. vol.44, no.10, pp513-522 (1961).

52. Brown, J.A.
Senior Thesis.
Dept. of Met. Eng. Carnegie Inst. Tech. (1950).

53. Kellock, B.
Complex Components Via 'New' Techniques.
Machinery and Prod. Eng. (Apr. 1988). pp 111-113,115,117.

54. Anderson, R.L. Groza, J.
High Speed Consolidation of Rapidly Solidified High Temperature Powder Preforms.
Proc. of Int. Conf. on PM Aerospace Materials '87 (1987). pp 37.1-37.8.

55. Arkens, O. Libowton, J. Dalaey, L. Buekenhout, L.
Dynamic Compaction and Hot Isostatic Pressing of Nickel Aluminides.
Proc. of Int. Conf. on HIP (1988). pp 2.41-2.43.

56. Miller, D.J. Sears, J.W. Fraser, H.L.
Microstructure and Properties of Rapidly Solidified Material Consolidated by Dynamic Compaction and Hot Isostatic Pressing.
Processing of Structural Metals by Rapid Solidification (1987). pp 133-141.

57. Konvica, H.R.
Hot Isostatic Pressing: an Advanced Technique in Materials Technology.
Adv. Mat. Technol.: Monitor (May 1985). pp 36-42.

58. Buekenhout, L. Tempels, M. Sleurs, J. Schrijvers, J.
Recent Results Related to the Development of Encapsulation Techniques.
Proc. of the Int. Conf. on HIP (1988). pp 1.35-1.36.

59. Abouaf, M. Chenot, J.L. Baudin, P. Raisson, G.
Prediction of the Deformation During the Production of Near-Net-Shape Superalloy Parts by Hot Isostatic Pressing.
Proc. of the 2nd Int. Conf. on Isostatic Pressing (1982). pp 9.1-9.20.

60. Aren, B. Li, W.-B.
Investigation of Hot Isostatic Pressing of Metal Powder to Near Net Shape.
Proc. of the Int. Conf. on HIP (1987). pp 117-124.

61. Cotta, A. Bannani, A.
Influence of Geometric Shapes and Welding Seams of Metallic Cans on the Dimensional Variation of Components made by HIP.
Proc. of the 1st Int. Conf. on Isostatic Pressing (1981). pp 7.1-7.21.

62. Fallman, S. Jaktlund, L.-L. Tegman, R. Garvare, T.
Numerical Modelling of Shrinkage During HIP.
Proc. of Int. Conf. on HIP (1987). pp 89-96.

63. Ingelstrom, N. Ekstrom, T.
Silicon Nitride Made by the Encapsulated HIP Technique.
Proc. of Int. Conf. on HIP (1987). pp 307-314.

64. Pejryd, L.
Yttria Doped Si_3N_4 Consolidated at Different Temperatures Using the Encapsulated HIP Technique.
Proc. of Int. Conf. on HIP (1987). pp 353-357.

65. Nyce, A.C.

Containerless HIPing of PM Parts: Technology, Economics and Equipment Productivity.
MPR (July 1983). pp 387,389-392.

66. Kaysser, W.A.
Sintering and HIP with a Liquid Phase.
Ceramic Powder Science IIB vol.1 (1988). pp 955-968.

67. Kaysser, W.A. Petzow, G.
Microstructural Development During Sintering and HIPing of some Multicomponent Systems.
Proc. of IISS Symposium vol.2 (1987). pp 743-748.

68. 'Proposal'
Pressure Assisted Sintering (PAS).
Gorham Advanced Materials Inst. (1990).

69. Bose, A. German, R.M.
Potential of Powder Injection Moulding and Hot Isostatic Pressing of Nickel Aluminide Matrix Composites.
Ind. Heat (May 1988). pp 38-41.

70. Diehl, W.
Properties of Injection Moulded, Containerless HIP'ed UDIMET 700 Parts.
Proc. of Int. Conf. on HIP (1988). pp 2.11-2.15.

71. Diehl, W. Buchkremer, H.P. Kaiser, H. Stover, D.
Injection Moulded Superalloy Parts Containerless HIP'ed.
Proc. of Int. Conf. on PM Aerospace Materials '87 (1987). pp 11.1-11.10.

72. Hecker, R. Stover, D. Buchkremer, H.P. Diehl, W. Duringer, Th.
Development of Sinter-HIP-Processes for Shaped Parts of Superalloy and Oxide-Ceramics.
Proc. of 12th Int. Plansee Seminar '89 vol.3 (1989). pp 353-370.

73. Kalavainen, P.
Sinter-HIP Technology for New Materials Processing.
Proc. of 12th Int. Plansee Seminar '89 (1989). pp 251-266.

74. Bauer,I.R.E.
Sinter HIP Furnaces - Sintering and Compacting in a Combined Cycle.
Modern Developments in PM vol.18 (1988). pp 91-103.

75. Minabe, M. Endoh, H.
The Development of High Density Sintered Titanium Alloys using a Sinter-

HIP Process.
Proc. of 1989 PM Conf. and Exib. (1989). pp 481-491.

76. Jeadin, M. Trottier, J.P. Koutny, J.L. Bienvenu, Y.
A Two-Stage Compaction Process for Superalloy Powders: Presintering + HIP.
MPR (Sept. 1984). pp 495-500.

77. German, R.M.
Fundamental Sintering Theory and Practise.
Advanced Sintering Technology. (1988). pp 1-33.

78. ASM Handbook Committee.
Physical Fundamentals of Consolidation.
Metals Handbook 9th Edition vol.7: Powder Metallurgy (1984). pp 308-321.

79. Elliot, A.G. Munir, Z.A.
The Sintering of Nickel/Aluminium Spheres to Nickel Plates.
J. Mater. Sci. 3 (1968). pp 150-157.

80. Aslan, M. Kaysser, W.A.
Deformation of Spheres under Non-Constraint Conditions and during HIPing.
Proc. of Int. Conf. on HIP (1987). pp 51-55.

81. Arzt, E. Ashby, M.F. Easterling, K.E.
Practical Applications of Hot-Isostatic Pressing Diagrams: Four Case Studies.
Metall. Trans. A (14A) (Feb. 1983). pp 211-221.

82. Arzt, E. Ashby, M.F. Verral, R.A.
Overview no.33. Interface Controlled Diffusional Creep.
Acta. Metall. (31(12)) (1983). pp 1977-1989.

83. Coble, R.L.
Sintering Crystalline Solids I. Intermediate and Final State Diffusion Models.
J. Appl. Physics (32(5)) (1961). pp 787-792.

84. Coble, R.L.
Diffusion Models for Hot Pressing with Surface Energy and Pressure Effects as Driving Forces.
J. Appl. Physics (41(12)) (1970). pp 4798-4807.

85. Crossman, F.W. Ashby, M.F.
The Non-Uniform Flow of Polycrystals by Grain-Boundary Sliding Accommodated by Power-Law Creep.
Acta. Metall. (23(4)) (1975). pp 425-440.

86. Helle, A.S. Easterling, K.E. Ashby, M.F.
Hot-Isostatic Pressing Diagrams: New Developments.
Acta. Metall. (33(12)) (1985). pp 2163-2174.

87. Matthews, J.R.
Indentation Hardness and Hot Pressing.
Acta. Metall. (28) (1980). pp 311-318.

88. McCoy, J.K. Wills, R.R.
Densification by Interface-Reaction Controlled Grain-Boundary Diffusion.
Acta. Metall. (35) (1987). pp 577-585.

89. Swinkels, F.B. Ashby, M.F.
A Second Report on Sintering Diagrams.
Acta. Metall. (29) (1981). pp 259-281.

90. Swinkels, F.B. Wilkinson, D.S. Arzt, E. Ashby, M.F.
Mechanisms of Hot-Isostatic Pressing.
Acta. Metall. (31) (1983). pp 1829-1840.

91. Wilkinson, D.S. Ashby, M.F.
Pressure Sintering by Power-Law Creep.
Acta. Metall. (23(11)) (1975). pp 1277-1285.

92. Carrol, M.M.
An Empirical Model for Hot Isostatic Pressing of Metal Powders.
Metall. Trans. A. (17A) (Nov. 1986). pp 1977-1984.

93. Laptev, A.M. Samarov, V.N. Podlesnyi, S.V.
Hot Isostatic Compaction Parameters for Porous Materials.
Russ. Metall. (5) (1988). pp 92-99.

94. Abouaf, M. Chenot, J.L. Raisson, G. Bauduin, P.
Finite Element Simulation of Hot Isostatic Pressing of Metal Powder.
Proc. of NUMIFORM '86 Conf. (1986). pp 79-83.

95. Abouaf, M. Raisson, G. Wey, E.
Influence of Cycle and Geometrical Parameters on the HIP'ing of a Turbine Disk.
Proc. of 3rd Int. Conf. on Isostatic Pressing vol.2 (1986). pp 10.1-10.11.

96. Cassenti, B.N.
A Nonvolume Preserving Plasticity Theory with Applications to Powder Metallurgy.
Nonlinear Constitutive Relations for High-Temperature Applications (1983).

pp 239-266.

97. Courtney, T.P. Krankota, J.L.
Finite Element Analysis of Hot Isostatic Pressing of Beryllium Powder into Near Net Shapes.
Maths. Modelling of Material Processing Operations. (1988). pp 1127-1146.

98. Nohara, A. Nakagawa, T. Soh, T.
Numerical Simulation of the Densification Behaviour of Metal Powder During Hot Isostatic Pressing.
Proc. of IISS Symposium vol.2 (1987). pp 749-754.

99. Nohara, A. Soh, T. Nakagawa, T.
Numerical Simulation of the Hot Isostatic Pressing Process.
Proc. of 3rd Int. Conf. on Isostatic Pressing vol.2 (1986). pp 11.1-11.25.

100. Soh, T. Nohara, A. Nakagawa, T.
HIP Process Simulation by the Finite Element Method.
Proc. of Int. Conf. on Hot Isostatic Pressing (1987). pp 81-88.

101. Traserras, J. Krauss, T.M. Ferguson, B.L.
Modelling of Powder Compaction using the Finite Element Method.
Proc. of 1989 PM Conf. and Exib. vol.1 (1989). pp 85-104.

102. Weber, G.G. Brown, S.B.
Simulation of the Compaction of Powder Components.
Proc. of 1989 PM Conf. and Exib. vol.1 (1989). pp 105-118.

103. Aren, B. Navara, E.
Modelling the Shape Change of Parts Produced by Hot Isostatic Pressing of Powders.
Proc. of Int. Conf. on Hot Isostatic Pressing (1987). pp 107-115.

104. Aren, B. Navara, E.
Modelling the Shape Change of Parts Produced by Hot Isostatic Pressing of Powders.
Powder Metall. (31(2)) (1988). pp 101-105.

105. Aren, B.G. Navara, E.
Shape Development of Powder Bodies Modelled as a Result of the Densification Process in Hot Isostatic Pressing.
Modern Devel. in PM vol.18 (1988). pp 23-36.

106. Bouvard, D. Cheynet, M.C. Saint-Antonin, F.
Densification Behaviour of Argon Atomised Powders During Hot Isostatic

Pressing.
Proc. of 3rd Int. Conf. on Isostatic Pressing vol.1 (1986). pp 14.1-14.17.

107. Bouvard, D. Lafer, M.
Determination of the Densification Kinetics of Metal Powders by Interrupted Hot Isostatic Pressing Tests.
Powder Metall. Int. (21(4)) (1989). pp 11-15.

108. Bouvard, D. Ouedraogo, E.
Modelling of Hot Isostatic Pressing: A New Formulation Using Random Variables.
Acta. Metall. (35(9)) (1987). pp 2323-2328.

109. Bouvard, D. Onedraogo, E. Cheynet, M.C.
A Model for the Densification of Powder by Particle Deformation During Hot Isostatic Pressing.
Proc. of Int. Conf. on Hot Isostatic Pressing (1987). pp 73-80.

110. Frish, A. Kaysser, W.A. Petzow, G.
Densification Maps and Defect Healing During Sinter/HIP of Polyphase Materials.
Proc. of 1989 PM Conf. and Exib. vol.2 (1989). pp 431-444.

111. Kaysser, W.A. Petzow, G.
Densification and Defect Healing by Hot Isostatic Pressing.
High Temp.-High Press. (21) (1989). pp 569-574.

112. Laag, R. Kaysser, W.A. Manser, R. Petzow, G.
Production and Consolidation of Ni-Al Powders.
Proc. of 1989 Pm Conf. and Exib. vol.2 (1989). pp 493-502.

113. Frish, A. Kaysser, W.A. Aslan, M. Petzow, G.
Prediction of the HIP Behaviour of Complex Materials.
Modern Devel. in PM vol.18 (1988). pp 11-21.

114. Kaysser, W. Aslan, M. Petzow, G.
Prediction of HIP Behaviour from the Deformation of Single Spheres.
Proc. of Int. Conf. on Hot Isostatic Pressing (1988). pp 1.11-1.16.

115. Kaysser, W.A. Aslan, M. Arzt, E. Mitkov, M. Petzow, G.
Microstructural Development and Densification During HIPing of Ceramics and Metals.
Powder Metall. (31(1)) (1988). pp 63-69.

116. Mitkov, M. Aslan, M. Kaysser, W.A.

Densification and Microstructure Development During HIPing of AP1.
Powder Metall. Int. (21(1)) (1989). pp 7-10.

117. Mitkov, M. Kaysser, W.A. Petzow, G.
Densification of AP1 Superalloy Powder During HIPing.
Contemporary Inorganic Materials: Progress in Ceramics, Metals and Composites (1985). pp 247-256.

118. Ashby, M.F.
HIP487: A Program for Constructing HIPing Diagrams.
(1987).

119. Ashby, M.F.
A First Report on Sintering Diagrams.
Acta. Metall. (22(3)) (1974). pp 275-289.

120. Frost, H.J. Ashby, M.F.
Deformation-Mechanism Maps.
Pergamon Press (1982).

121. Ashby, M.F.
The Role of Modelling in the Control of Hot-Isostatic Pressing.
Proc. of Int. Conf. on Hot Isostatic Pressing (1988). pp 1.1-1.9.

122. Arzt, E.
The Influence of an Increasing Particle Co-ordination on the Densification of Spherical Powders.
Acta. Metall. (30) (1982). pp 1883-1890.

123. Easterling, K.E.
Hot Isostatic Pressing of Metallic and Ceramic Powders.
Proc. of IISS Symposium vol.2 (1987).

124. Li, W.-B. Ashby, M.F. Easterling, K.E.
On Densification and Shape Change During Hot Isostatic Pressing.
Acta. Metall. (35(12)) (1987). pp 2831-2842.

125. Li, W.-B. Easterling, K.E.
Stresses Developed in the Hot Isostatic Pressing of Metals and Ceramics.
Proc. of Int. Conf. on Hot Isostatic Pressing (1987). pp 97-105.

126. Wlassich, J.J. Ashby, M.F. Blanchard, D.R. Henniges, B.L. O'Brien, D.W.
Modelling of Densification and Coarsening During Hot Isostatic Pressing.
Intelligent Processing of Materials (1990). pp 207-224.

127. Nair, S.V. Hendrix, B.C. Tien, J.K.
Obtaining the Radial Distribution of Random Dense Packed Hard Spheres.
Acta. Metall. (34(8)) (1986). pp 1599-1605.

128. Borofka, J.C. Caulfield, T. Tien, J.K.
Understanding the Kinetics and Densification Mechanisms in HIPing of Superalloy Powders.
MPR (Oct. 1986). pp 745-747.

129. Kissinger, R.D. Nair, S.V. Tien, J.K.
Hot Isostatic Consolidation of P/M Superalloys.
Mat. Res. Soc. Symp. Proc. (28) (1984).

130. Nair, S.V. Tien, J.K.
Densification Mechanism Maps for Hot Isostatic Pressing (HIP) of Unequal Sized Particles.
Metall. Trans. A. (18A) (Jan. 1987). pp 97-107.

131. Tien, J.K. Borofka, J.C.
Bimodal Modelling of HIP of Superalloys.
Proc. of Int. Conf. on Hot Isostatic Pressing (1987). pp 41-50.

132. Li, E.K.H. Funkenbusch, P.D.
Modelling of the Densification Rates of Monosized and Bimodal-Sized Particle Systems During Hot Isostatic Pressing (HIP).
Acta. Metall. (37(6)) (1989). pp 1645-1655.

133. Li, E.K.H. Funkenbusch, P.D.
Geometrical Considerations Regarding the Densification Rates of Monosize or Bimodal-Size Particle Systems during Hot Isostatic Pressing.
Solid State Powder Processing. (1990). pp 127-134.

134. Funkenbusch, P.D. Li, E.K.H.
HIP of Powder Mixtures.
Mat. Res. Soc. Proc. vol.251 (1992). pp 15-20.

135. Duva, J.M. Crow, P.D.
The Densification of Powders by Power-Law Creep During Hot Isostatic Pressing.
Acta. Metall. Mater. vol.40 no.1. (1992). pp 31-35.

136. McMeeking, R.M. Kuhn, L.T.
A Diffusional Creep Law for Powder Compacts.
Acta. Metall. Mater. vol.40 no.5. (1992). pp 961-969.

137. Teer, D.G.
Evaporation and Sputter Techniques.
Proc. of Conf. on Eng. Coatings: Vapour Deposited Coatings (1987).

138. Advanced Surface Coatings: a Handbook of Surface Engineering.
eds. Rickerby, D.S. Matthews, A.
Blackie and Son Ltd. (1991).

139. Rudki, G.J.
Surface Finishing Systems.
Finishing Publications Ltd. (1983).

140. Lawson, K.J.
Physical Vapour Deposition.
Proc. of Conf. on Eng. Coatings: Vapour Deposited Coatings (1987).

141. Hochman, R.F. Mattox, D.M.
Ion Plating.
Metals Handbook 9th Edition vol.5: Surface Cleaning, Finishing, and Coating (1984). pp 417-421.

142. Hocking, M.G. Vansantasree, V. Sidky, P.S.
Metallic and Ceramic Coatings.
Longman Scientific and Technical (1989).

143. Fielder, H.C. Sawyer,T.F. Kopp, R.W.
Spray-Forming - An Evaluation using IN718.
Proc. 1986 Vacuum Metall. Conf. on Speciality Metals and Processing (1987). pp 157-165.

144. Gupta, M. Marinkovich, J. Mohamed, F.A. Lavernia, E.J.
Processing of Two Al-Li-X-Zr (X=Cu, Mg and Ge) Alloys using Spray Atomisation and Deposition.
Proc. of 1989 PM Conf. and Exib. vol.2 (1989). pp 139- 160.

145. Pfender, E.
Fundamental Studies Associated with the Plasma Spray Process.
Proc. of Nat. Spray Conf. (1987).

146. Hannotian, M. Schrijvers, J. Sleurs, J.
Upgrading of Coatings by HIP Treatment.
Proc. of Int. Conf. on HIP (1988). pp 3.33-3.36.

147. Huber, P. Kress, H. Kaiser, H.
Vacuum Plasma Spraying in Combination with Hot Isostatic Pressing for the

Repair or Fabrication of Superalloy Components.
Thermal Spraying vol.2 (1989). pp 51-59.

148. Sampath, S. Herman, H. Rangoswamy, S.
Ni-Al Re-Evaluation.
Proc. of Nat. Thermal Spray Conf. (1987).

149. Houck, D.L. Whisenamt, W.
Wear Resistance of Five Molybdenum Containing Plasma Sprayed Coatings.
Proc. of Nat. Thermal Spray Conf. (1987).

150. Johner, G. Wilmms, V. Schmeitzer, K.K. Adam, P.
Experimental and Theoretical Aspects of Thick Thermal Barrier Coatings for Turbine Applications.
Proc. of Nat. Thermal Spray Conf. (1987).

151. Lugscheider, E.
Plasma Spraying for Wear Applications.
Proc. of Nat. Thermal Spray Conf. (1987).

152. Zhon, K.S. Wang, D.Z. Liu, M.
A Study of Ti-Ni Alloy Coatings and its Behaviour on Cavitation Erosion.
Proc. of Nat. Thermal Spray Conf. (1987).

153. Bunshah, R.F.
Evaporation.
Deposition Technologies for Films and Coatings: Developments and Applications. (1982). pp 83-167.

154. Blocher, J.M.
J. Vac. Sci. and Tech. vol.11, no.4, (1974).

155. Bunshah, R.F.
Deposition Technologies: An Overview.
Deposition Technologies for Films and Coatings: Developments and Applications. (1982). pp 1-16.

156. Movchan, B.A. Demchishin, A.V.
Study of the Structure and Properties of Thick Condensates of Titanium, Nickel, Tungsten, Zirconia and Alumina.
Phys. Met. Metall. vol.28 (1969). pp 83-90.

157. Thornton, J.A.
High Rate Thick Film Growth (of Metals).
Ann. Rev. Mater. Sci. vol.7 (1977). pp 239-260.

158. Grovenor, C.R.M. Hentzell, H.T.G. Smith, D.A.
The Development of Grain Structure During Growth of Metallic Films.
Acta. Metall. (32(5)) (1984). pp 773-781.

159. Messier, R. Yehoda, J.E.
Geometry of Thin-Film Morphology.
J. Appl. Phys. vol.58, no.15. pp3739-3746 (1985).

160. Downing, M. Nicholls, J.R. Stephenson, D.J.
Physical Vapour Deposition Coating Processes for Encapsulation of Powder Metal Components Before Hot Isostatic Pressing.
Mat. Sci. and Tech. vol.7. (dec. 1991). pp 1138-1142.

161. Power, D.
Encapsulation of Powdered Metal Compacts for Hot Isostatic Pressing using PVD Coatings.
M.Sc. Thesis. Cranfield Institute of Technology. (1989).

162. Major, M.R.
The Closure of Artificial Porosity by Hot Isostatic Pressing.
M.Sc. Thesis. Cranfield Institute of Technology. (1985).

163. Petzow, G. Kaysser, W.A. Kunesch, J.
Advanced Materials by Powder Metallurgy - Science and Technology.
Sintering of Multiphase Metals and Ceramic Systems. (1990). pp 3-36.

164. Stephenson, D.J.
Private Communication (1989).

165. Hansen, M.
Constitution of Binary Alloys.
Metallurgy and Metallurgical Engineering Series. (1958). pp 601-603.

166. Darken, L.S. Gurry, R.W.
Physical Chemistry of Metals.
McGraw-Hill (1953).

167. Morrel, R.
Density and Porosity.
Handbook of Properties of Technical and Engineering Ceramics (1982). pp 67-72.

168. Manual - Mini-Magiscan/IAS25/IV25.
Joyce-Loebl Ltd. (1989).

169. Image Analysis: Principles and Practise.
Joyce-Loebl Ltd. (1989).

170. Prybylowski, J. Pelloux, R.M. Price, P.
Effects of Argon Contamination in PM Hot Isostatically Pressed Nickel Base Superalloy.
Powder Metall. vol.27. no.27. (1984). pp 107-111.

171. Eylon, D. Schwenker, S.W. Froes, F.H.
Thermally Induced Porosity in Ti-6Al-4V Prealloyed Powder Compacts.
Metall. Trans. A vol.16A. (Aug. 1985). pp 1526-1531.

172. Thamburaj, R. Koul, A.K. Wallace, W. de Malherbe, M.C.
Prior Particle Boundary Precipitation in P/M Superalloys.
Mod. Devel. in PM vol.16. (1988). pp 635-673.

173. Warren, R. Ingesten, N.G. Winberg, L. Ronnhult, T.
Particle Surface and Prior Particle Boundaries in Hf Modified PM Astroloy.
Powder Metall. vol.27. no.3. (1984). pp 141-146.

174. German, R.M.
The Sintering of 304L Stainless Steel Powder.
Metall. Trans. A vol.7A. (Dec. 1976). pp 1879-1885.

APPENDICES

Appendix A

To give the effective radii for a log-normal distribution of particle size the simulation needs a maximum and minimum size to be entered. When a plot is requested the following procedure is performed to calculate the effective radii:

```
procedure reffln (maxs,mins : real ; var bdr,vol : real);

var     i,n : integer ;
        inc, t, t2, y, sd, mean, x : real ;
        s, stot, tot, totrefv, totrefb : real ;
        mas,mis : real ;

begin

        totrefb := 0;
        totrefv := 0;
        tot := 0;
        t := 0;
        t2 := 0;
        mas := ln(maxs);
        mis := ln(mins);
        n := 100;
        inc := (mas-mis)/n;

        for i := 1 to n+1 do
                t := t + mis + (i-1)*inc;

        mean := t/n;

        for i := 1 to n+1 do
        t2 := t2 + ((mis+(i-1)*inc) - mean) * ((mis+(i-1)*inc) - mean);

        sd := sqrt(t2/(n-1));

        for i := 1 to n+1 do
        begin
                x := (mis+(i-1)*inc);
                s := (x-mean)/sd;
                y := (1/(sd*2.5066283)) * exp(-0.5*s*s);
                y := y*(mas-mis)/n;
                tot ;+ tot + y;
        end;
```

```
stot := tot;
tot := 0;

for i := 1 to n+1 do
begin
        x := (mis+(i-1)*inc);
        s := (x-mean)/sd;
        y := (1/(sd*2.5066283)) * exp(-0.5*s*s);
        y := y*(mas-mis)/n;
        y: = y*(1/stot);
        tot := tot + y;

        bdr := exp(x)*exp(x)*exp(x)*y;
        totrefb := totrefb + bdr;
        vol := exp(x)*exp(x)*y;
        totrefv := totrefv + vol;

end;

        bdr := exp(ln(totrefb)/3);
        vol := exp(ln(totrefv)/2);
        particlerad := exp(mean);

end;
```

The effective radii are used in the rate equations for boundary and lattice densification while the mean size is used by the other mechanisms, thus:

```
procedure DIFFUSION_RATES;    (File: DIFFRATE.PRC)

{--Calculates the rates of diffusion and the reference creep rate--}

var
        arg1 : real;
        arg2 : real;
        arg3 : real;
        arg4 : real;

begin

{--Evaluate exponent and temperature T--}

arg1 := qvolmN*(1/TN - 1); if arg1 > 60.0 then arg1:= 60.0;
arg2 := qbdryN*(1/TN - 1); if arg2 > 60.0 then arg2:= 60.0;
arg3 := q_crpN*(1/TN - 2); if arg3 > 60.0 then arg3:= 60.0;
```

```
{--Evaluate diff. coefficient, normalised by R, at T; units: /s--}

        diff1 := dmeltvolm*(exp(-arg1)/(reffvol*reffvol));
        diff2 := dmeltbdry*(exp(-arg2)/(reffbdy*reffbdy*reffbdy));
        dorn := 1.e-6*exp(-arg3);

end;    {DIFFUSION_RATES.       File: DIFFRATE.PRC}

procedure SINTERING_RATES;    {File: DIFFRATE.PRC}

{-Calculate the rates of densification by each mechanism-}

var
        c1,c2,c3,c4 : real;             c5,c6,c7,c8 : real;
        S1,S2 : real;
        L : integer;

begin

        for L := 0 to numberofmechanisms do DNrate[L] := 0.0:
        if DN <= 1.00001*DI then DNrate[5] := 100.0;
                {Set initial creep rate high}

        if (DN > 1.00001*DI) and (DN < 0.99995) then begin
                {Overflow protect}

        c1 := (atvol/boltz)/(TN*tmelt);
        c7 := (diff1 +pi*diff2*particlerad/Gsize)*particlerad*particlerad/
                (Gsize*gsize);

{--START STAGE 1 CALCULATIONS--}

        if DN < 0.95 then begin     {Limit Stage 1 to < 0.95}

        PN_crp := (pn*yield - porepressure)/S_crp;
        if PN_crp < 1.e-6 then PN_crp := 1.e-6;

        c2 := (1 - DO)/(DN - DO);
        c3 := exp(n_crp*ln(PN_crp*c2/(3*DN*DN)));

        S1 := 1 - (DN - DO)/(0.95 - DO)*(DN - DO)/(0.95 - DO);
        if S1 < 0.0 then S1 := 0.0;
                {Smoothing factor, stage 1}

        P_force1 := (PN*yield - porepressure)*1.e-6*c1;
```

```
{Driving forces}
        Sb_force1 := (sfeng/reffbdy)*c1;
        Sv_force1 := (sfeng/reffvol)*c1;
        if P_force1 < 0.0 then P_force1 := 0.0;
        if Sb_force1 < 0.0 then Sv_force1 := 0.0;
        if Sv_force1 < 0.0 then Sv_force1 := 0.0;

        DNrate[1] := 72*DO*c2*diff1*Sv_force1*S1;
{Volm diff, stage 1}
        DNrate[2] := 43*c2*(1 - DO)*diff1*P_force1*S1;        {Helle et al.
eqn(19)}
        DNrate[3] := 18*DN*c2/(DN - DO)*diff2*Sb_force1*S1; {Bdry diff, stage
1}
        DNrate[4] := 43*c2*c2*diff2*P_force1*S1;
{Helle et al. eqn(19)}
        DNrate[5] := 3.06*DN*sqrt(1/c2)*dorn*c3*S1;
{P-L creep, stage 1}
        if Gsize < particlerad then  {Helle et al. eqn(23)}
        DNrate[6] := 14.4*c7*sqrt(c2)/DN*P_force1*S1;
{N-H creep, stage 1}
{Helle et al. eqn(26)}
        end;

{--START STAGE 2 CALCULATIONS--}

        if DN > 0.85 then begin     {Limit Stage 2 to > 0.85}

        P_internal := porepressure*((1 - DNcrit)*DN/((1 - DN)*DNcrit) - 1);
        if P_internal < porepressure then P_internal := porepressure;
        PN_crp := (PN*yield - P_internal)/S_crp;
        if PN_crp < 1.e-6 then PN_crp := 1.e-6;

        c4 := exp(ln(1 - DN)/6)/3);
        c5 := 270*sqrt(1 - DN);
        c6 := 1.5*PN_crp/(n_crp*(1 - exp((1/n_crp)*ln(1 - DN))));

        S2 := 6.67*DN - 5.67;       {Smoothing factor, stage 2}
        if S2 < 0.0 then S2 := 0.0;

        P_force2 := (PN*yield - P_internal)*1.e-6*c1;
        Sv_force2 := (2*sfeng/(c4*reffvol) - P_internal*1.e-6)*c1;
        Sb_force2 := (2*sfeng/(c4*reffbdy) - P_internal*1.e-6)*c1;

        if P_force2 < 0.0 then P_force2 := 0.0;
        if Sv_force2 < 0.0 then Sv_force2 := 0.0;
```

```
        if Sb_force2 < 0.0 then Sb_force2 := 0.0;

        DNrate[7] := 18*c4*diff1*Sv_force2*S2;
{Volm diff, stage 2}
        DNrate[8] := c4*c5*diff1*P_force2*S2;
{Helle et al. eqn(21)}
        DNrate[9] := 9*diff2*Sb_force2*S2;
{Bdry diff, stage 2}
        DNrate[10] := c5*diff2*P_force2*S2;
{Helle et al. eqn(21)}
        DNrate[11] := 1.5*dorn*DN*(1 - DN)*exp(n_crp*ln(c6));
{P-L creep, stage 2}
        DNrate[11] := DNrate[11]*S2;
{Helle et al. eqn(24)}
        if Gsize < particlerad then  {N-H creep, stage 2}
        DNrate[12] := 32*c7*(1 - DN)*P_force2*S2;
{Helle et al. eqn(27)}
        end;
        end;

{--Sum the sintering rates--}

        DNratetotal := DNrate[1] + DNrate[2] + DNrate[3] + DNrate[4] +
                       DNrate[5] + DNrate[6] + Dnrate[7] + DNrate[8] + DNrate[9]
                       + DNrate[10] + DNrate[11] + DNrate[12];

        if DNratetotal < 1.e-12 then DNratetotal := 1.e-12;

        end;    {SINTERING RATES.       File: SNTRRATE.PRC}
```

The next upgrade incorporates a bimodal distribution by prompting for two maximum and minimum particle size values plus, the weight ratio of the sizes in the mixture. The effective radii are produced for each size then input back using the ratio as f_i, giving two new effective radii. Finally, the particle radius used by the other rate equations is calculated from the two means and the ratio. Thus:

```
if c3 + 1 then
begin
(*Calculate effective radii using normal dist for both sizes*)
        reffn( e.pmax1,e.pmin1,bdr1,vol1);
        reffn( e.pmax2,e.pmin2,bdr2,vol2);
end
else
begin
(*Calculate effective radii using log normal dist for both sizes*)
```

```
        reffln( e.pmax1,e.pmin1,bdr1,vol1);
        reffln( e.pmax2,e.pmin2,bdr2,vol2);
end;

        (*Calculate effective boundary/volume and particle radii using the ratios of the
        two sizes*)

        reffbdy := exp(ln(bdr1*bdr1*bdr1*e.ratio1/100
+bdr2*bdr2*bdr2*e.ratio2/100)/3);
        reffvol := exp(ln(vol1*vol1*e.ratio1/100 + vol2*vol2*e.ratio2/100)/2);
        particlerad  :=  (e.pmin1  +  e.pmax1)/2*e.ratio1/100  +  (e.pmin2
                        +e.pmax2)/2*e.ratio2/100;
```

The final modification was to extend the analysis to include a normal distribution:

```
        procedure reffn ( maxs,mins : real ; var bdr,vol : real ) ;

        var     i,n : integer ;
                inc, t, t2, y, sd, mean, x : real ;
                s, stot, tot, totrefb : real ;
                mas,mis : real ;

        begin

                totrefb := 0;
                totrefv := 0;
                tot := 0;
                t := 0;
                t2 := 0;
                mas := (maxs);
                mis := (mins);
                n := 100;
                inc := (mas-mis)/n;

                for i : 1 to n+1 do
                        t := t + mis + (i-1)*inc;

                mean := t/n;

                for i := 1 to n+1 do
                        t2  :=  t2  +  ((mis+(i-1)*inc) - mean)  *  (( mis+(i-1)*inc) -
                                mean);

                sd := sqrt(t2/(n-1));
```

```
for i := 1 to n+1 do
begin
        x := (mis+(i-1)*inc);
        s := (x-mean)/sd;
        y := (1/(sd*2.5066283)) * exp(-0.5*s*s);
        y := y*(mas-mis)/n;
        tot := tot + y;
end;

stot := tot;
tot := 0;

for i := 1 to n+1 do
begin
        x := (mis+(i-1)*inc);
        s := (x-mean)/sd;
        y := (1/(sd*2.5066283)) * exp(-0.5*s*s);
        y := y*(mas-mis)/n;
        y := y*(1/stot);
        tot := tot + y;

        bdr := (x)*(x)*(x)*y;
                totrefb := totrefb + bdr;
                vol := (x)*(x)*y;
                totrefv := totrefv + vol;
        end;

        bdr := exp(ln(totrefb)/3);
        vol := exp(ln(totrefv)/2);
        particlerad := exp(mean);
end;
```

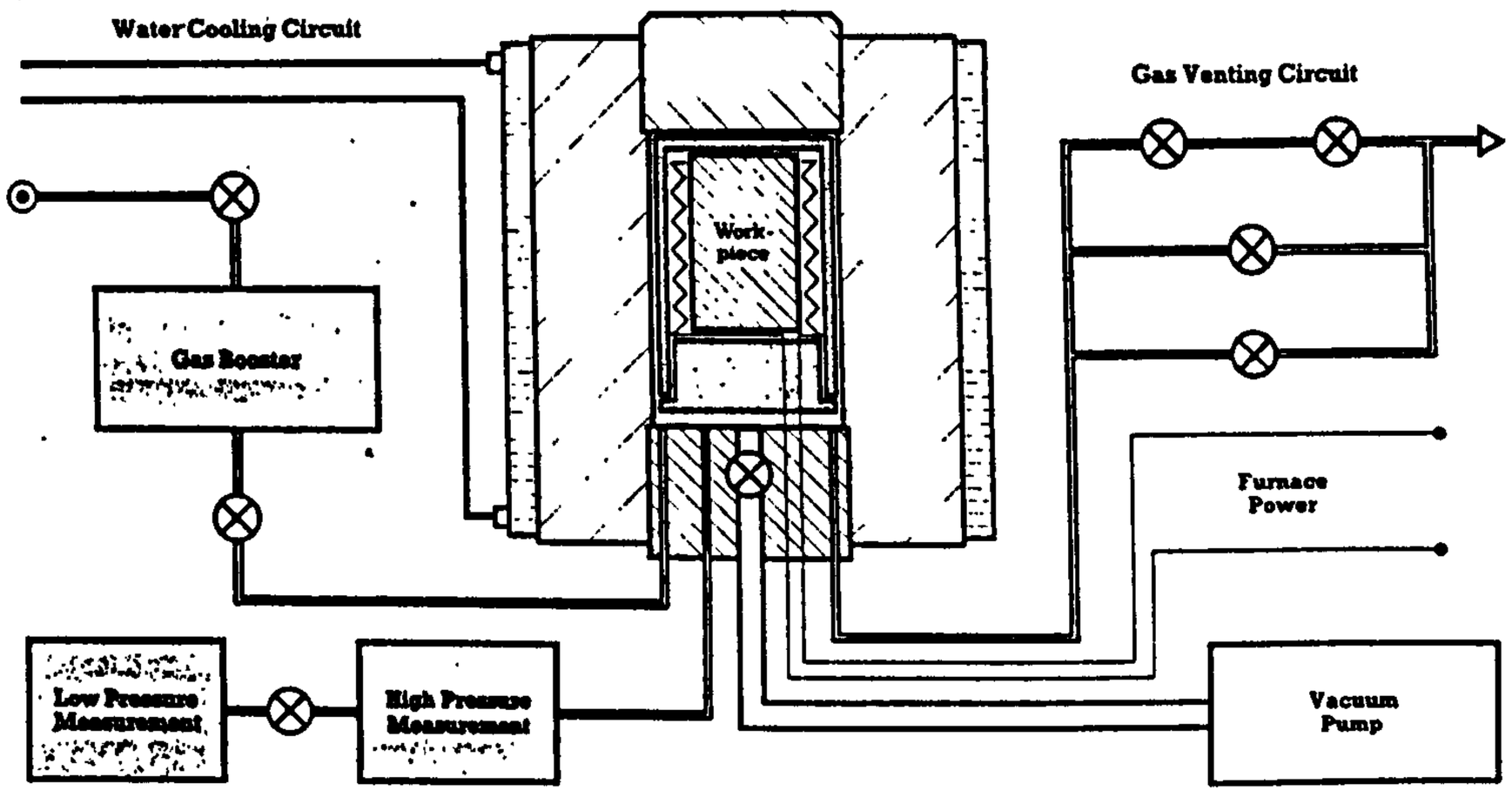

Figure 1. Schematic Diagram of the Superhipper Process Module.[16]

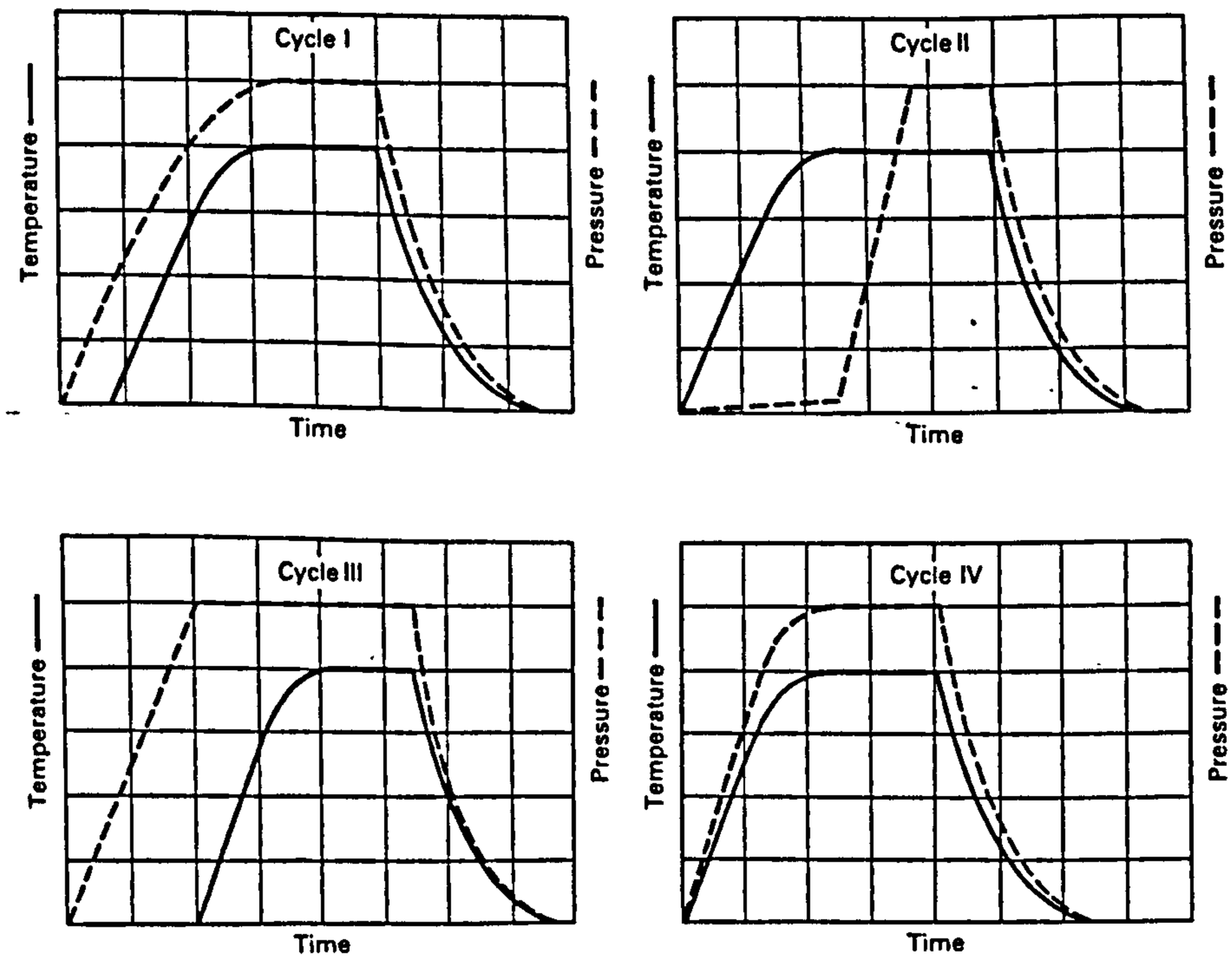

Figure 2. Schematic Process Cycles for Hot Isostatic Pressing.[13]

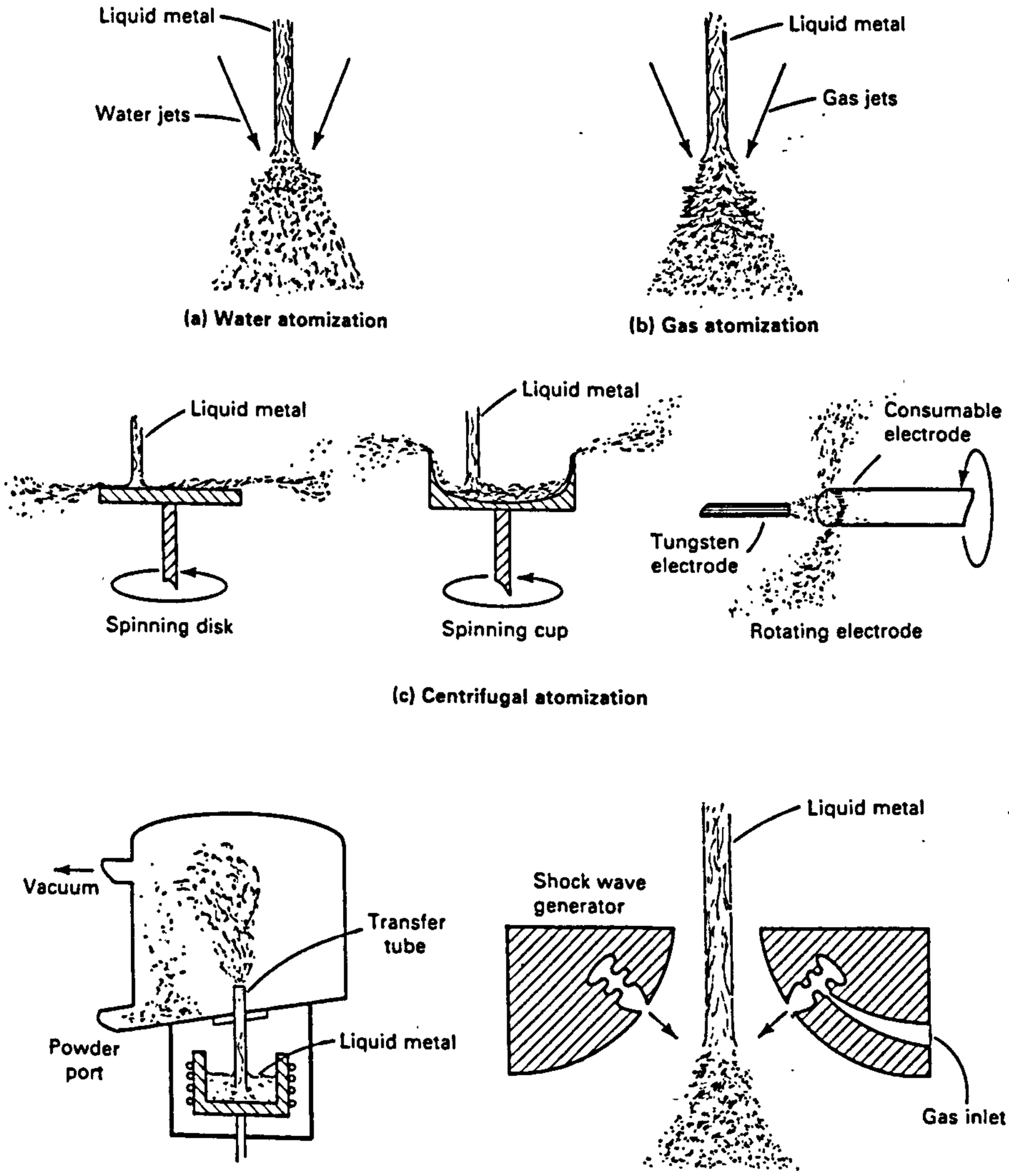

Figure 3. Schematic of Atomization Processes.[30]

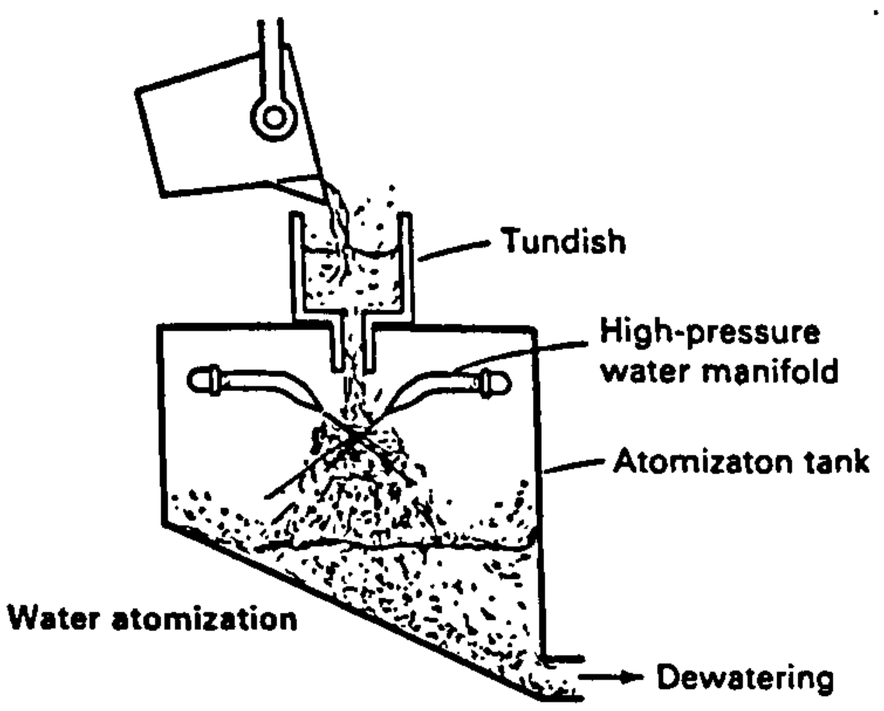

Gas atomization with fluidized bed cooling

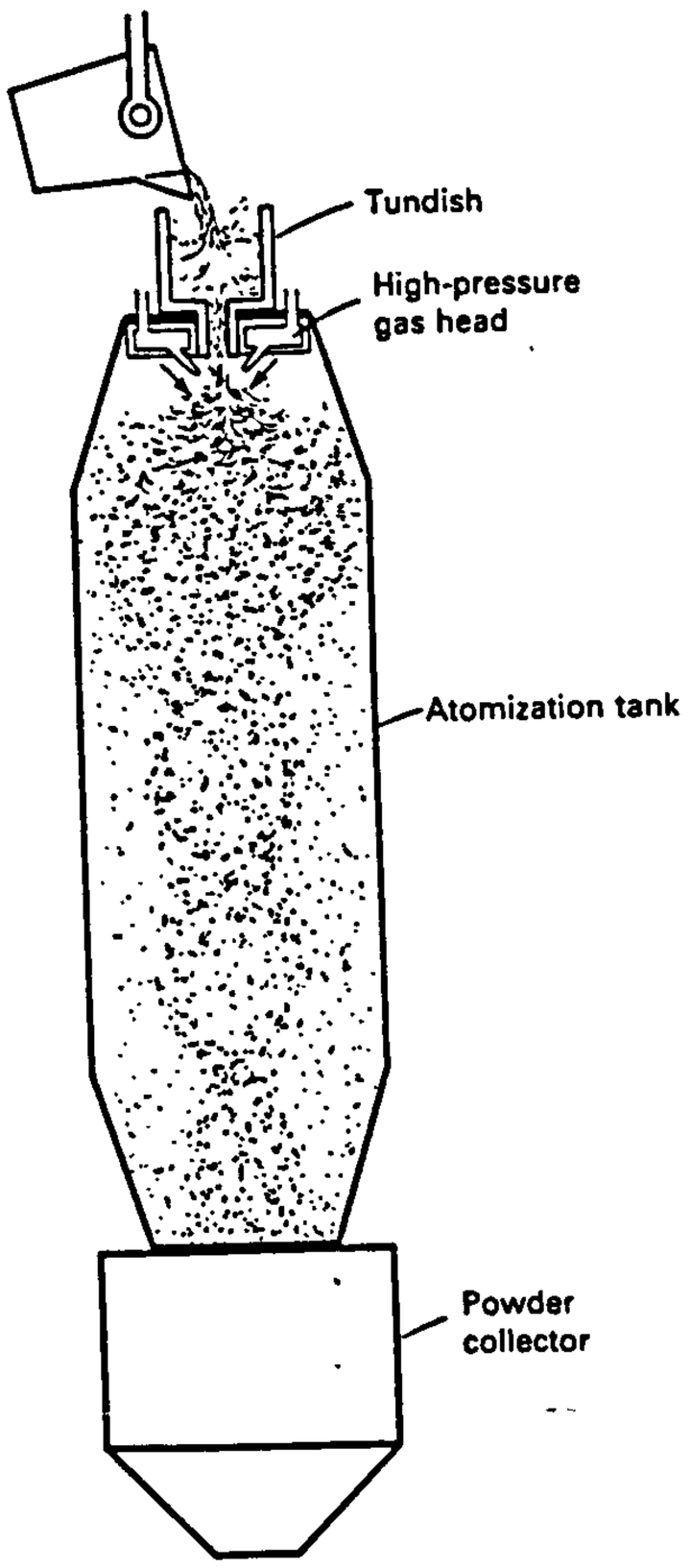

Gas atomization

Figure 4. Schematic of Water and Gas Atomisation Processes.[30]

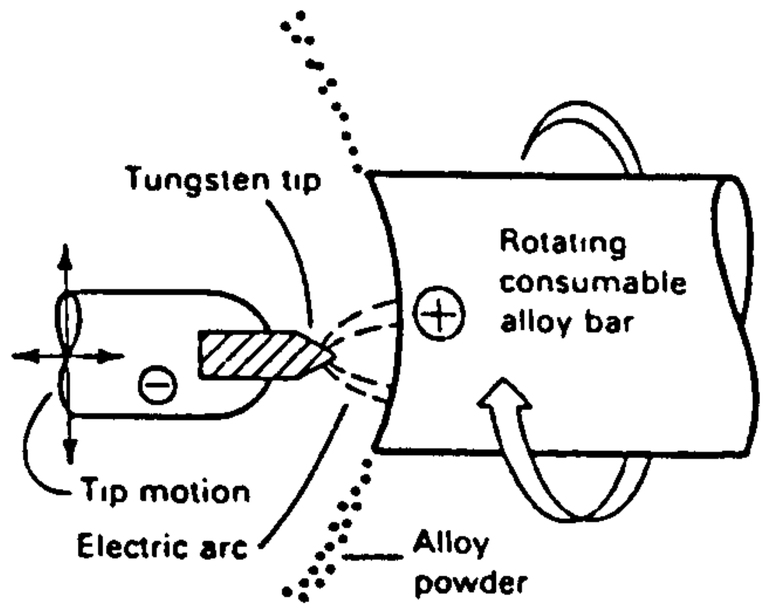

Figure 5. Schematic of Rotating Electrode Process.[34]

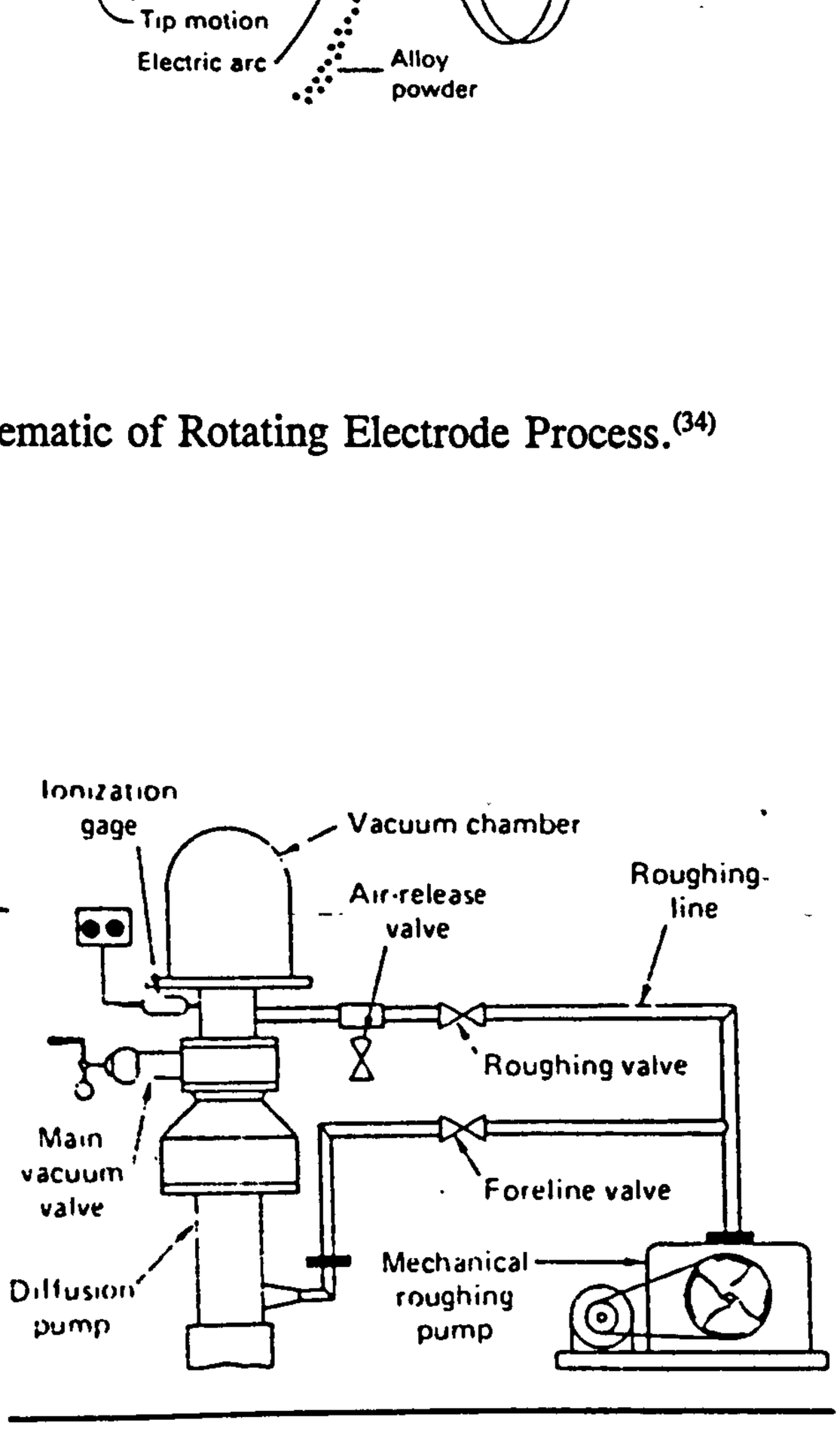

Figure 6. Schematic of Vacuum Atomization Process.[35]

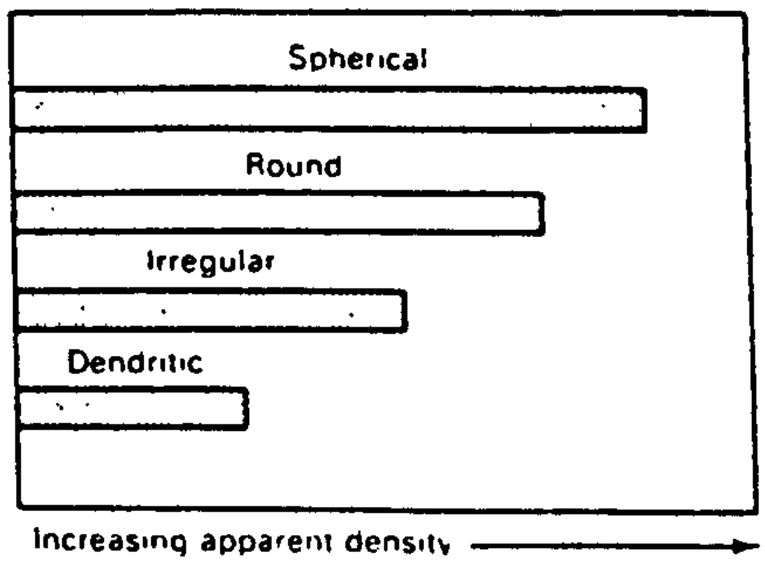

Figure 7. Effect of Particle Shape on Apparent Density of a Metal Powder.[36]

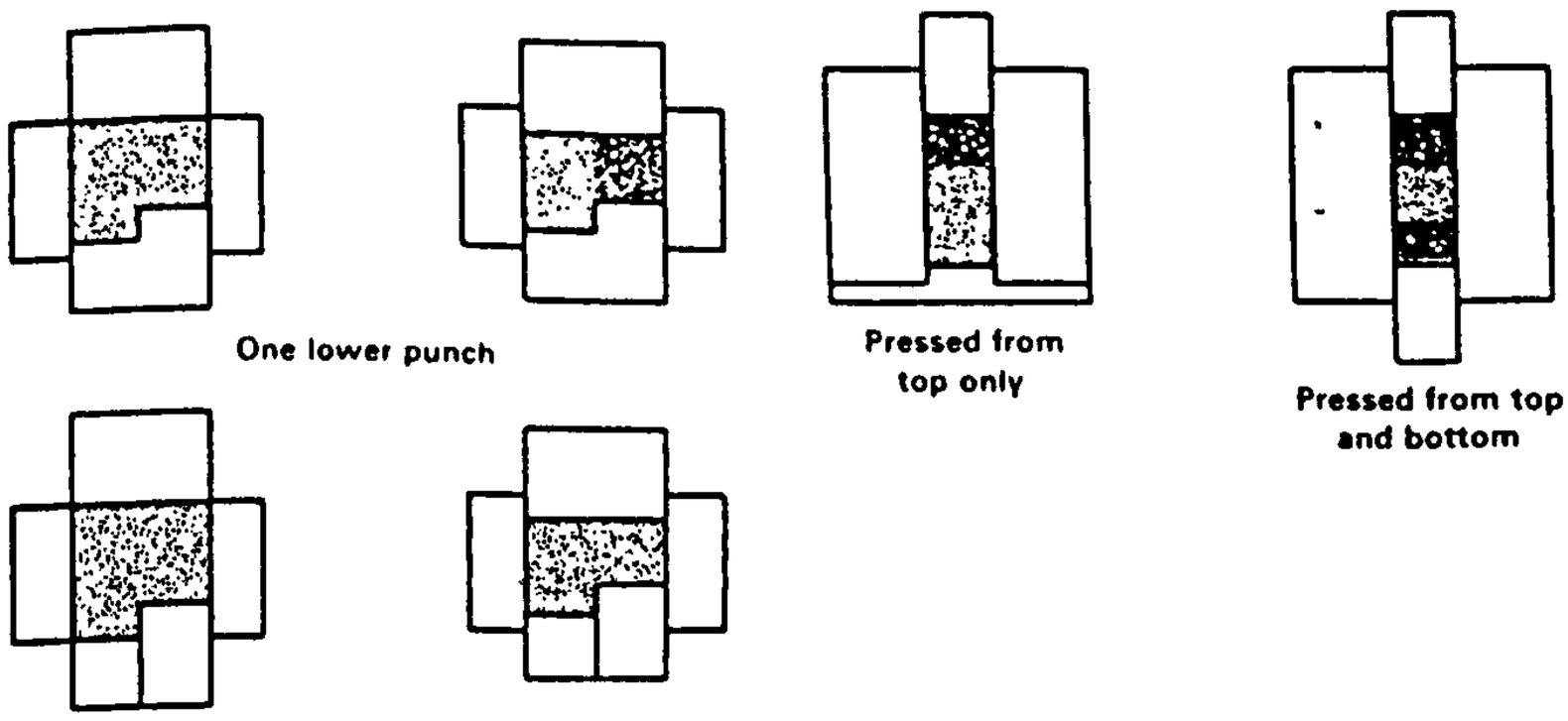

Figure 8. Density Distribution in Compacts.[37]

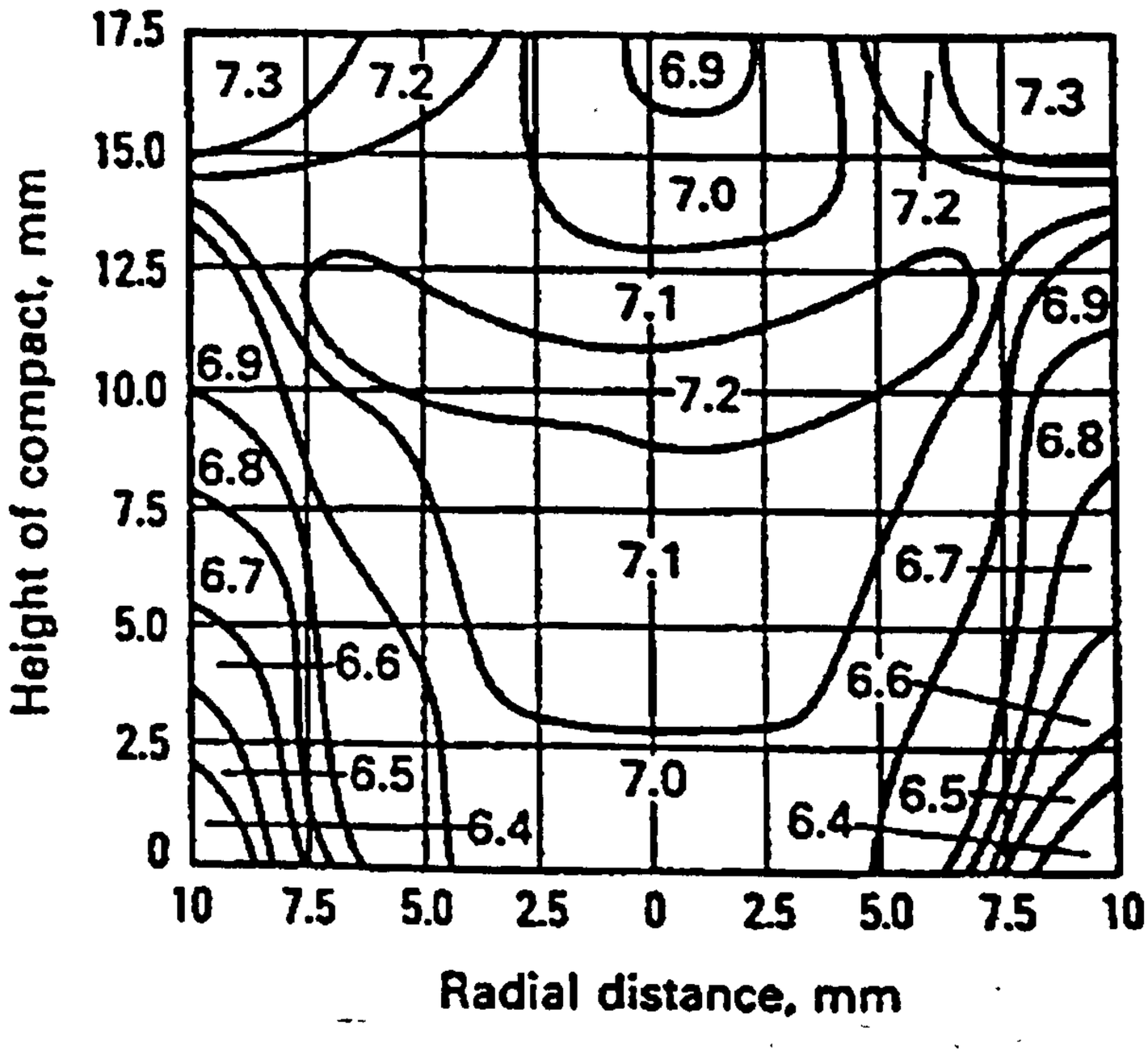

Figure 9. Density Distribution in a Cylindrical Nickel Powder Compact.[50]

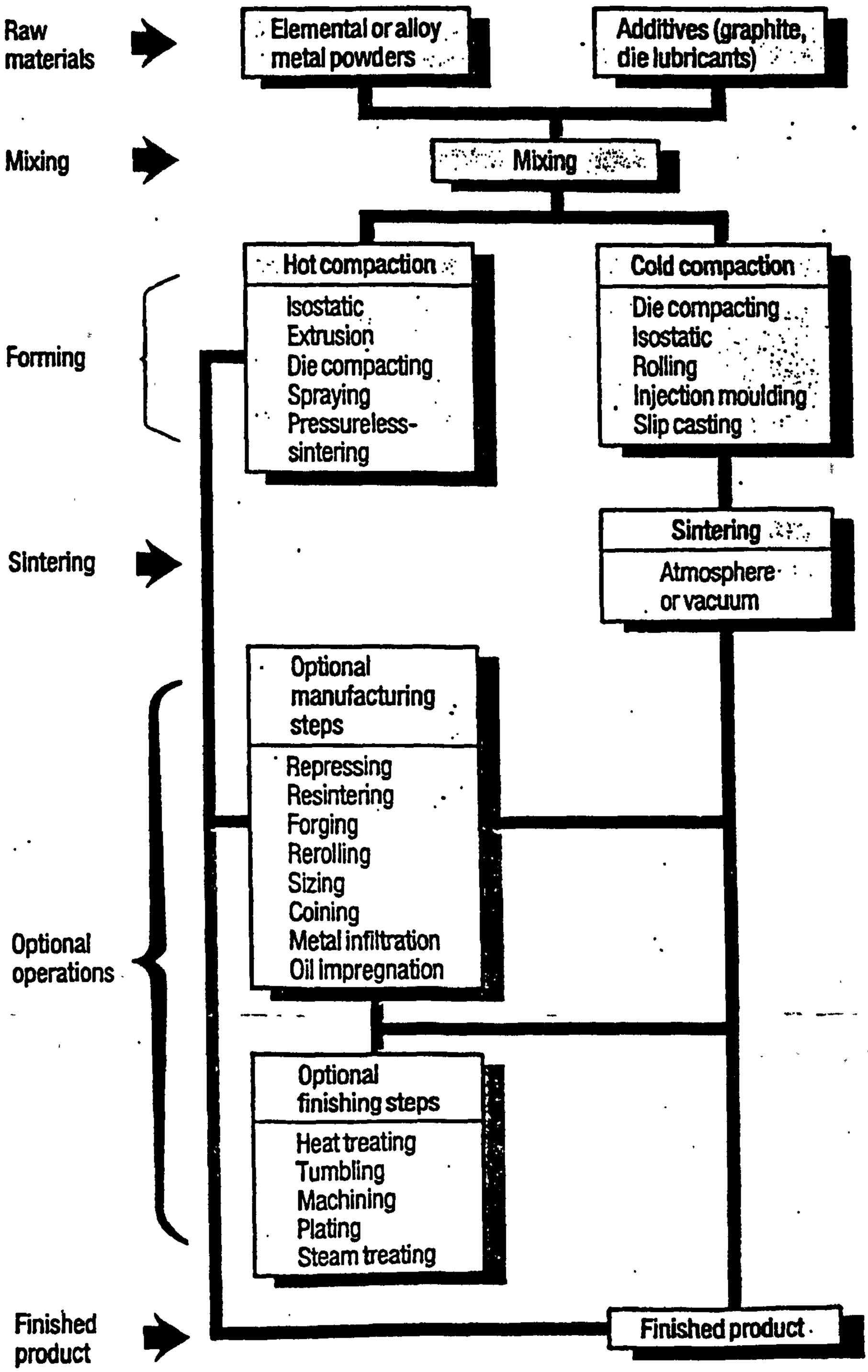

Figure 10. Processing Techniques for Powder Metallurgy.[53]

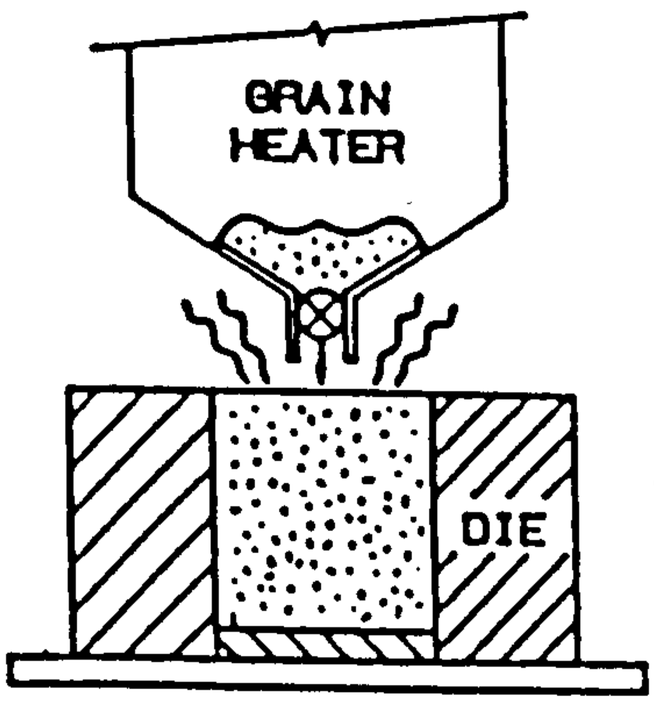

1. HEATED GRAIN FILLS THE DIE

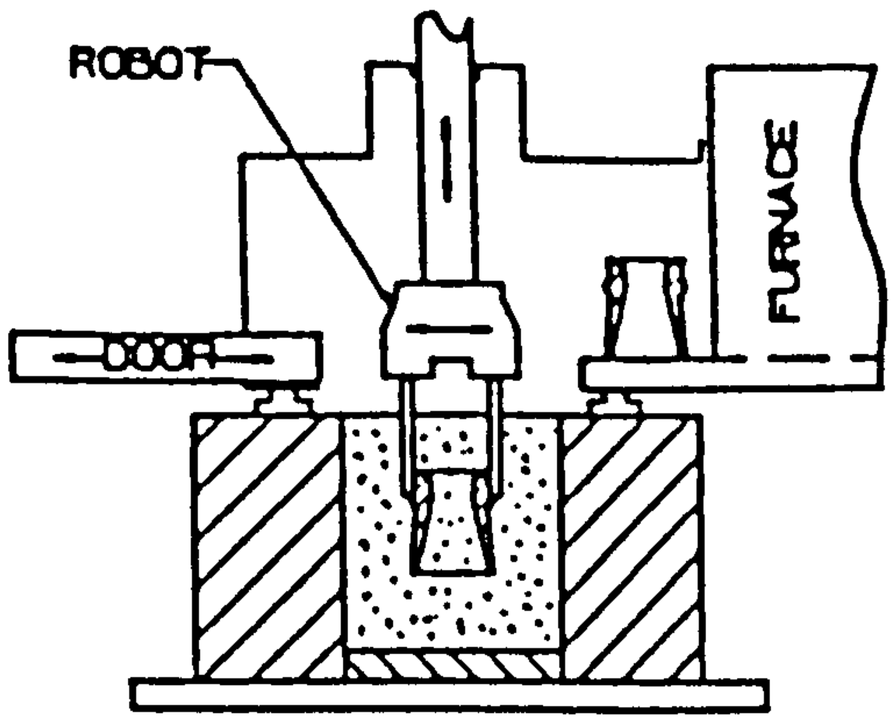

2. HEATED PREFORM IS INSERTED IN THE GRAIN BY ROBOT

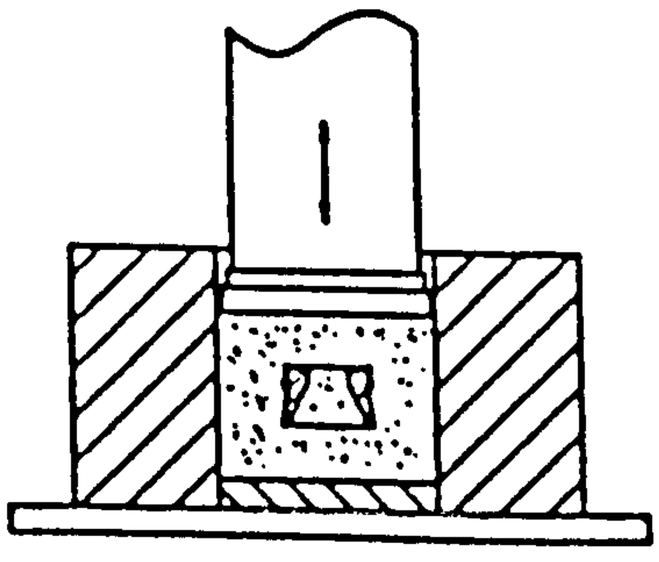

3. HYDRAULIC PRESS RAM PRESSURIZES THE GRAIN & CONSOLIDATES THE PART TO 100% DENSITY

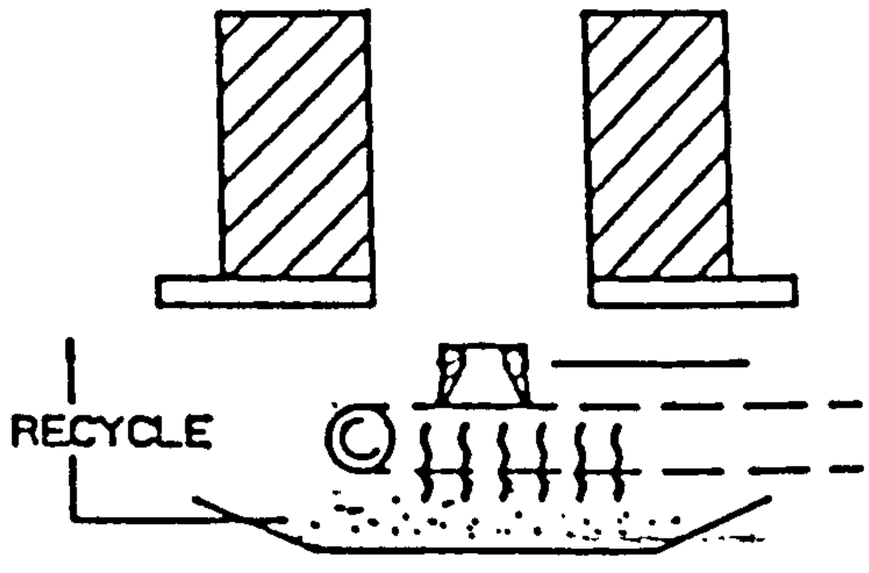

4. THE DIE IS CLEARED AND THE GRAIN IS RECYCLED

Figure 11. Ceracon Process Manufacturing Steps.[54]

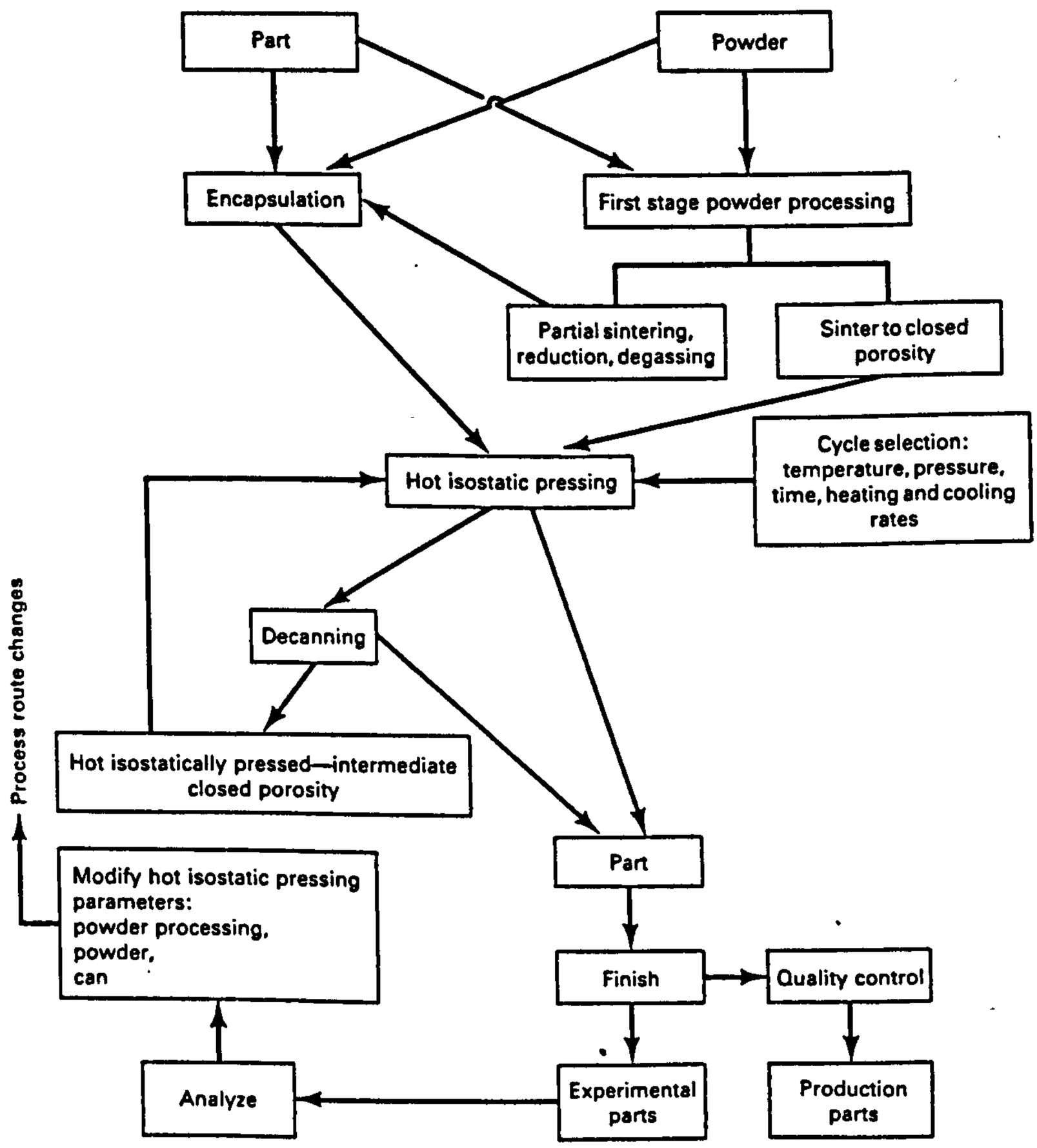

Figure 12. Flowchart for Powder Metallurgy Manufacture of Metal Parts by Hot Isostatic Pressing.[13]

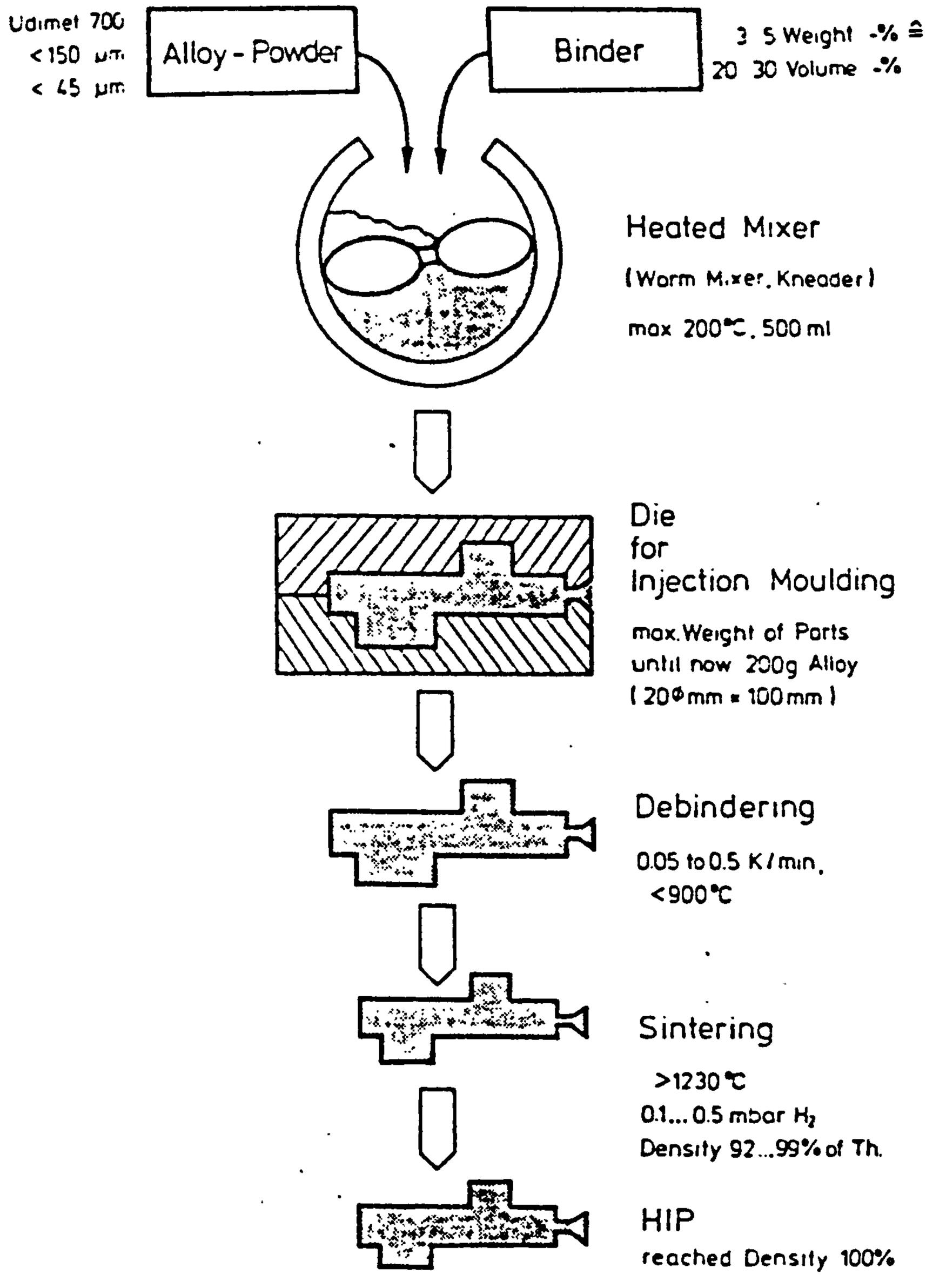

Figure 13. Scheme of the MIM-Process with Parameters for UDIMET 700.[72]

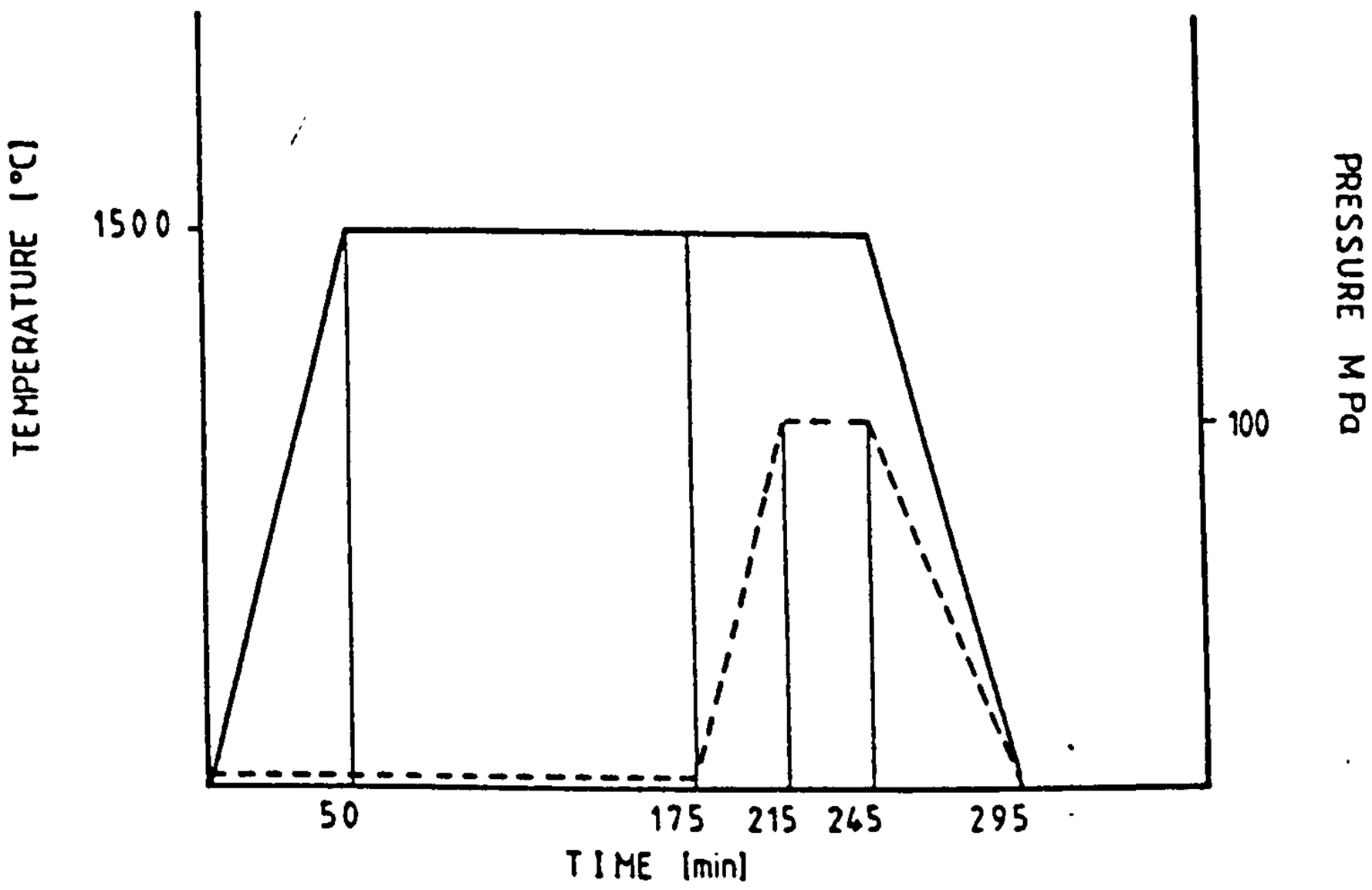

Figure 14. Sinter-HIP Cycle for Cr_2O_3 Powder.[72]

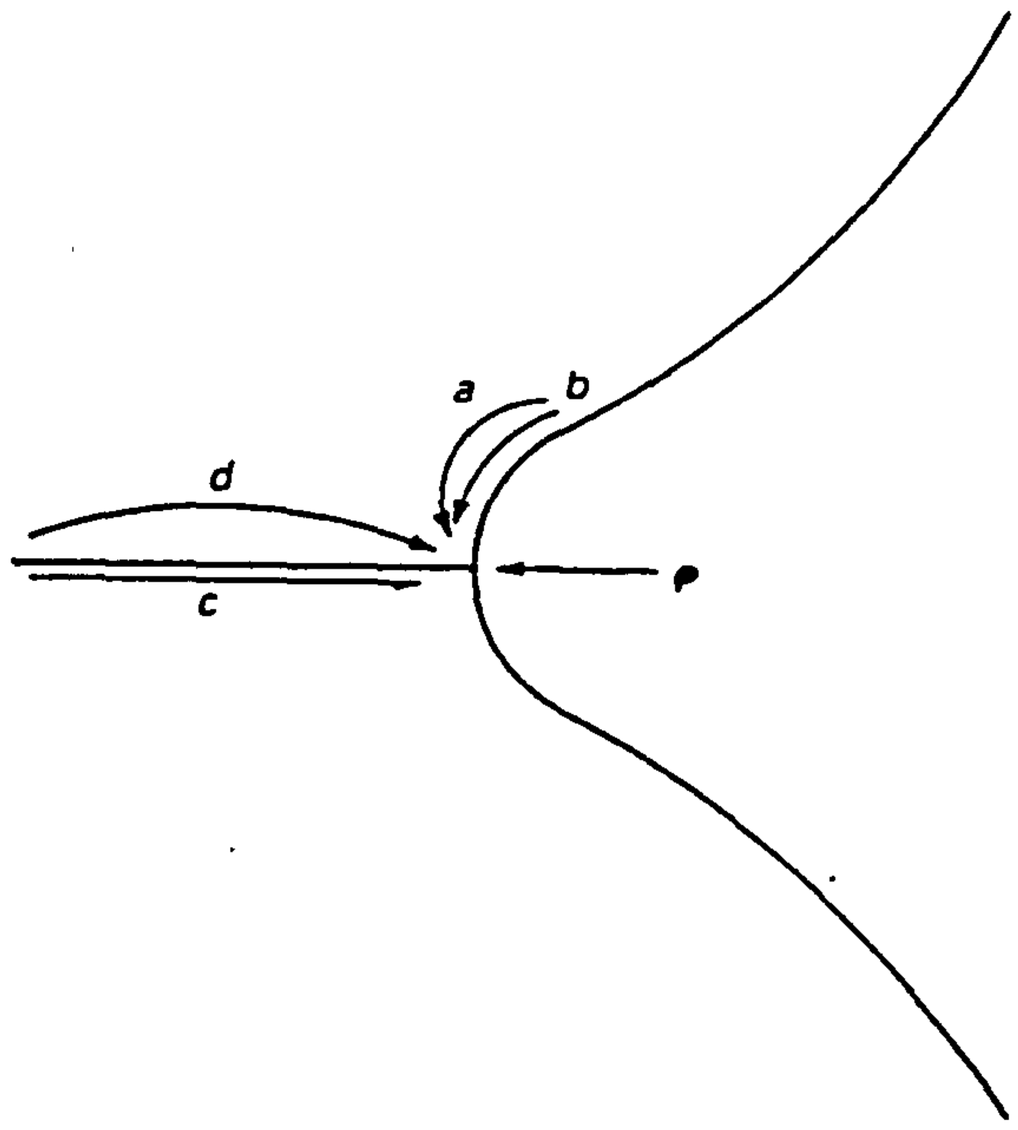

Figure 15. Types of Material Transport when Two Single Crystal Spheres with a Grain Boundary at the Interface Sinter Together.[78]

Path a - volume diffusion from the flat surface to the neck. Path b - surface diffusion from the flat surface to the neck. Path c - grain-boundary diffusion from the grain boundary to the neck. Path d - volume diffusion from the grain boundary to the neck.

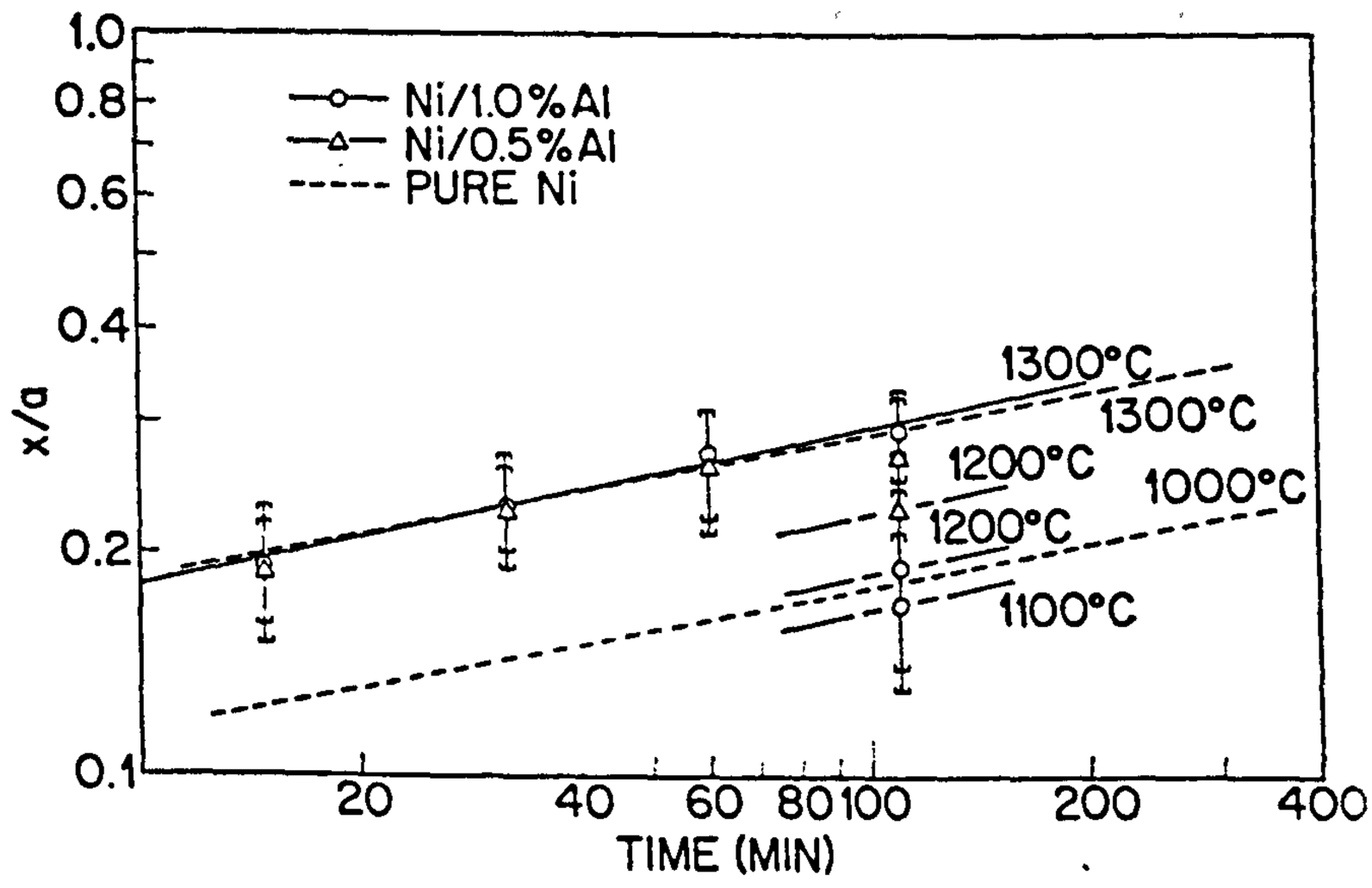

Figure 16. Neck Radius as a Function of Time During Sintering of Spherical Nickel and Nickel-Alloy Powders on to a Nickel Plate.[79]

x is the neck radius, a is the particle radius.

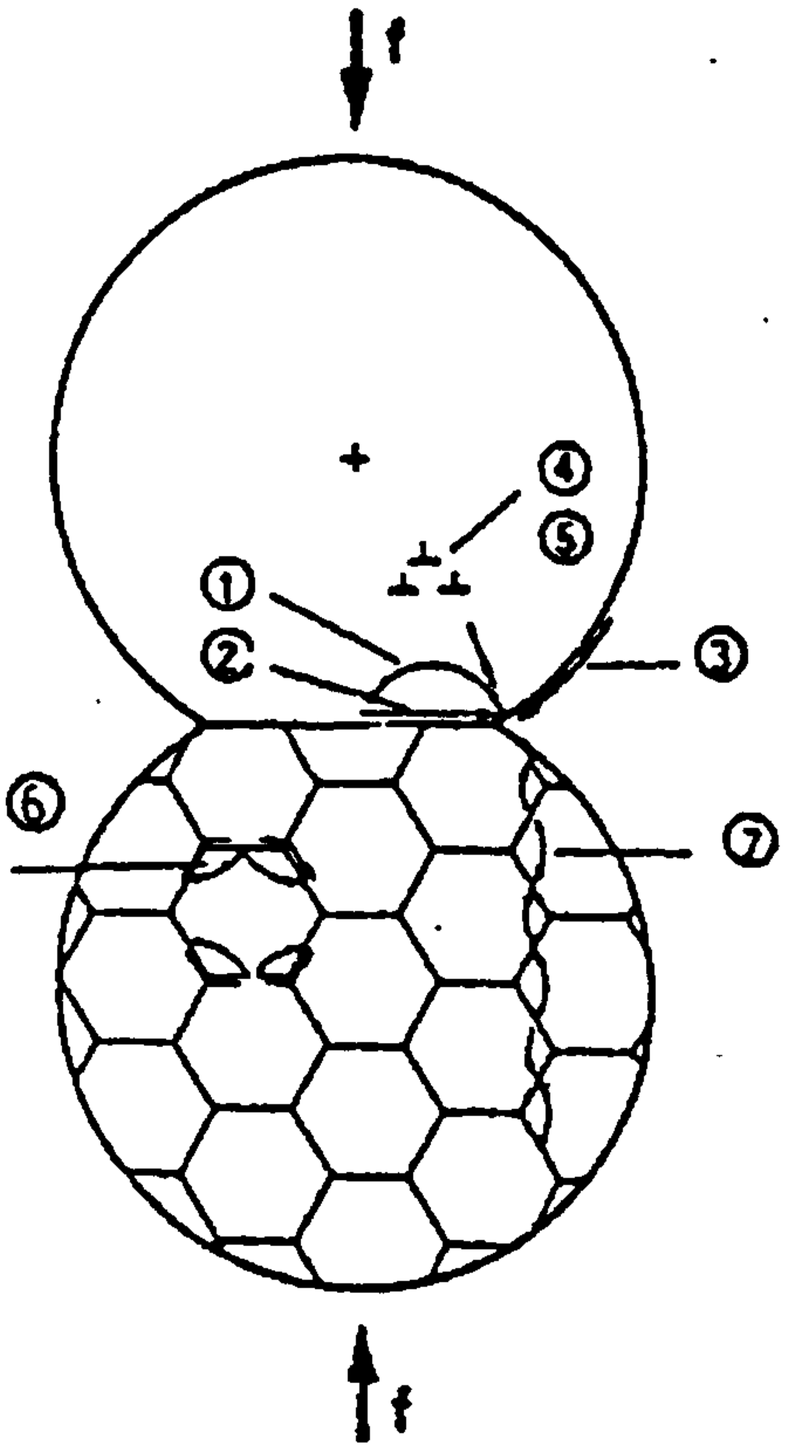

1 BULK DIFFUSION
2 GRAIN BOUNDARY DIFFUSION
3 SURFACE DIFFUSION

4 PLASTIC DEFORMATION
5 POWER-LAW CREEP

6 DIFFUSIONAL CREEP
(NH-C CREEP)
7 GRAIN BOUNDARY SLIDING

Figure 17. Transport Processes During Hot Isostatic Pressing.[80]

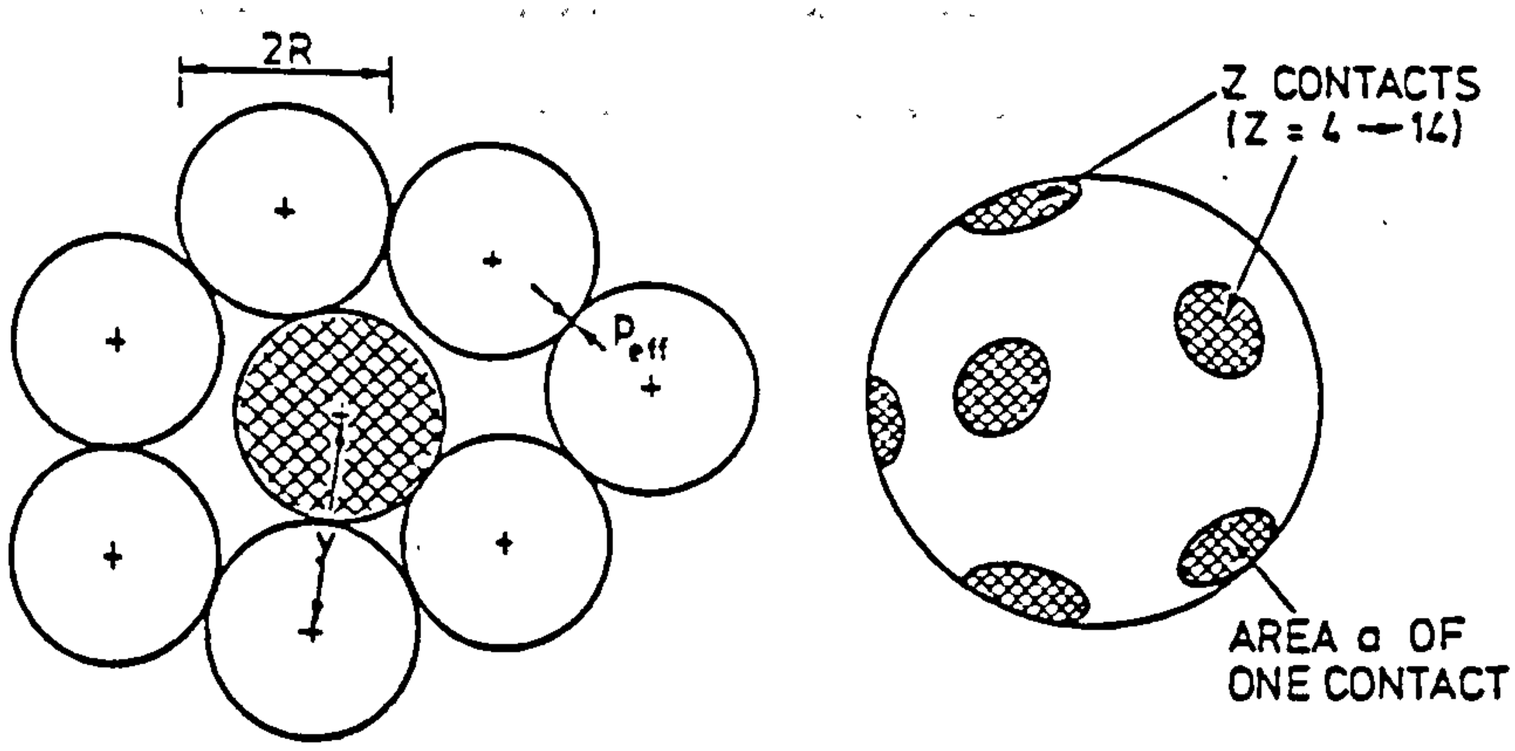

Figure 18. A Particular Particle (shaded) Contacts a Number Z of its Neighbours in Small Contact Areas, a.[121]

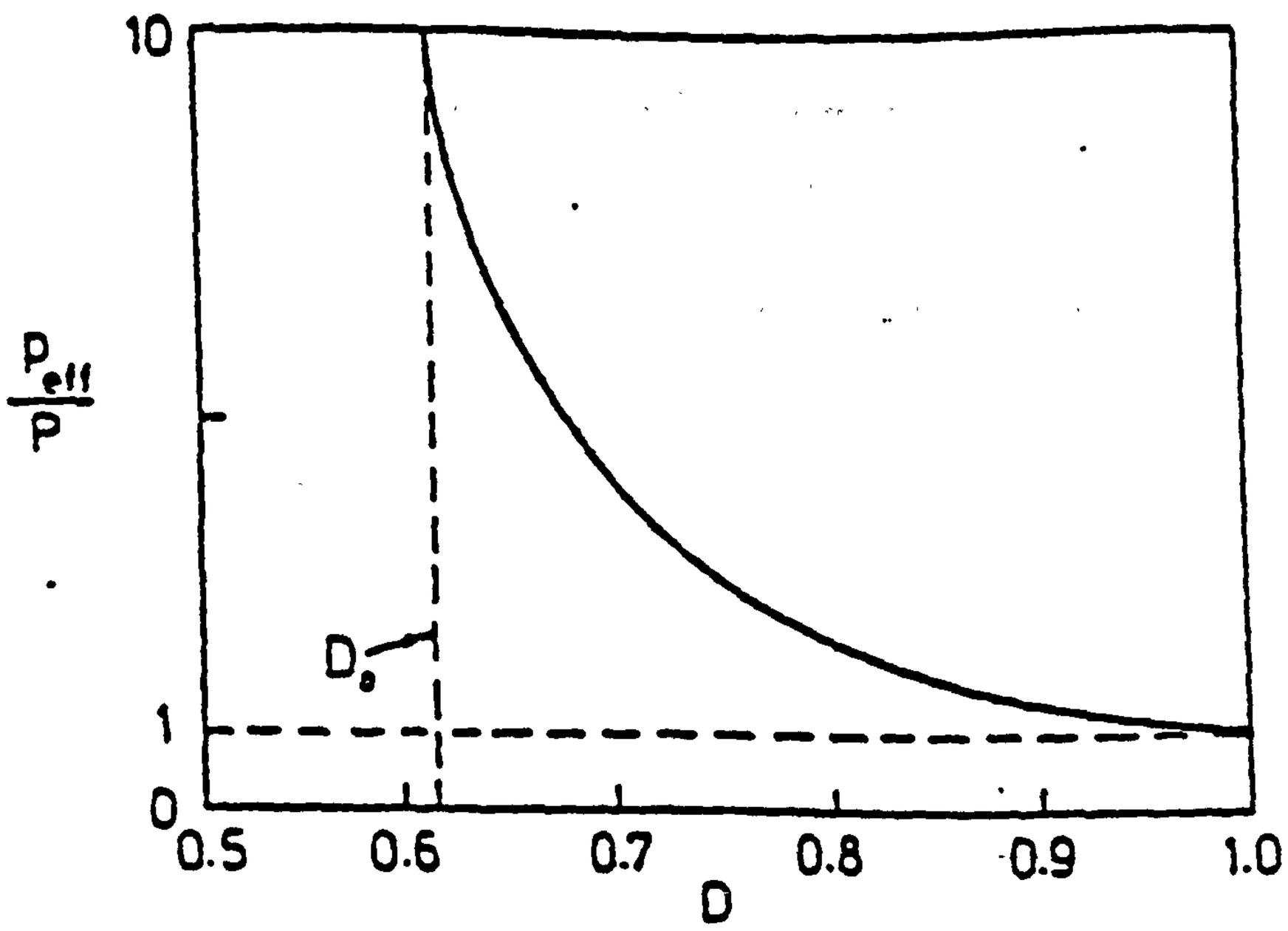

Figure 19. The Effective Pressure at a Contact (the force per unit area).[121]

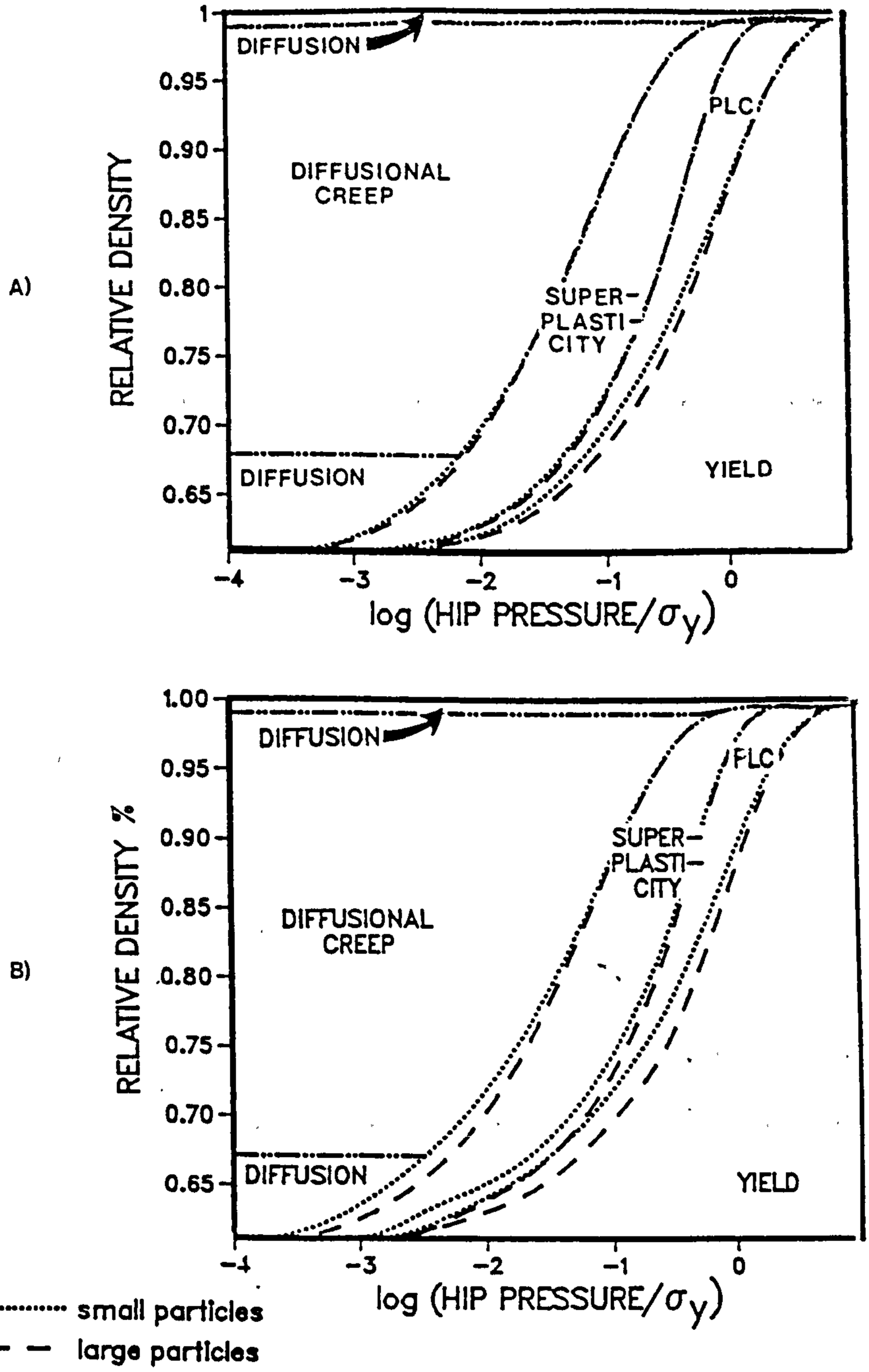

Figure 20. HIP Maps for Bimodal Distributions of Rene 95 (weight fractions of 10% and 90% for the small and large particles respectively).[131]

HIP temperatures and R_2/R_1 are a) 1100 °C and 2.3, and b) 1100 °C and 5.0.

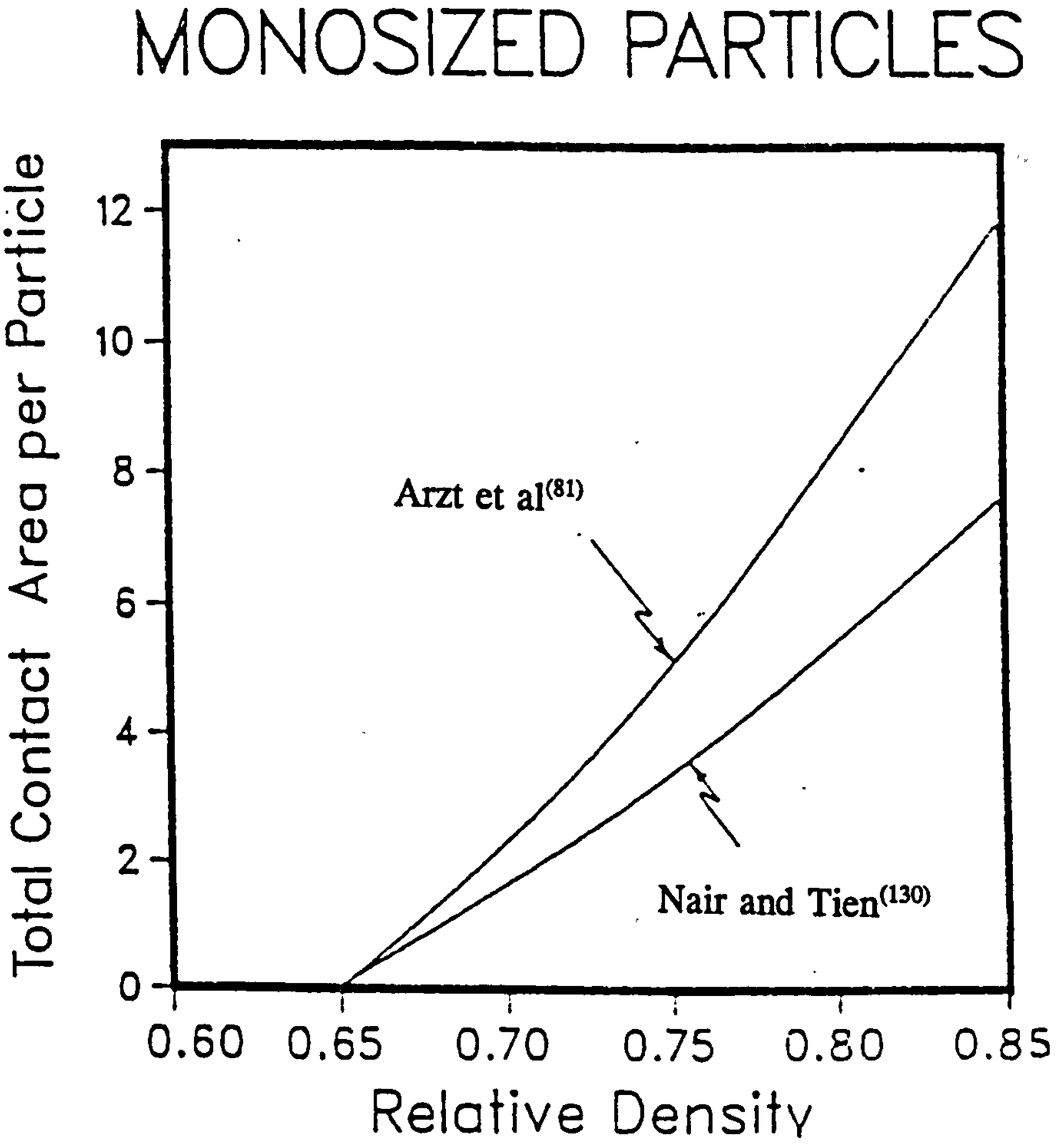

Figure 21. The Growth of the Total Contact Area on Each Particle as Densification Progresses for the Monosized Case.[130]

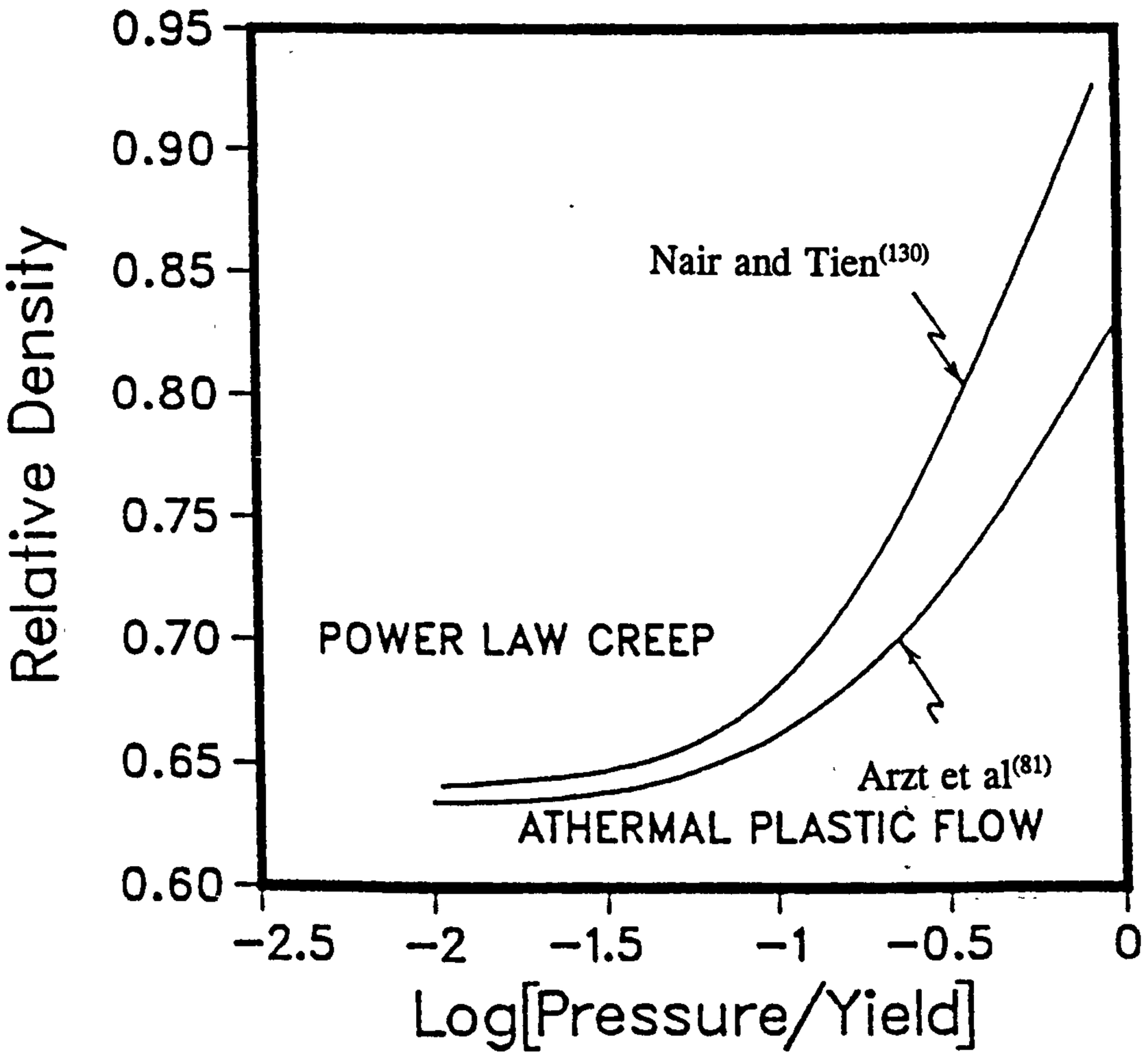

Figure 22. The Densification Mechanism Map for the Monosized Case.[130]

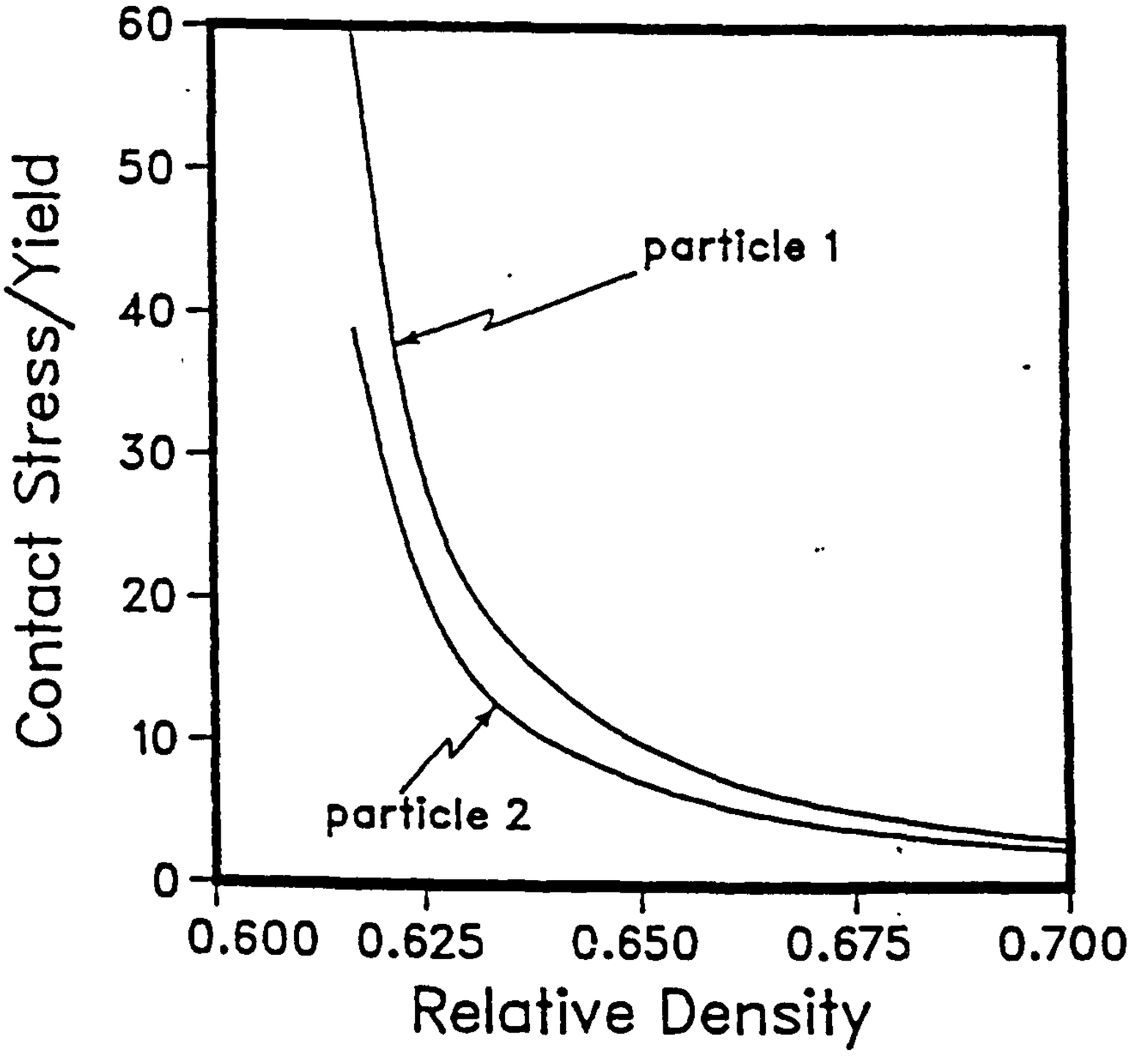

Figure 23. The Average Interparticle Contact Stress Normalised to the Yield Stress Plotted as a Function of the Relative Density for Particles 1 and 2 (small and large respectively).[130]

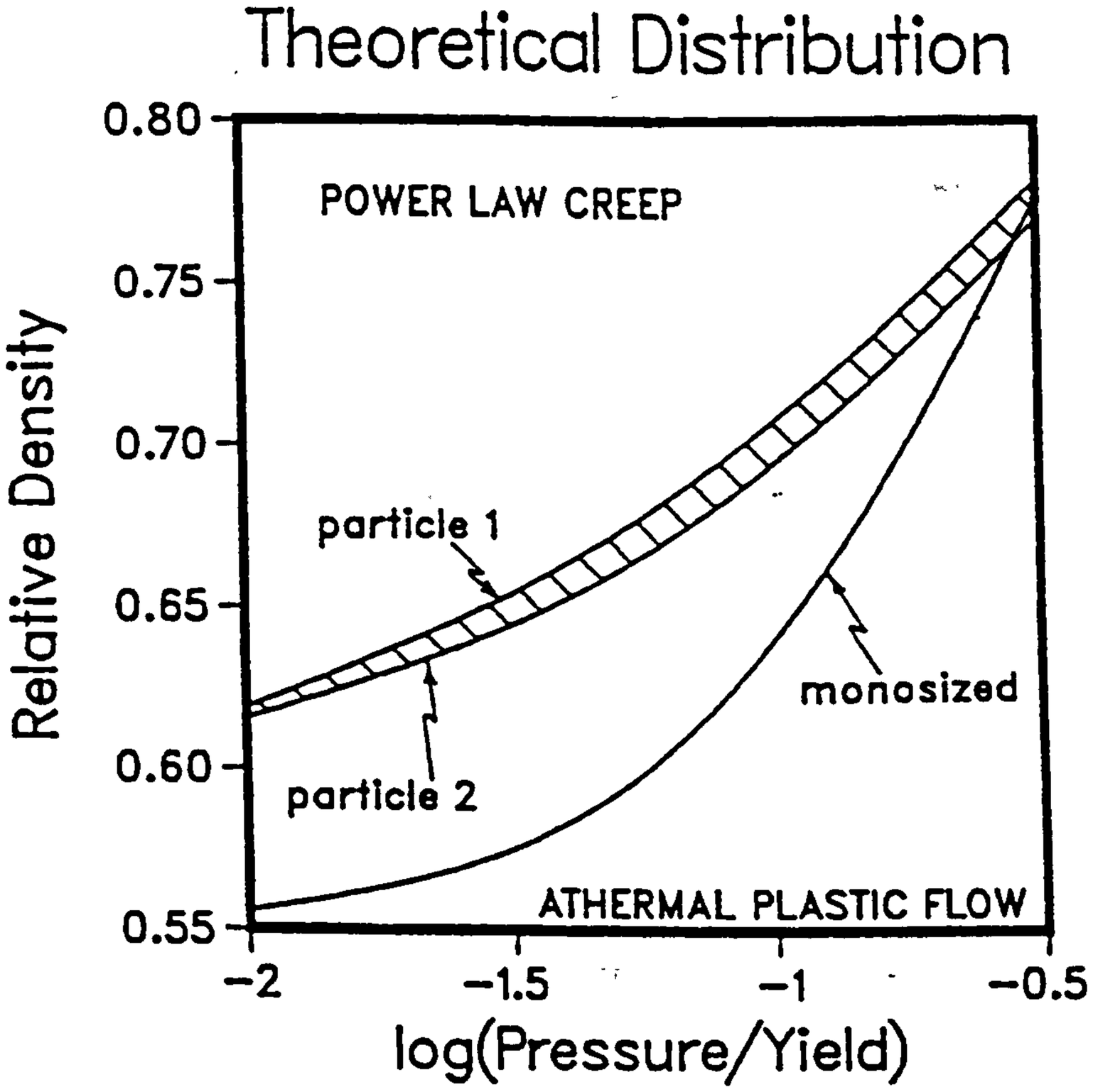

Figure 24. Densification Mechanism Map for a Bimodal Distribution of Powders in Comparison with that for the Monosized Case.[130]

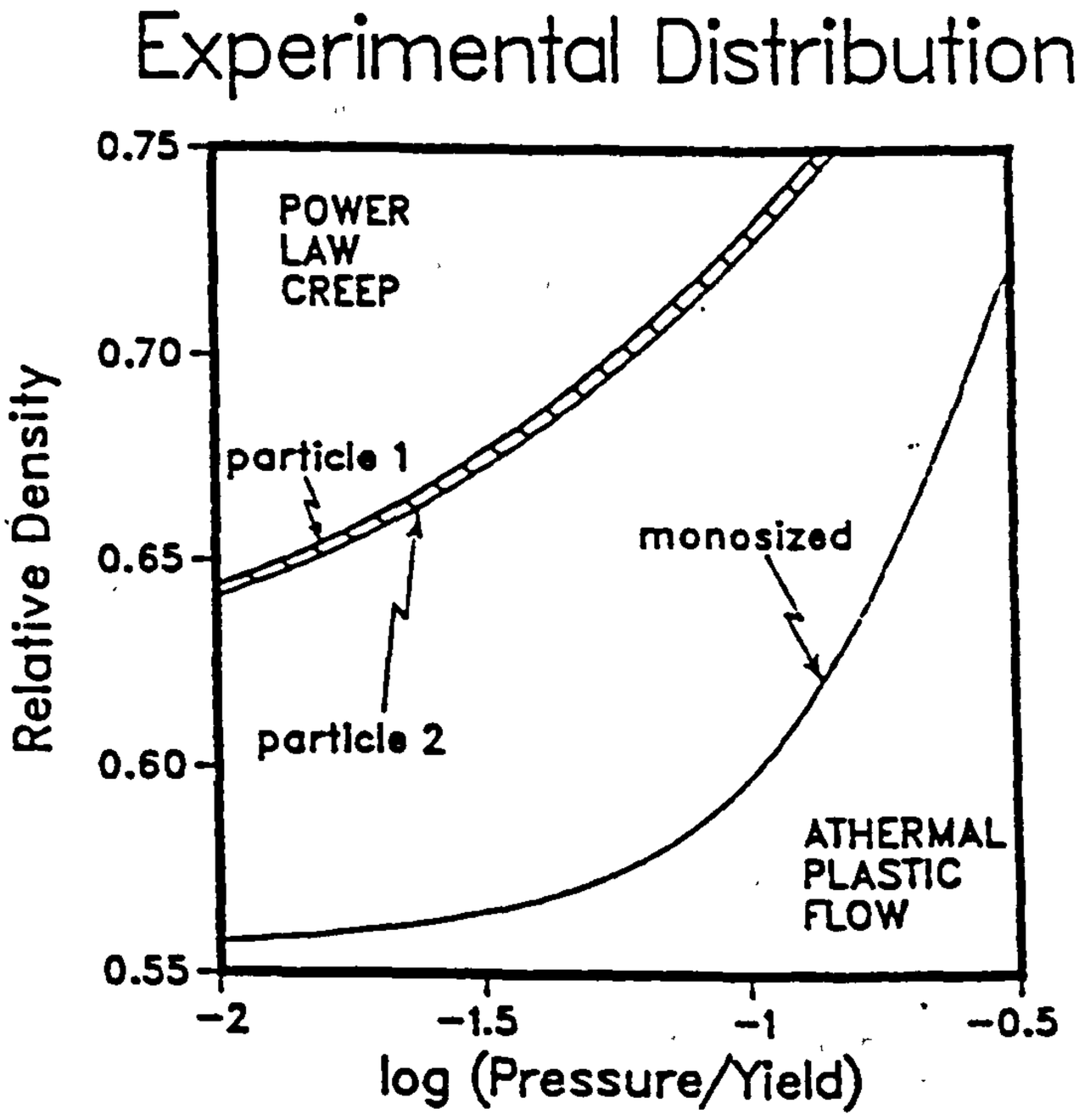

Figure 25. Densification Mechanism Map for a Bimodal Distribution of Powders in Comparison with that for the Monosized Case.[130]

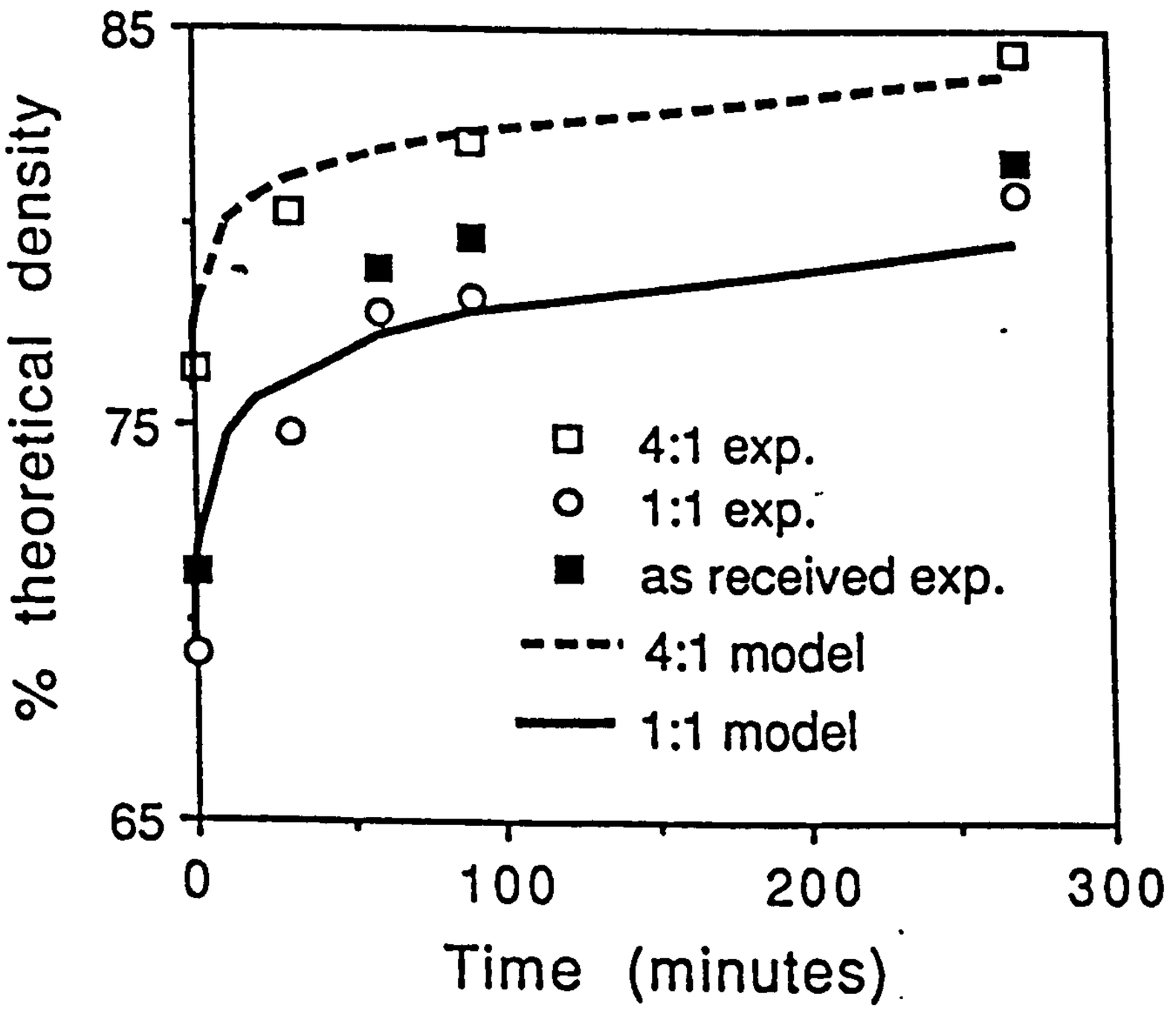

Figure 26. Consolidation Behaviour of Monosized, Bimodal, and As-Received Packings for a 316L Stainless Steel Powder.[134]

HIP was performed at 840 °C and 44 MPa.

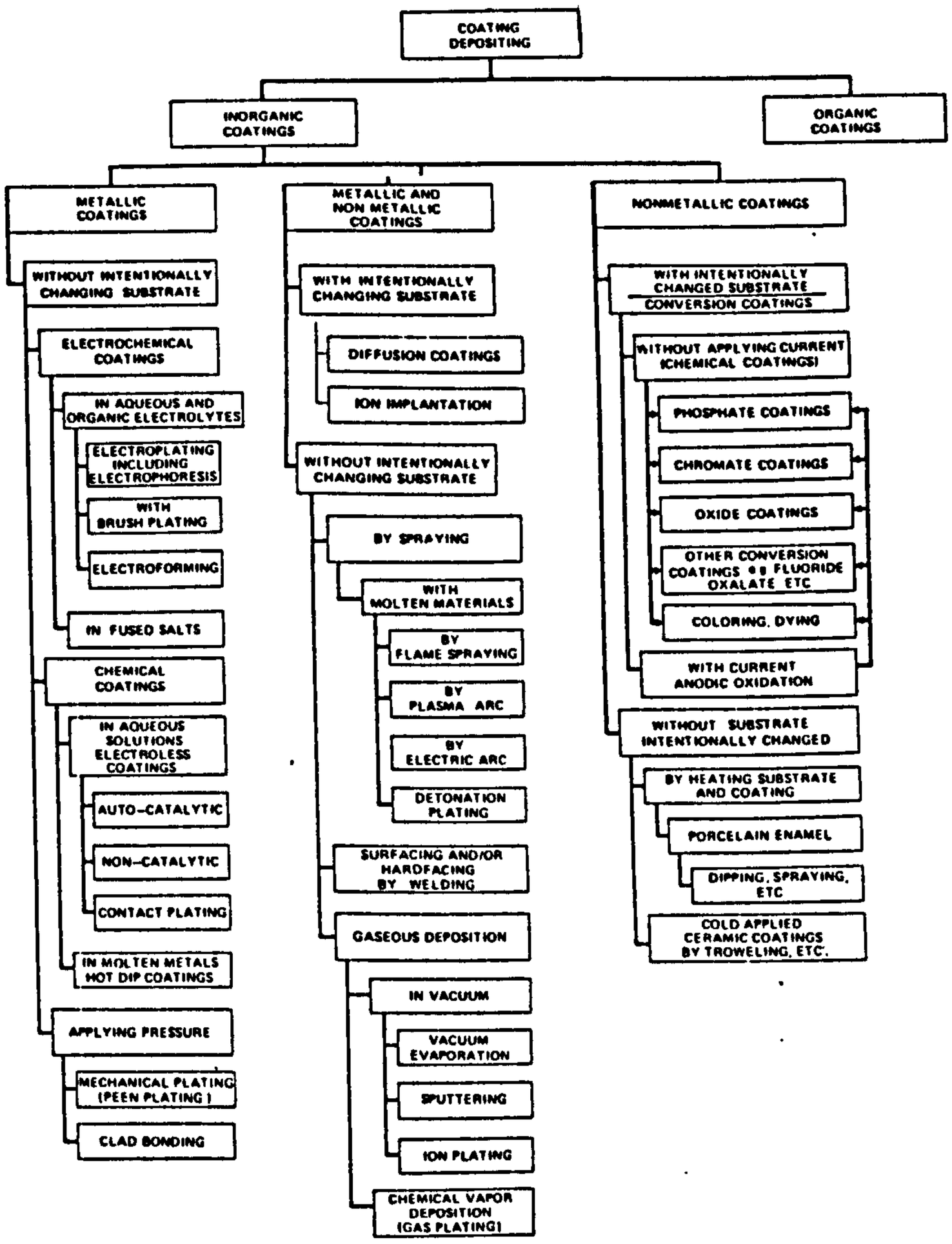

Figure 27. Heterogeneous System for Coating Classification.[137]

	Gaseous (vapour) phase			Liquid phase		Molten, semi-liquid phase		
	PVD	CVD	Ion implantation	Sol-gel	Electro-deposition	Laser	Thermal spraying	Welding
Thickness (mm)	Up to 0.3	Up to 0.5	~0.005	0.002	0.02–0.5	0.05–2	0.05–2	1–20 or more
Deposition rate (kgh^{-1})	Up to 0.5 per source	Up to 1	–	0.1–0.5	0.1–0.5	0.1–1	0.1–10	3–50
Component size	Limited by chamber size			Limited by solution bath		No practical limits*		
Substrate material	Wide choice	Limited by deposition temperature	Wide choice	Wide choice	Wide choice	Wide choice		Mostly steels
Pre-treatment	Chemical plus ion bombardment	Various	Chemical plus ion bombardment	Grit blast and/or chemical clean	Chemical cleaning and etching	Mechanical and chemical cleaning		
Post-treatment	None	Substrate stress relief/mechanical properties	None	High temperature calcine		None/Substrate stress relief		
Control of deposit thickness	Good	Fair/Good	Good	Fair/Good	Fair/Good	Manual – Variable Automated – Good		
Bonding mechanism	Atomic	Atomic	–	Surface forces		Mechanical/Chemical		Metallurgical
Distortion of substrate	Low	Can be high	Low	Low	Low	Low/Moderate		Can be high

* Some variants of these processes have chamber size limitations.

Figure 28. Comparison of Surface Engineering Techniques.[138]

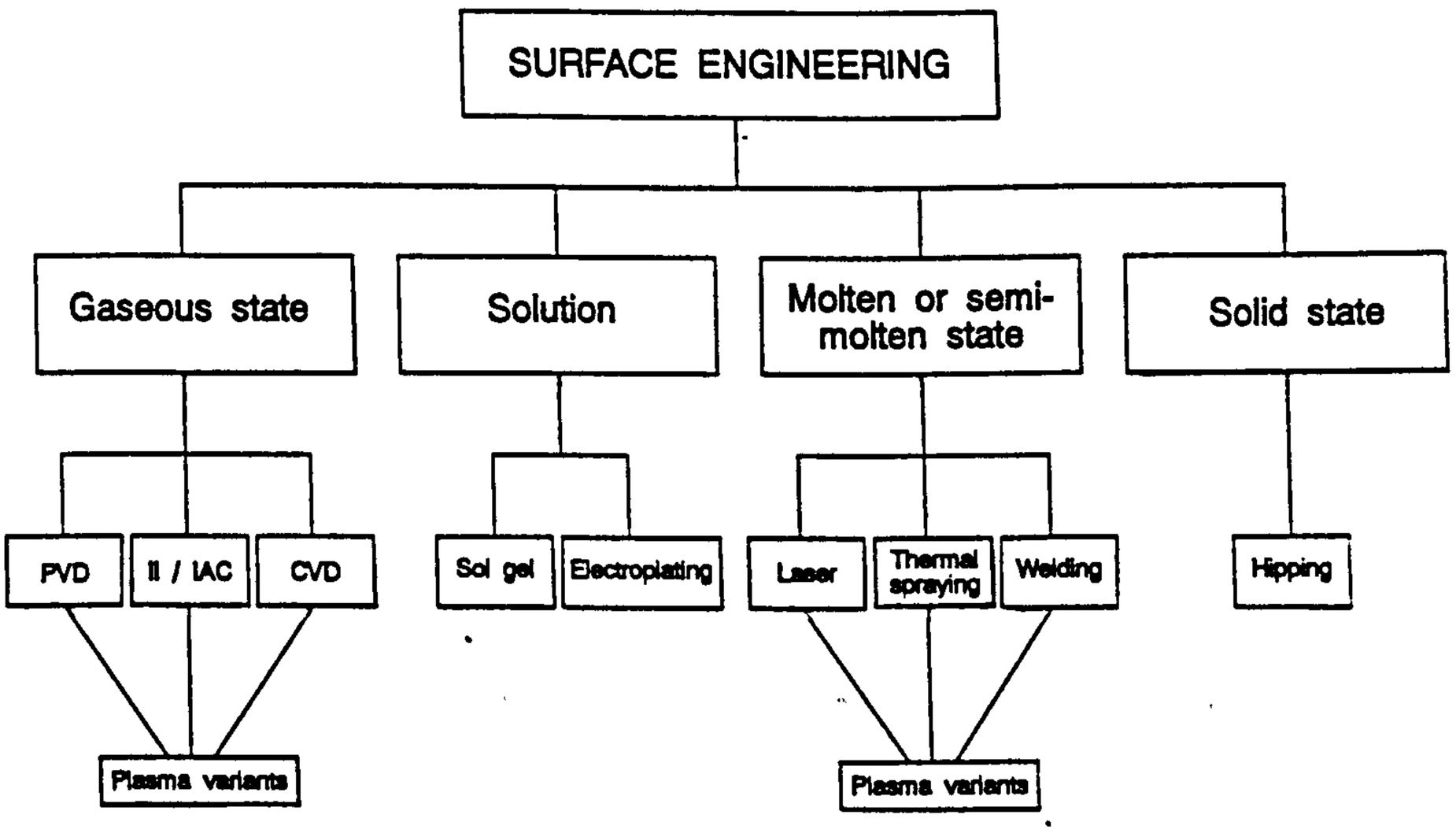

Figure 29. A General Classification of Surface Engineering Techniques.[138]

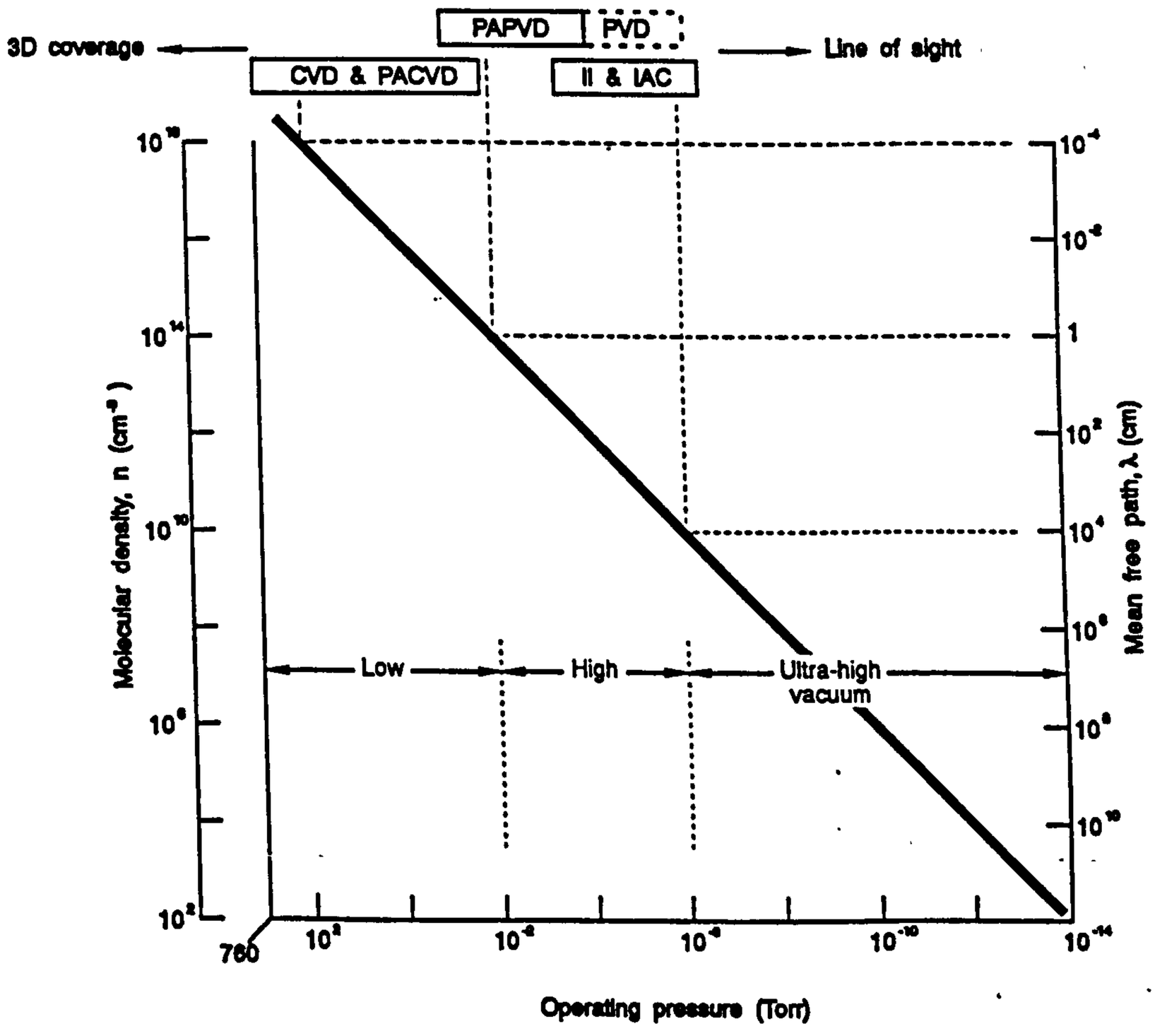

Figure 30. The Ability of Vapour Phase Processes to Coat Complex Component Geometry is Dictated by the Degree of Gas-Scattering, as Determined by the Mean Free Path.[138]

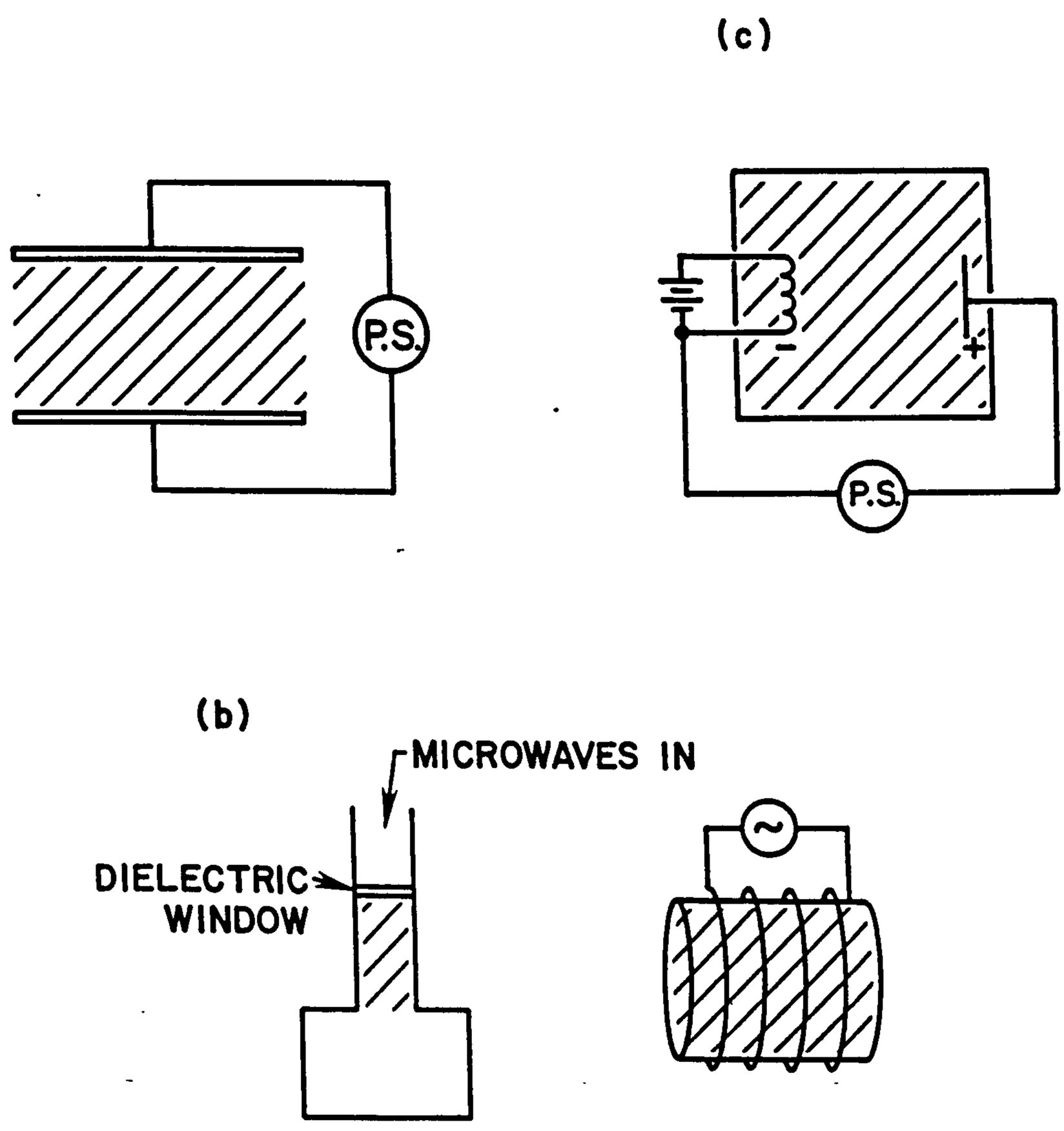

Figure 31. The Generation of Plasmas.[138]
a) Typical Plasma Excited Between Two Powered Electrodes.
b) Plasma Induced by Electric Fields Through a Non-Conducting Wall or Window.
c) Plasma Induced by Acceleration of Electrons Emitted from a Hot Filament.

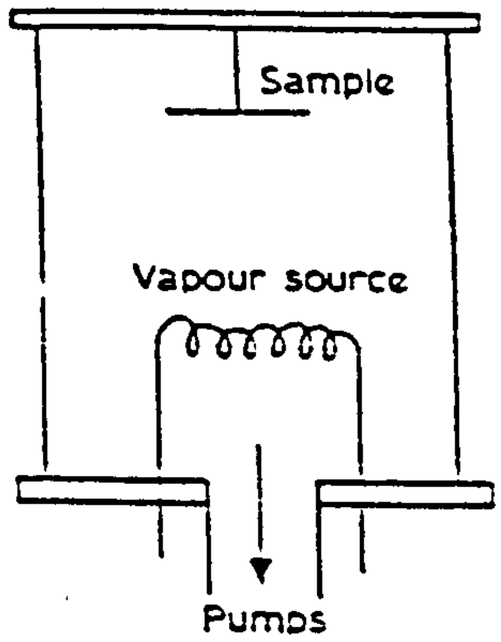

Figure 32. Schematic for Vacuum Evaporation.[137]

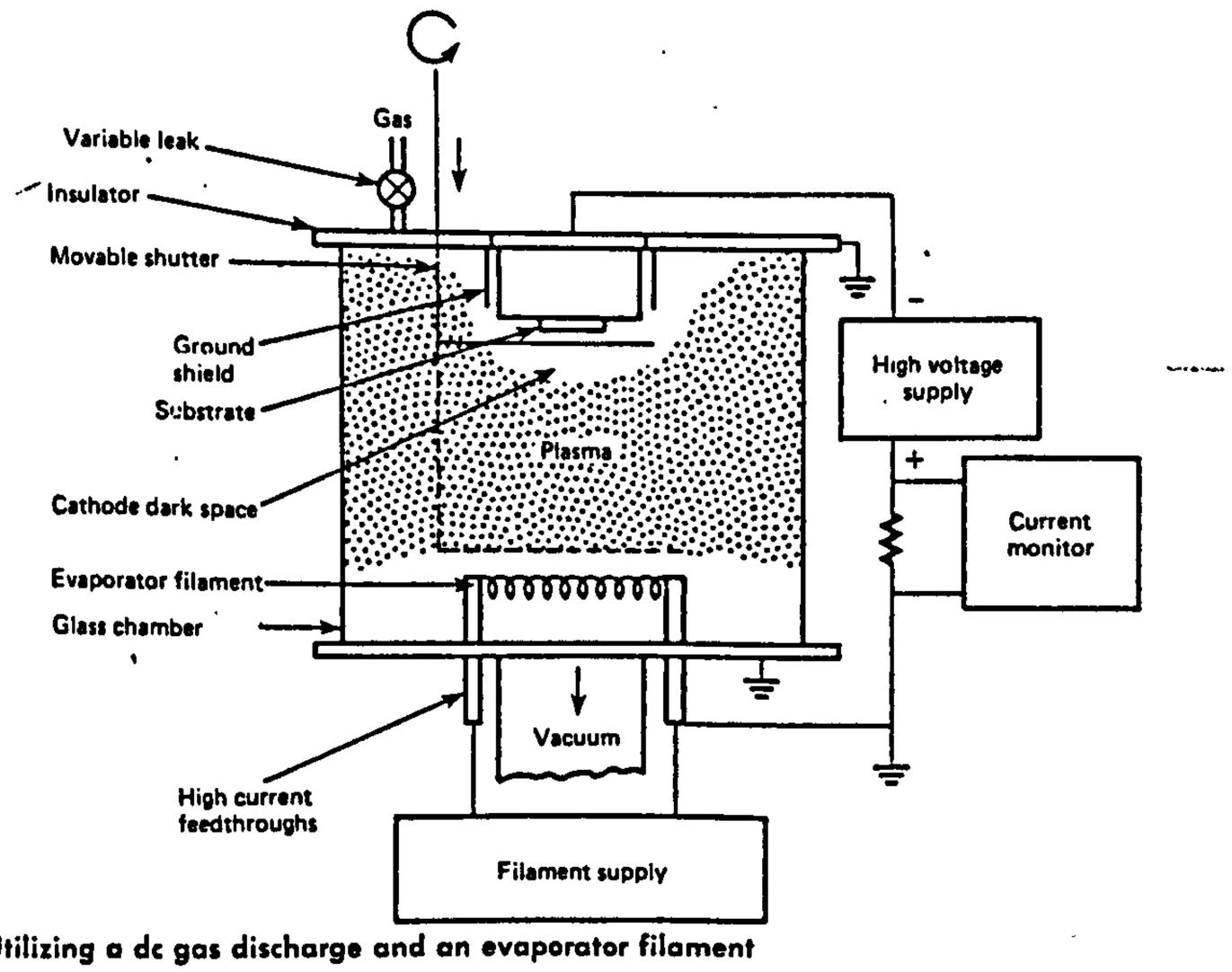

Figure 33. Schematic for Ion-Plating.[141]

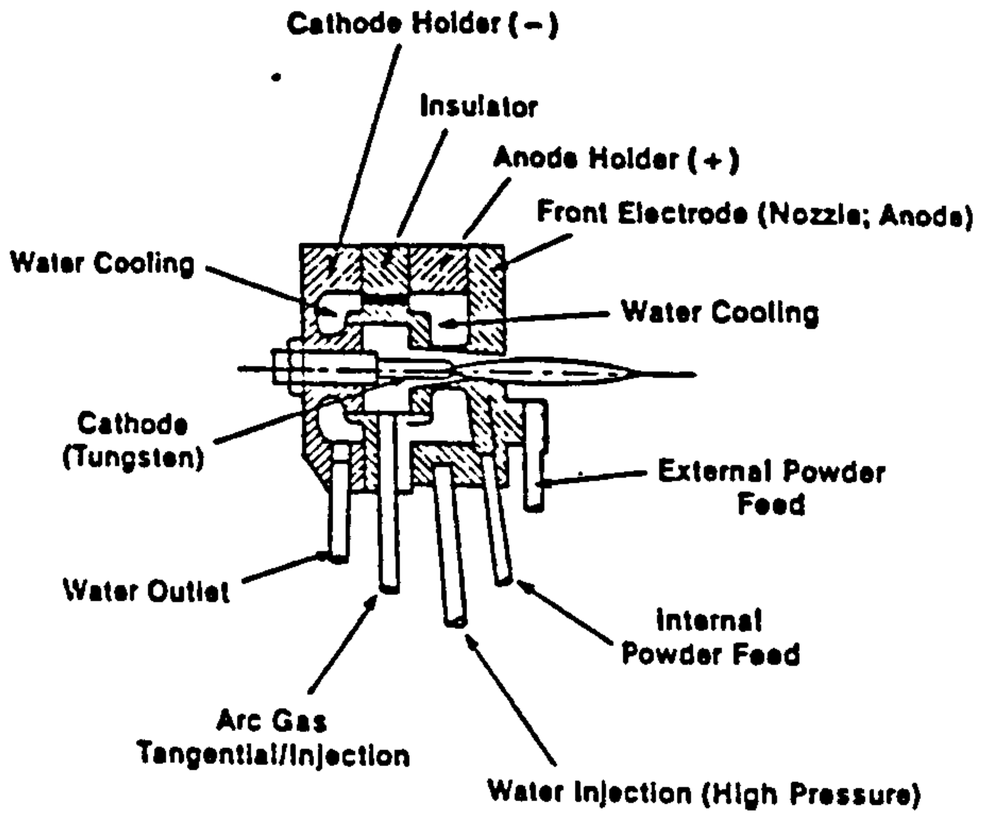

Figure 34. Schematic of Typical Plasma Spray Gun.[145]

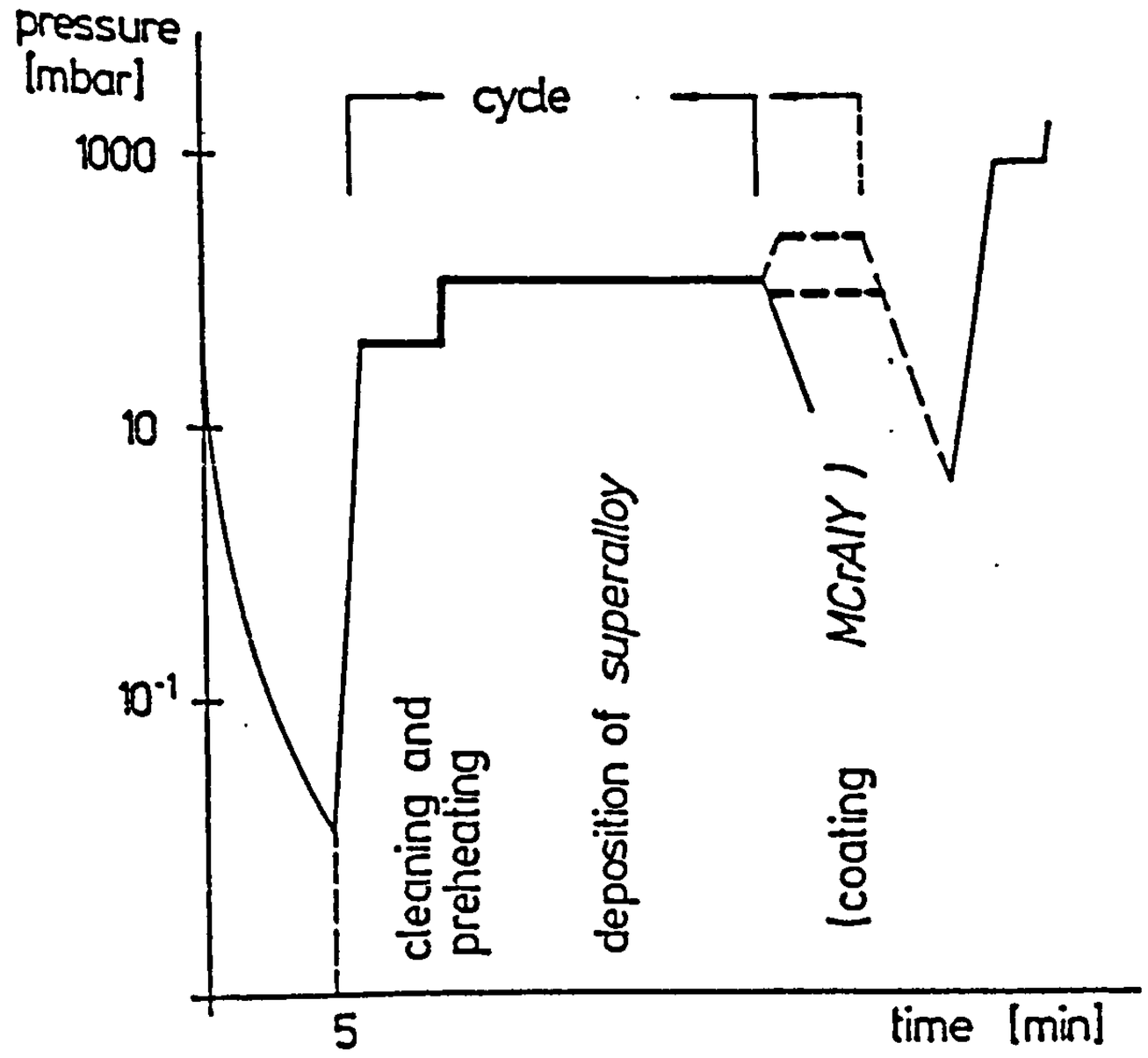

Figure 35. Time vs. Pressure Diagram of a Vacuum Plasma Spray Repair and Coating Process.[147]

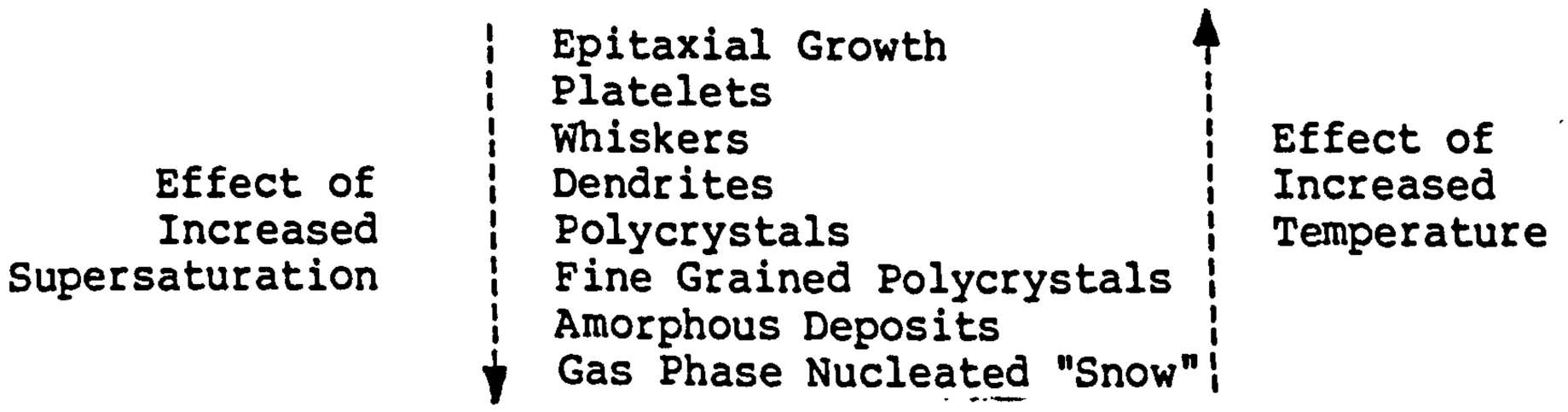

Figure 36. The Influence of Temperature and Supersaturation on the Substrate of Condensed Materials.[154]

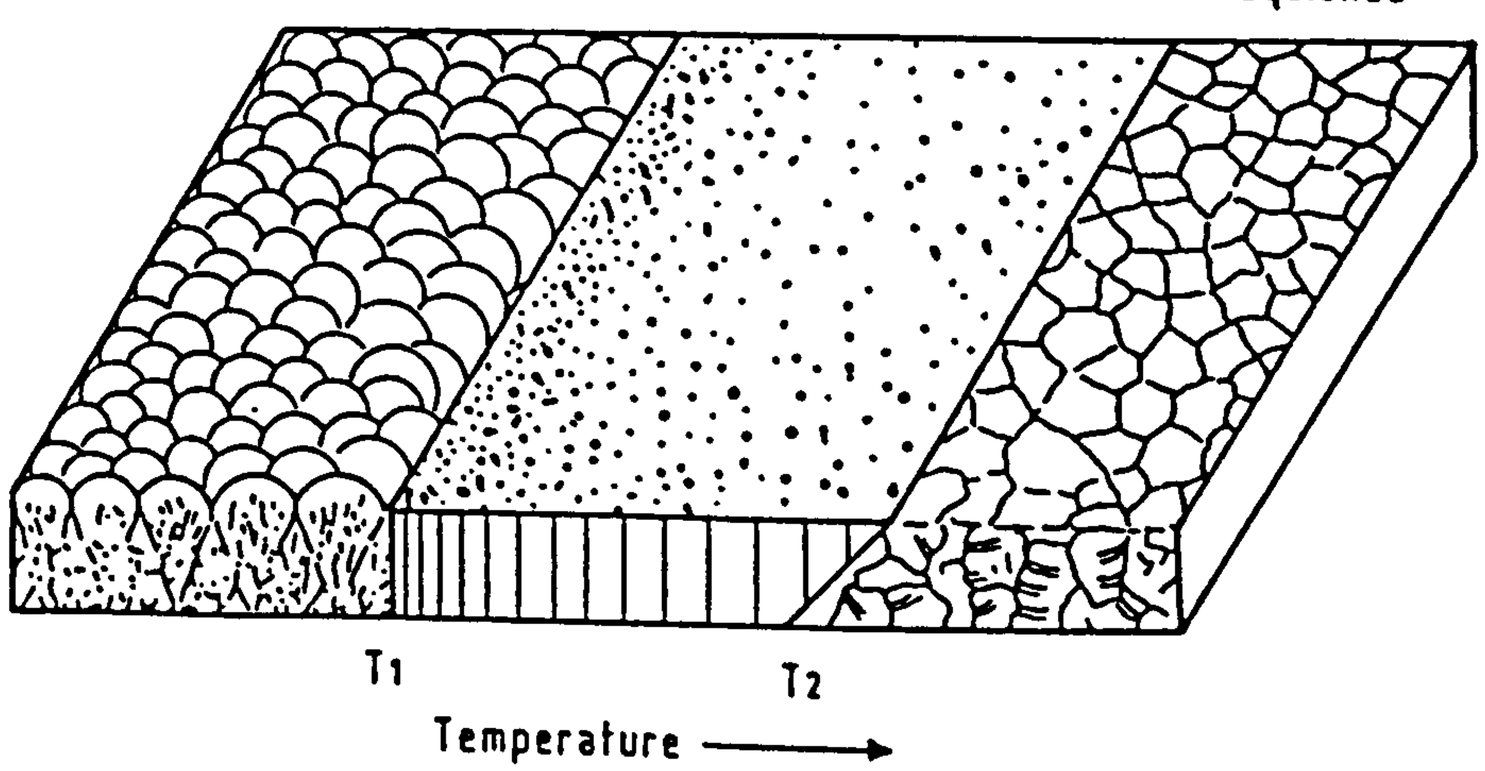

Figure 37. Movchan and Demchishin Model.[156]

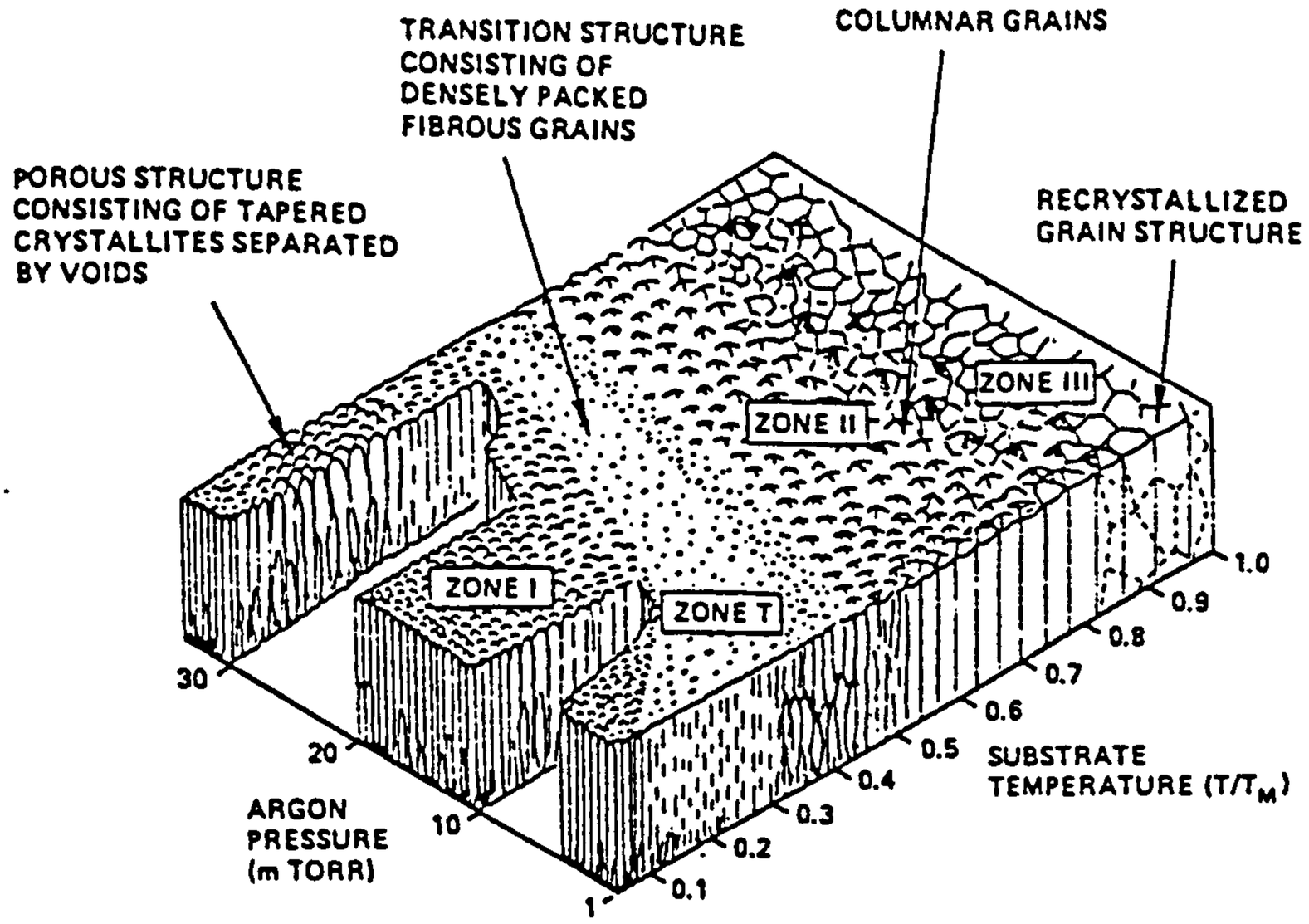

Figure 38. Thornton Model.[157]

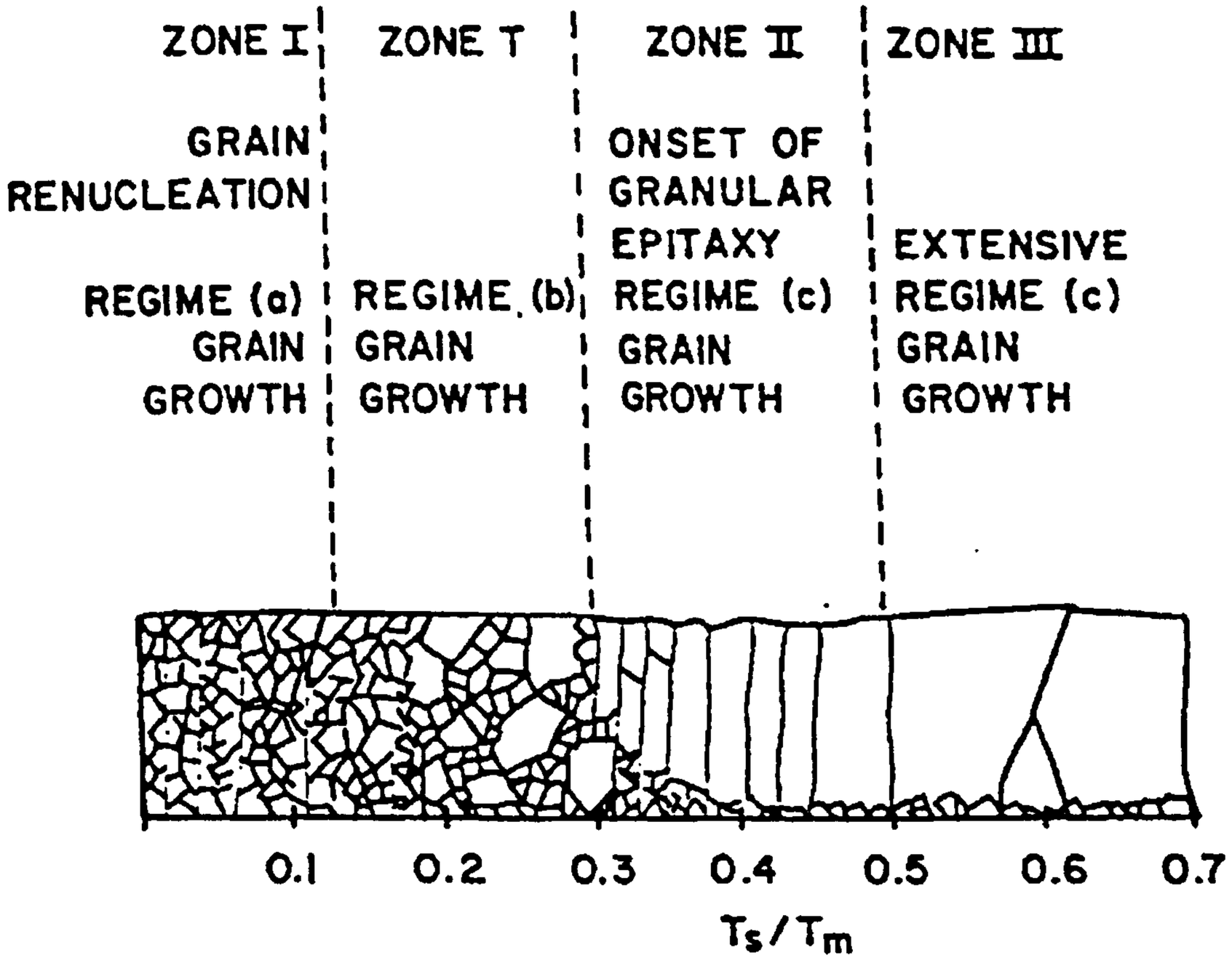

Figure 39. Grovenor Zone Model for the Grain Structure of Vapour Deposited Metal Films.[158]

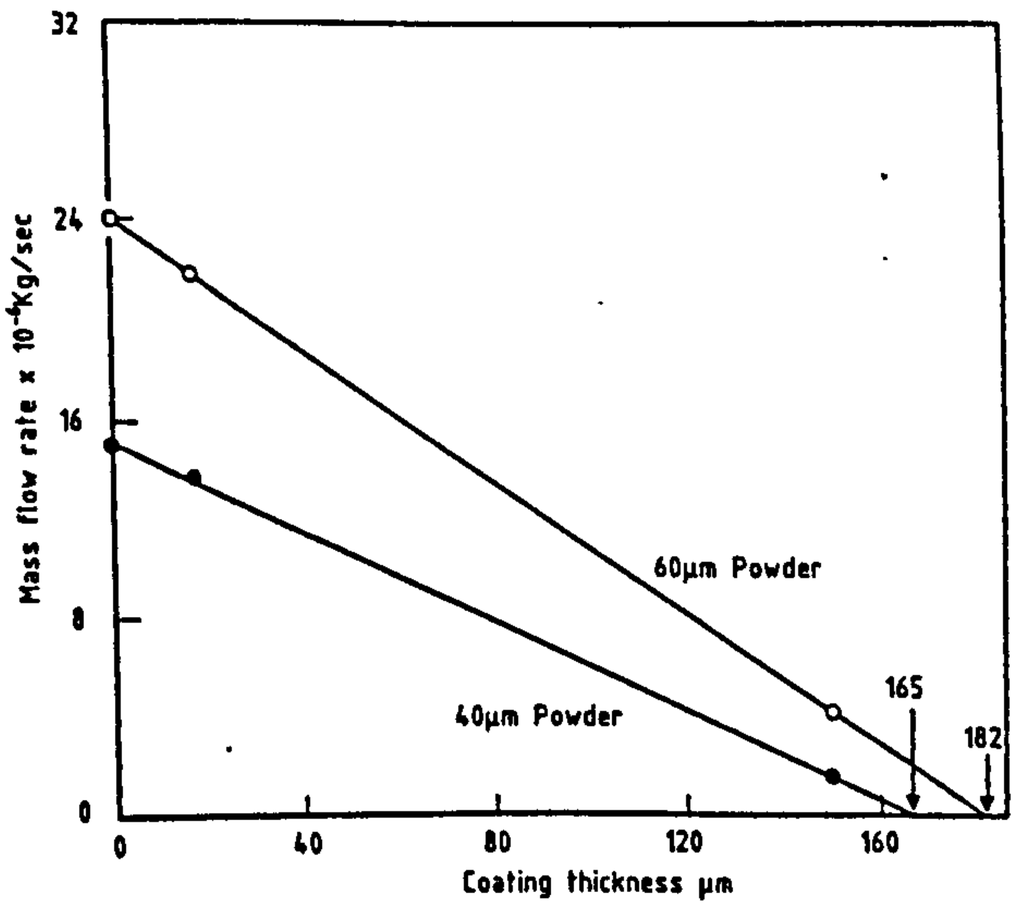

Figure 40. Influence of Nickel Coating Thickness on Closure of Surface Porosity on Phosphor Bronze Substrates.[160]

Figure 41. Metallic Preforms.

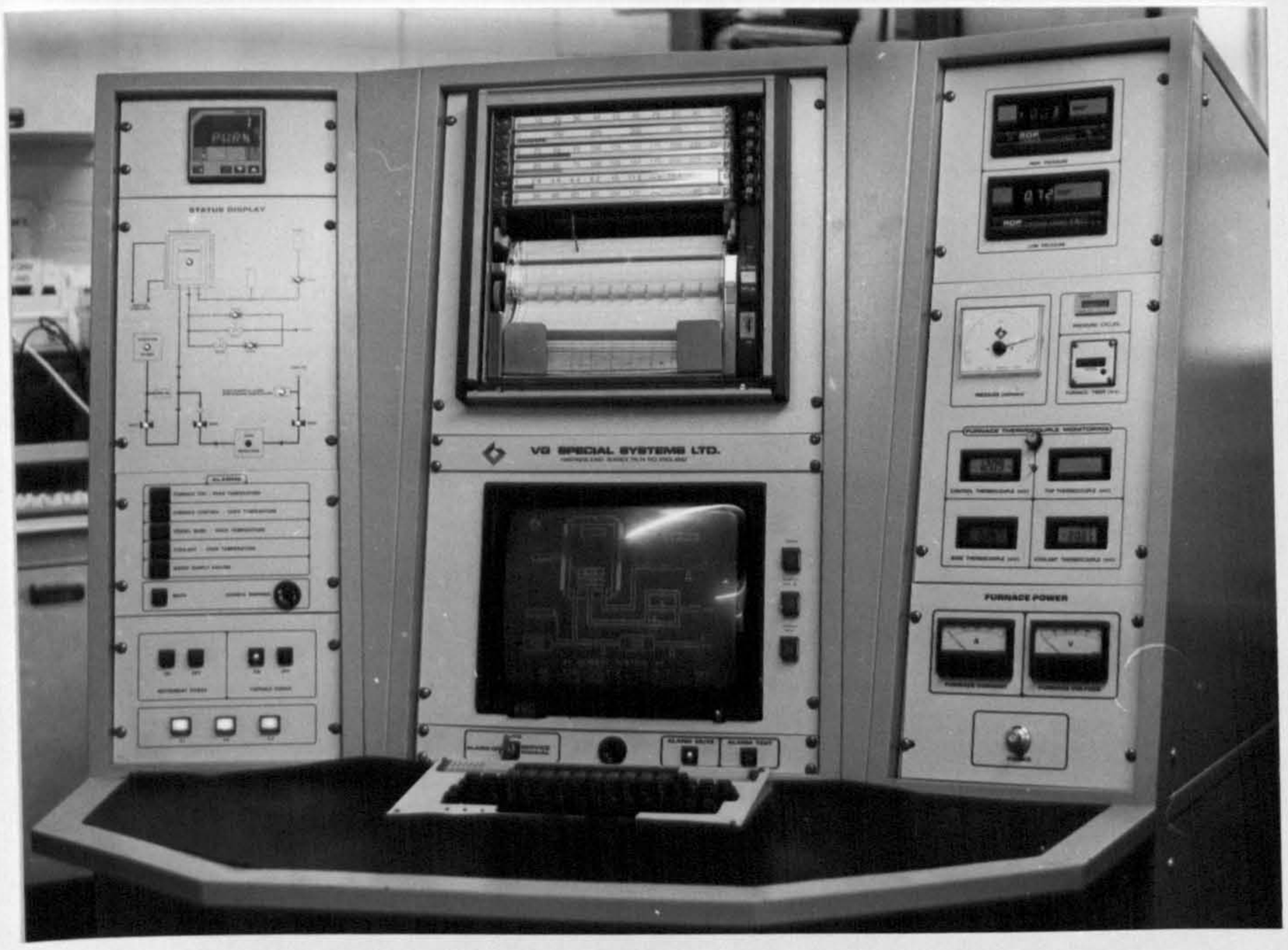

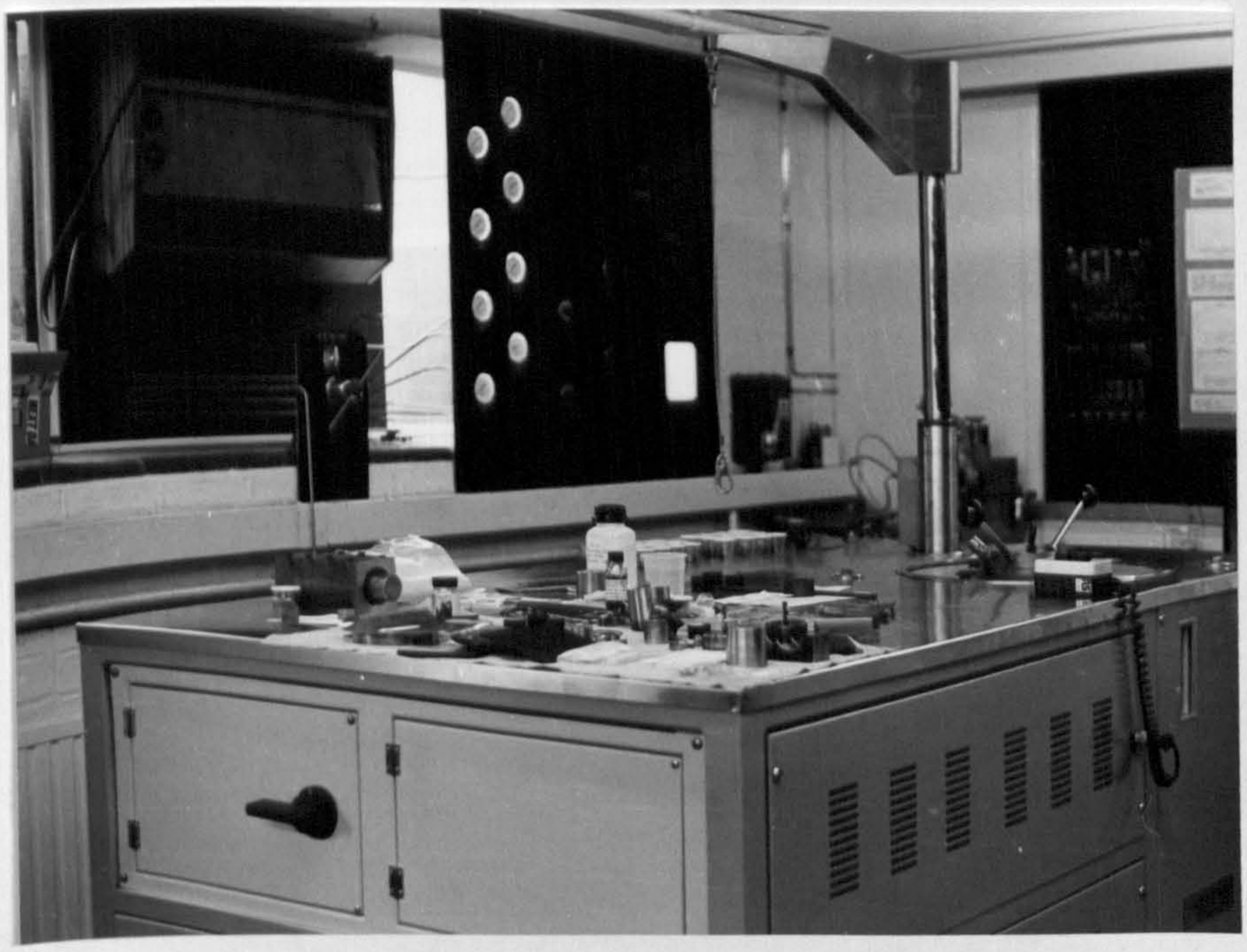

Figure 42. Superhipper Hot Isostatic Pressing Unit.

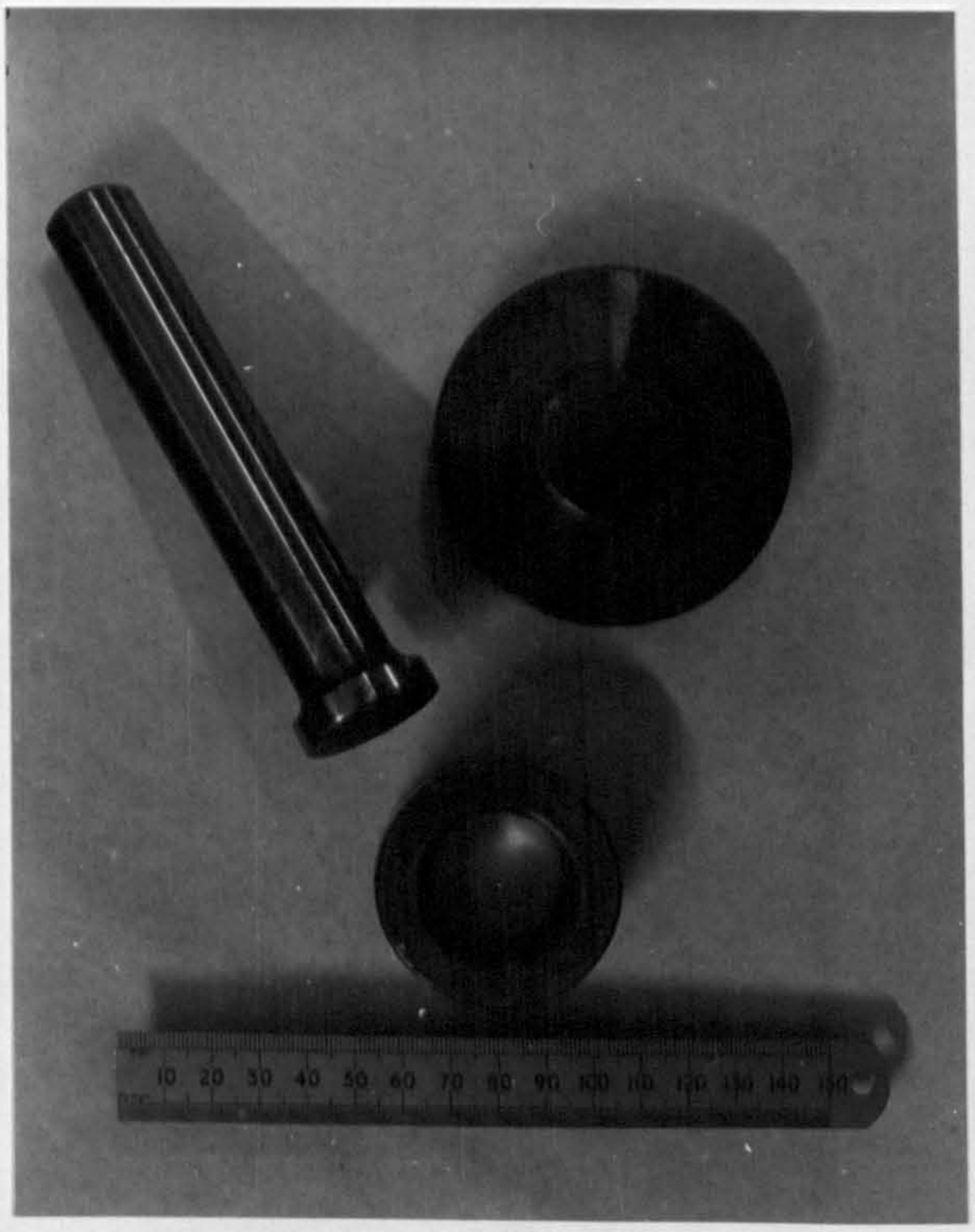

Figure 43. Simple Die for the Production of Pressed Metal Powder Discs.

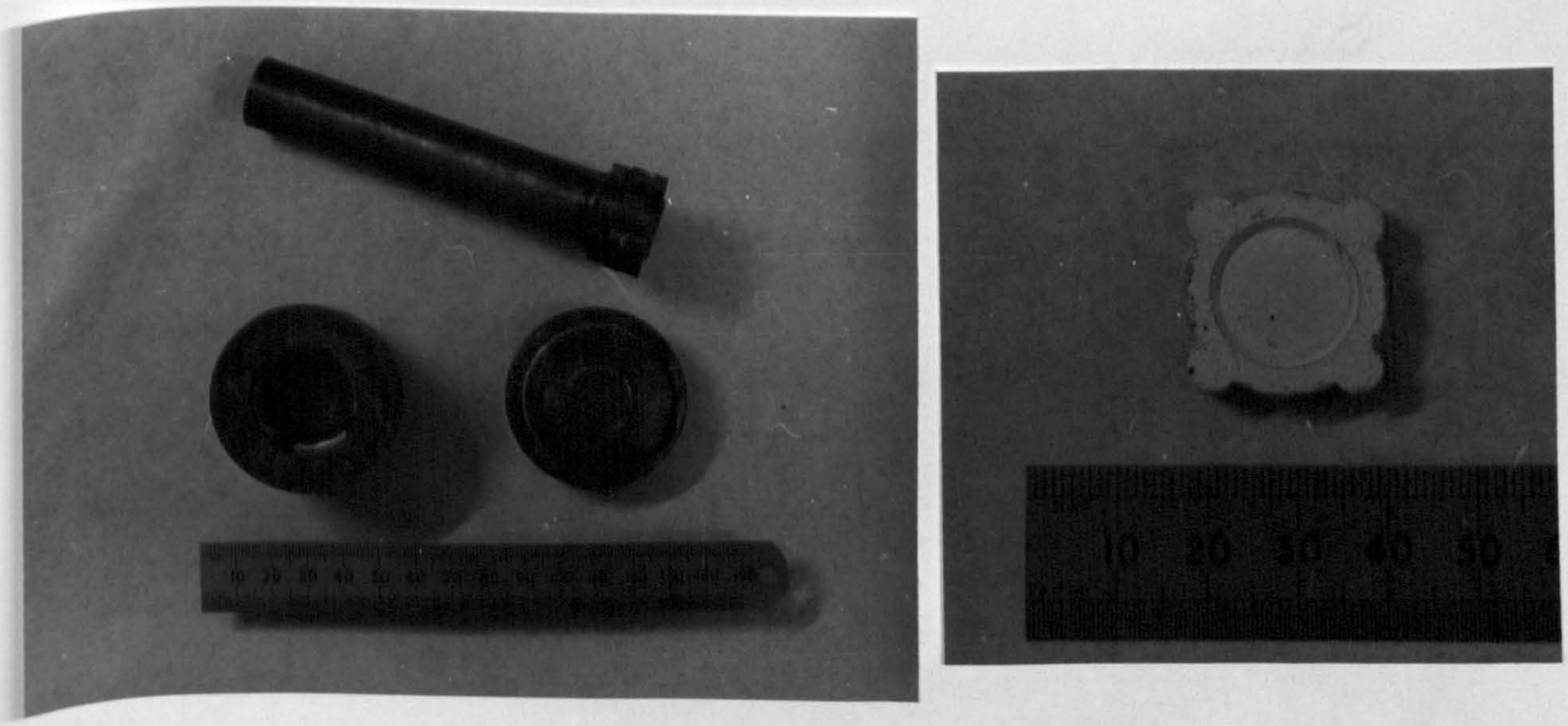

Figure 44. Complex Die for the Production of Pressed Metal Powder Discs.

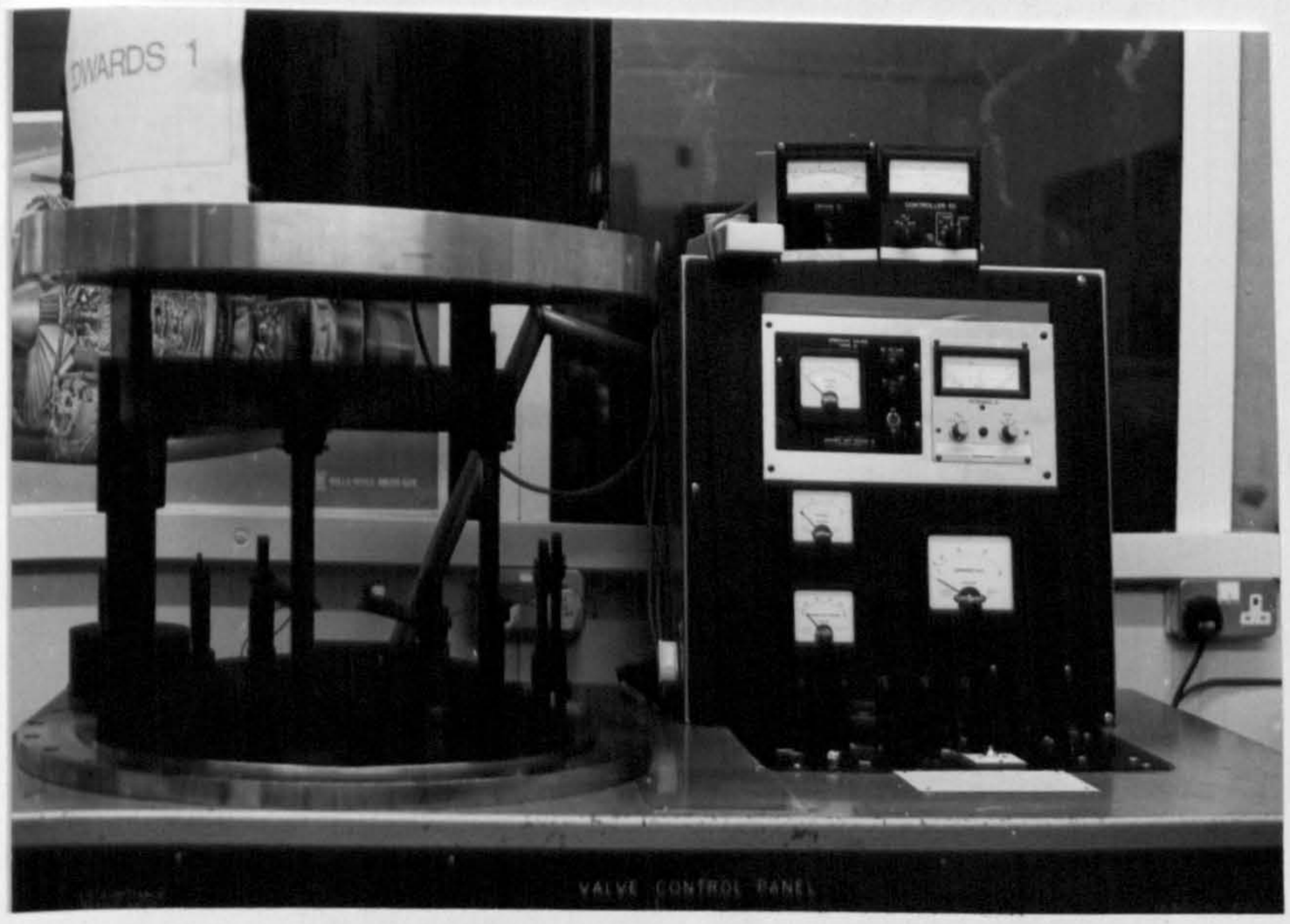

Figure 45. Edwards 19E2 Unit.

Figure 46. Electrotech SL10-20 Unit.

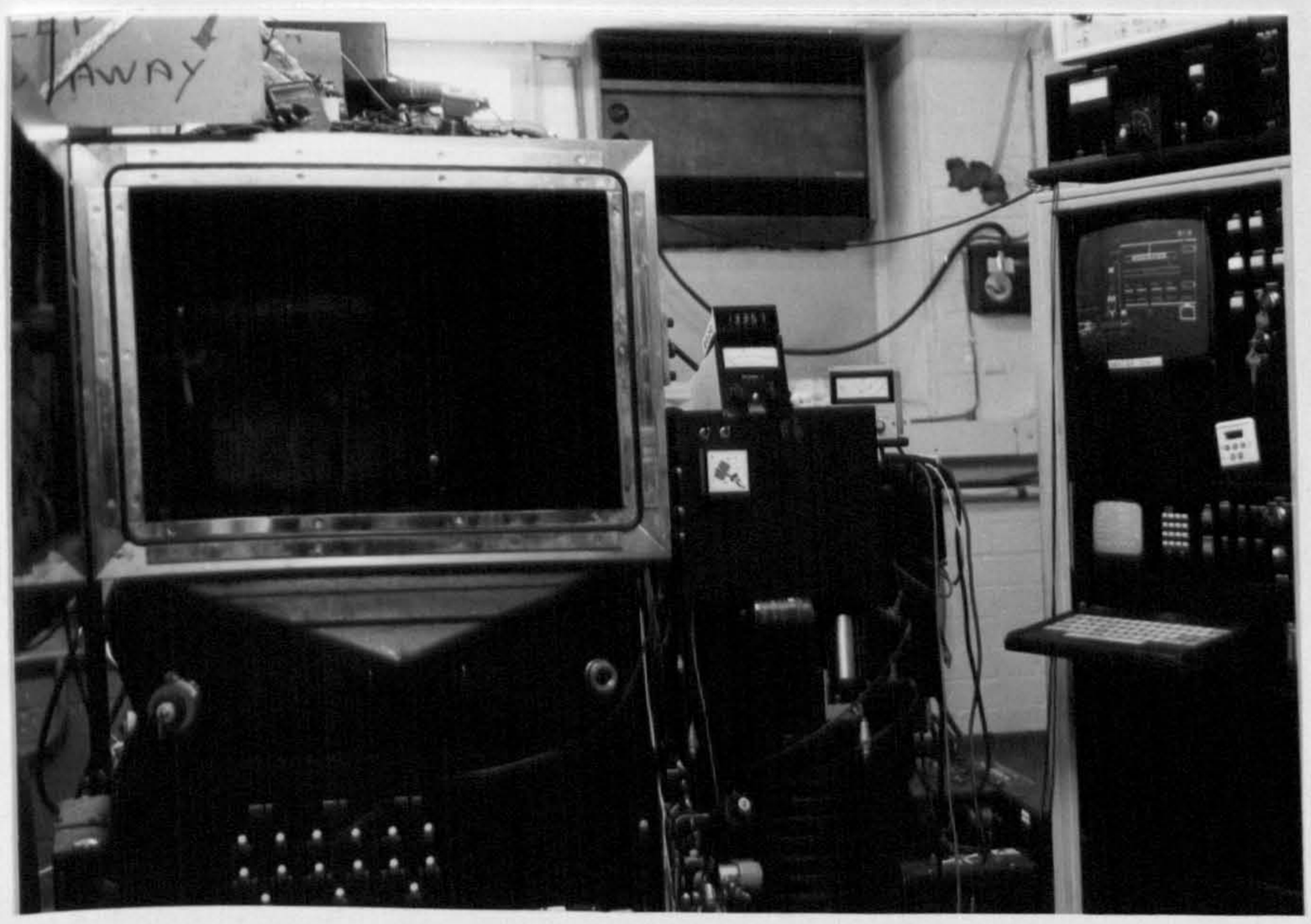

Figure 47. Cranfield Ion Plating System.

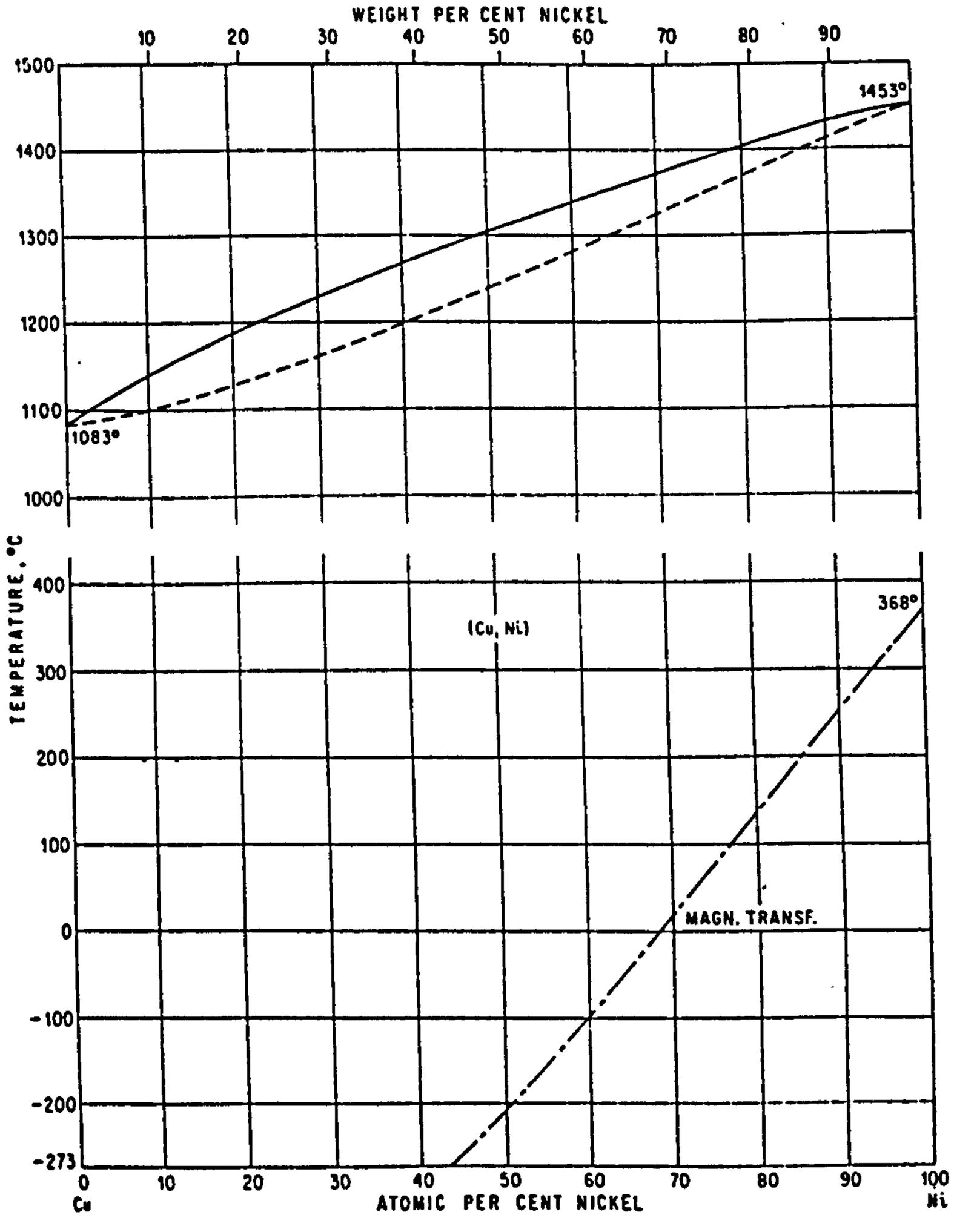

Figure 48. Phase Diagram for the Copper-Nickel Alloy System.[164]

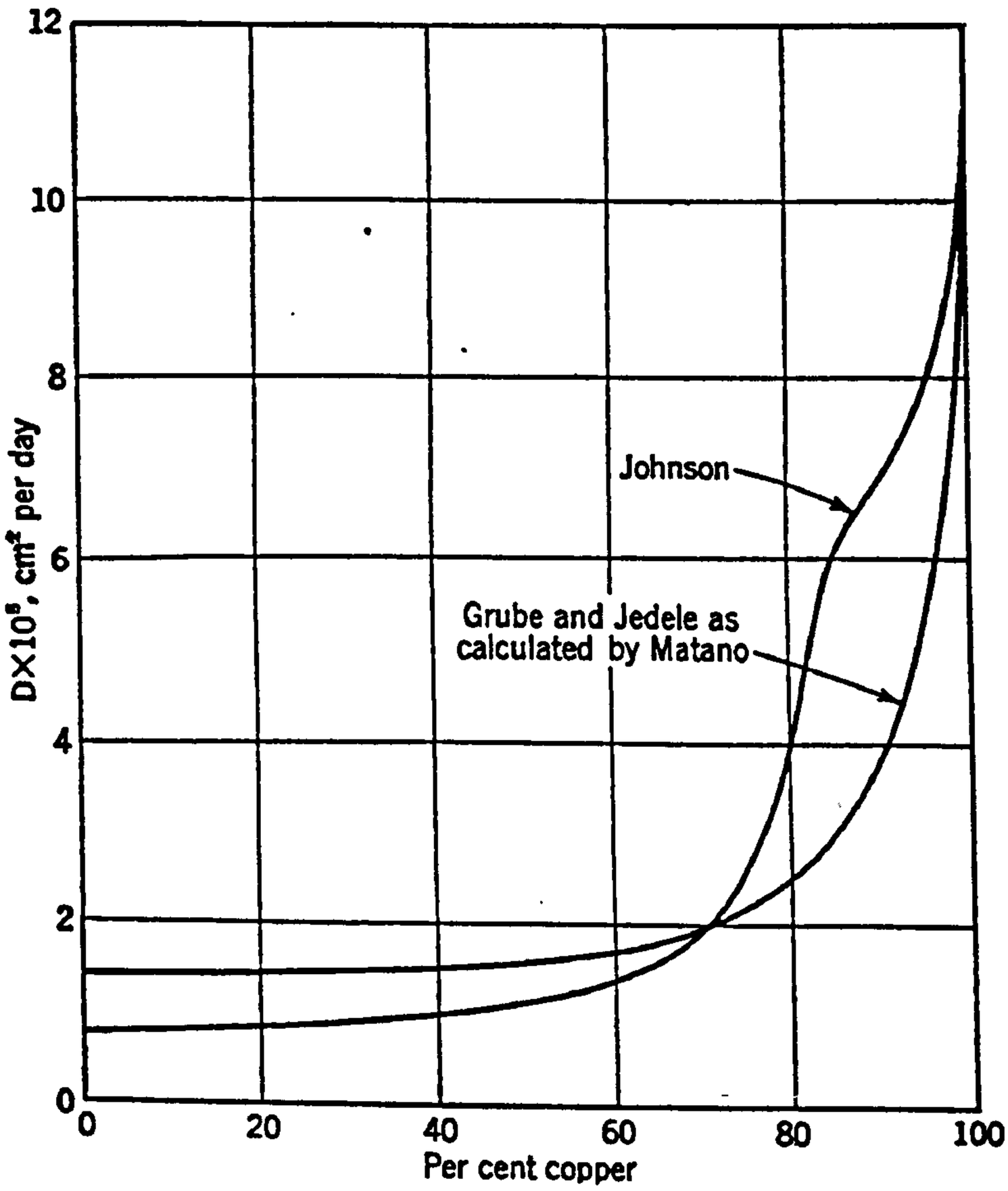

Figure 49. Variation of Diffusivity with Composition for the Nickel-Copper System at 1052 ° C.[166]

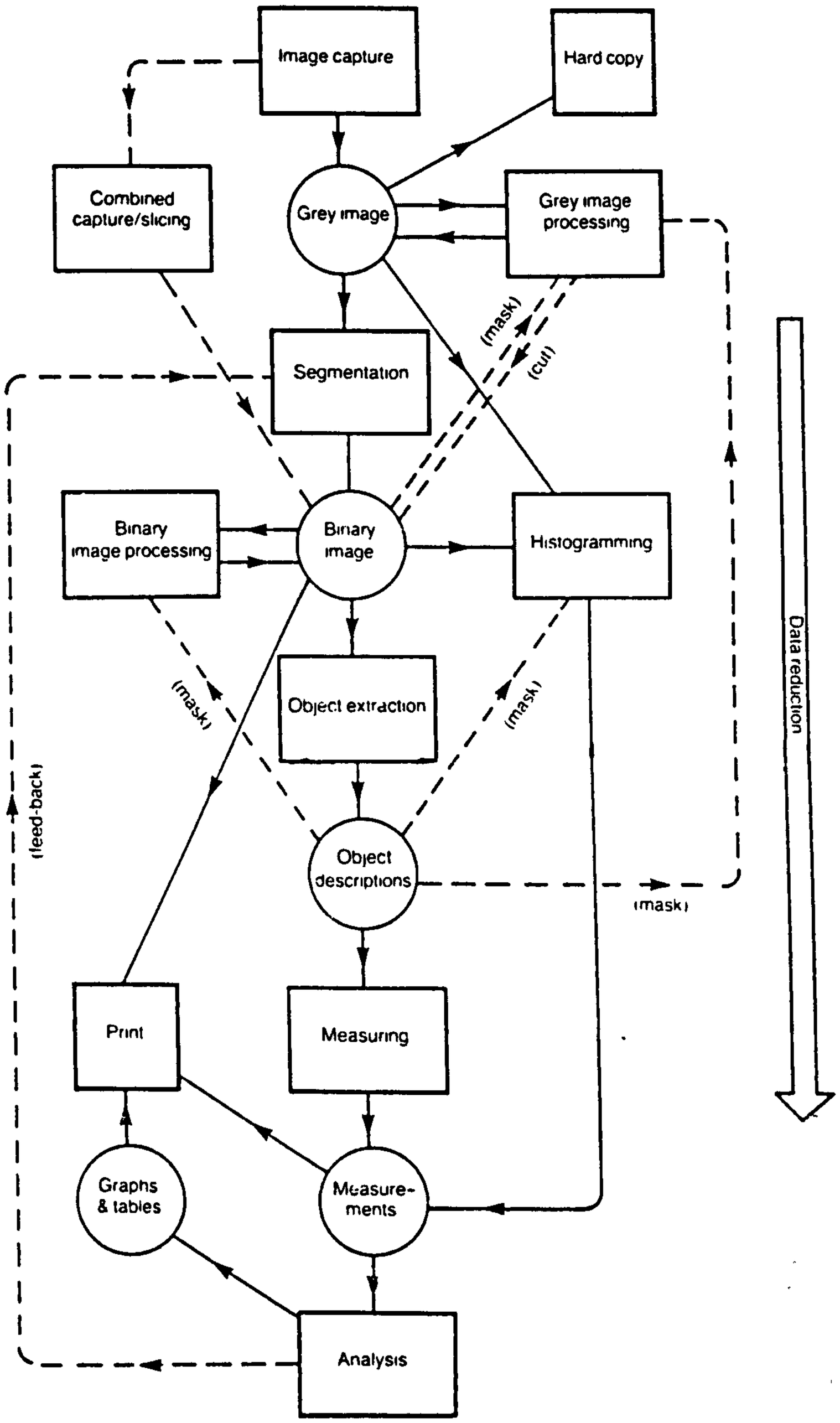

Figure 50. The Principal Stages of Image Analysis.[167]

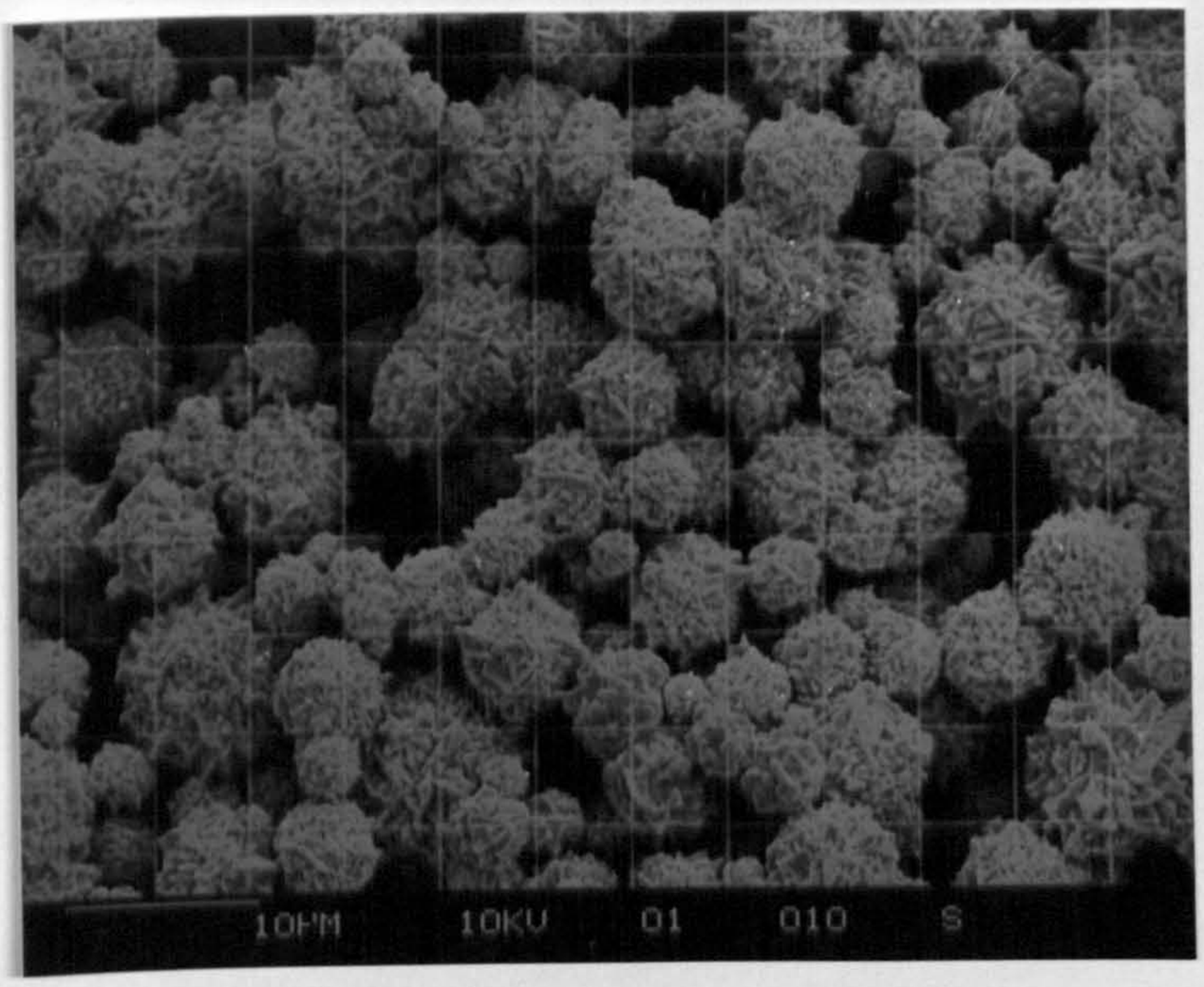

(a)

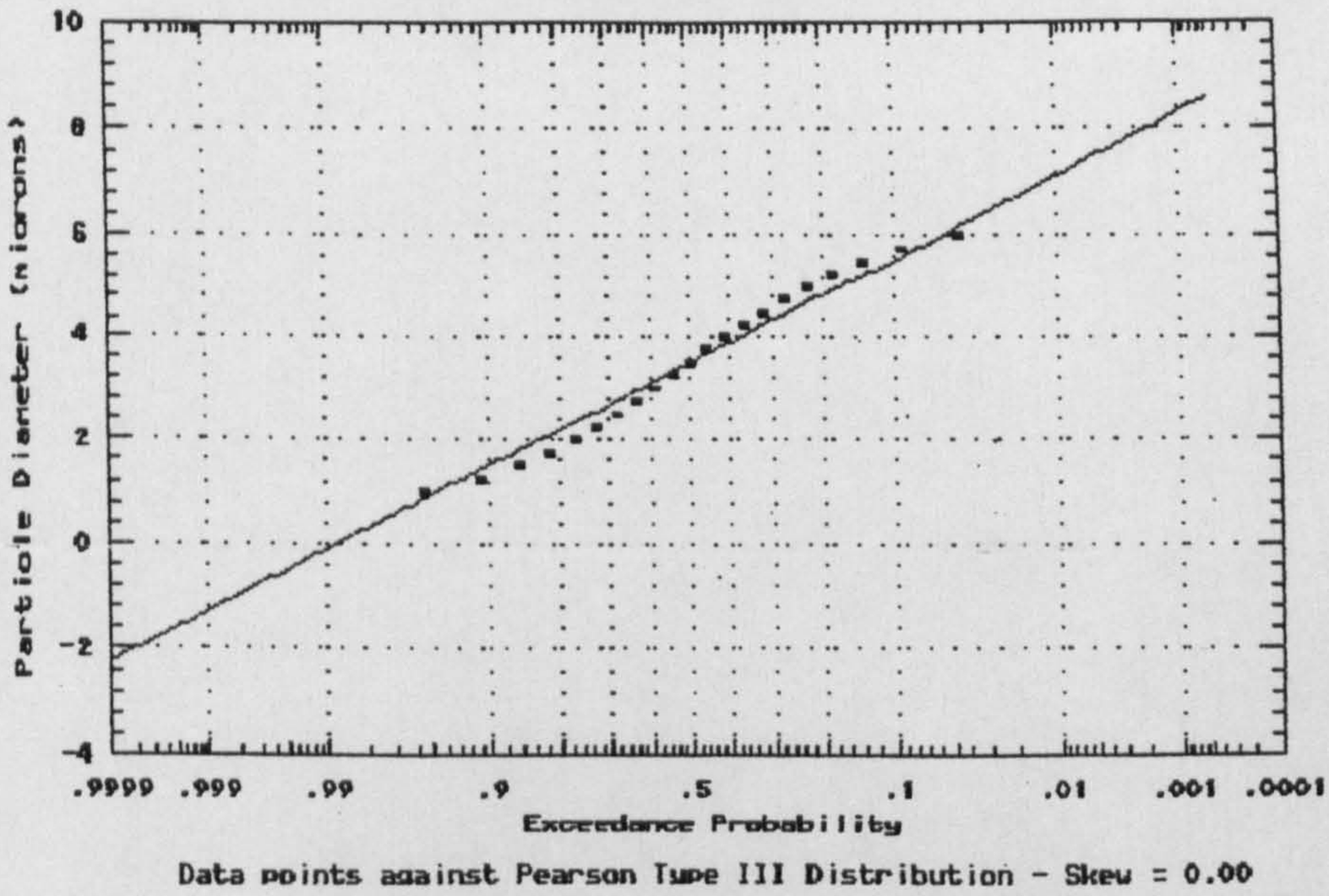

(b)

Figure 51. Ni123 Powder.
(a) SEM Micrograph.
(b) Particle Size Distribution.

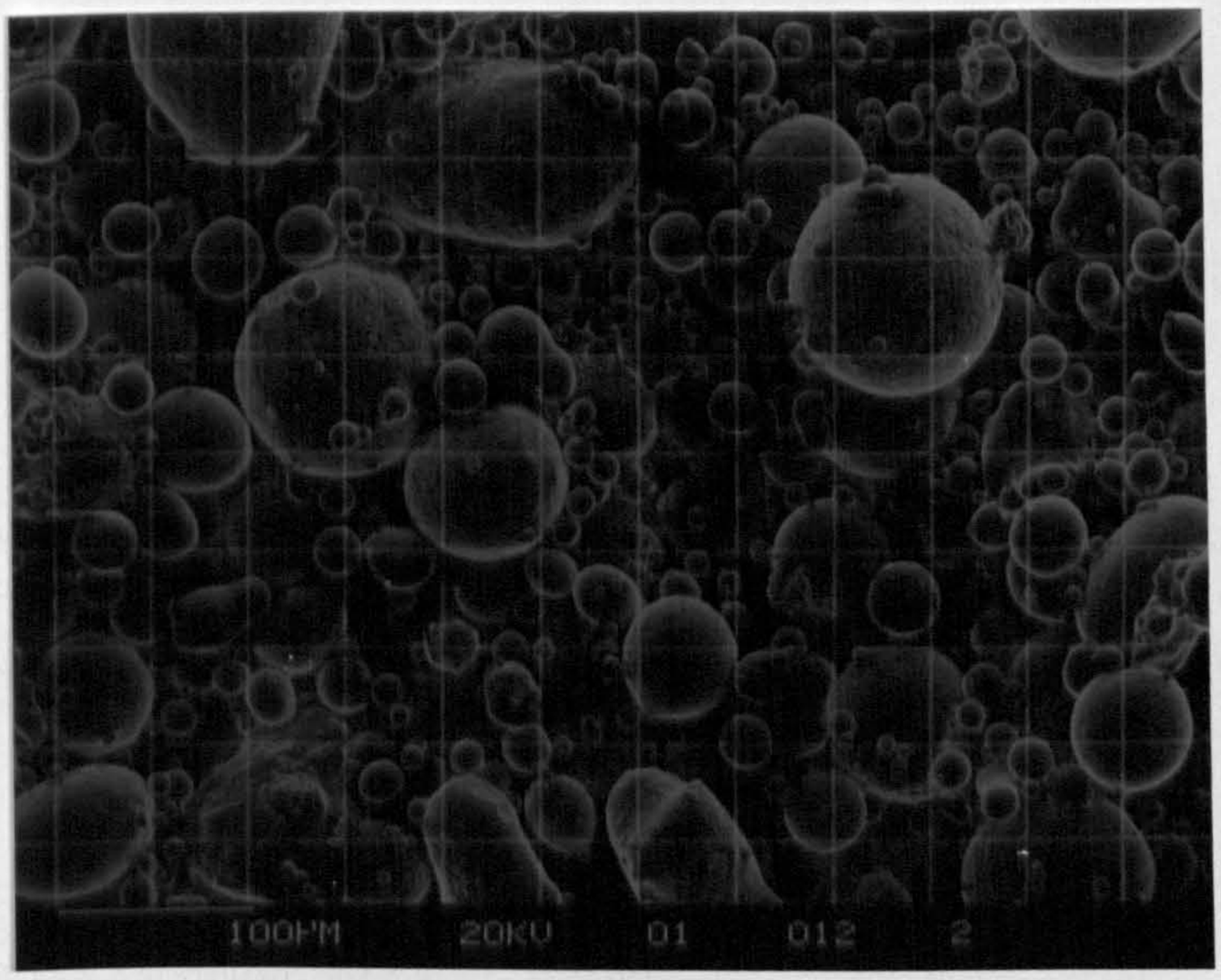

(a)

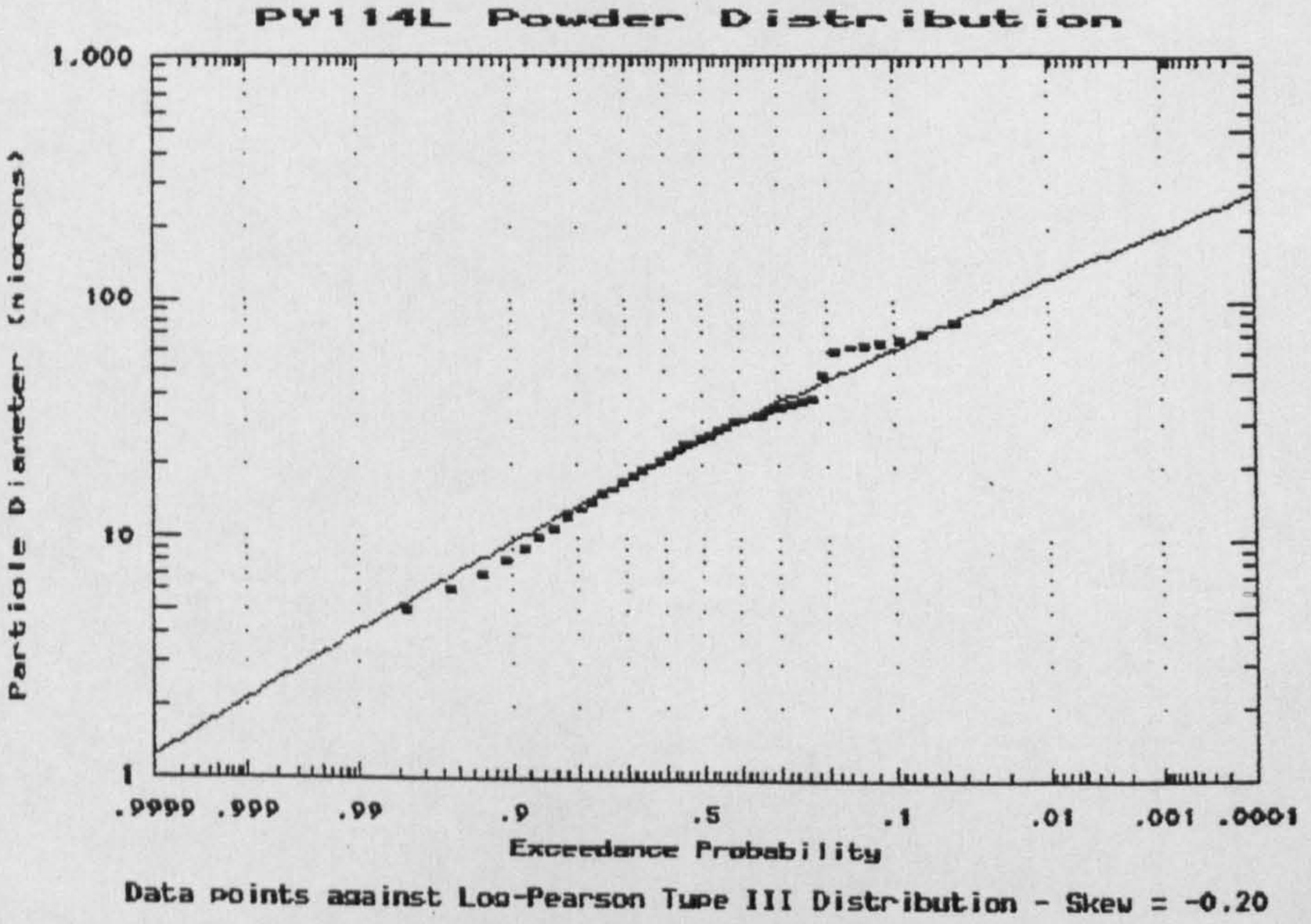

(b)

Figure 52. PY114L Powder.
(a) SEM Micrograph.
(b) Particle Size Distribution.

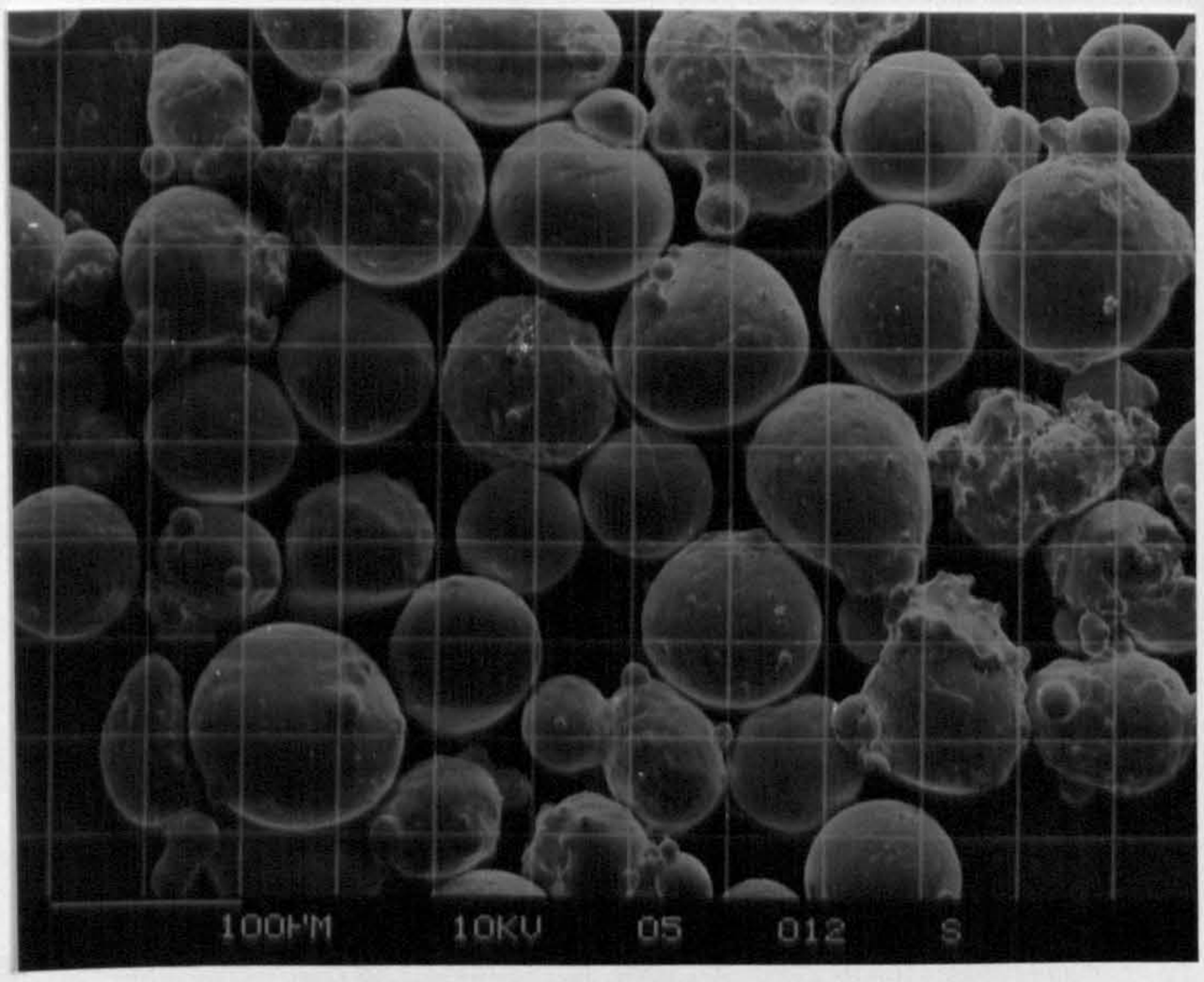

(a)

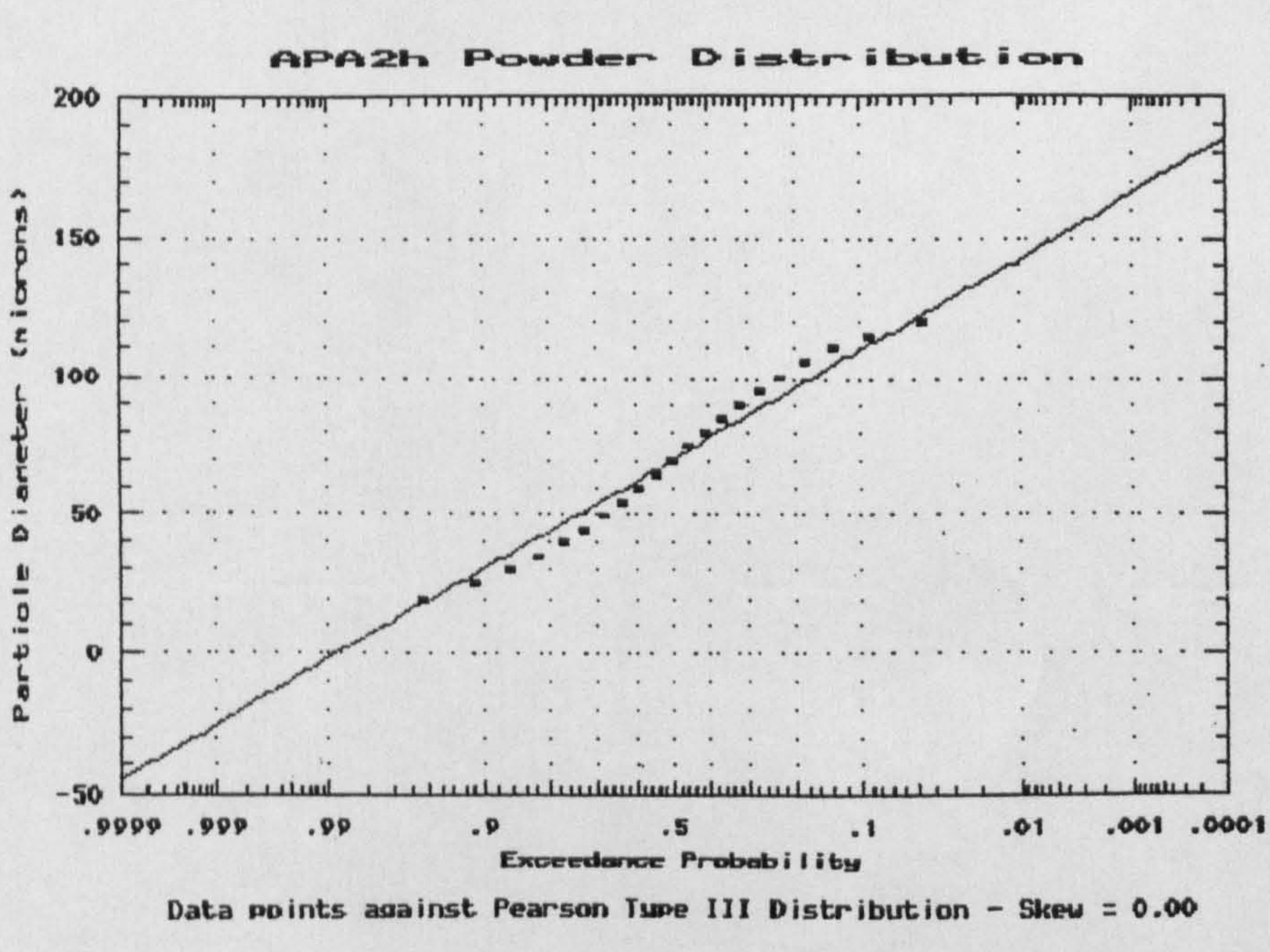

(b)

Figure 53. APA2h Powder (Sieved >N56-<N80 Mesh).
(a) SEM Micrograph.
(b) Particle Size Distribution.

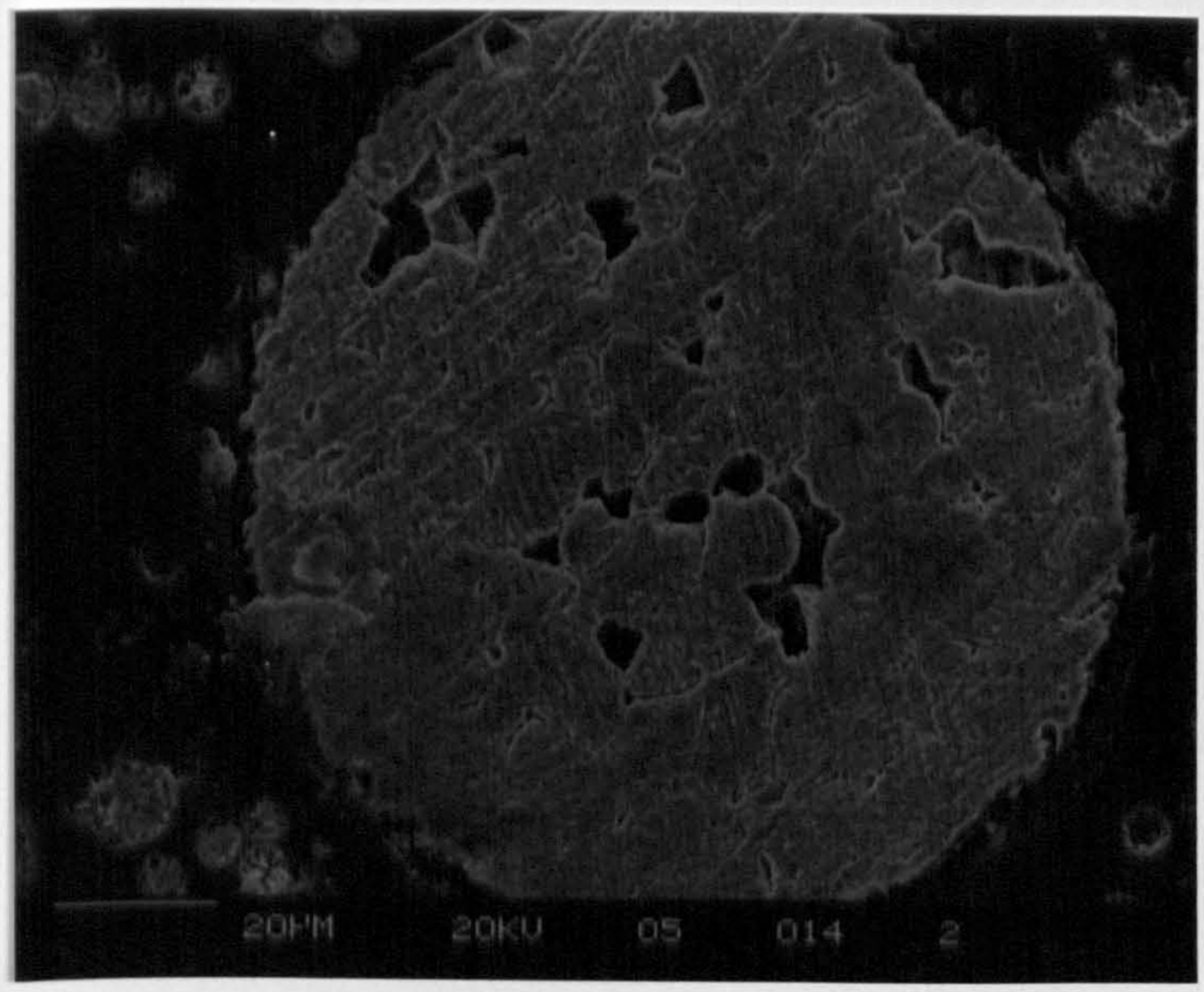

(a)

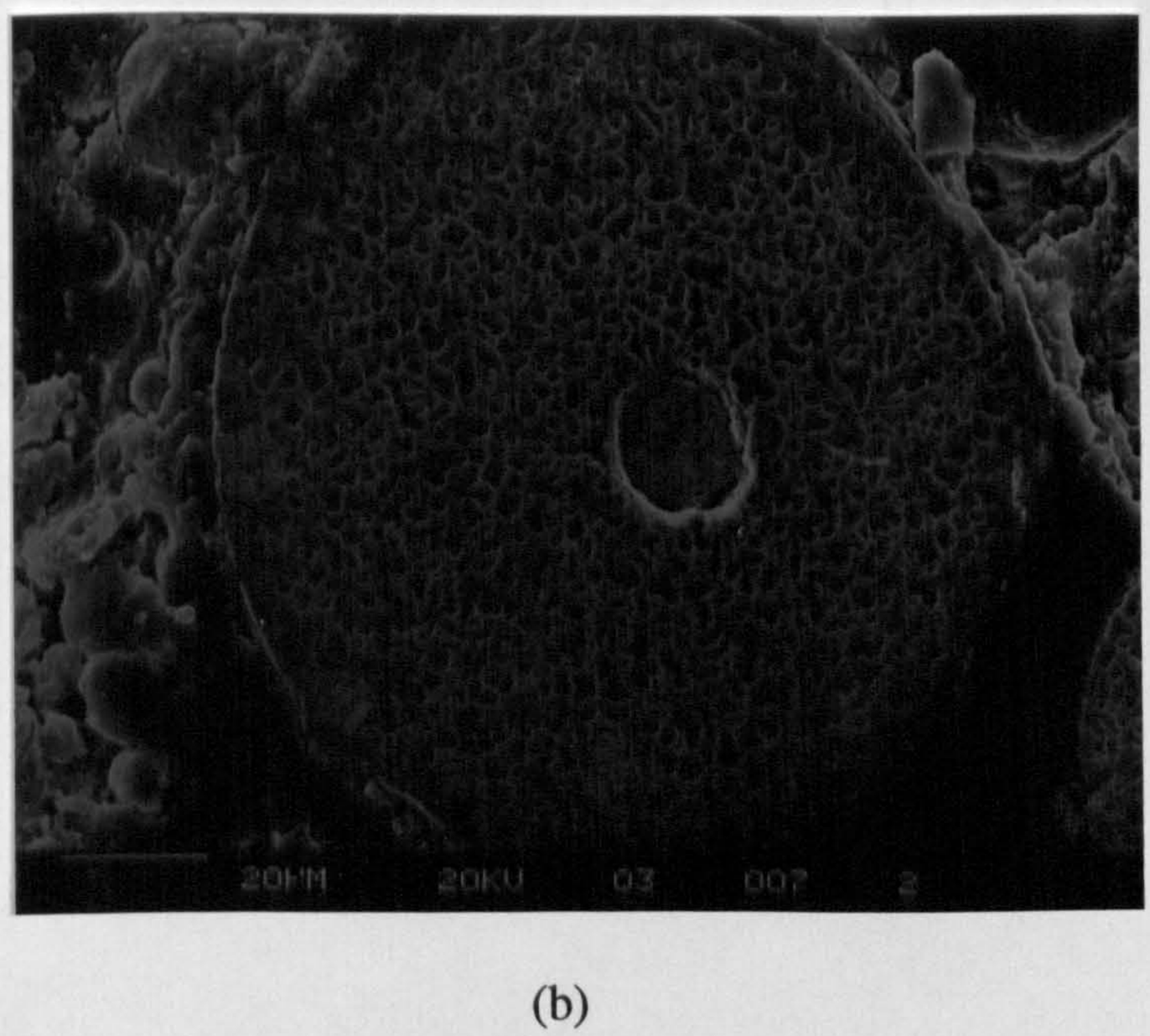

(b)

Figure 54. Grain Boundary Size Investigation.
(a) APA2 Powder (showing gas entrapment).
(b) PY114L Powder (showing an inclusion).

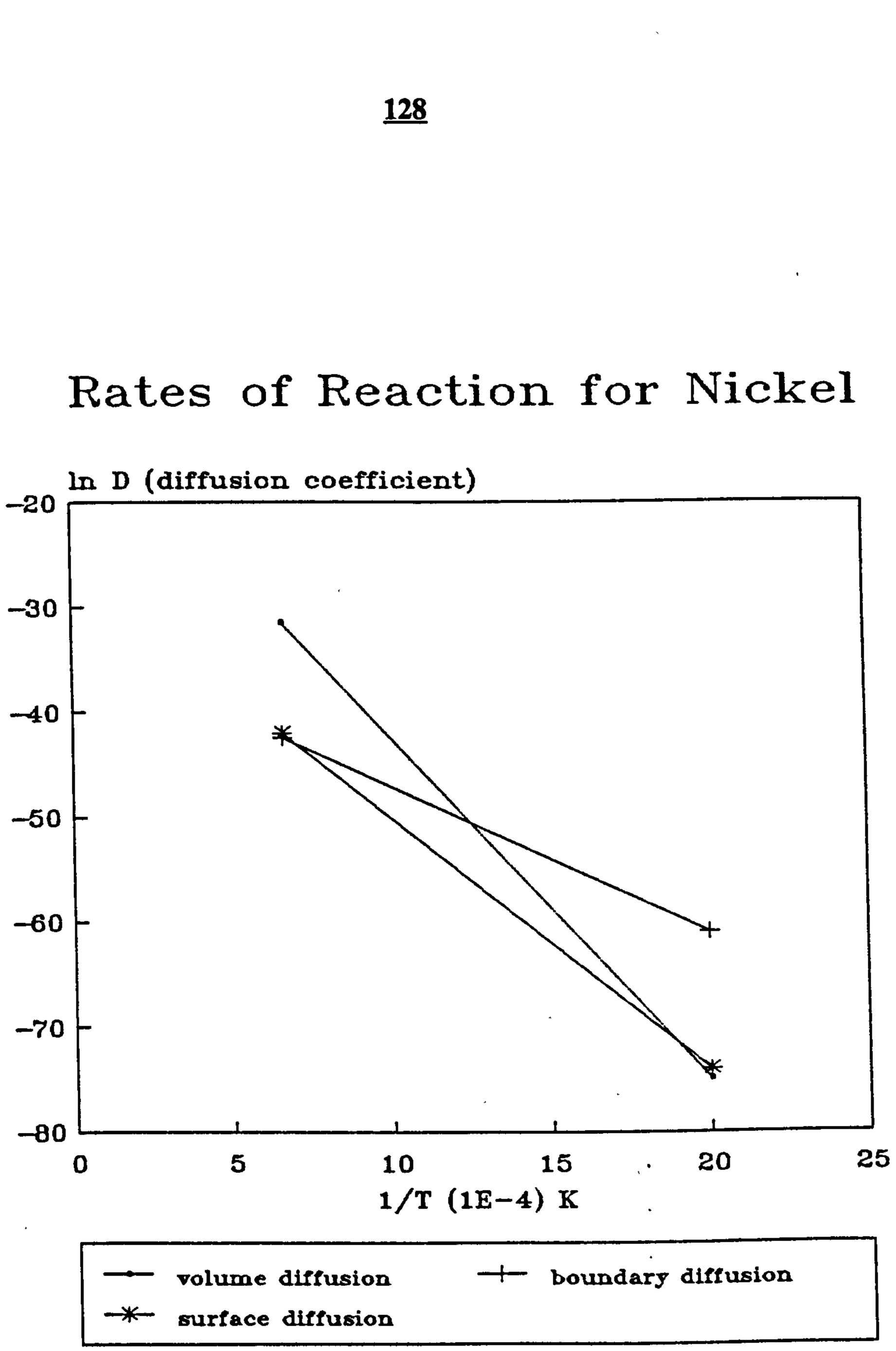

Figure 55. Rates of Reaction for Diffusion Mechanisms for Nickel, Calculated from HIP487 Data.[118]

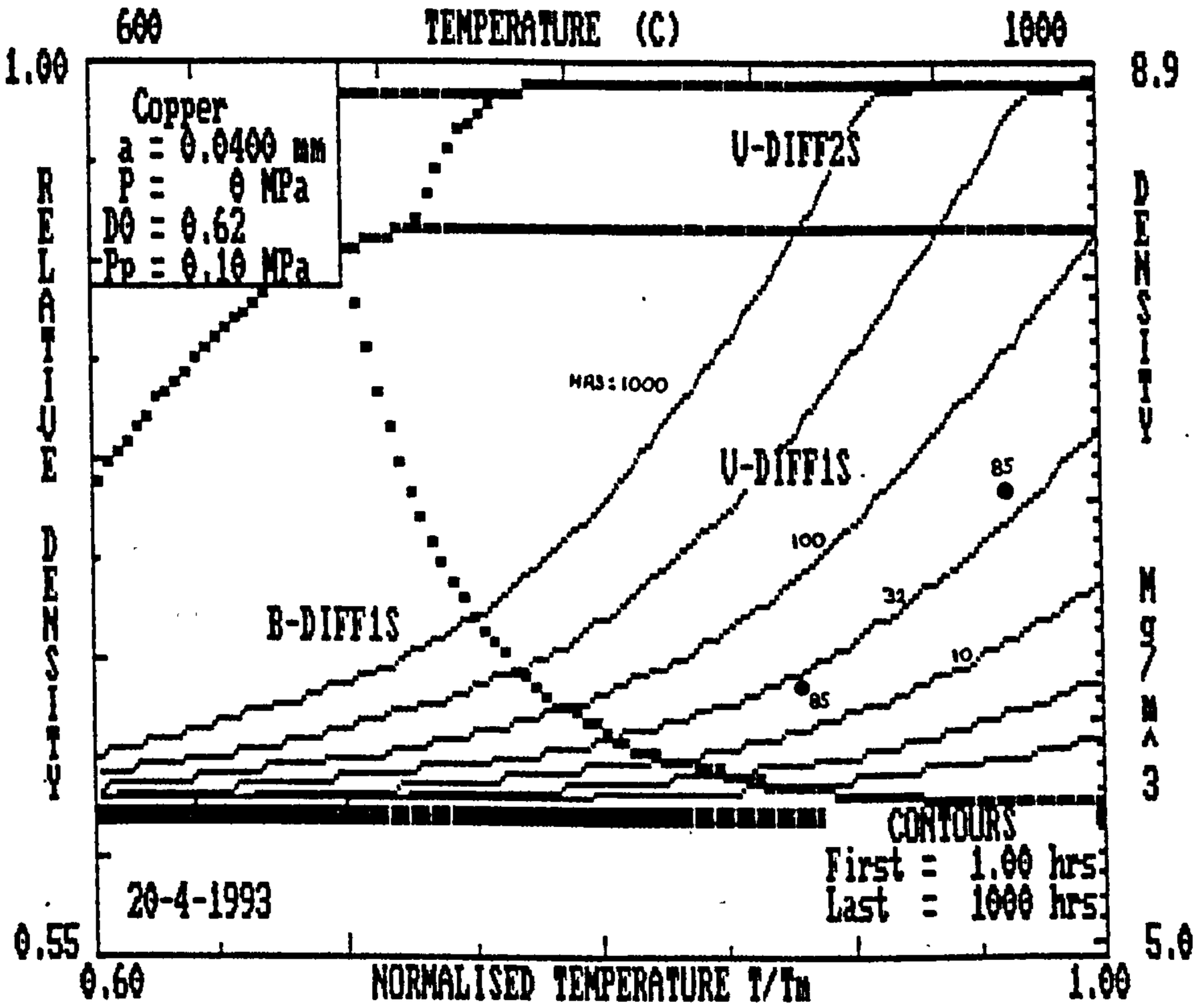

Figure 56. (a) HIP487 Map for Copper.

1.0 INPUT PARAMETERS for Copper

1	Melting Point	K	=	1.4E+0003
2	Surface Energy	J/m^2	=	1.7E+0000
3	Youngs Modulus	GPa	=	1.3E+0002
4	T-dependence of Modulus		=	3.4E-0001
5	Yield Stress	MPa	=	3.3E+0001
6	T-dependence of yield		=	3.4E-0001
7	Atomic Volume	m^3	=	1.2E-0029
8	Pre-exp. Volume Diffusion	m^2/s	=	6.2E-0005
9	Activ. energy, Vol. Diff.	kJ/mol	=	2.1E+0002
10	Pre-exp. Bdry Diffusion	m^3/s	=	3.1E-0015
11	Activ. energy, Bdry. Diff.	kJ/mol	=	1.1E+0002
12	Pre-exp. Surface Diffusion	m^3/s	=	6.0E-0010
13	Activ. energy, Surf. Diff.	kJ/mol	=	2.1E+0002
14	Power Law Creep Exponent		=	4.8E+0000
15	Reference stress, P-L creep	MPa	=	3.3E+0001
16	Activ. energy for P-L creep	kJ/mol	=	2.0E+0002
17	Solid Density	kg/m^3	=	9.0E+0003

Time

1.0 INPUT VARIABLES for Copper

1	Plot Option (1, 2 or 3)		=	3.0E+0000
2	Particle Radius	m	=	4.0E-0005
3	Initial Relative Density		=	6.2E-0001
4	Initial Pore Pressure	MPa	=	1.0E-0001
5	Grain diameter in particle	m	=	3.0E-0005
6	Lower limit, D/DS axis		=	5.5E-0001
7	Upper limit, D/DS axis		=	1.0E+0000
8	Fixed Pressure	MPa	=	0.0E+0000
9	Lower limit, P/BY axis		=	1.0E-0003
10	Upper limit, P/BY axis		=	1.0E+0001
11	Fixed Temperature	K	=	7.7E+0002
12	Lower limit, T/TM axis		=	6.0E-0001
13	Upper limit, T/TM axis		=	1.0E+0000
14	First time contour	s	=	3.6E+0003
15	Multiplier for time contour		=	3.2E+0000
16	Number of Time contours		=	7.0E+0000
17	Number of Program Steps		=	1.5E+0002

Figure 56. (b) Data Set for Copper.

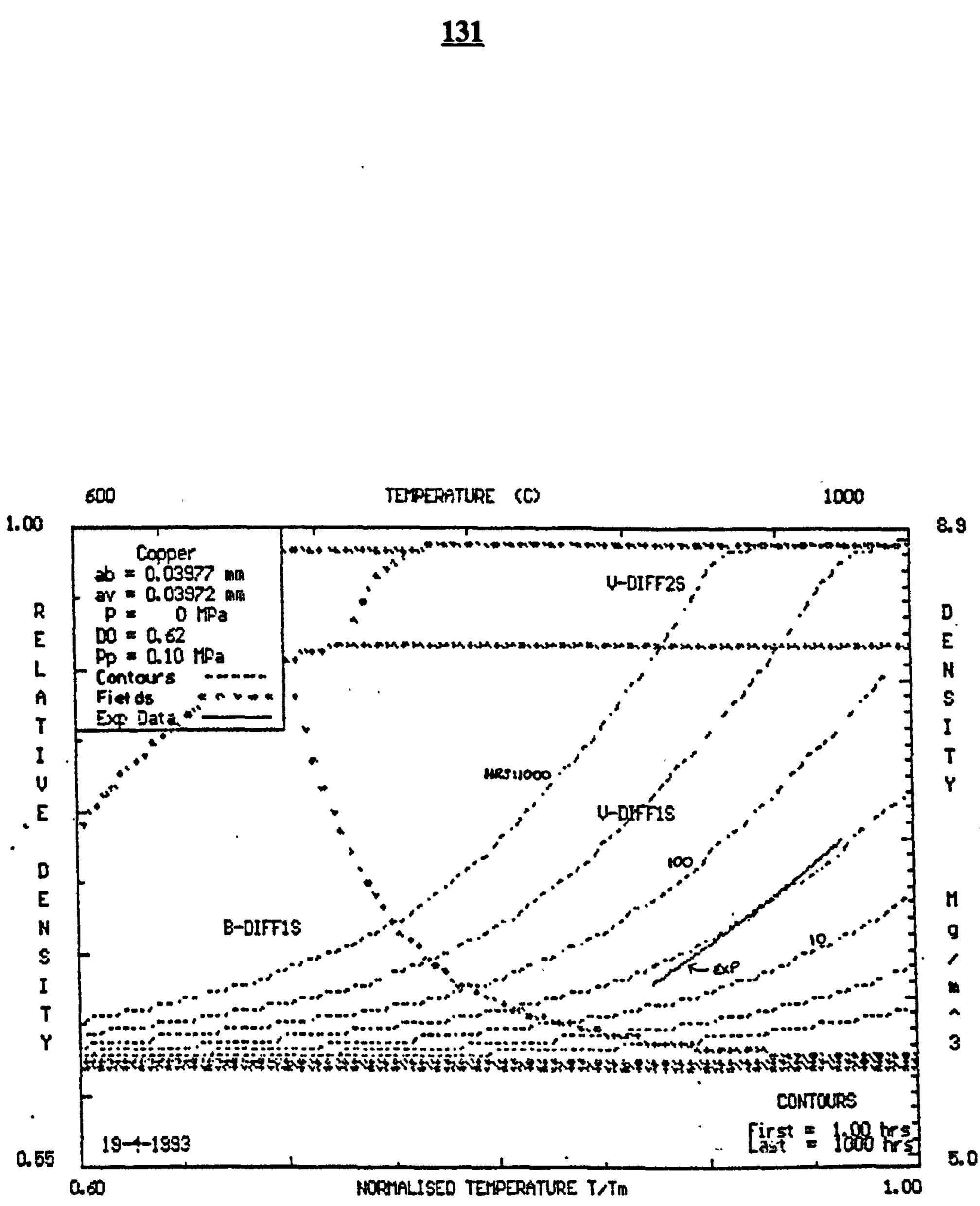

Figure 57. HIP792 Map for Copper.
(a) Assuming Normal Powder Distribution.

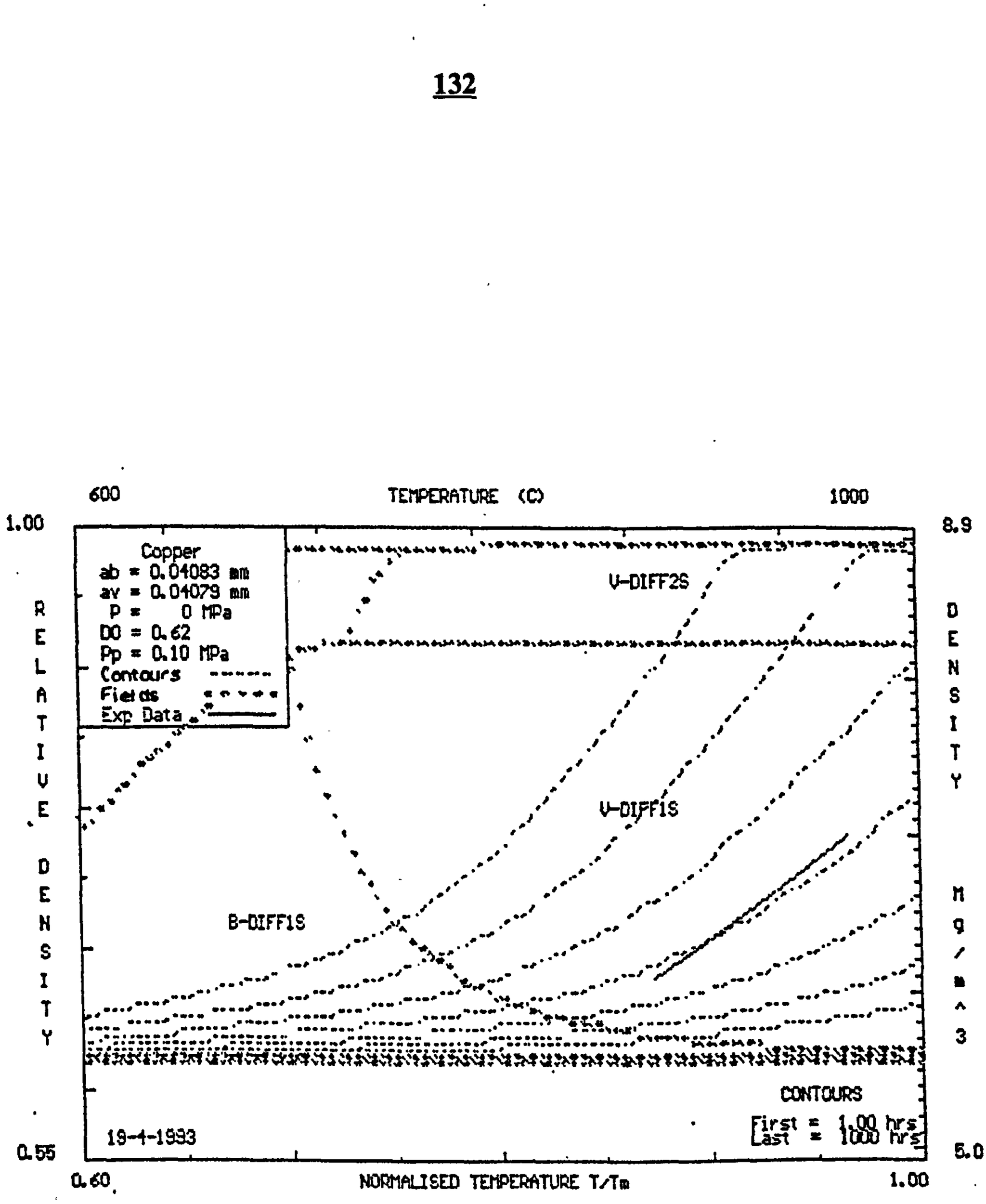

Figure 57. HIP792 Map for Copper.
(b) Assuming Log-Normal Distribution.

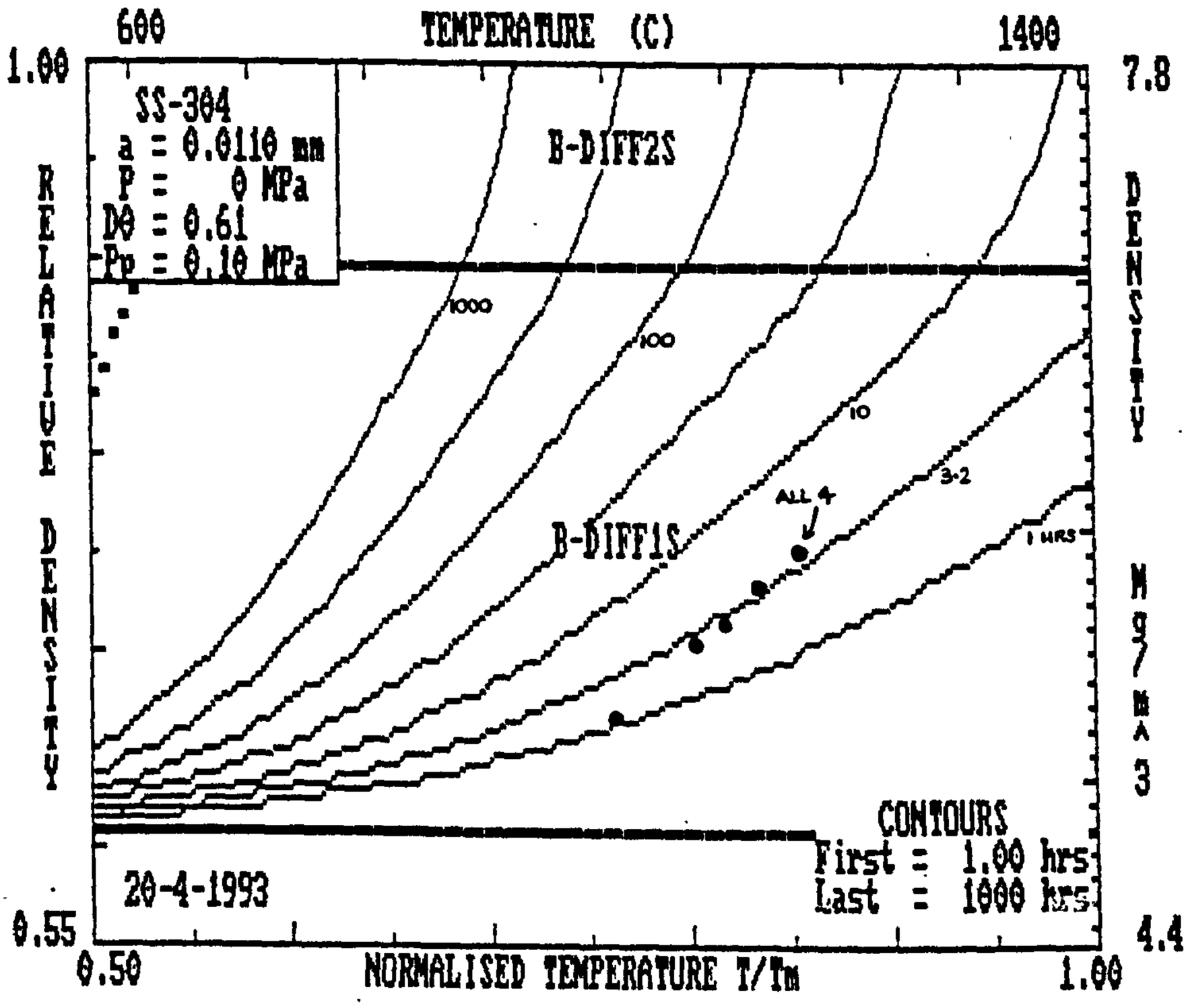

Figure 58. HIP487 Map for SS-304.

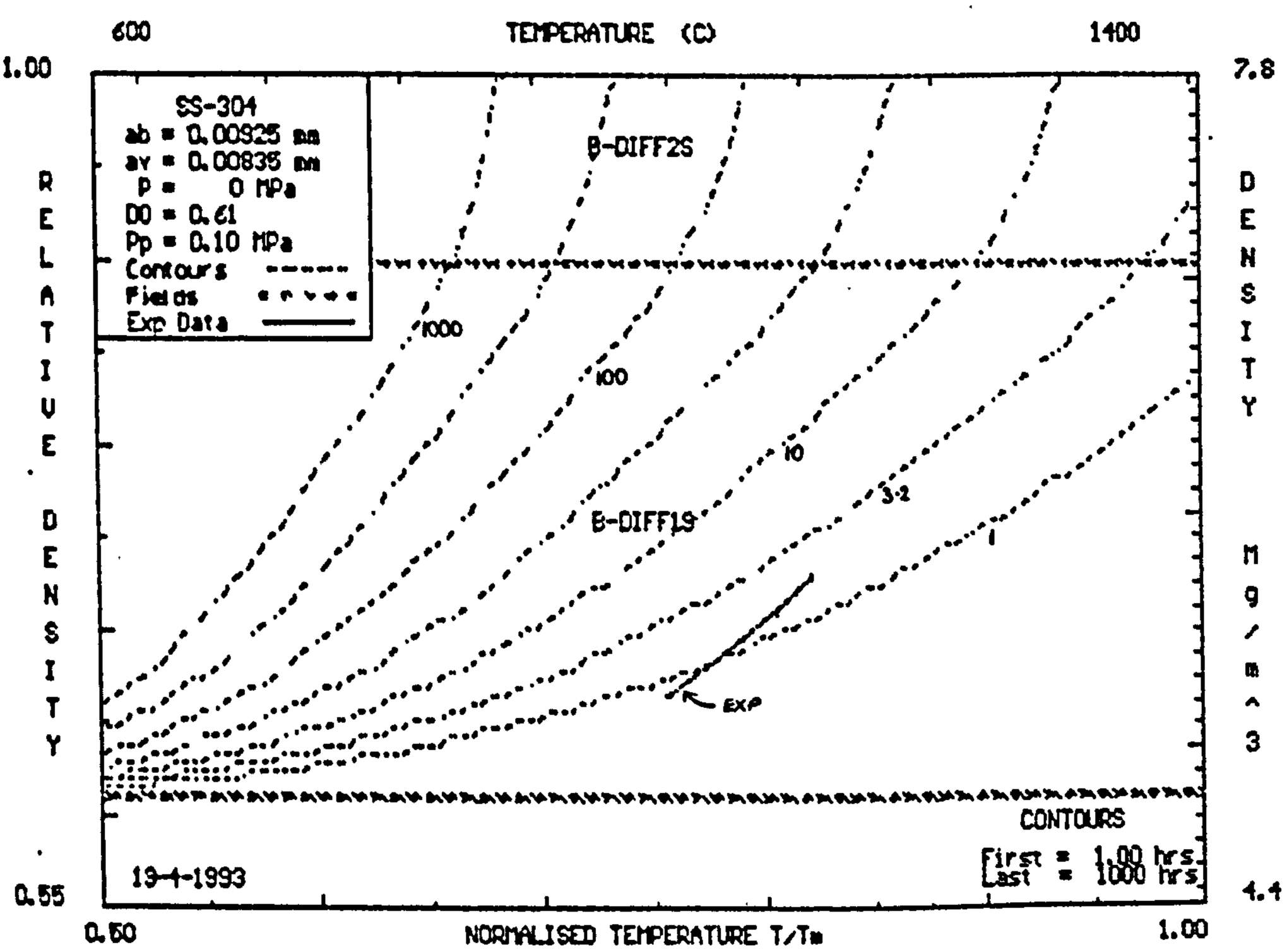

Figure 59. HIP792 Map for SS-304.
(a) Assuming Normal Powder Distribution.

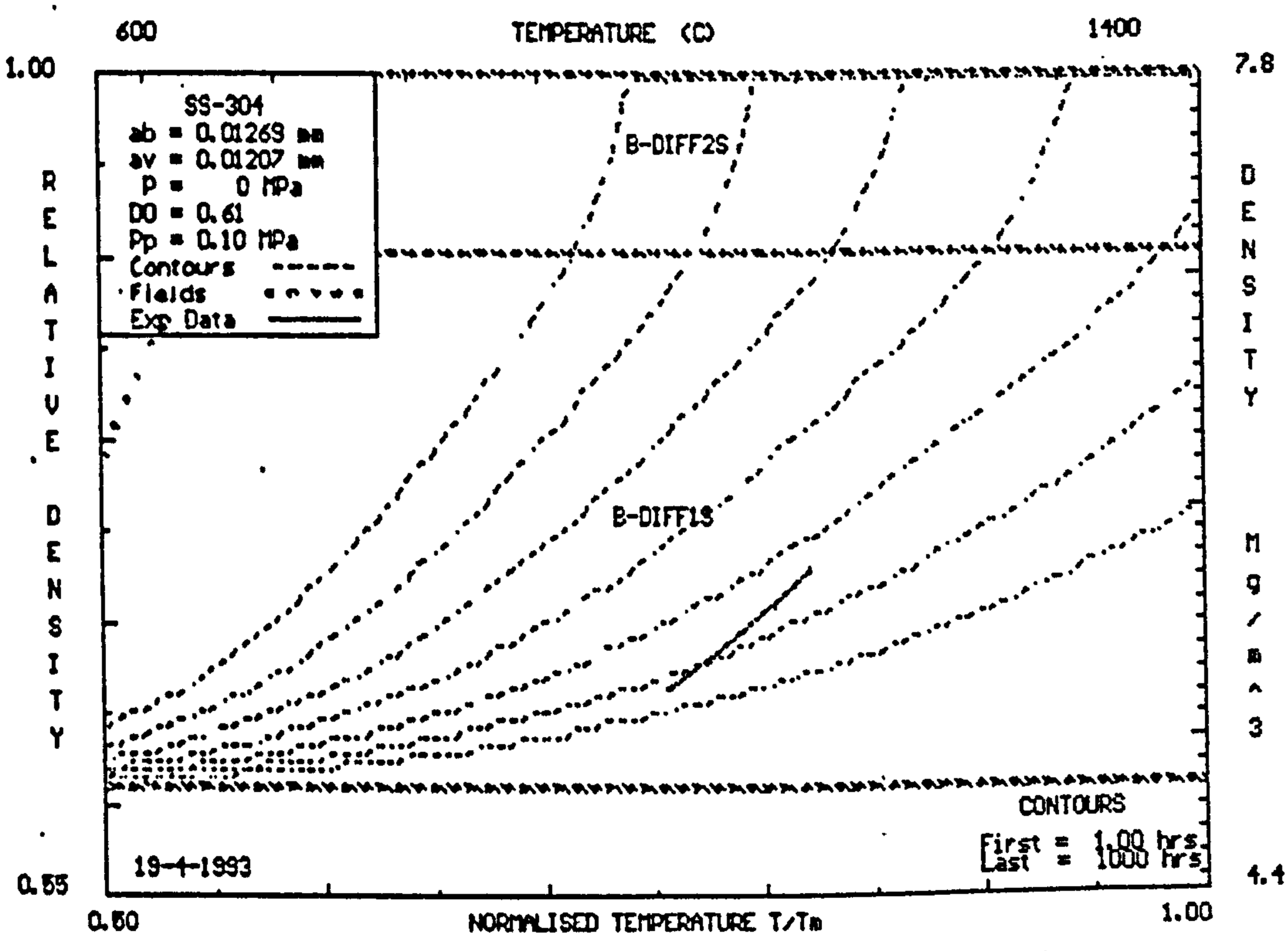

Figure 59. HIP792 Map for SS-304.
(b) Assuming Log-Normal Distribution.

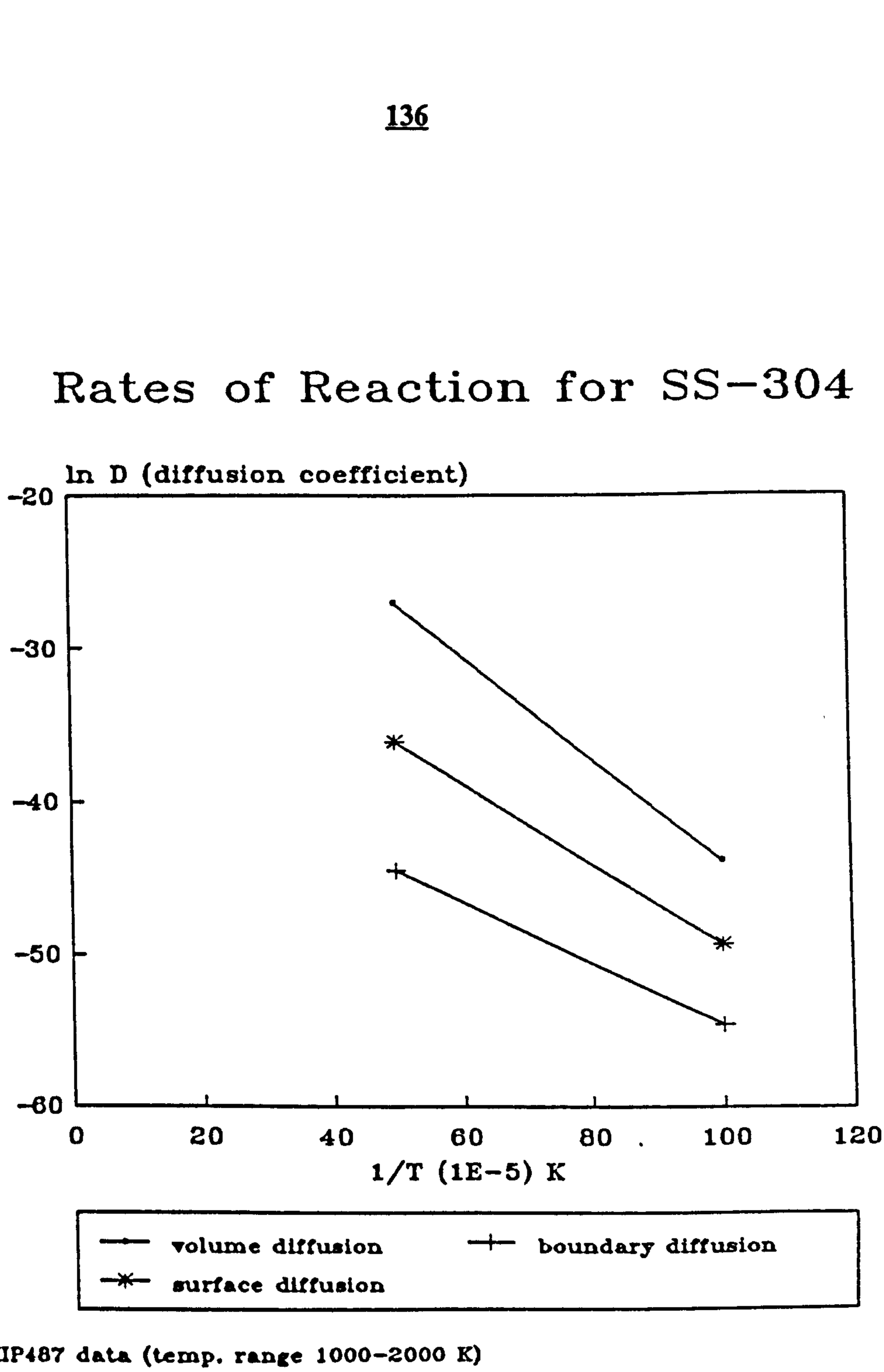

Figure 60. Rates of Reaction for Diffusion Mechanisms for SS-304, Calculated from HIP487 Data.[118]

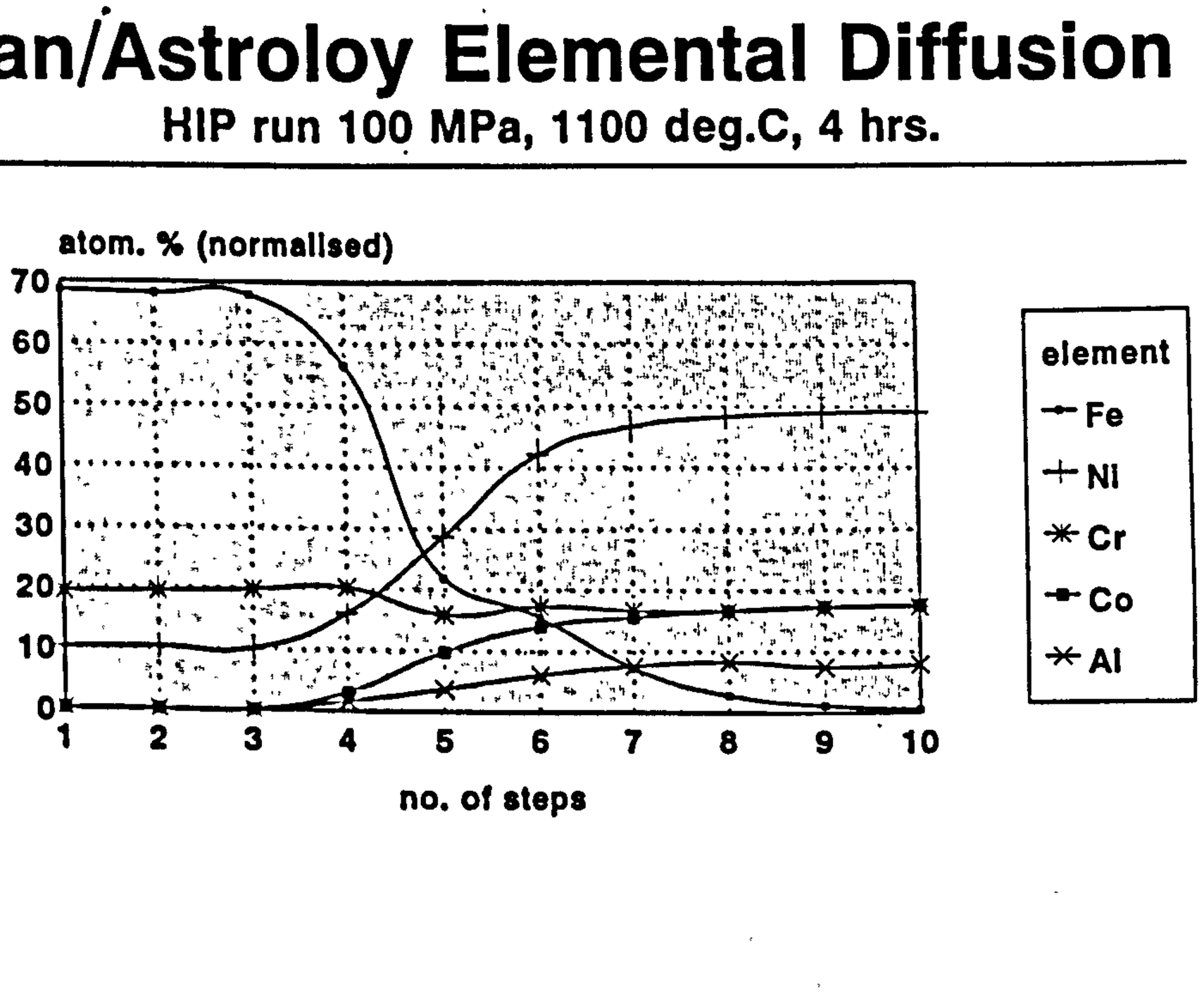

Figure 61. SEM Digipoint Analysis for Can/Astroloy Diffusion.

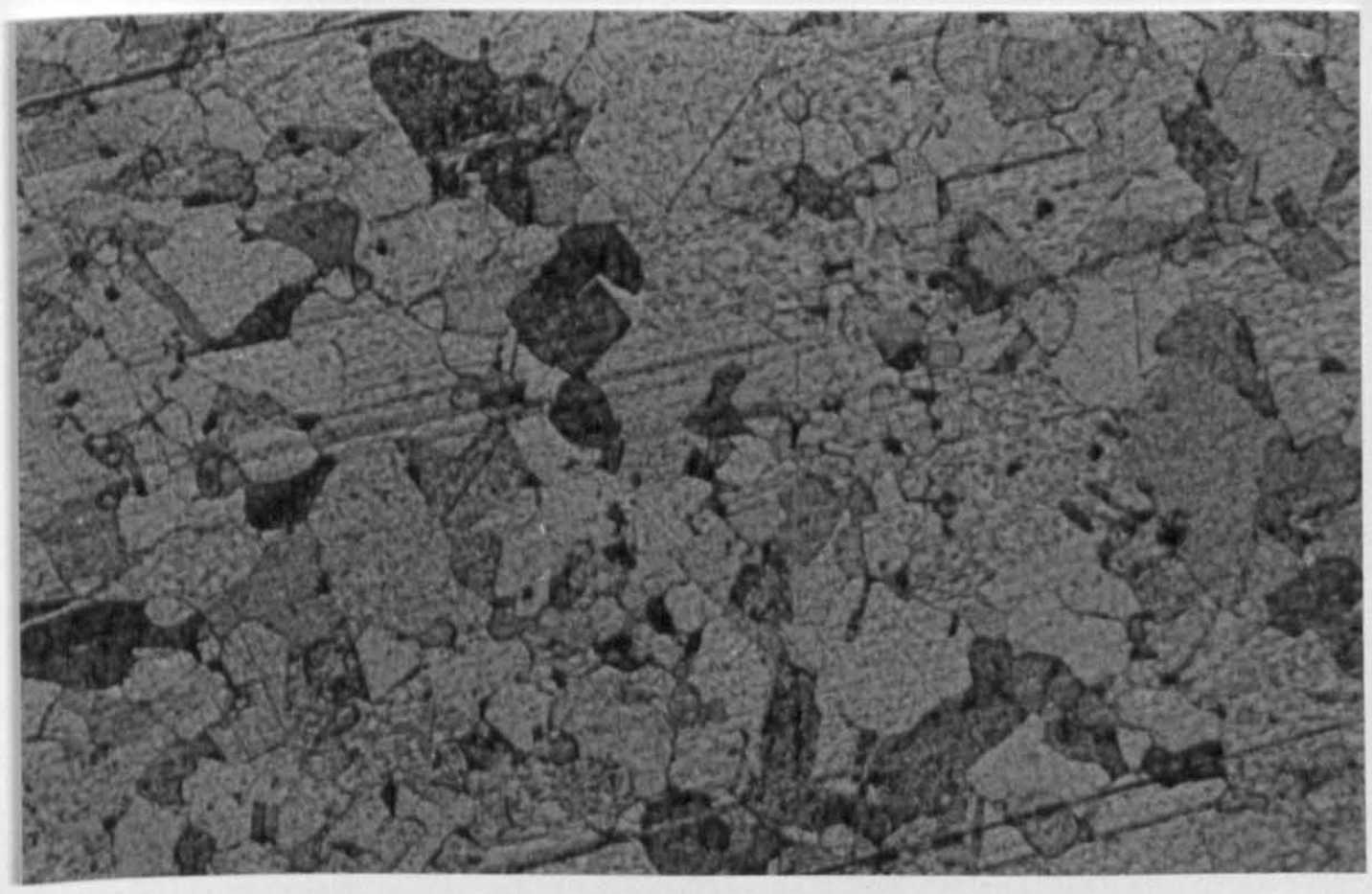

(a)

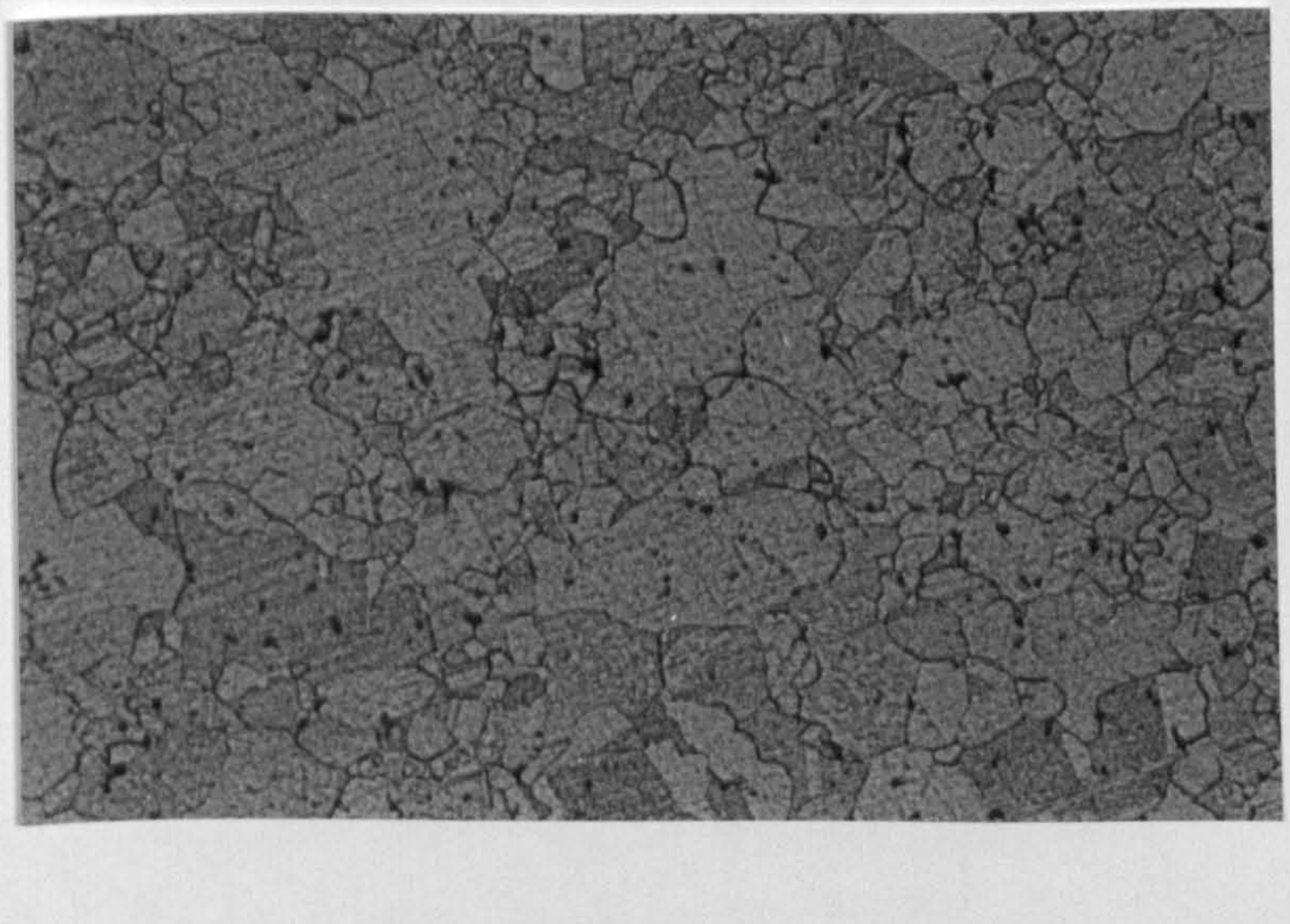

(b)

Figure 62. Comparison of Compact Microstructure with Differing Can Length Design (mag.X600).
(a) 20 mm Length Can.
(b) 30 mm Length Can.

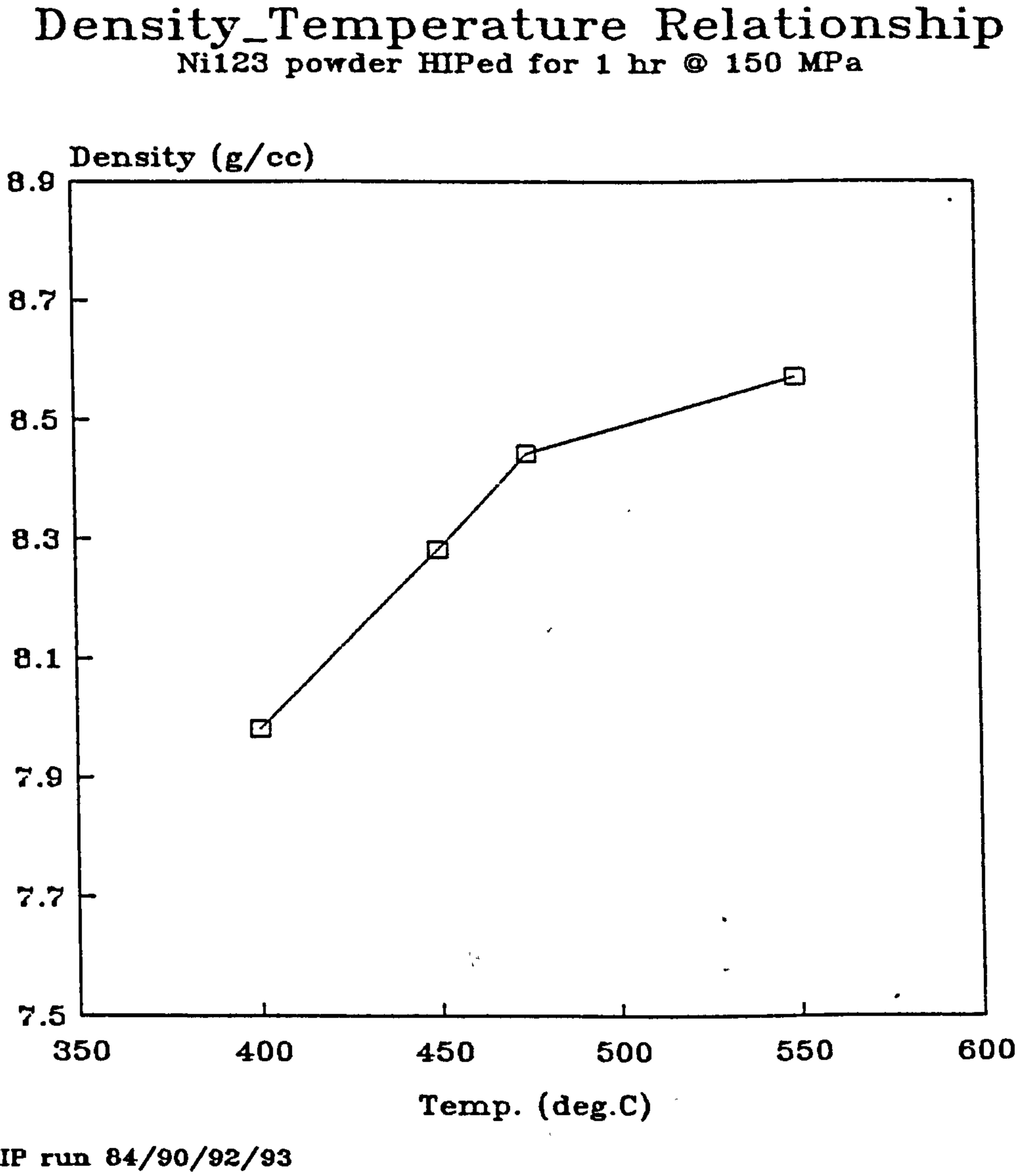

Figure 63. The Density-Temperature Relationship for HIP'ed Containerised Ni123 Powder.

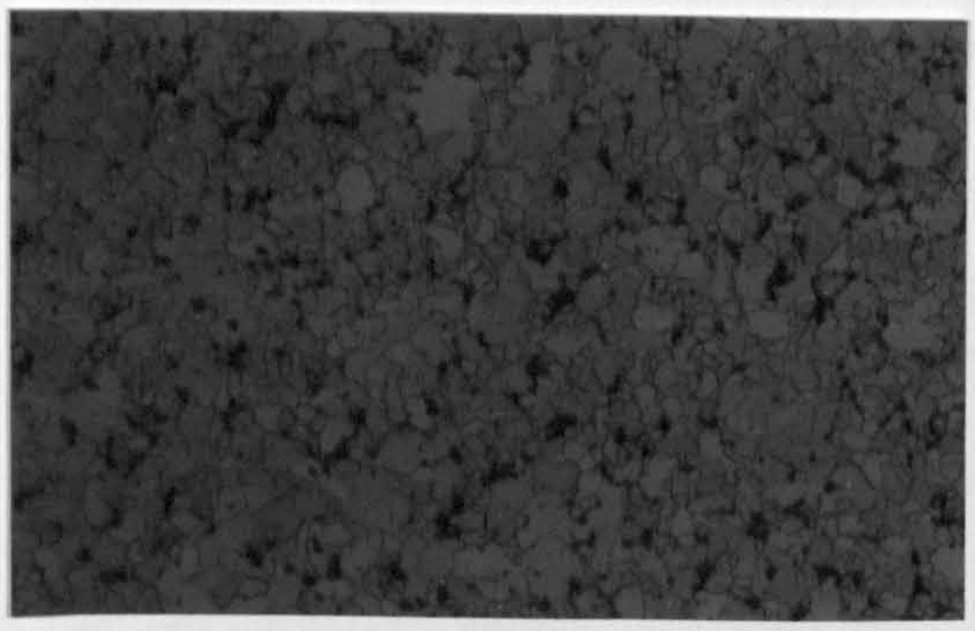

(a)

(b)

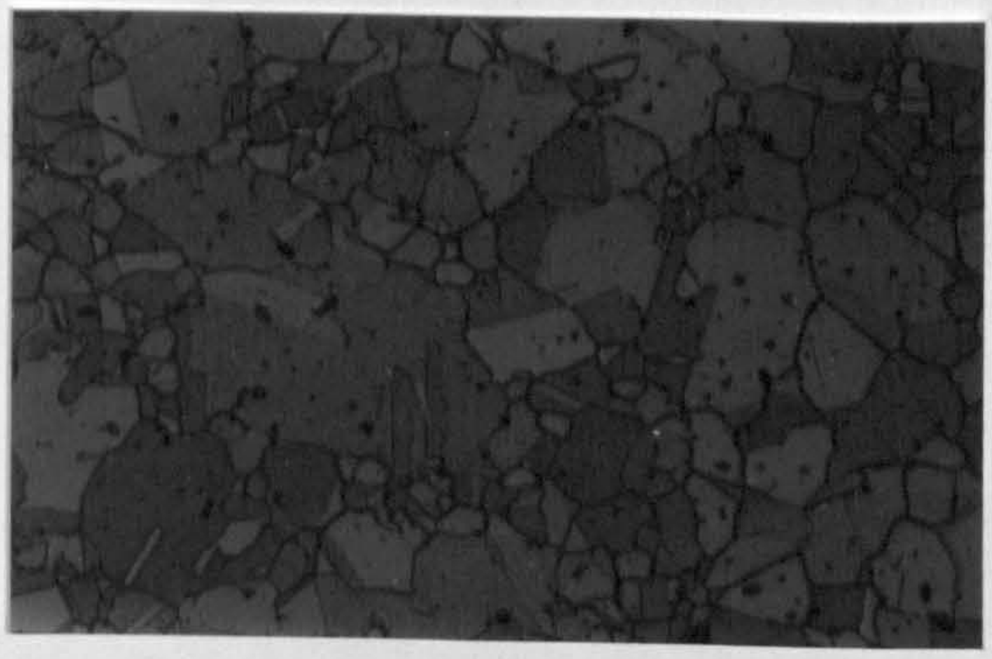

(c)

Figure 64. Microstructural Development (mag.X400).
(a) 400 °C (b) 475 °C (c) 550 °C.

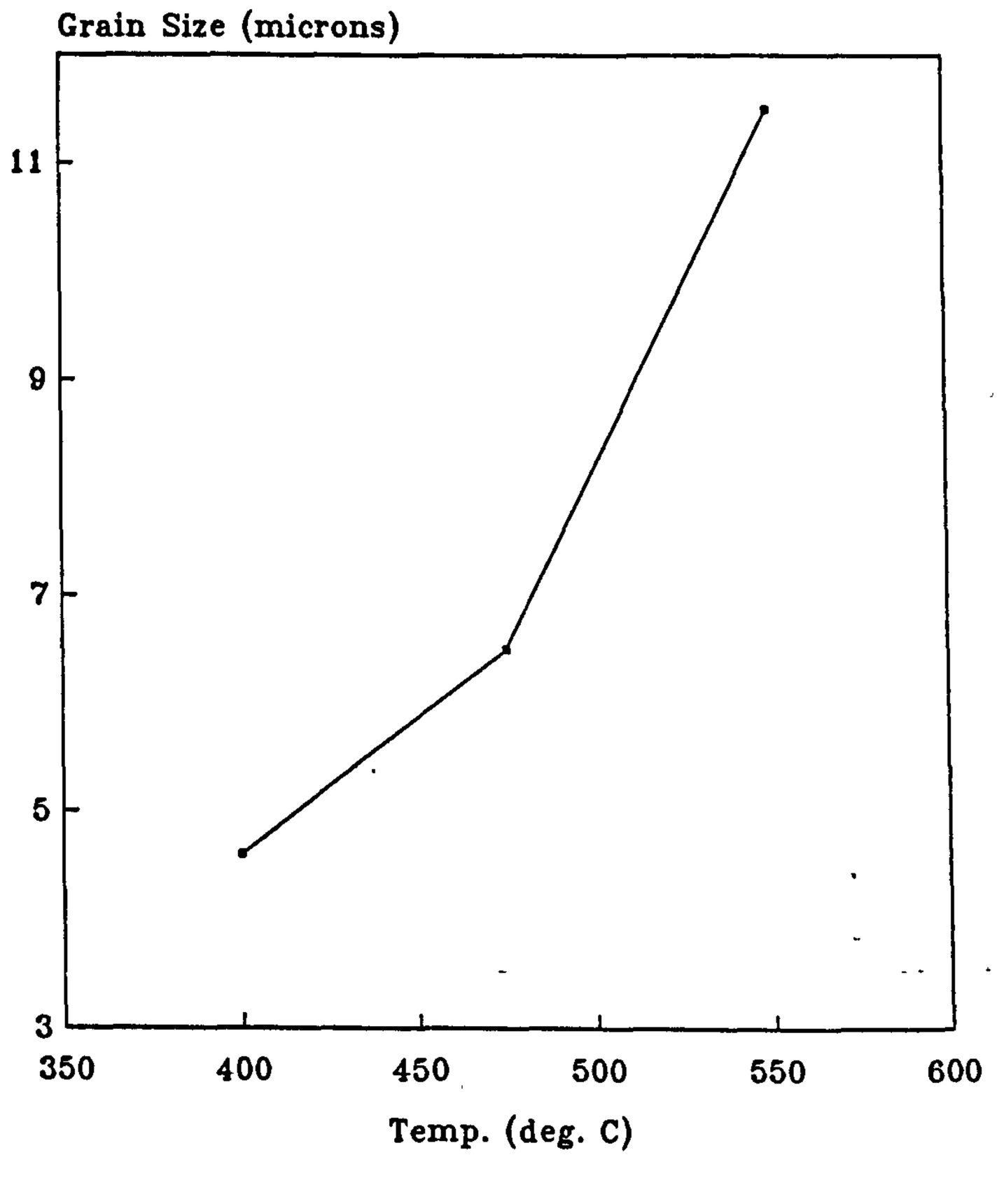

Figure 64. (d) Grain Growth as a Function of Temperature.

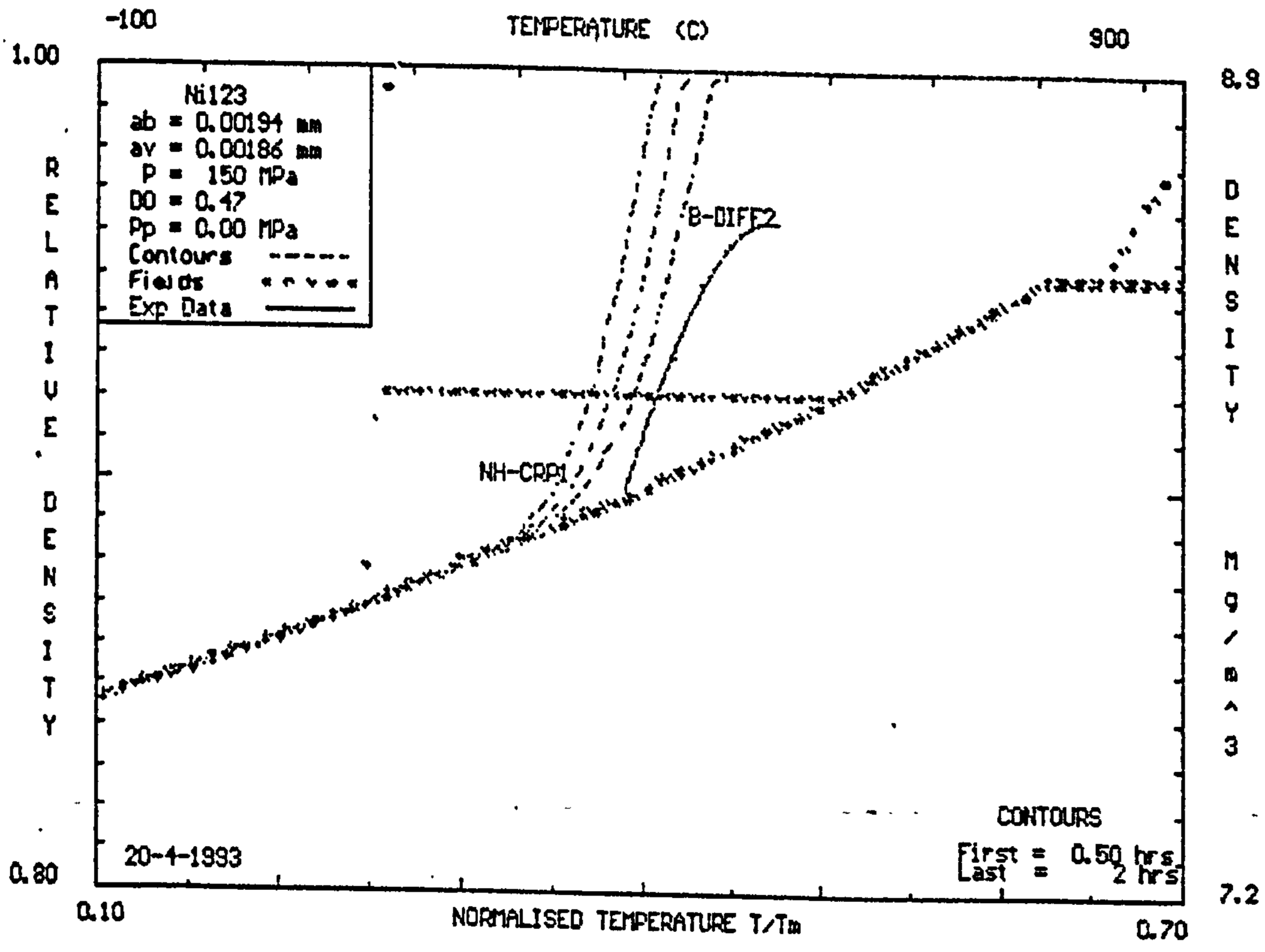

Figure 65. HIP792 Temperature Map.

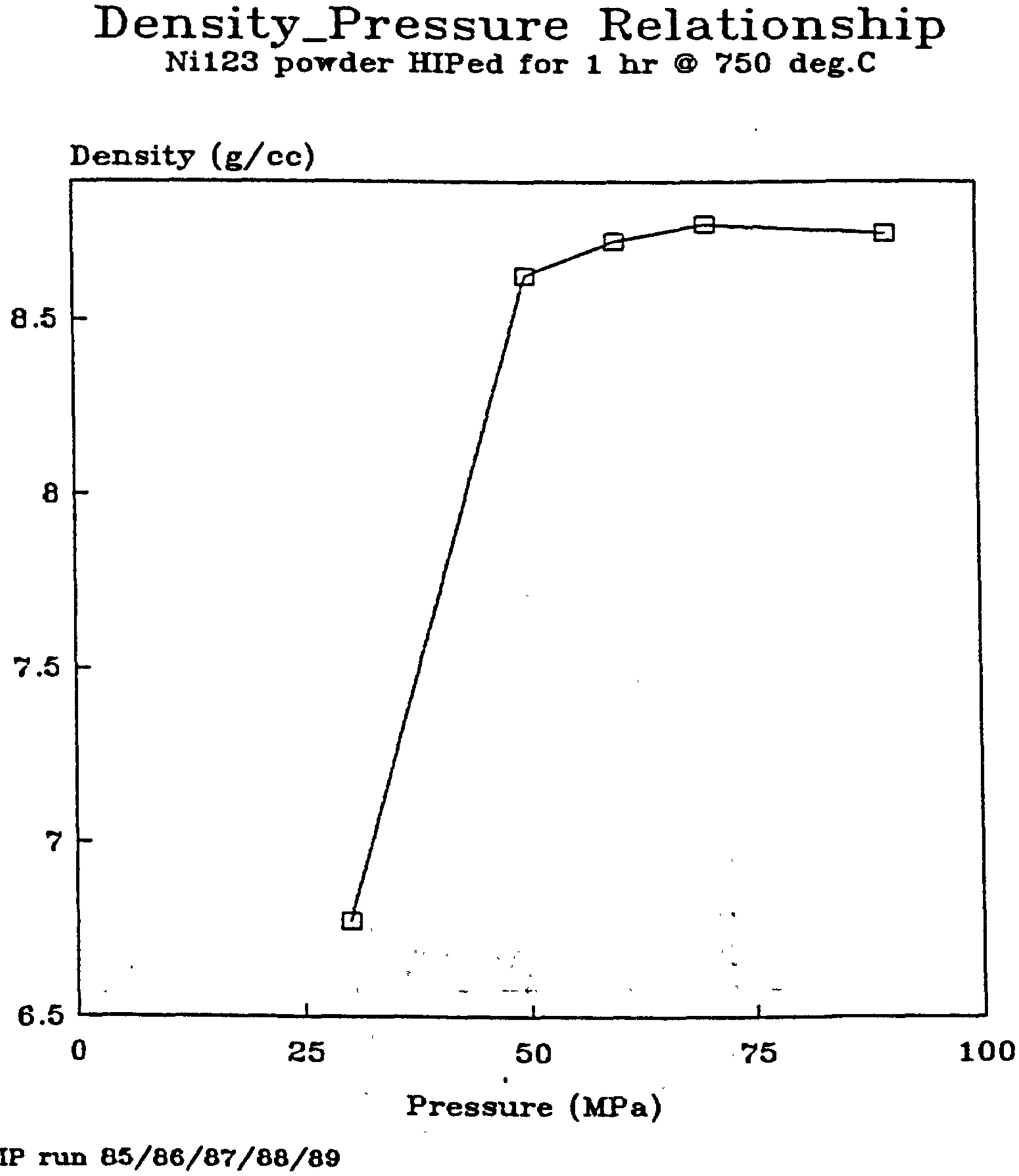

Figure 66. The Density-Pressure Relationship for HIP'ed Containerised Ni123 Powder.

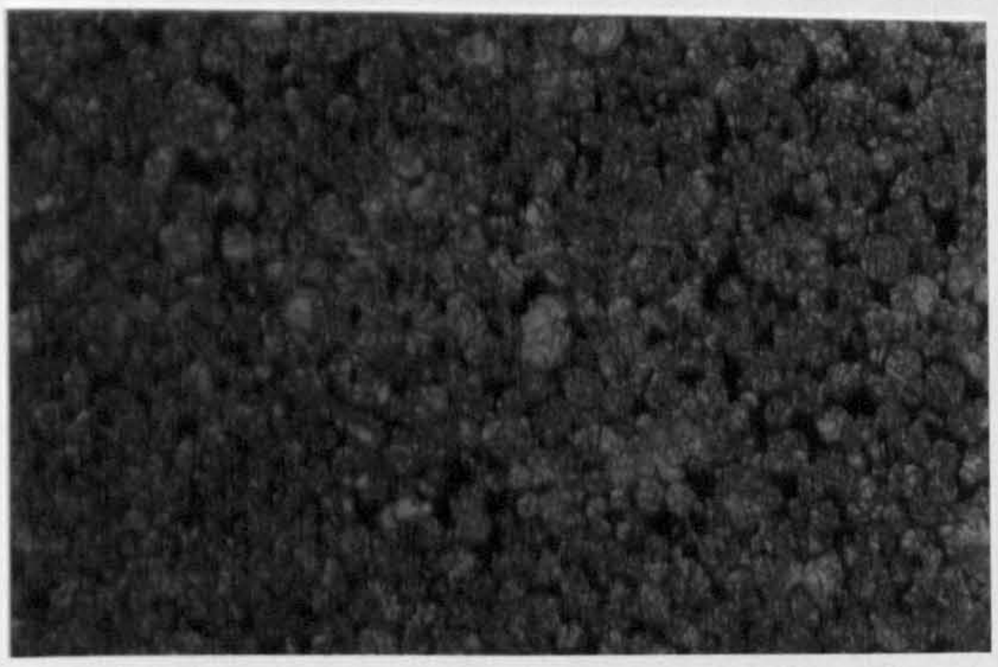

(a)

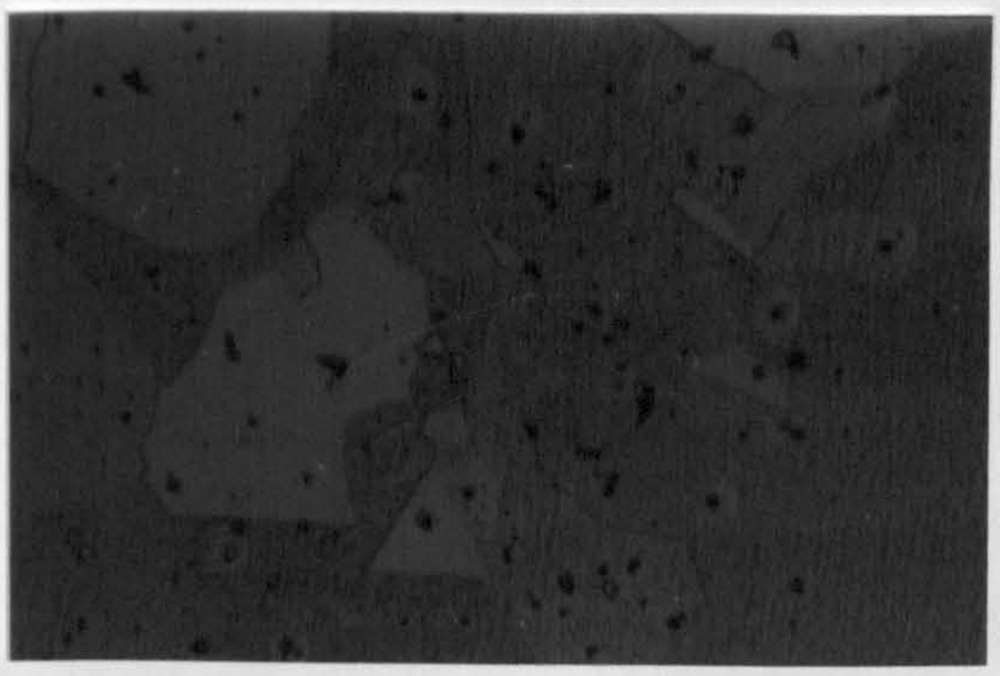

(b)

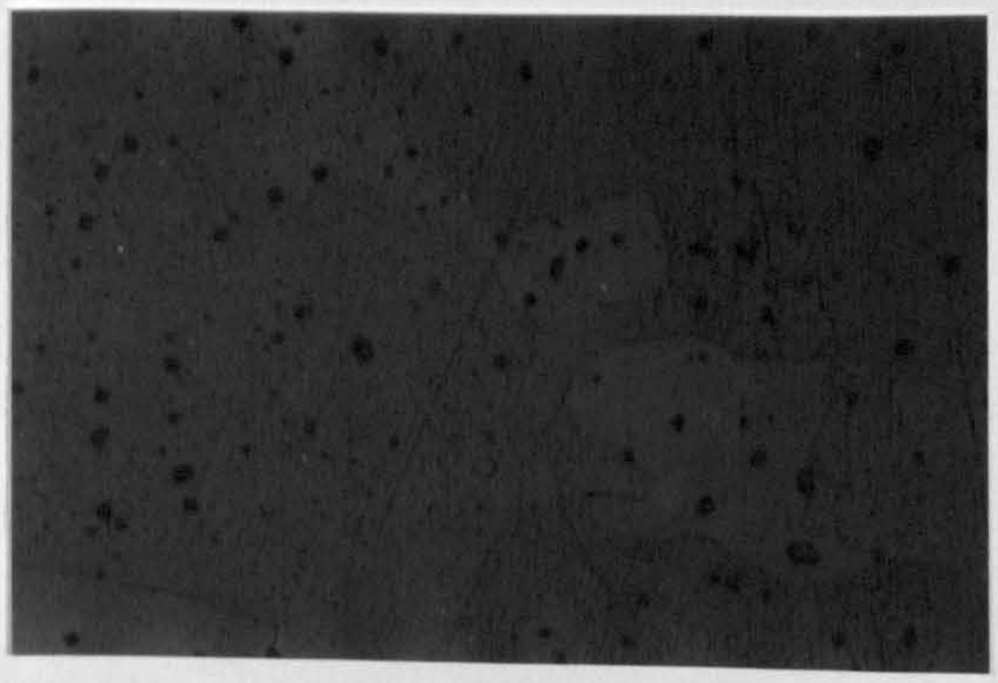

(c)

Figure 67. Microstructural Development (mag.X400).
(a) 30 MPa (b) 60 MPa (c) 90 MPa.

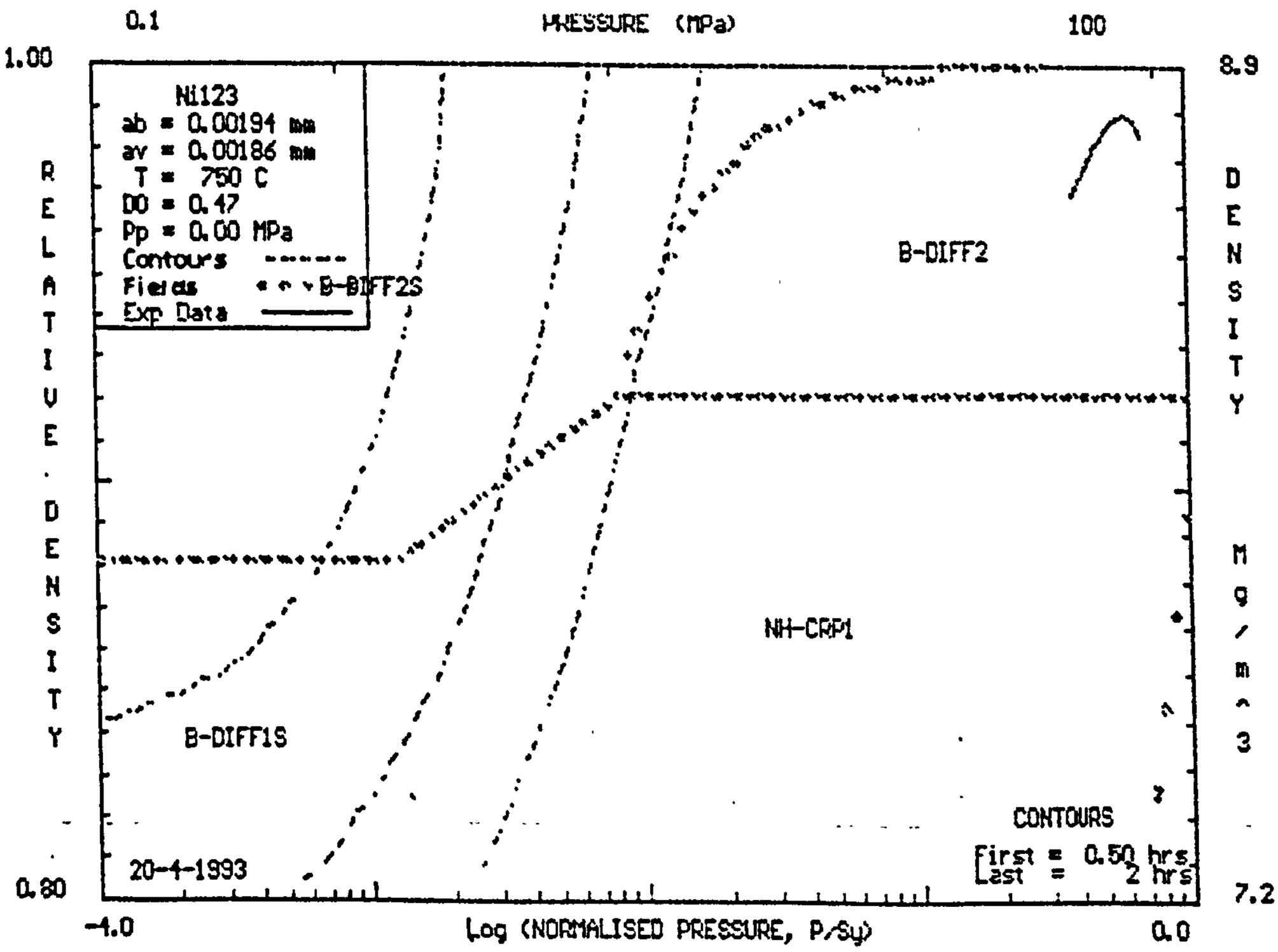

Figure 68. HIP792 Pressure Map.

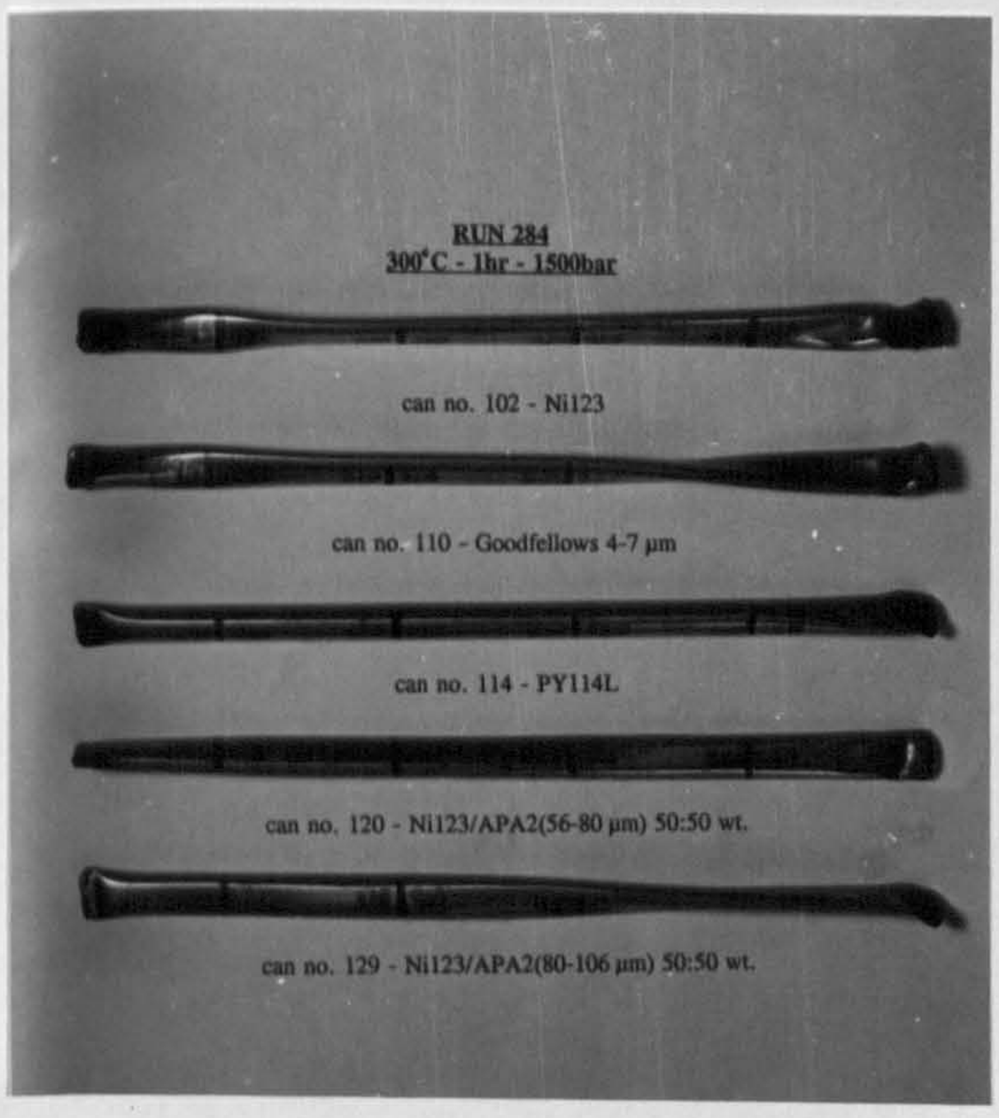

Figure 69. Deformation of Filled Cans following the Application of a HIP Cycle.

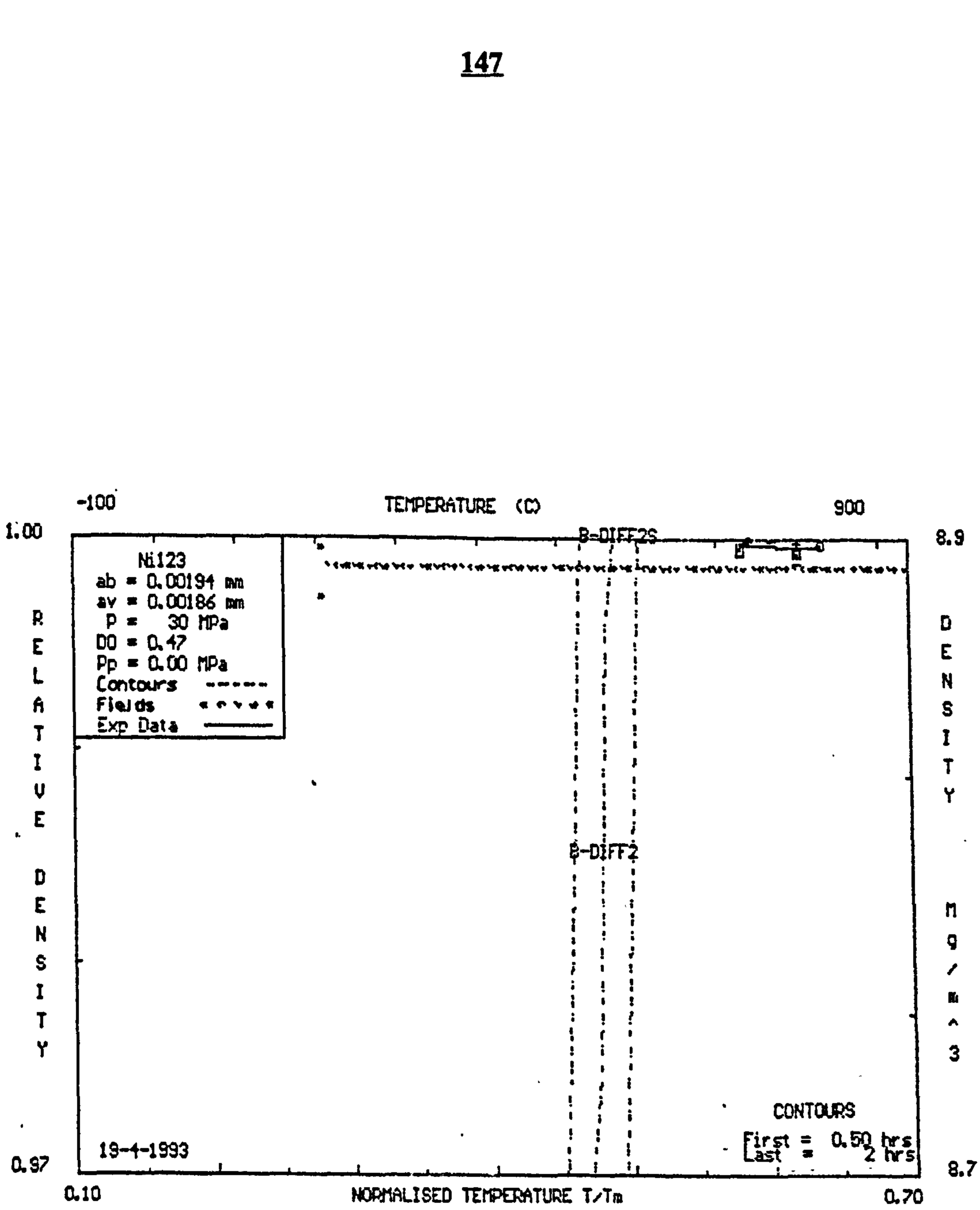

Figure 70. HIP792 Map for Ni123 Containerised Powder (Low Pressure).

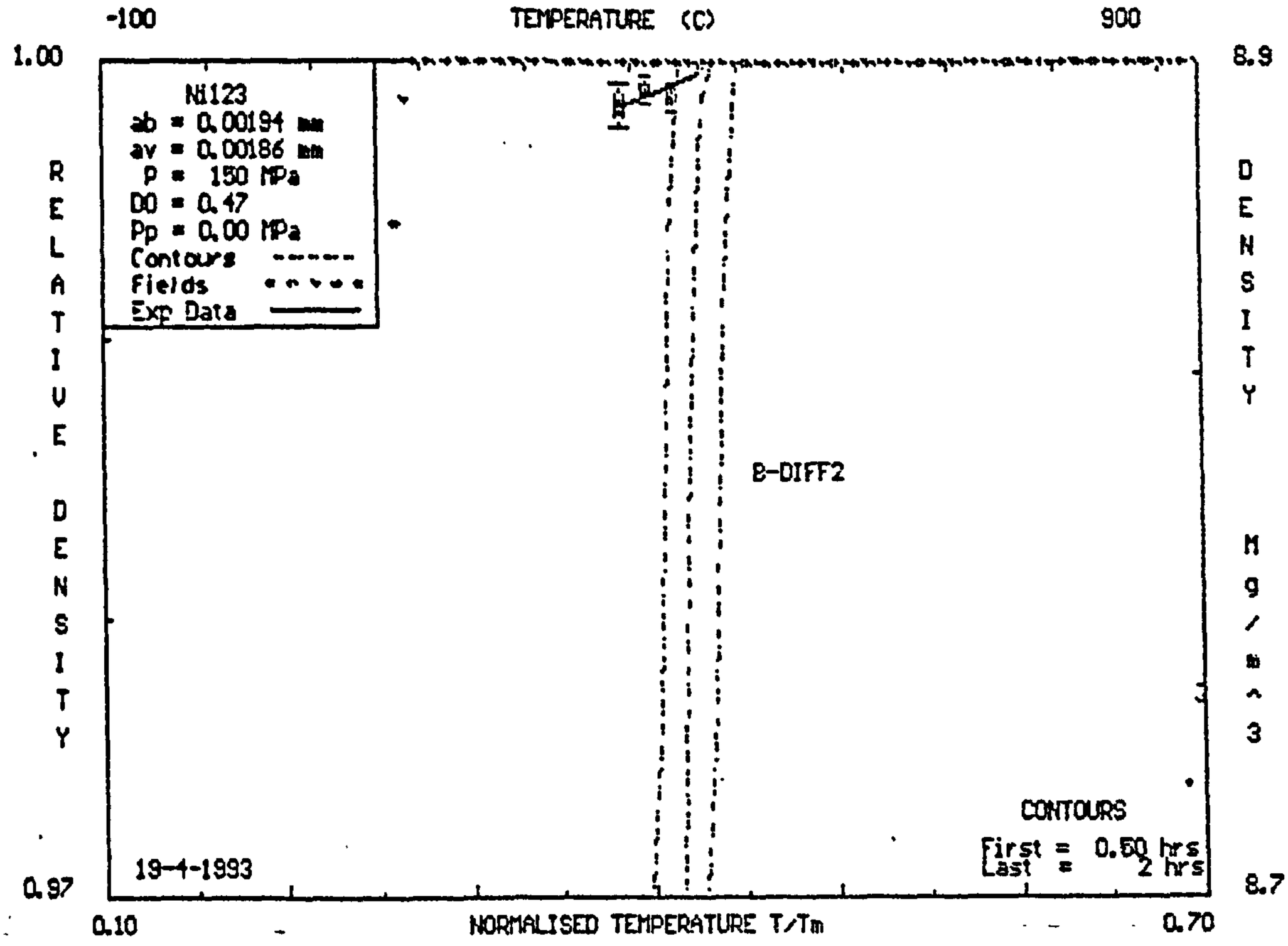

Figure 71. HIP792 Map for Ni123 Containerised Powder (High Pressure).

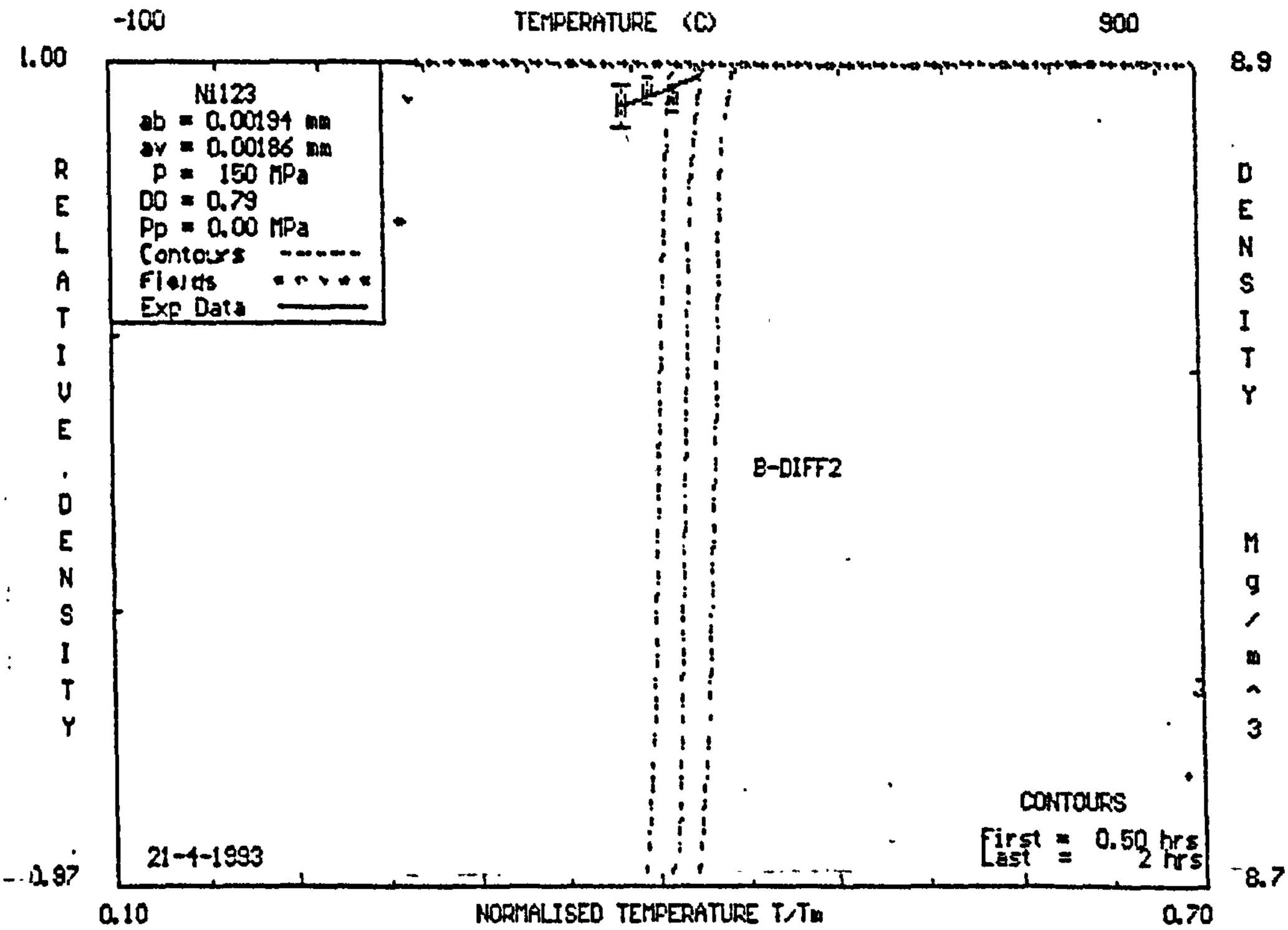

Figure 72. HIP792 Map for Ni123 Containerised Powder, with the Initial Packing Density Set High to Simulate Densification During Heat-Up.

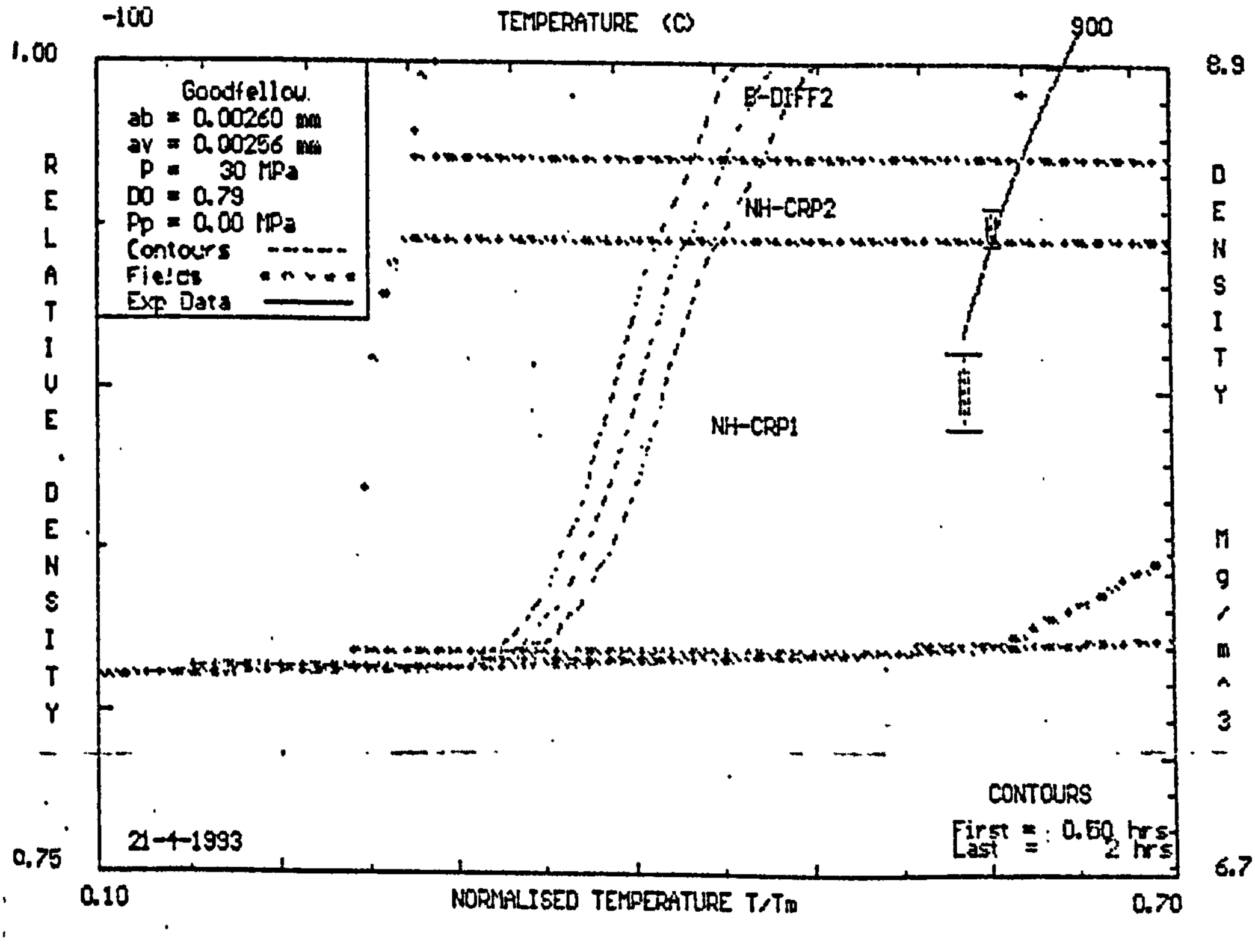

Figure 73. HIP792 Map for Containerised Goodfellow Powder (Low Pressure).

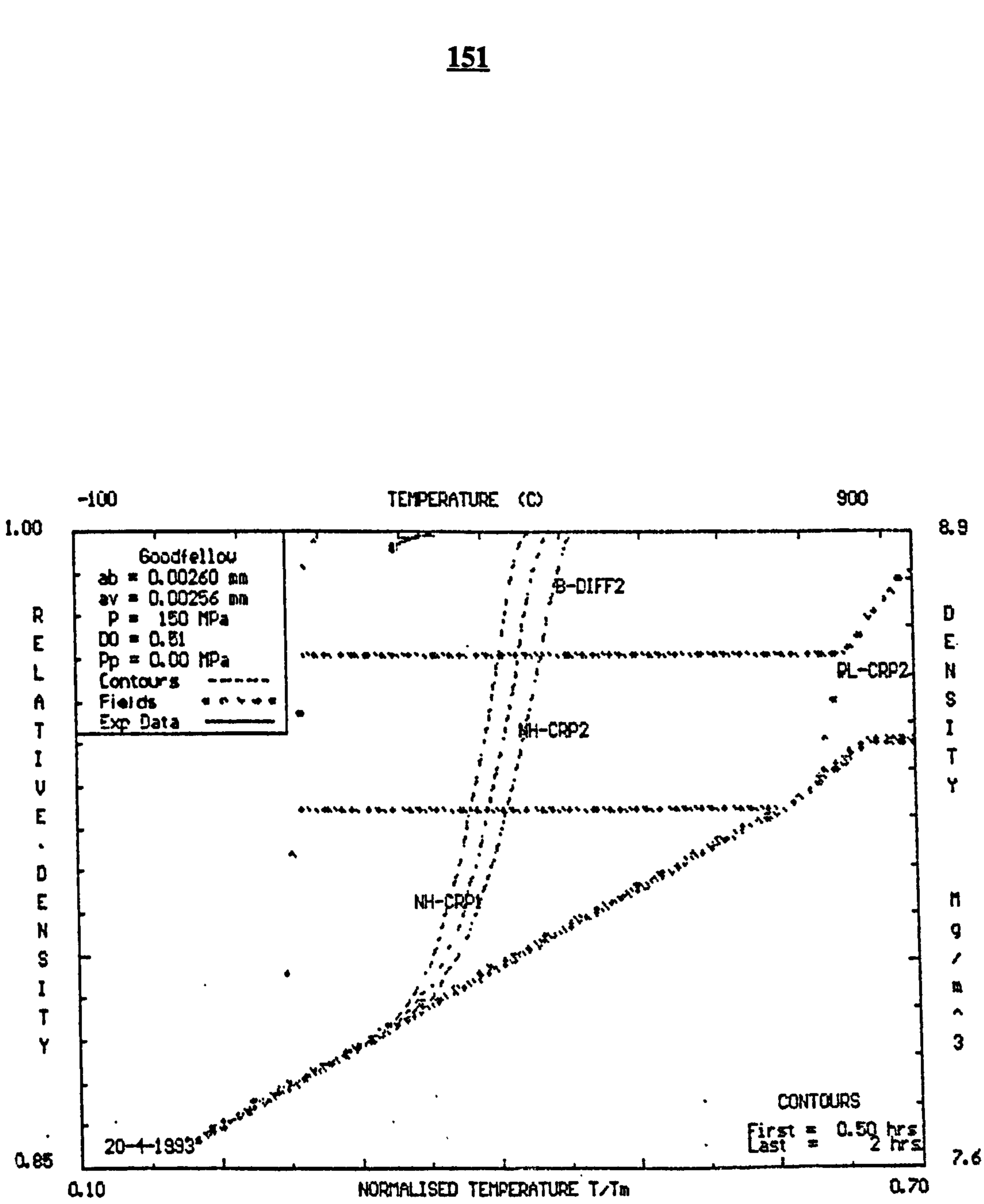

Figure 74. HIP792 Map for Containerised Goodfellow Powder (High Pressure).

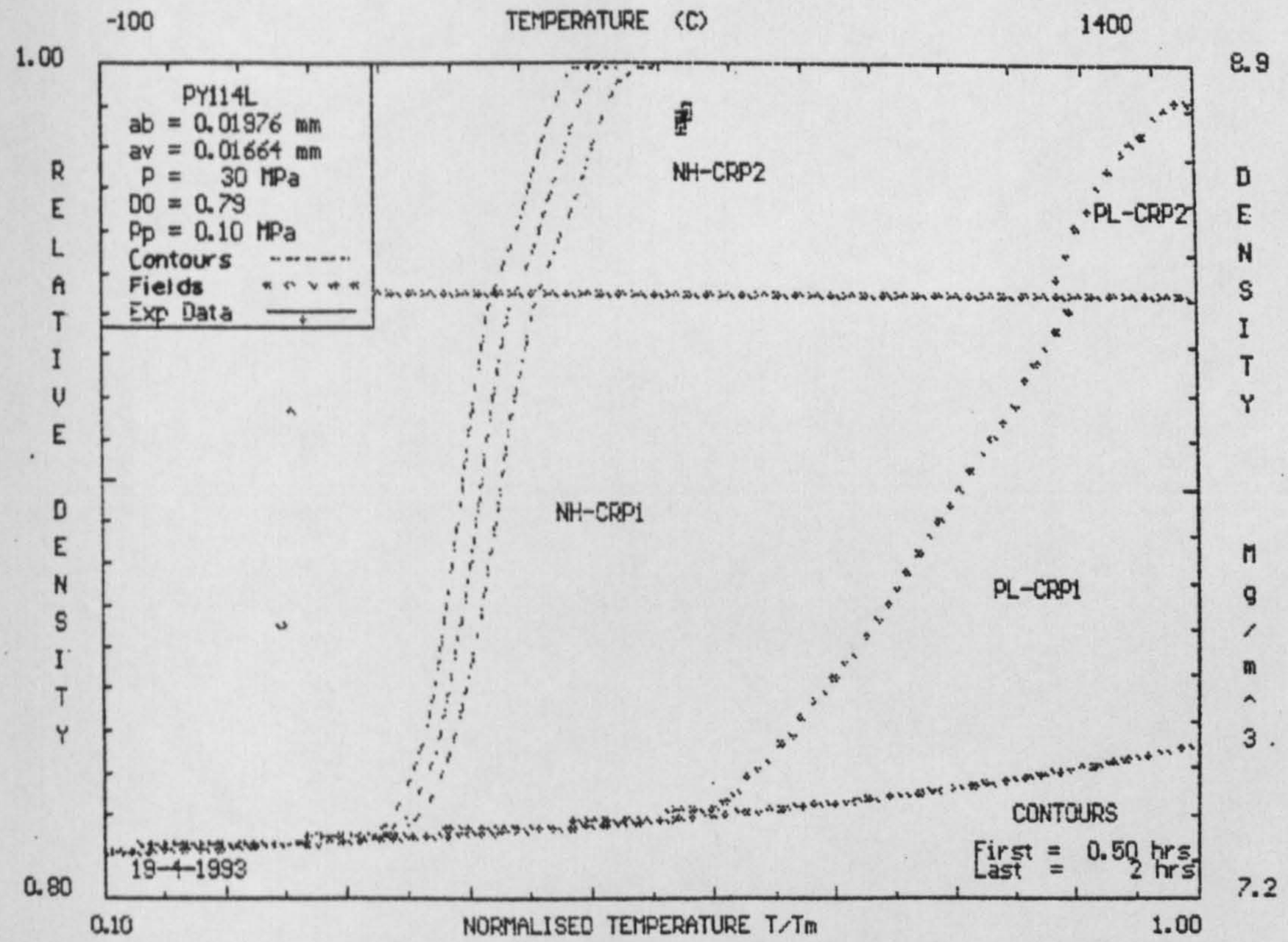

(a)

(b)

Figure 75. (a) HIP792 Map for Containerised PY114L Powder.
(b) Prior Particle Boundaries Still Visible at 800 °C (mag.X300).

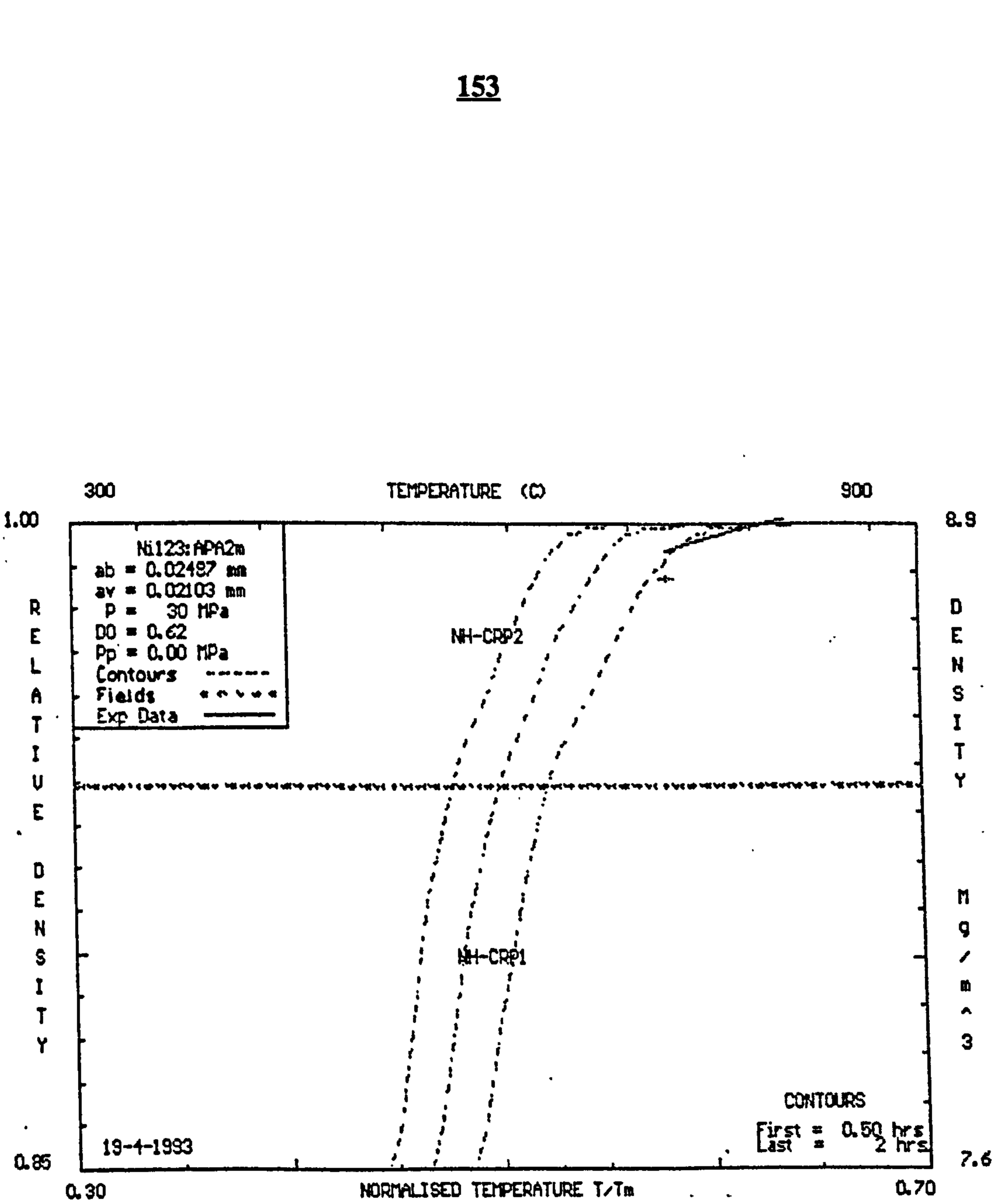

Figure 76. (a) HIP792 Map for Containerised Ni123:APA2m Bimodal Powder - Grain Size of 1 μm.

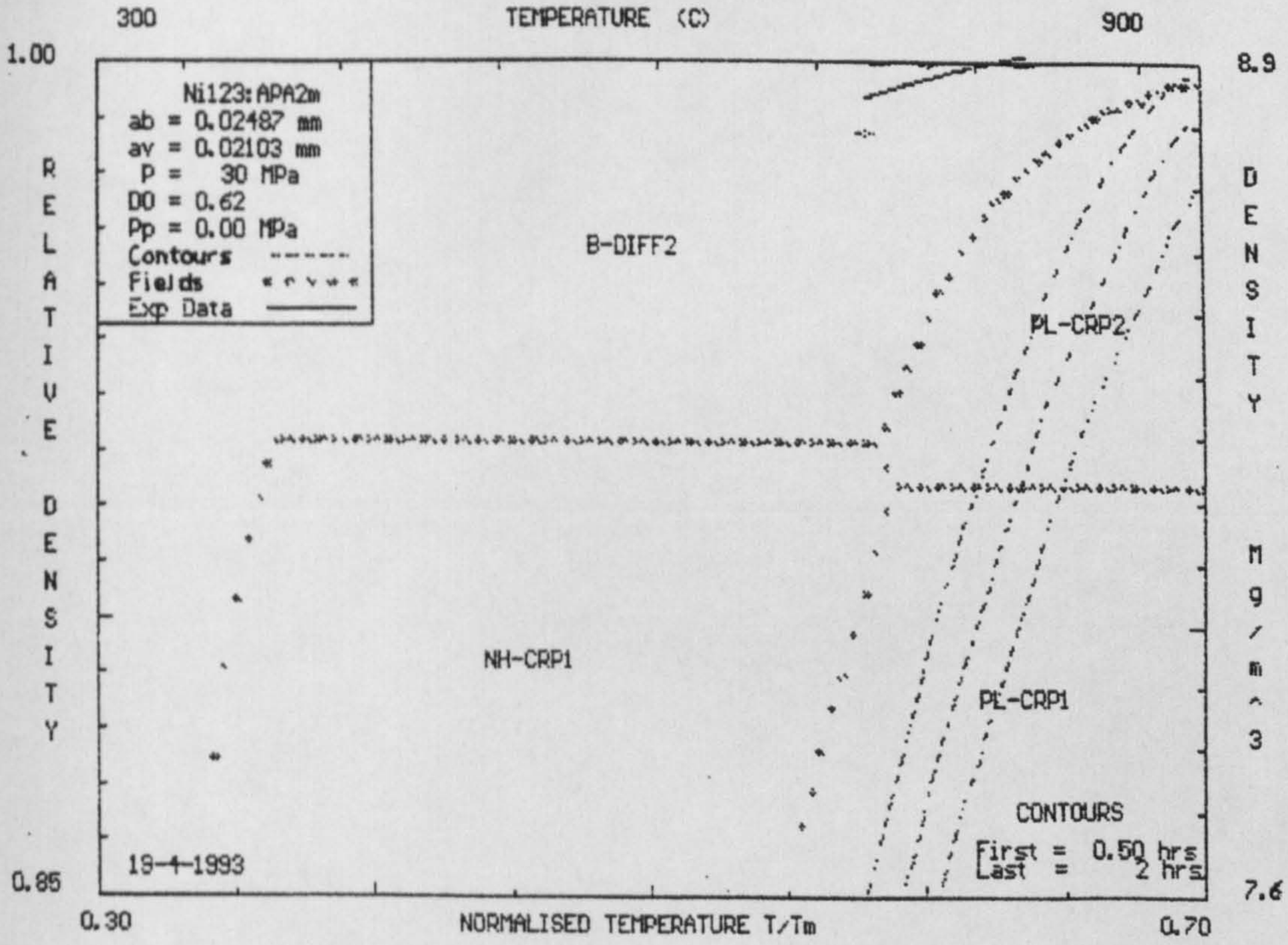

(b)

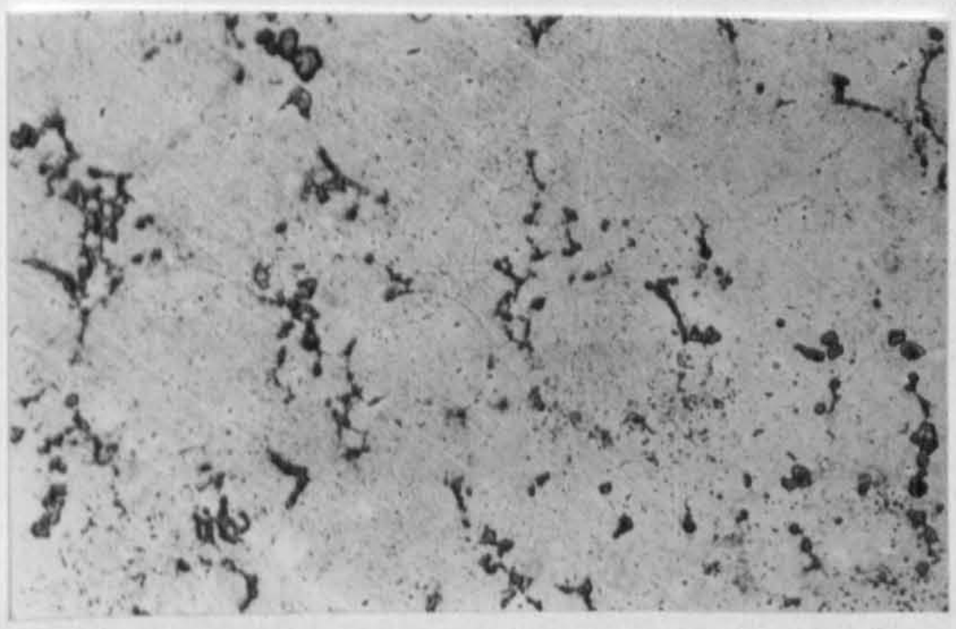

(c)

Figure 76. (b) HIP792 Map for Containerised Ni123:APA2m Bimodal Powder - Grain Size of 8 μm.
(c) Undeformed Large Size Fraction at 770 °C.

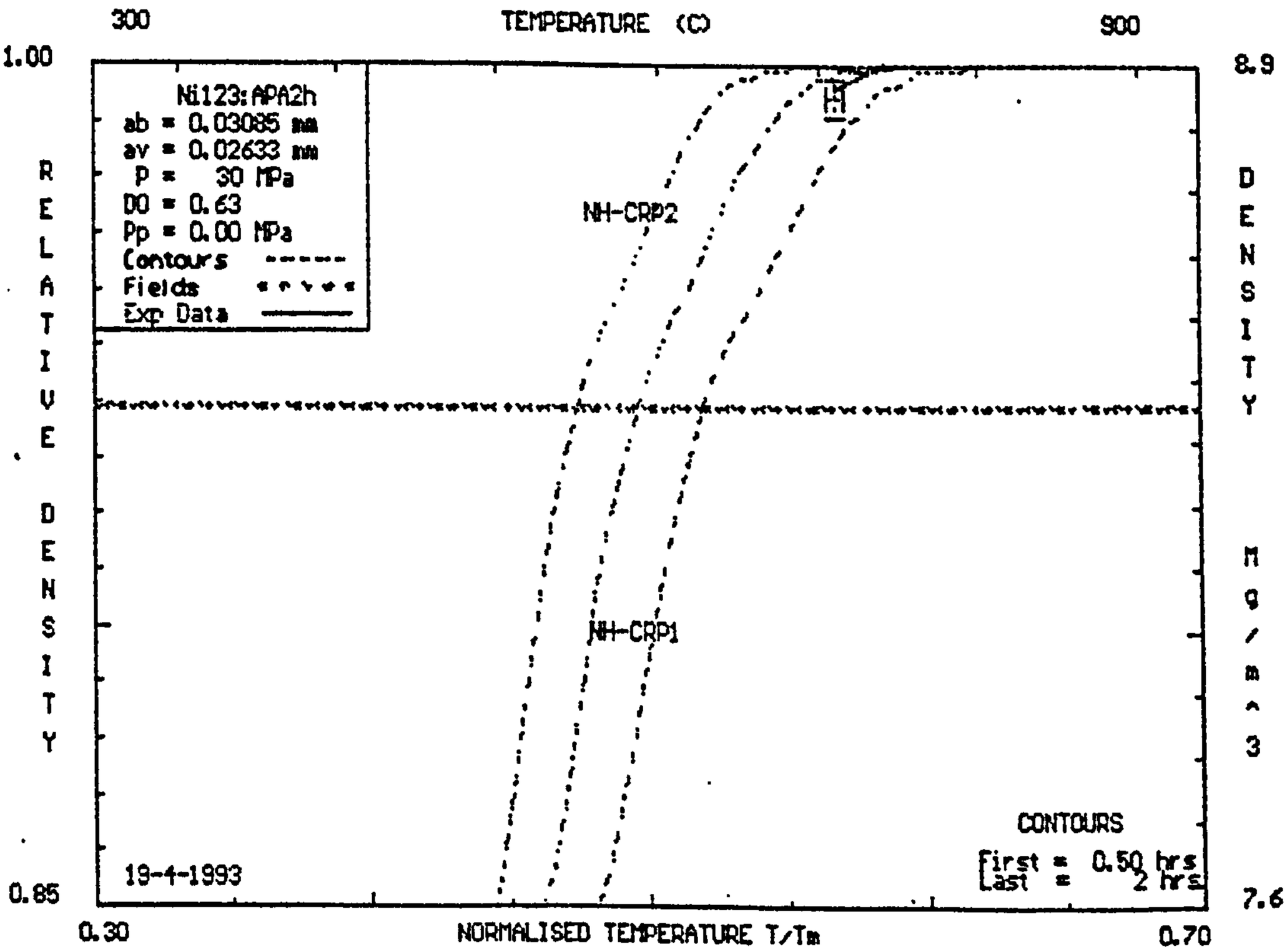

Figure 77. HIP792 Map for Containerised Ni123:APA2h Bimodal Powder.
(a) Grain Size of 1 μm.

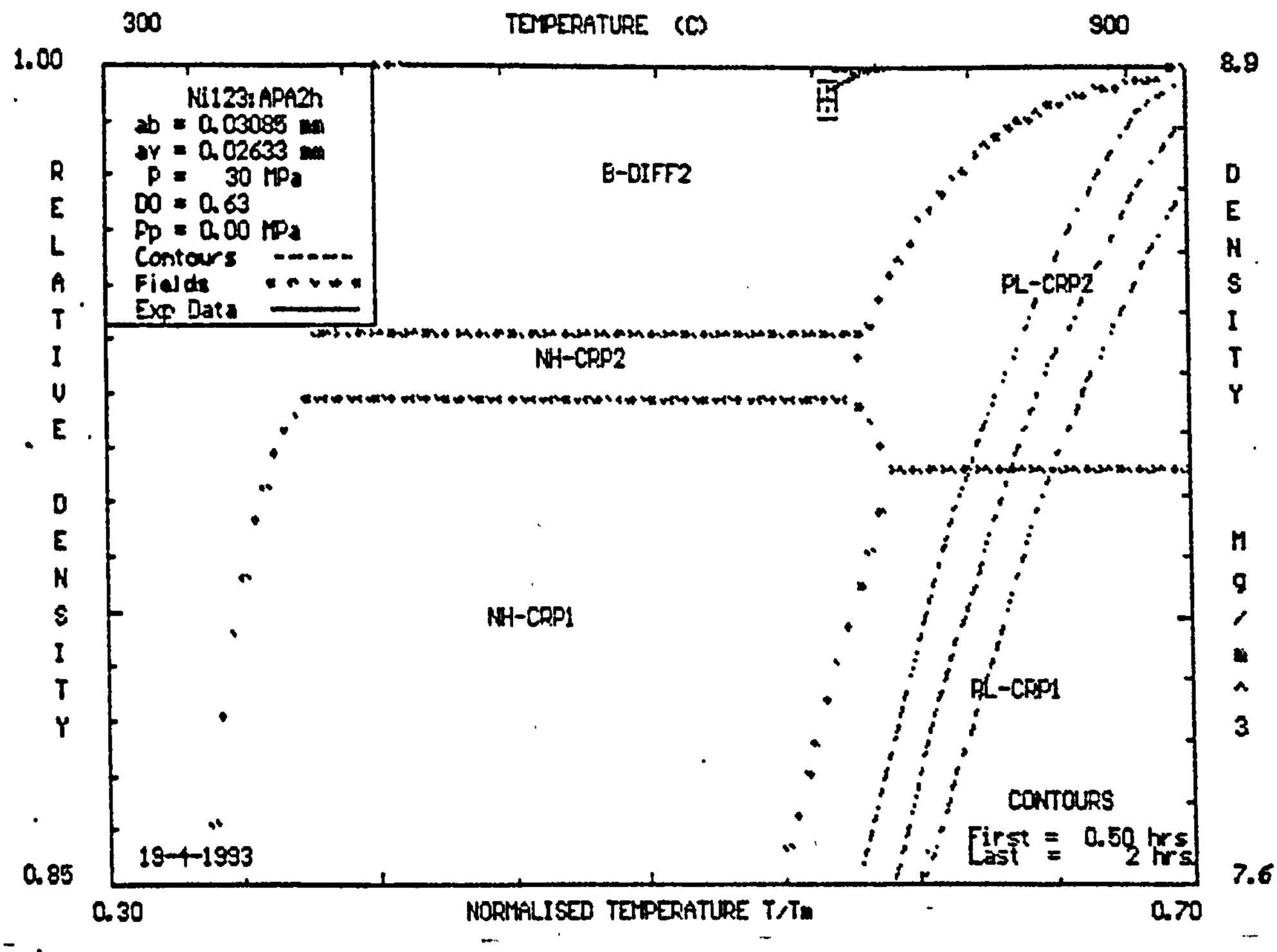

Figure 77. HIP792 Map for Containerised Ni123:APA2h Bimodal Powder. (b) Grain Size of 8 μm.

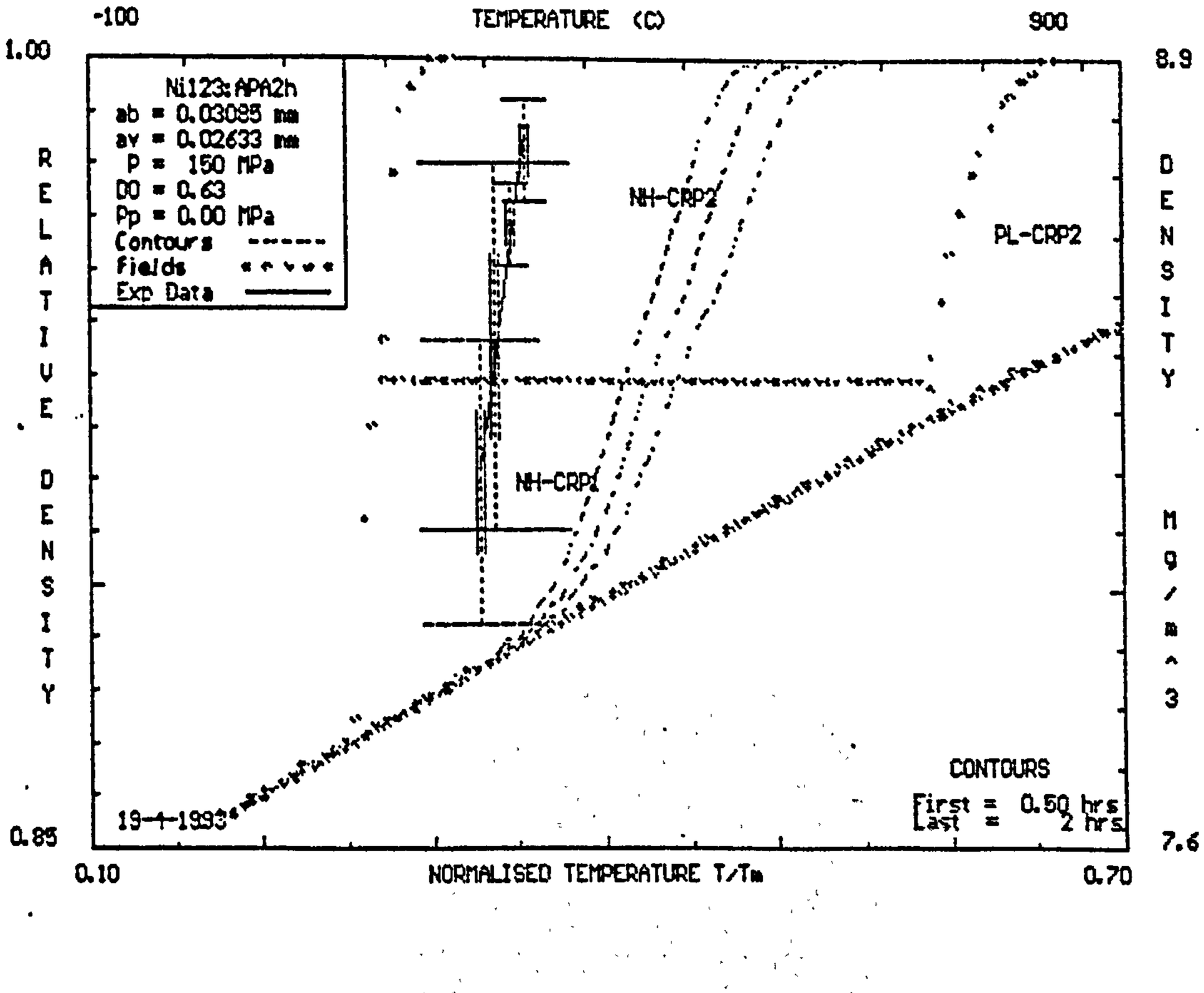

Figure 78. (a) HIP792 Map for Containerised Ni123:APA2h Bimodal Powder - Grain Size of 1 μm.

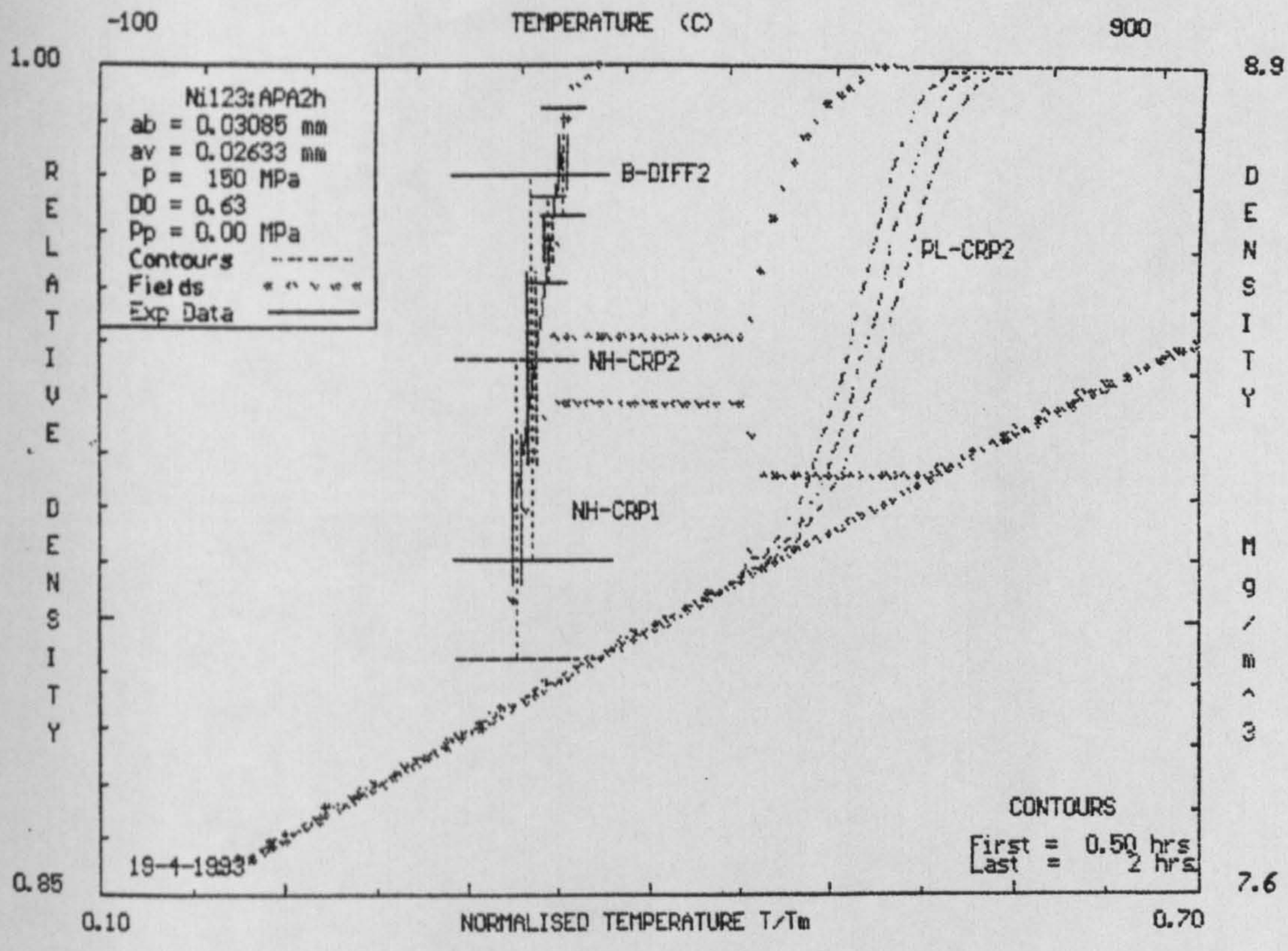

(b)

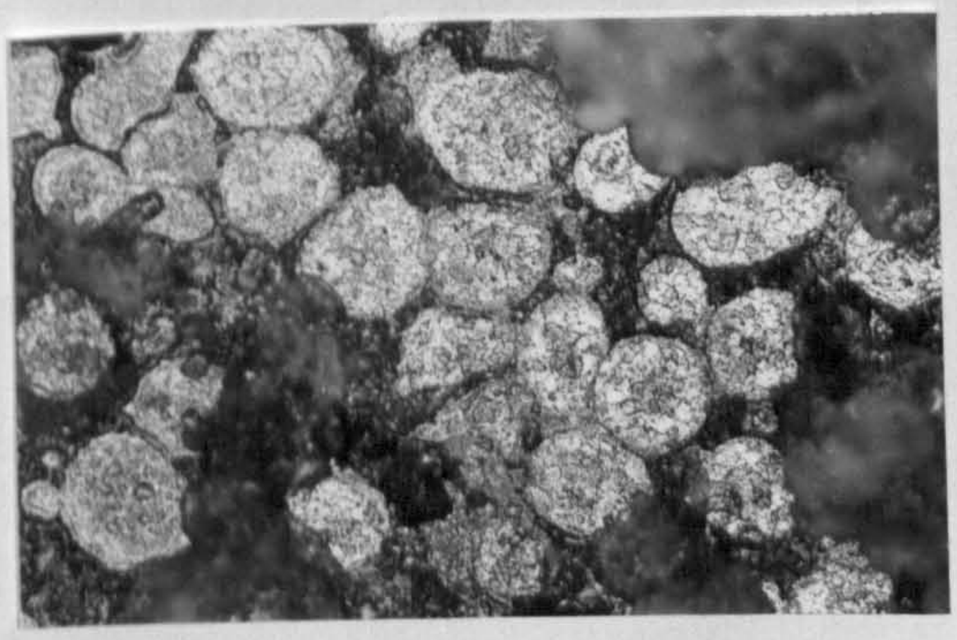

(c)

Figure 78. (b) HIP792 Map for Containerised Ni123:APA2h Bimodal Powder - Grain Size of 8 μm.
(c) Undeformed Large Size Fraction at 340 °C.

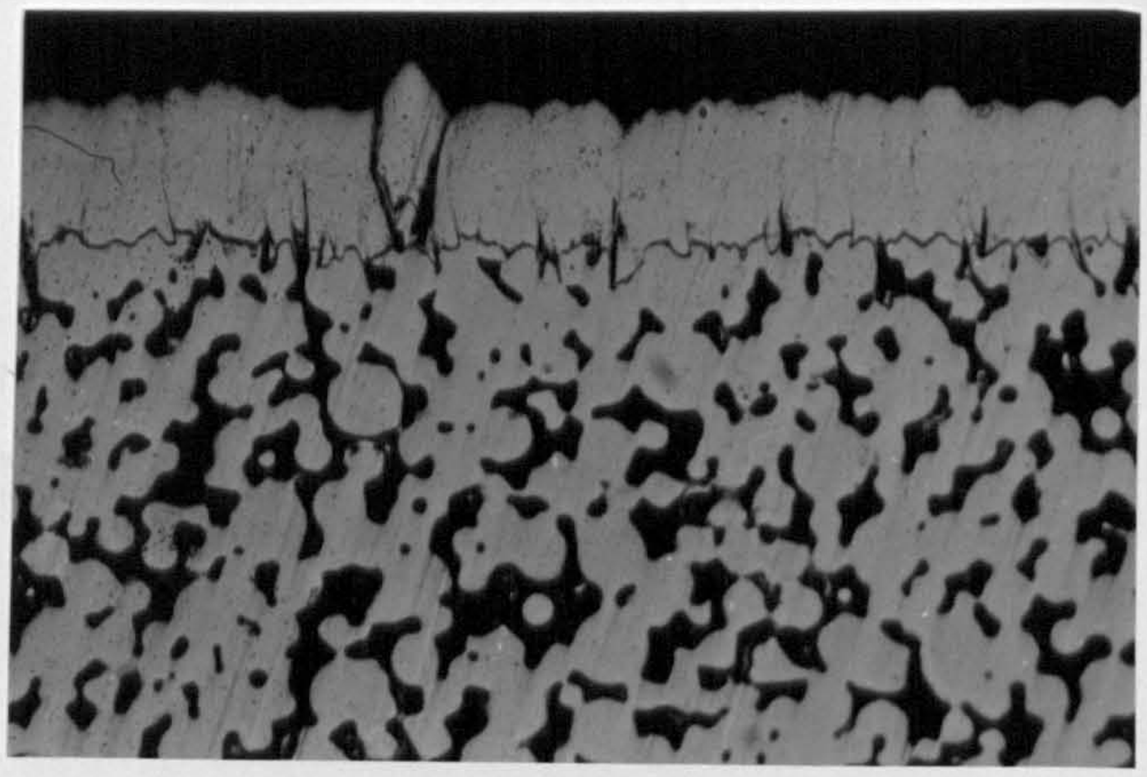

(a)

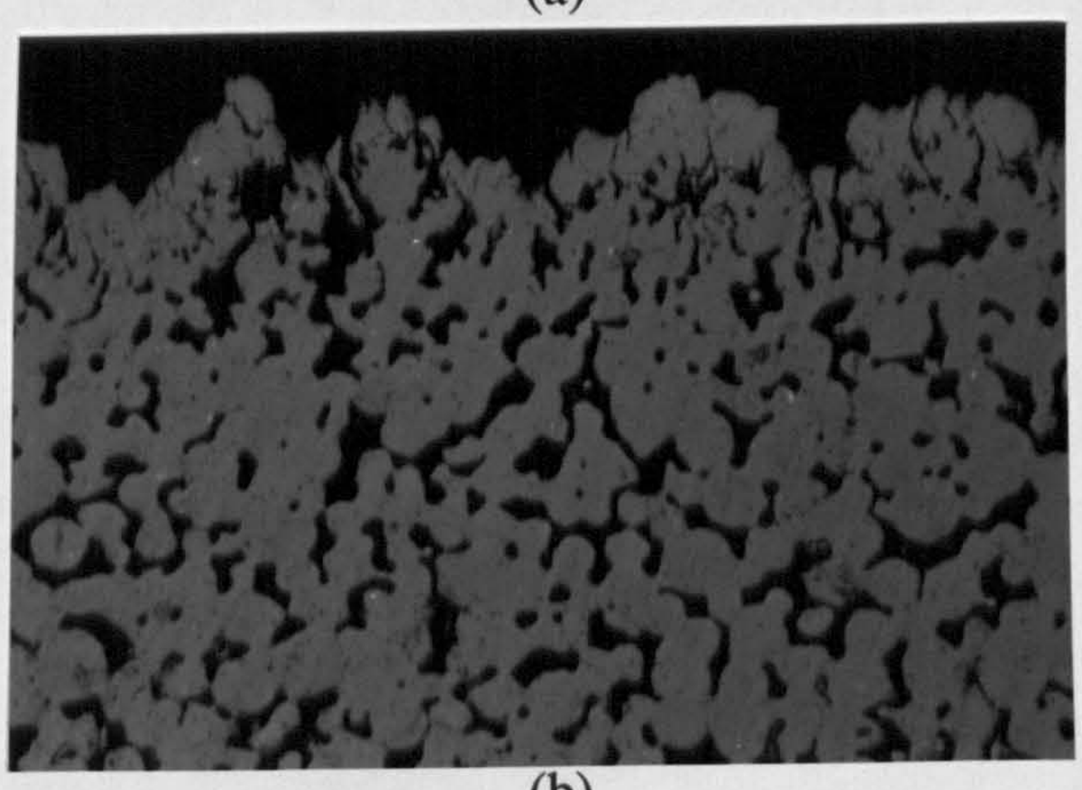

(b)

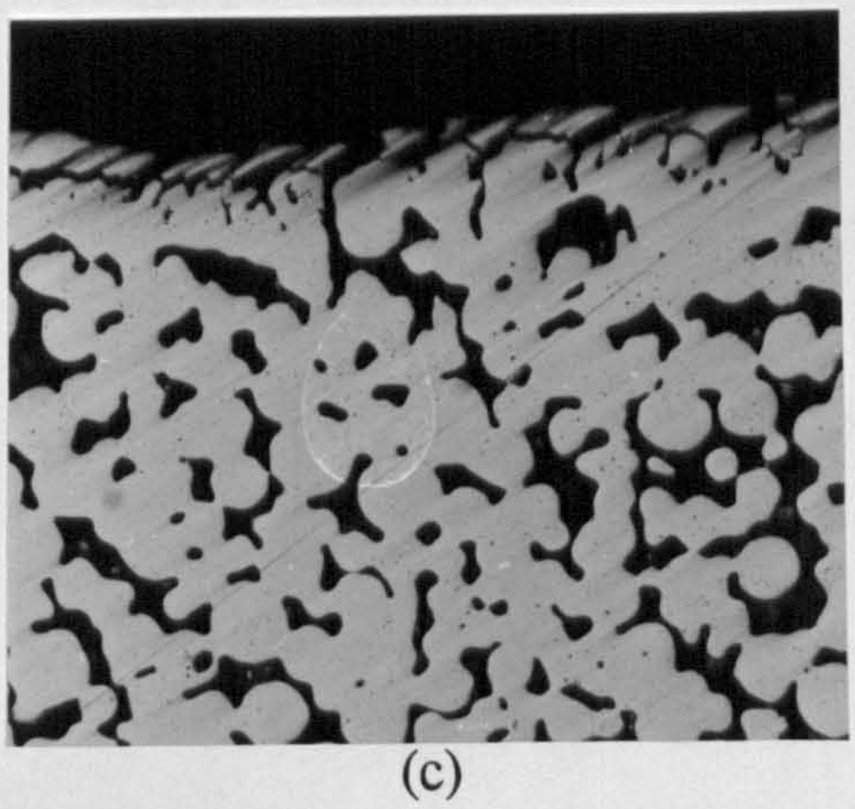

(c)

Figure 79. EB-PVD Ni Coating on Ni Substrate (mag.X150).
(a) (b) Coating Coverage Variation on Compact Surface.
(c) Coating Coverage on Compact Side.

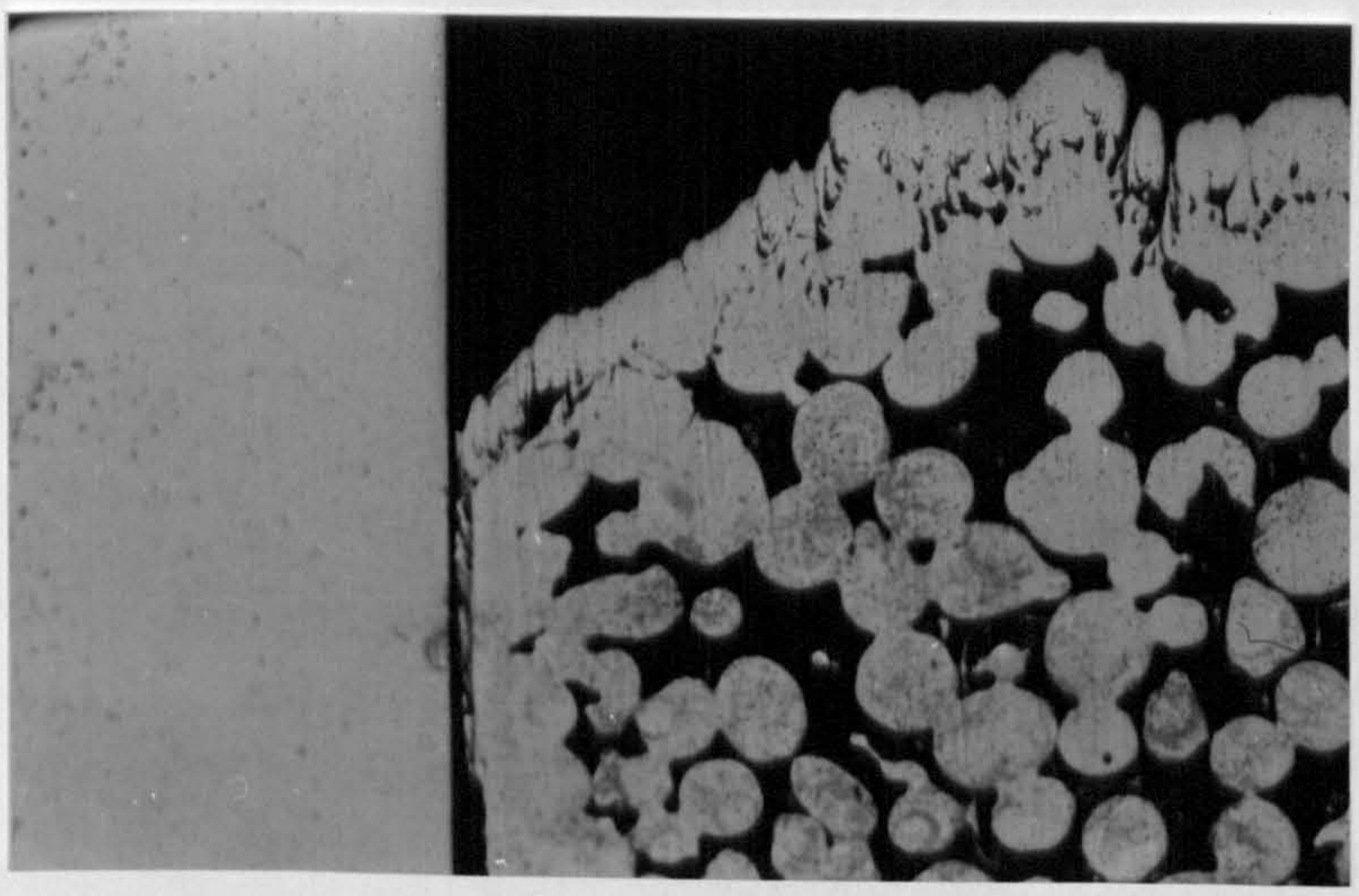

Figure 80. Coating Structural Weakness Caused by Proximity of Wire (mag.X150).

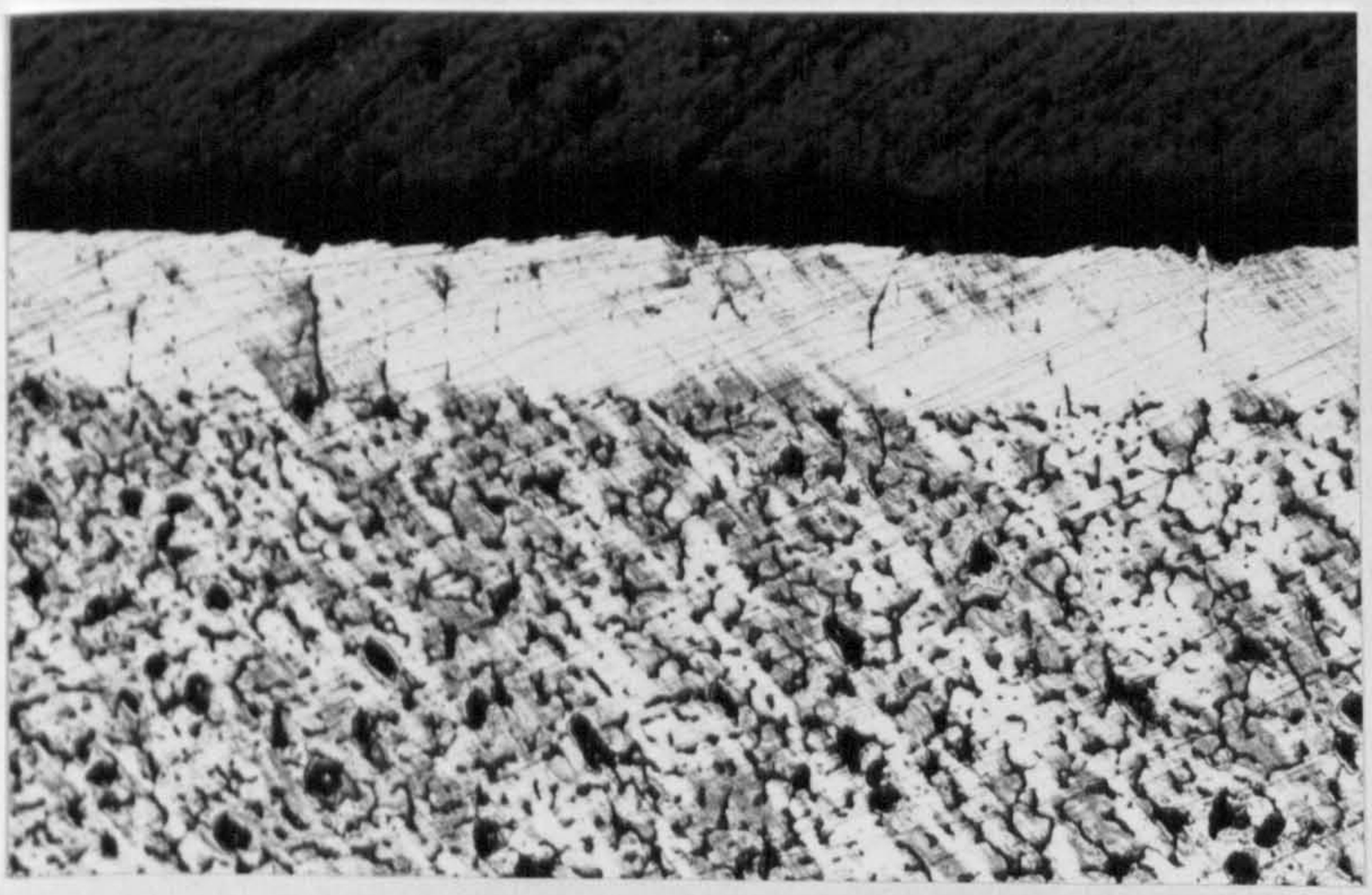

(a)

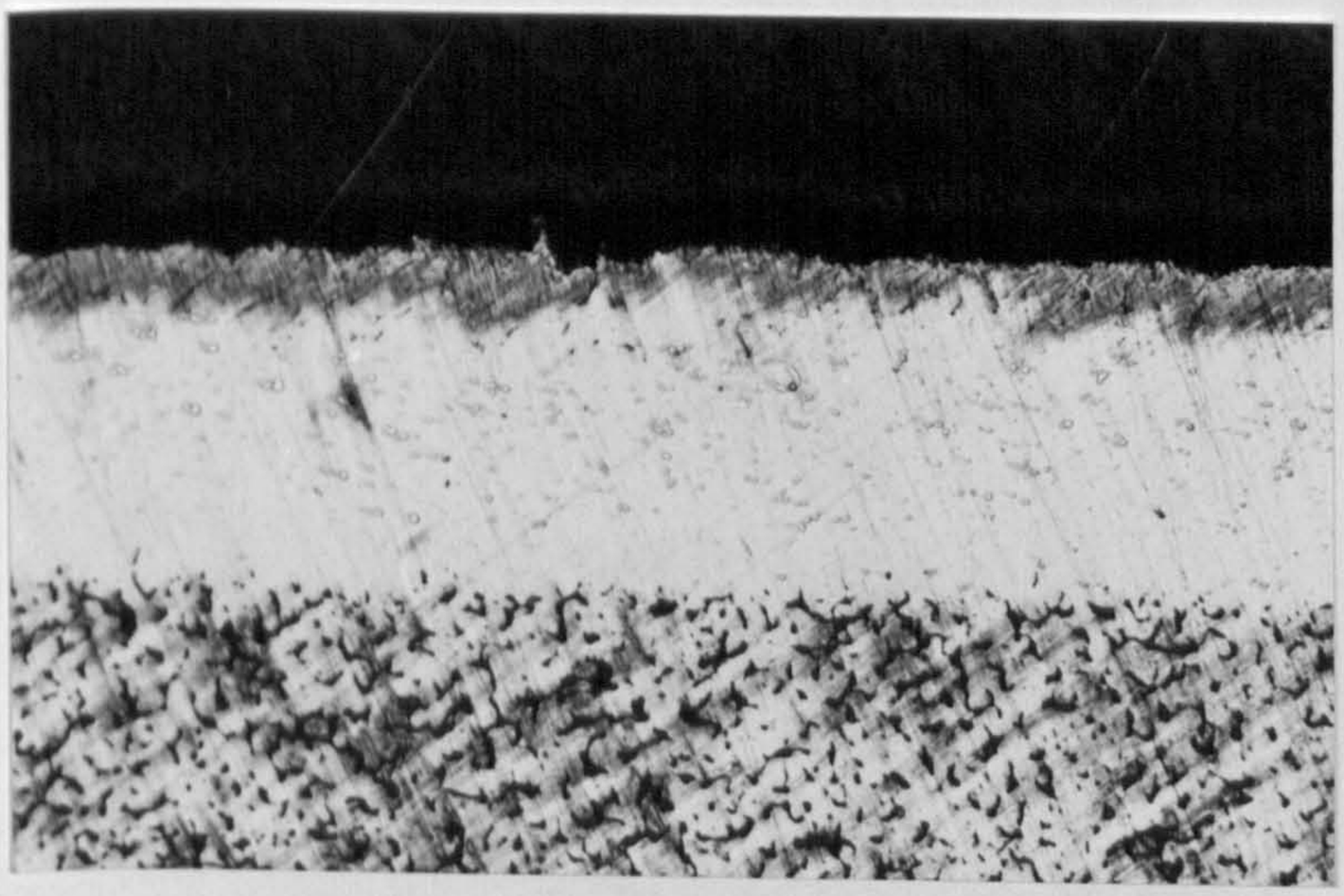

(b)

Figure 81. (a) Plasma PVD Ni Coating on Ni Substrate, Deposited at 400 °C (mag.X150).
(b) Plasma PVD Ni Coating on Ni Substrate, Deposited at 650 °C (mag.X150).

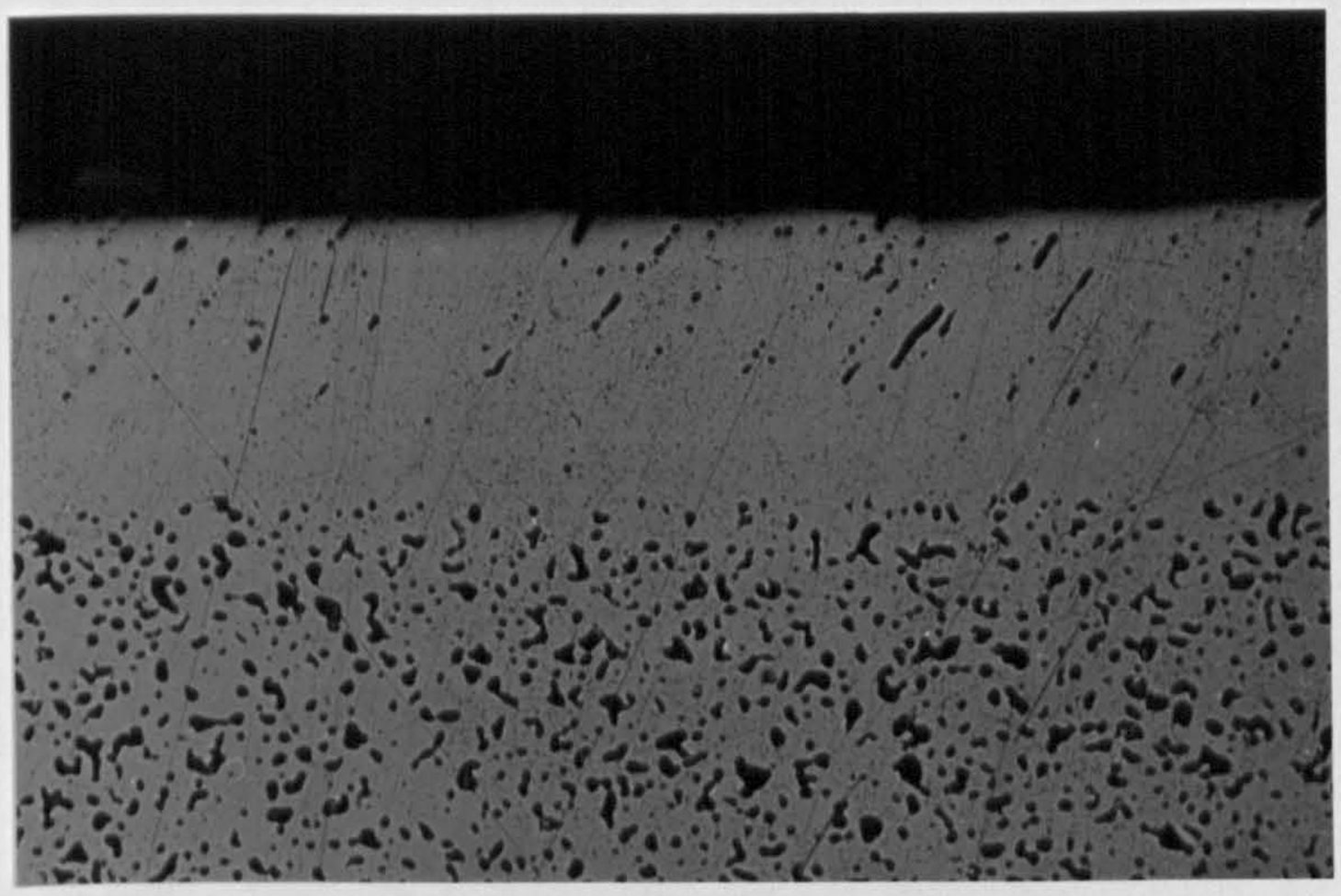

(a)

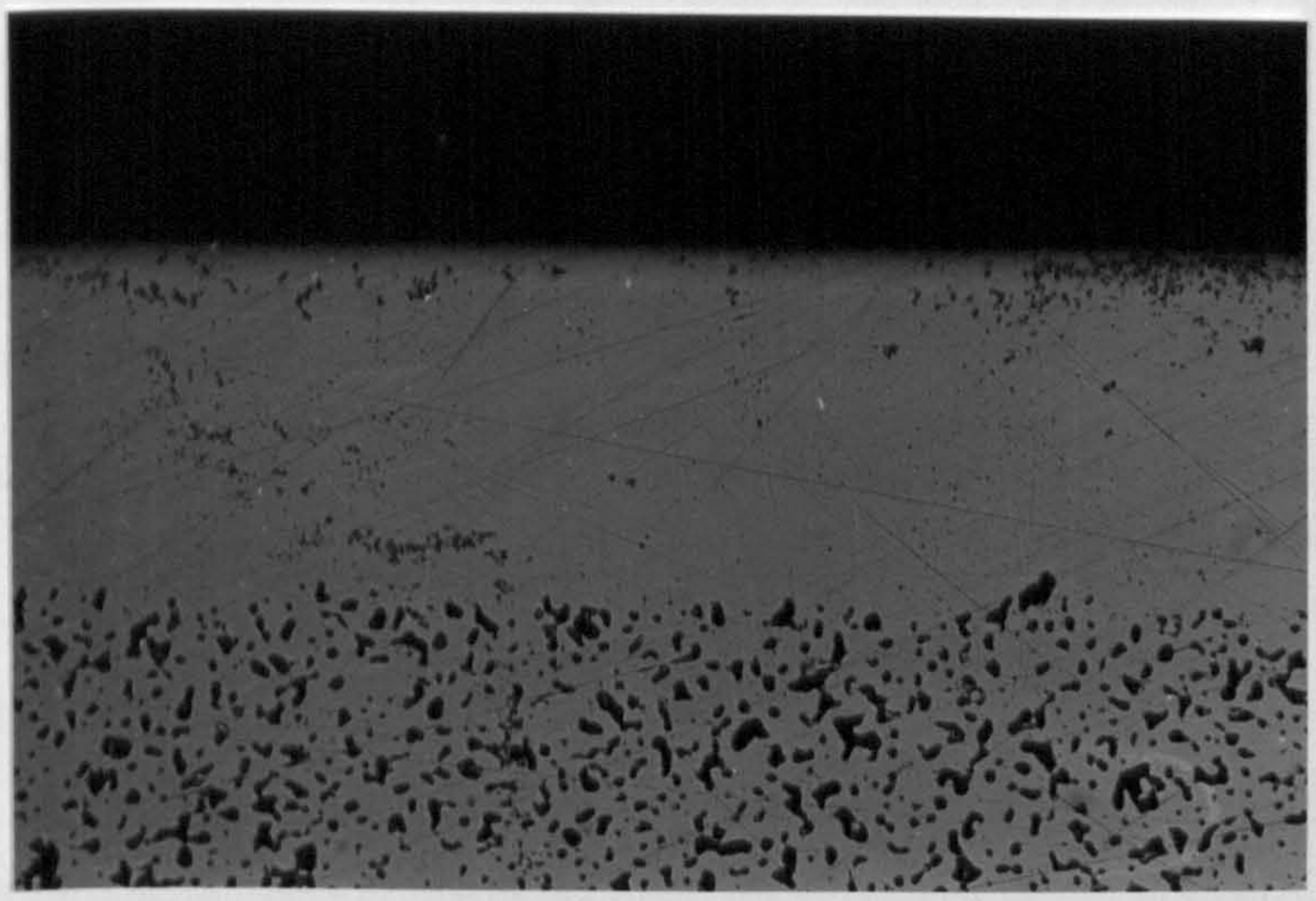

(b)

Figure 82. (a) Plasma PVD Ni Coated Ni Substrate (Deposited at 300 °C) HIP'ed at 1200 °C at 110 MPA for 1 hour (mag.X150).
(b) Plasma PVD Ni Coated Ni Substrate (Deposited at 800 °C) HIP'ed at 1200 °C at 110 MPa for 1 hour (mag.X150).

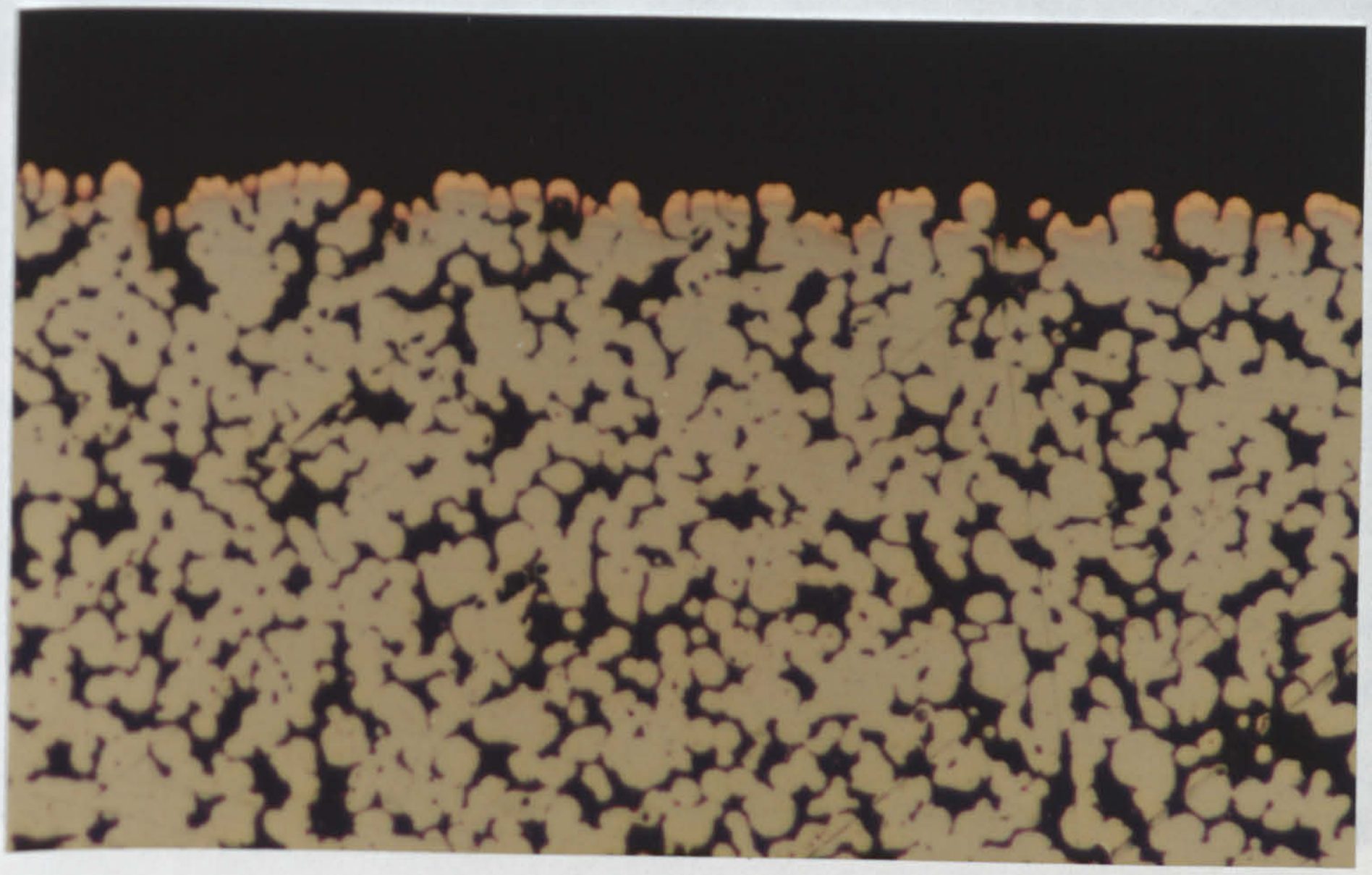

(a)

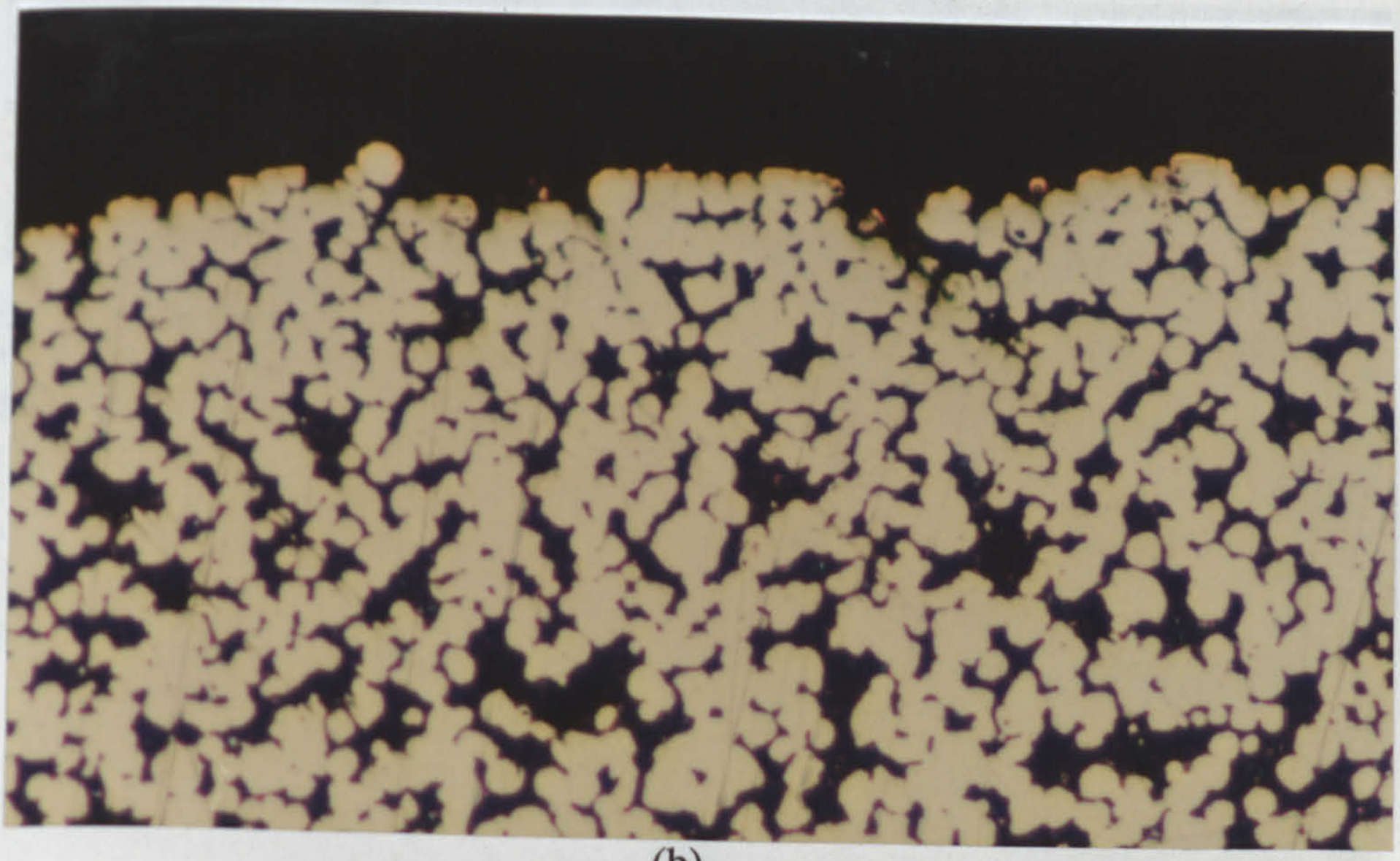

(b)

Figure 83. (a) 'Light' Loading PVD Cu Coating on Ni Substrate Surface (mag.X425).
(b) 'Light' Loading PVD Cu Coating on Ni Substrate Side (mag.X425).

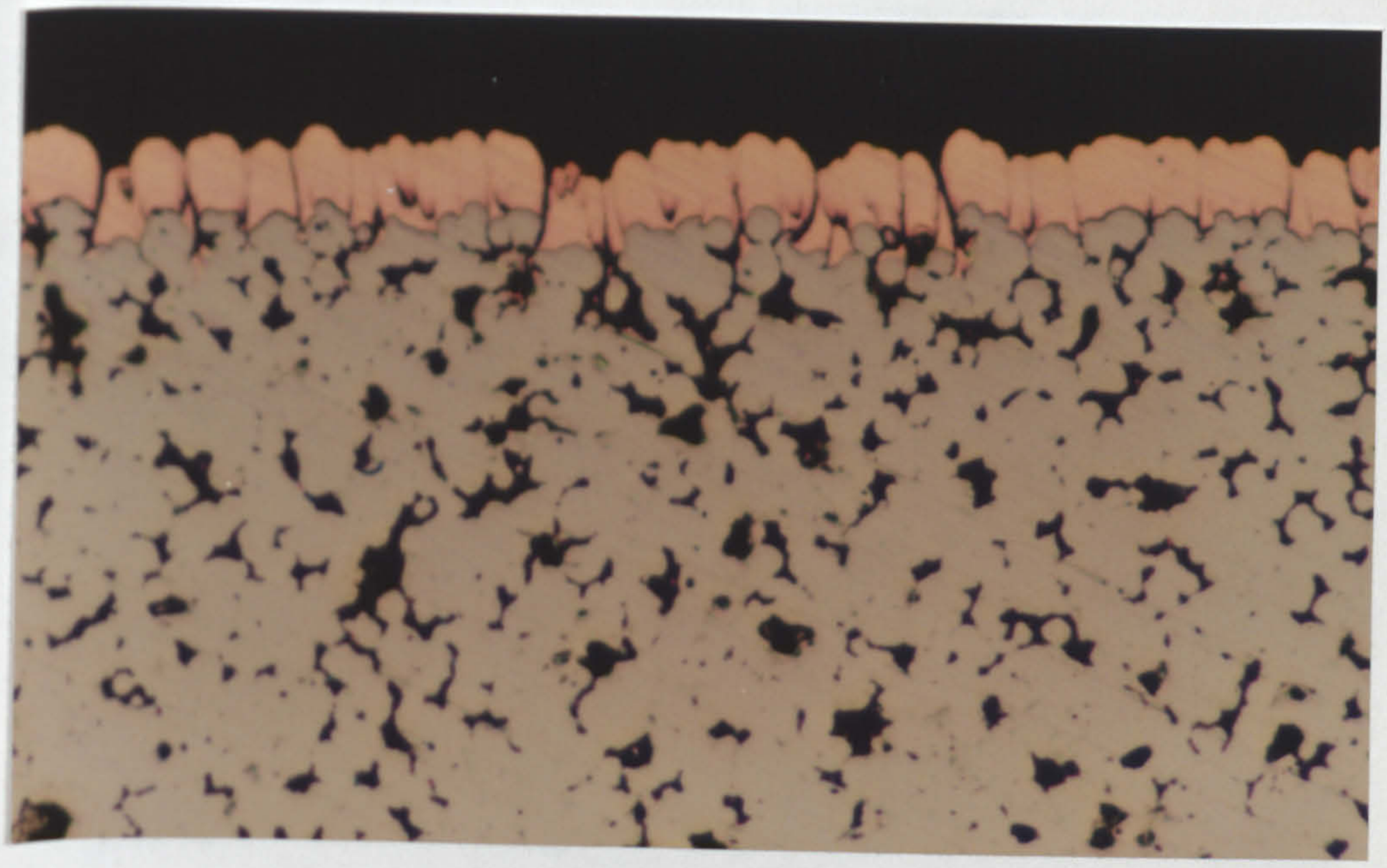

(a)

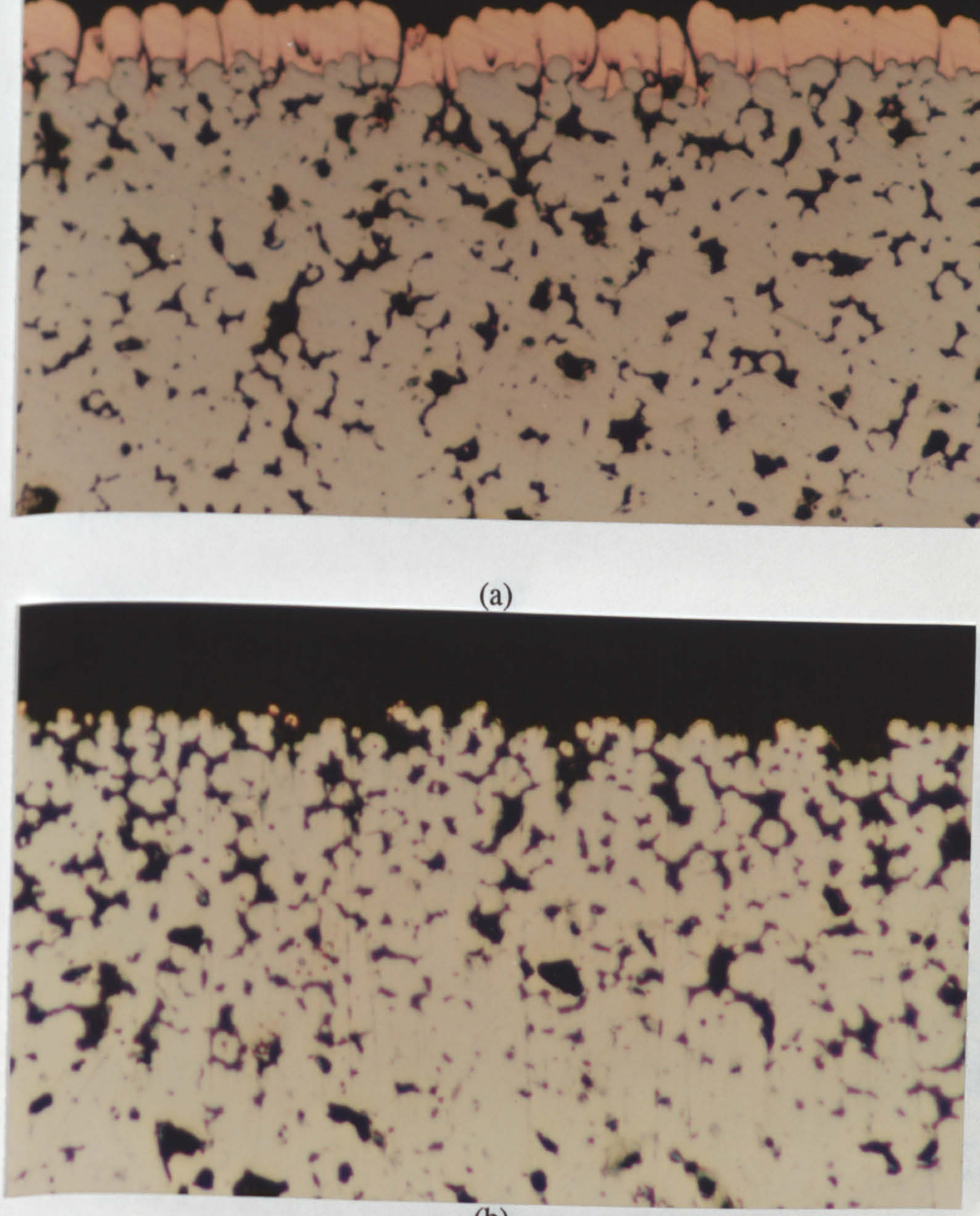

(b)

Figure 84. (a) 'Heavy' Loading PVD Cu Coating on Ni Substrate Surface (mag.X425).
(b) 'Heavy' Loading PVD Cu Coating on Ni Substrate Side (mag.X425).

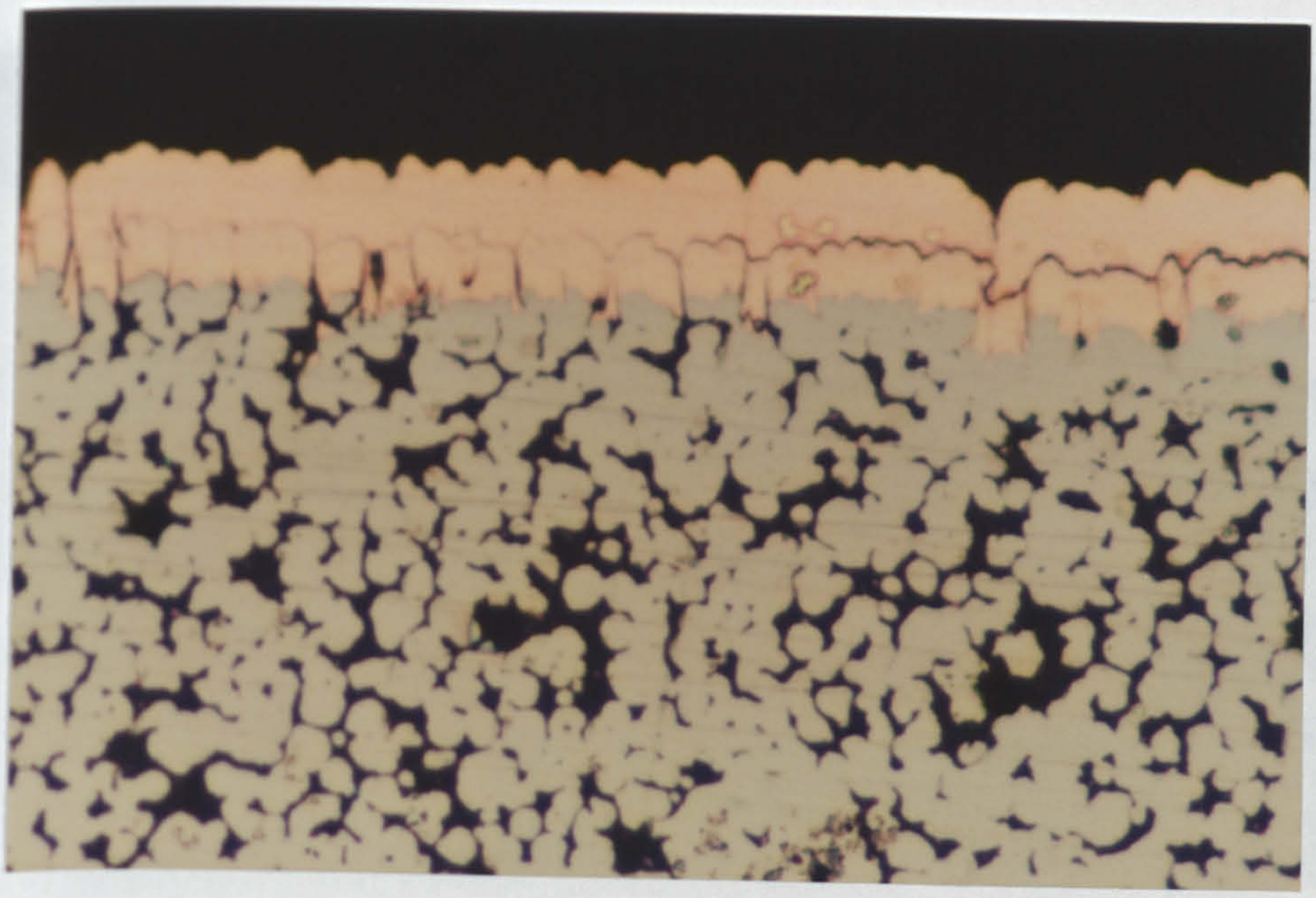

(a)

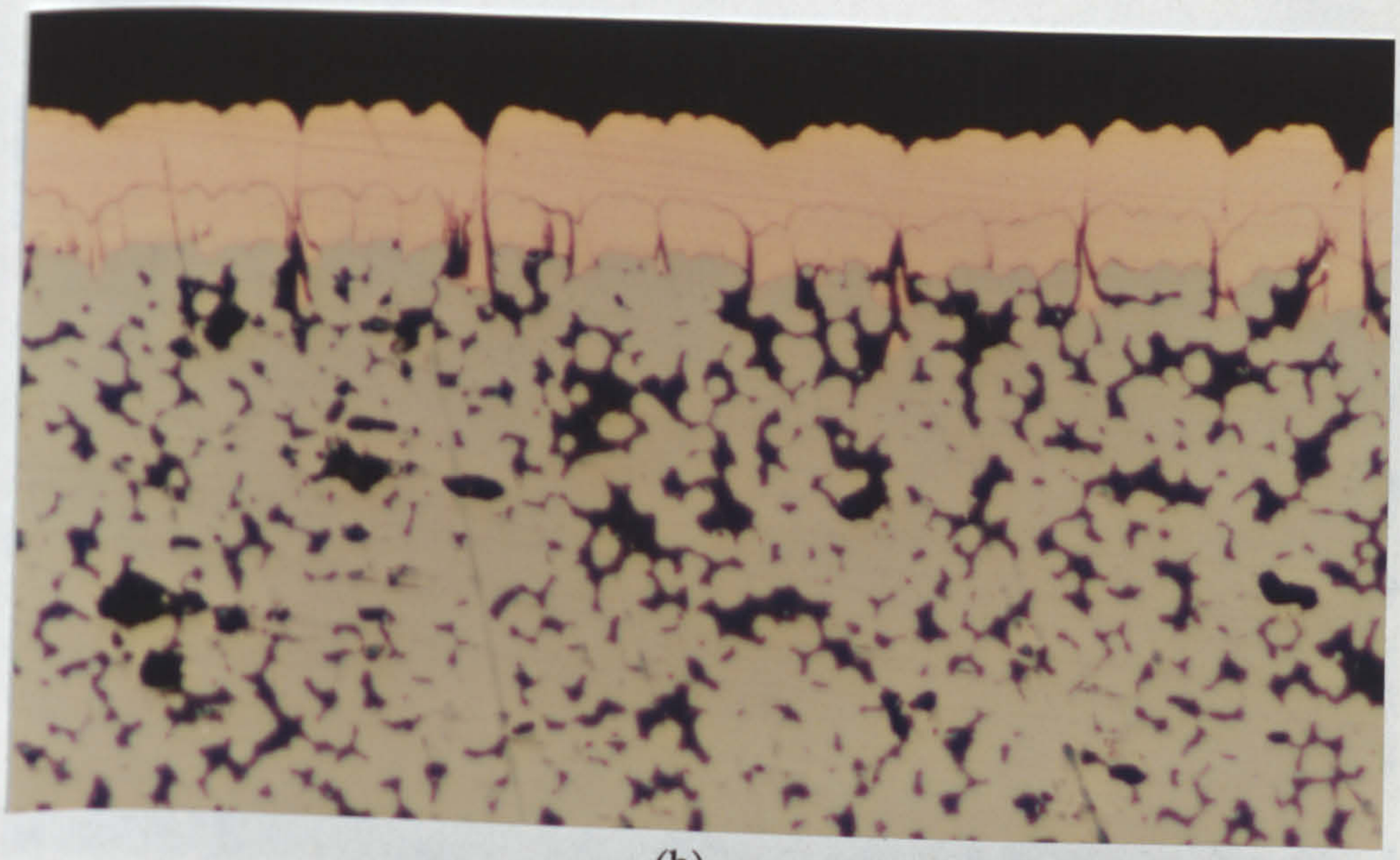

(b)

Figure 85. (a) (b) 'Heavy' Loading Cu PVD Multi-Coating on Ni Substrate Surface (mag.X425).

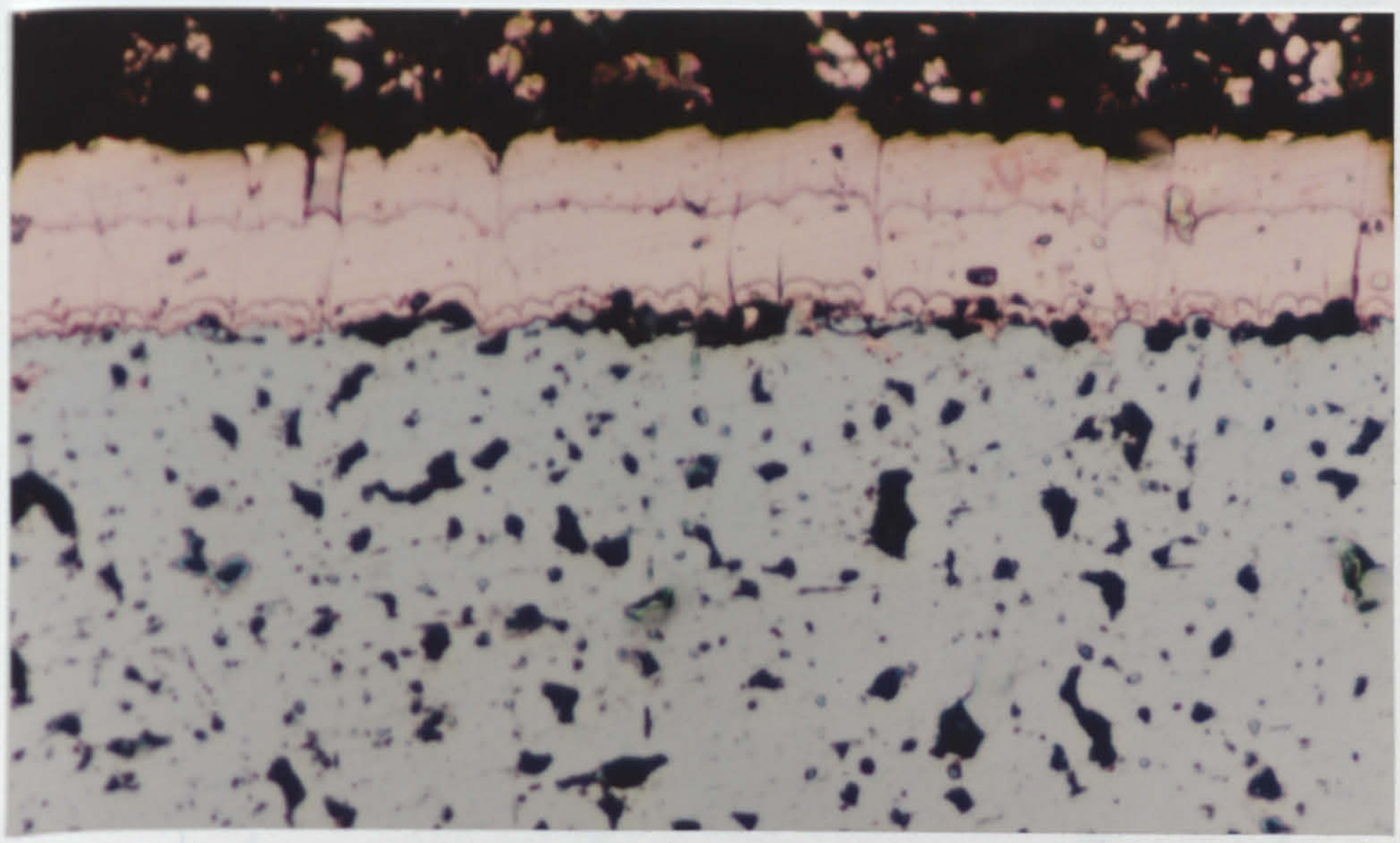

(a)

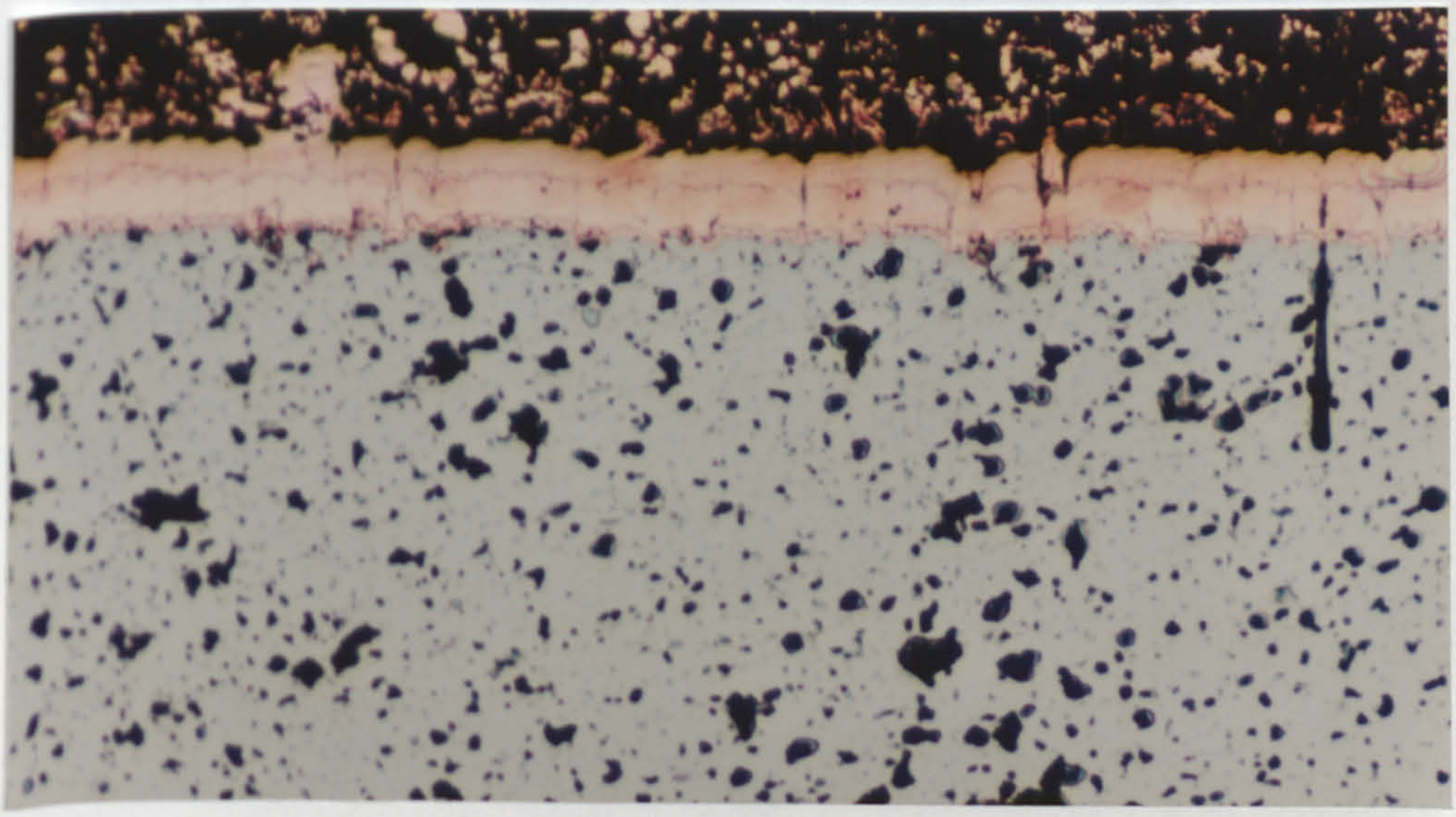

(b)

Figure 86. (a) (b) 'Heavy' Loading Cu PVD Multi-Coating on Ni Substrate Surface (mag.X425 and X215 respectively).

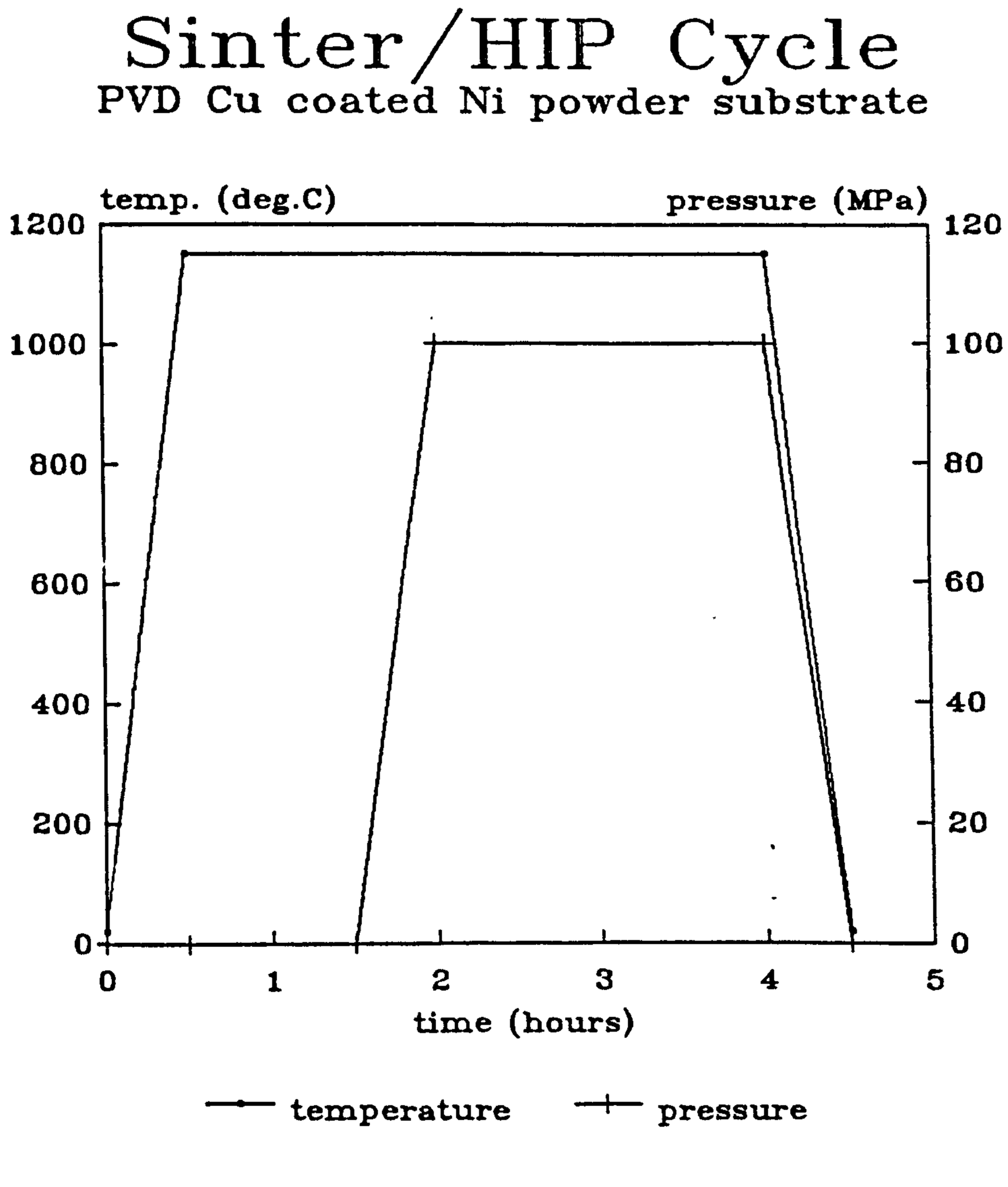

Figure 87. Schematic Representation of the Sinter-HIP Cycle.

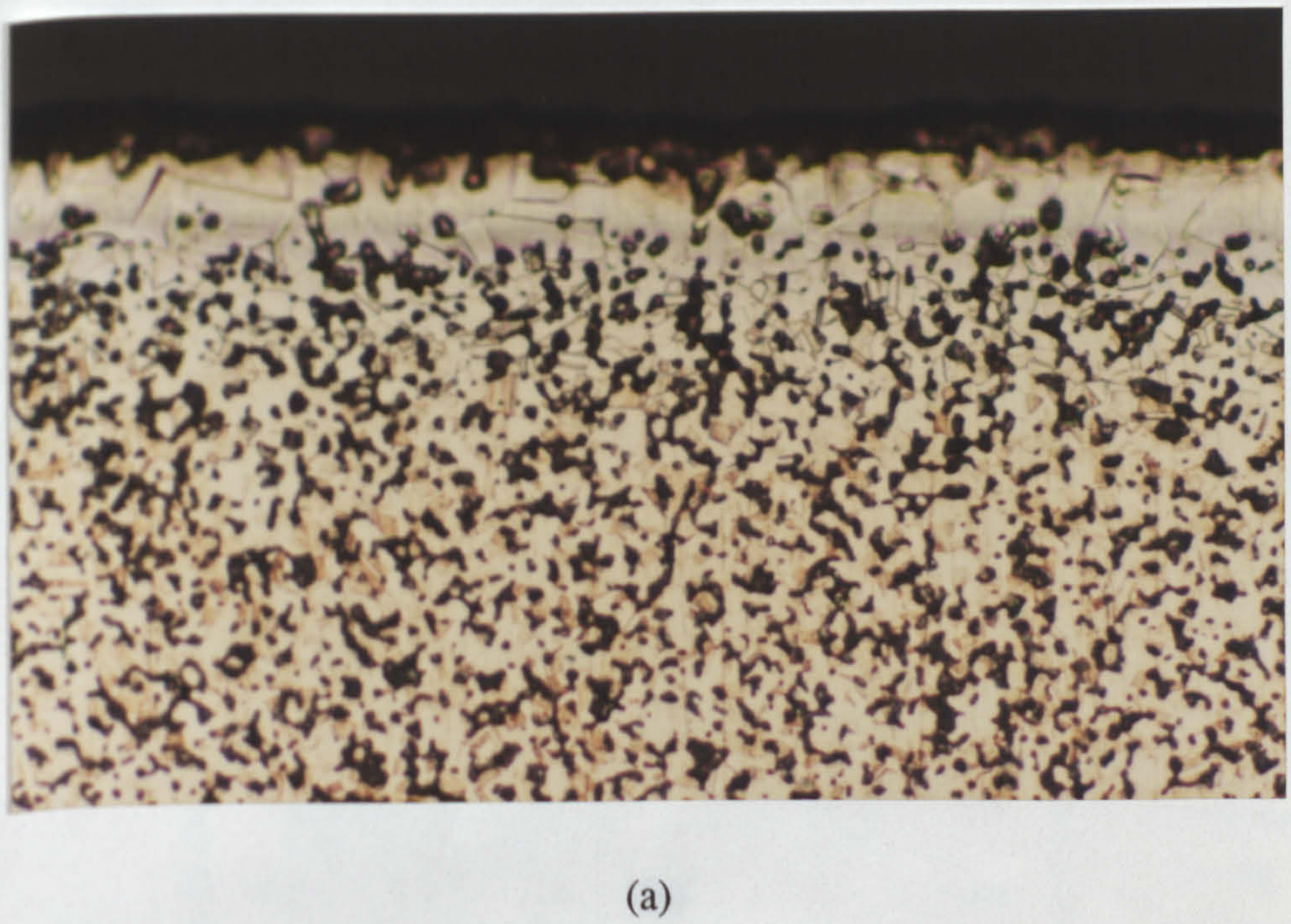

(a)

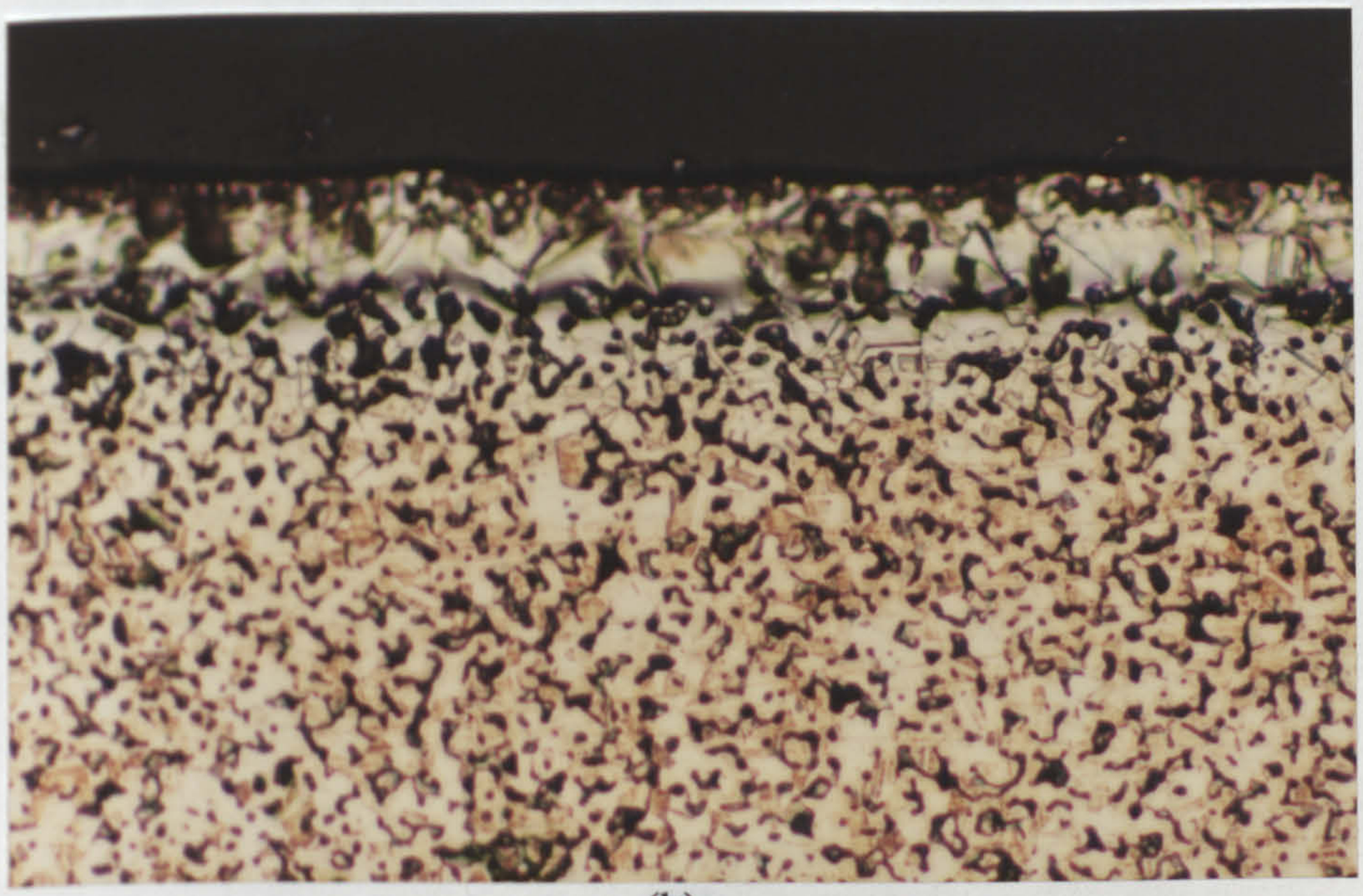

(b)

Figure 88. (a) (b) Cu PVD (Back-Filled) Multi-Coated Ni Substrate Defect-Healed after Sinter Cycle of 1150 °C for 1 hour (mag.X215 Surface and Side respectively).

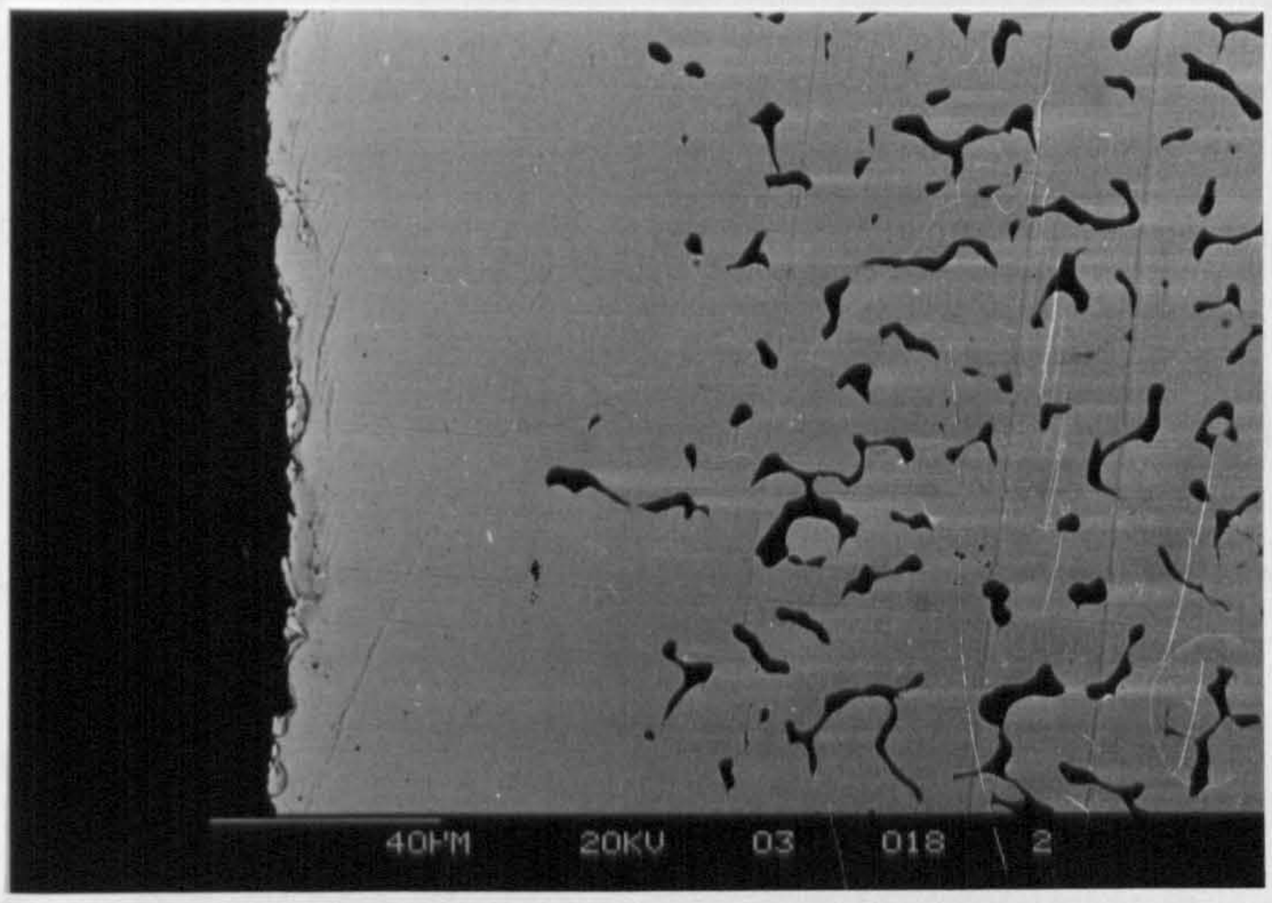

(a)

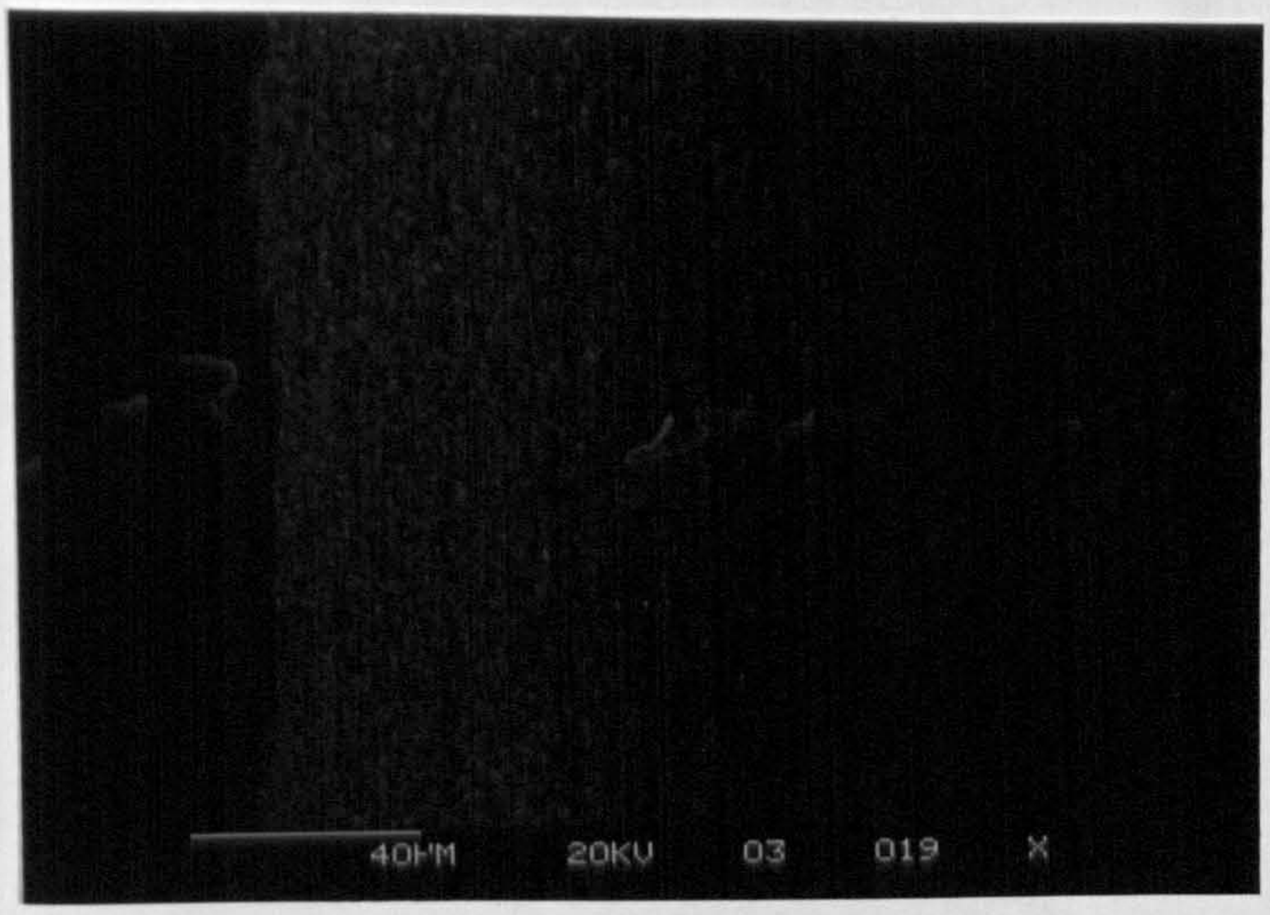

(b)

Figure 89. (a) SEM Micrograph of Cu-Coated Ni Substrate after Sinter Cycle.
(b) SEM Cu Elemental Map for above.

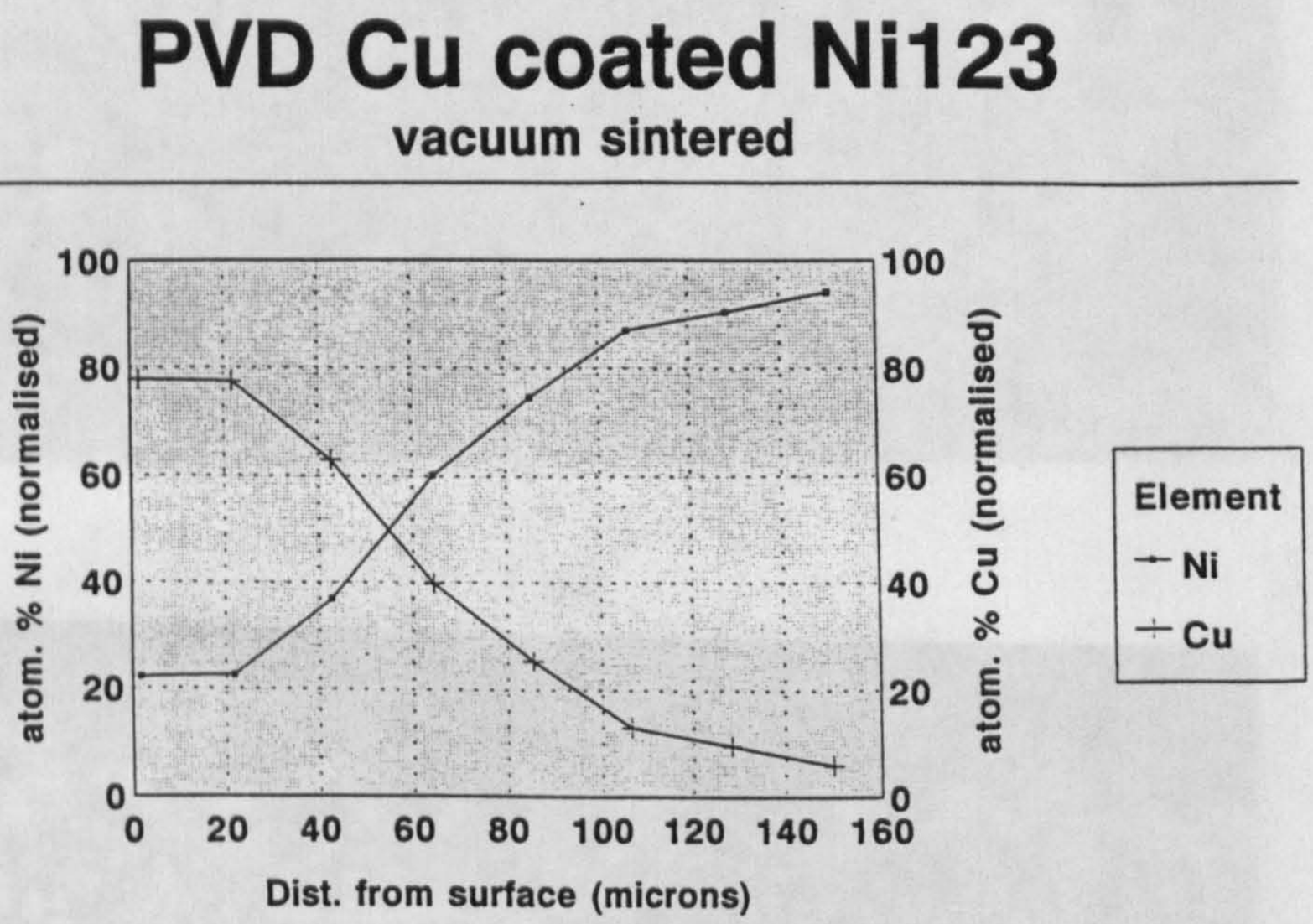

Figure 89. (c) SEM Digipoint Analysis for Vacuum Sintered Cu-Coated Ni Powder Substrate.

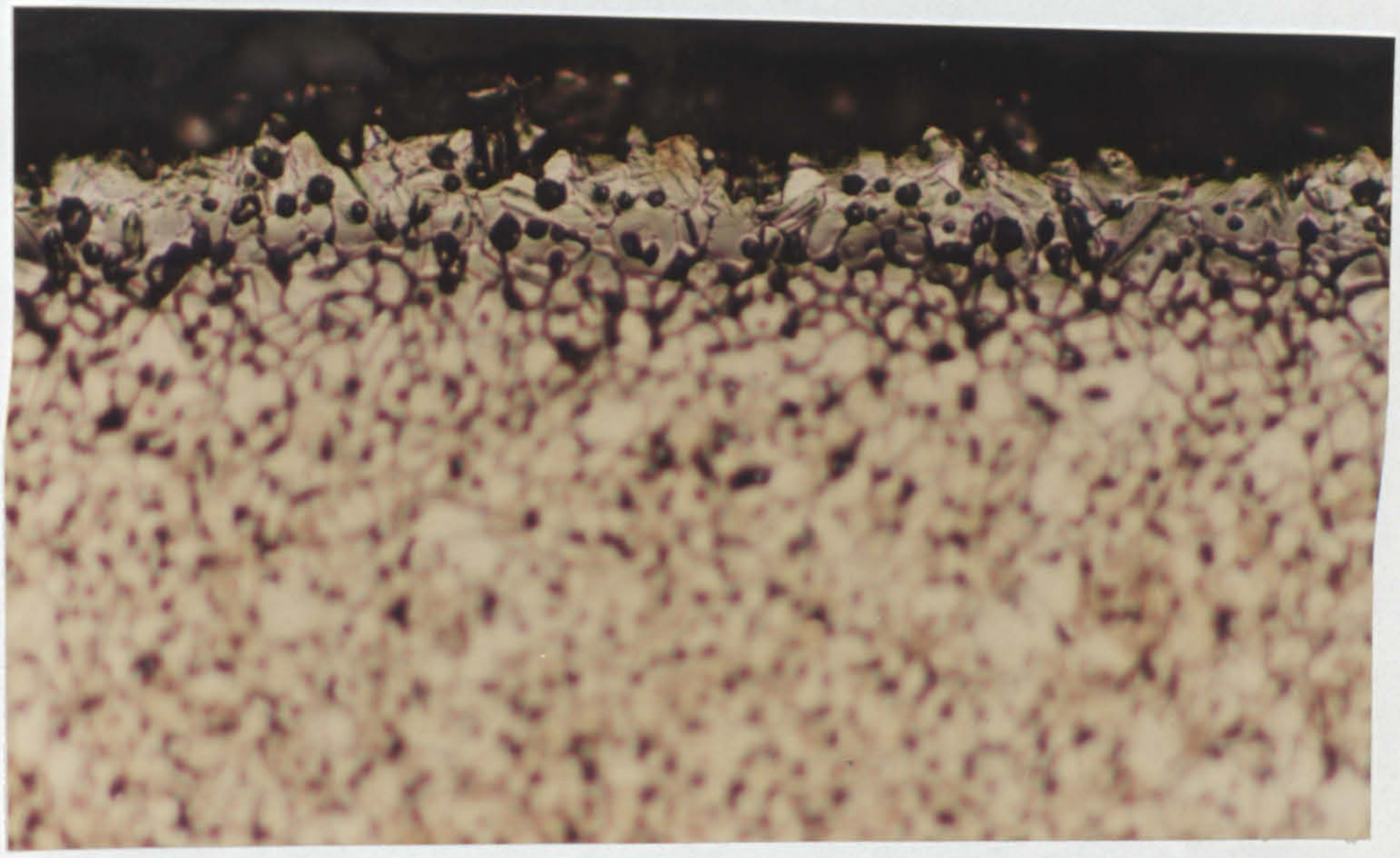

(a)

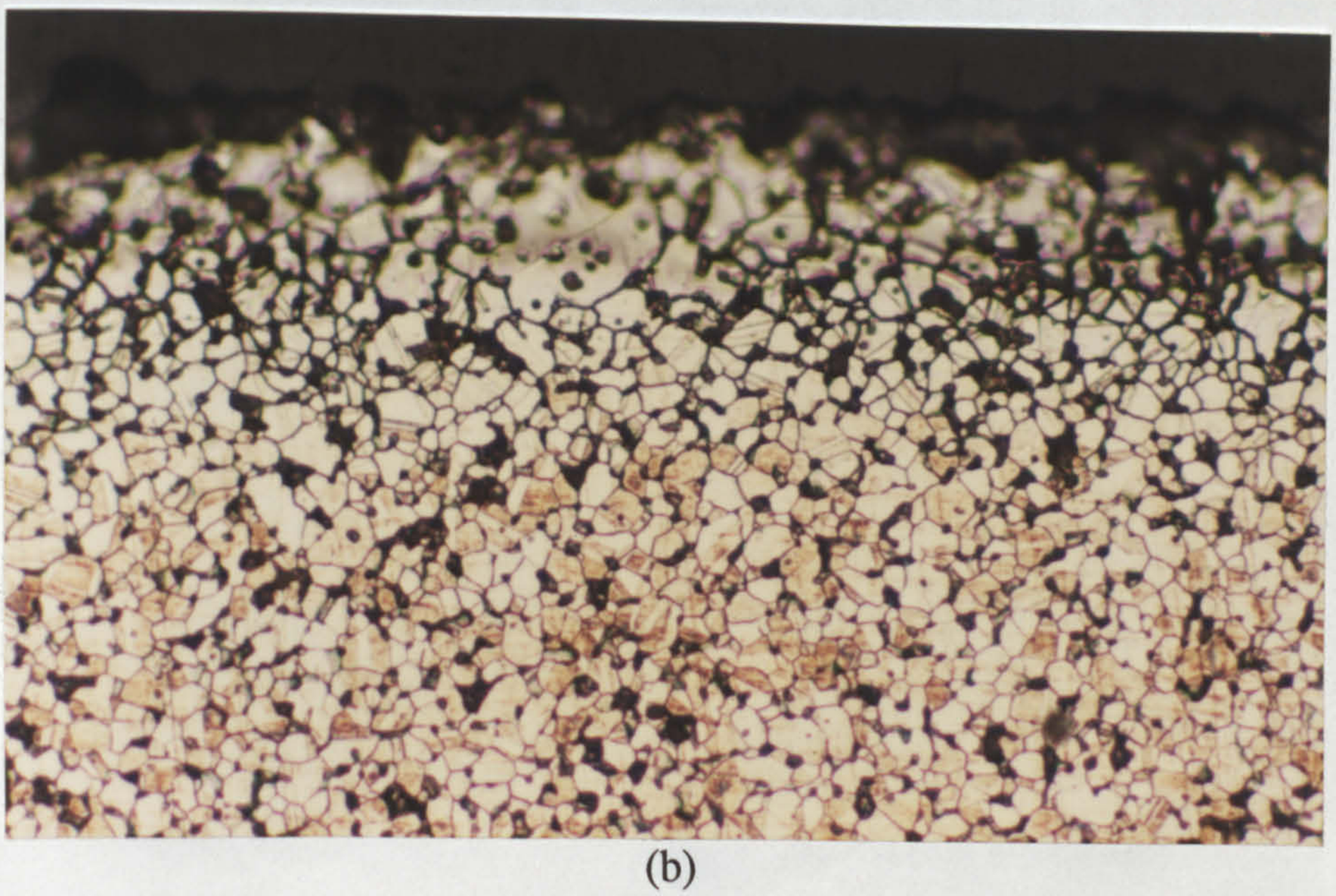

(b)

Figure 90. (a) (b) Cu PVD (Back-Filled) Multi-Coated Ni Substrate Fully Densified after Sinter-HIP Cycle (Pressure of 100 MPa applied for 2 hours) (mag.X215 Surface and Side respectively).

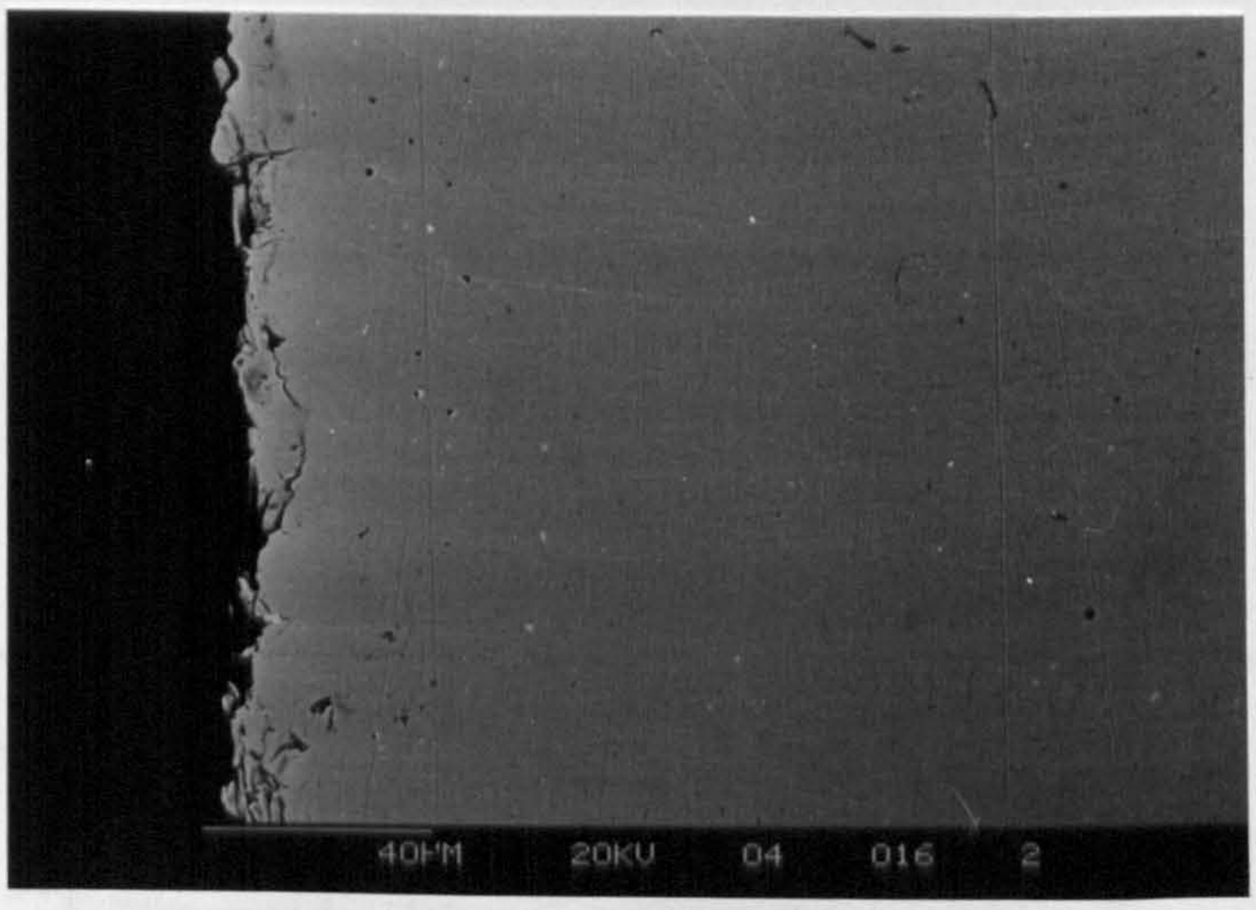

(a)

(b)

Figure 91. (a) SEM Micrograph of Cu-Coated Ni Substrate after Sinter-HIP Cycle.
(b) SEM Cu Elemental Map for above.

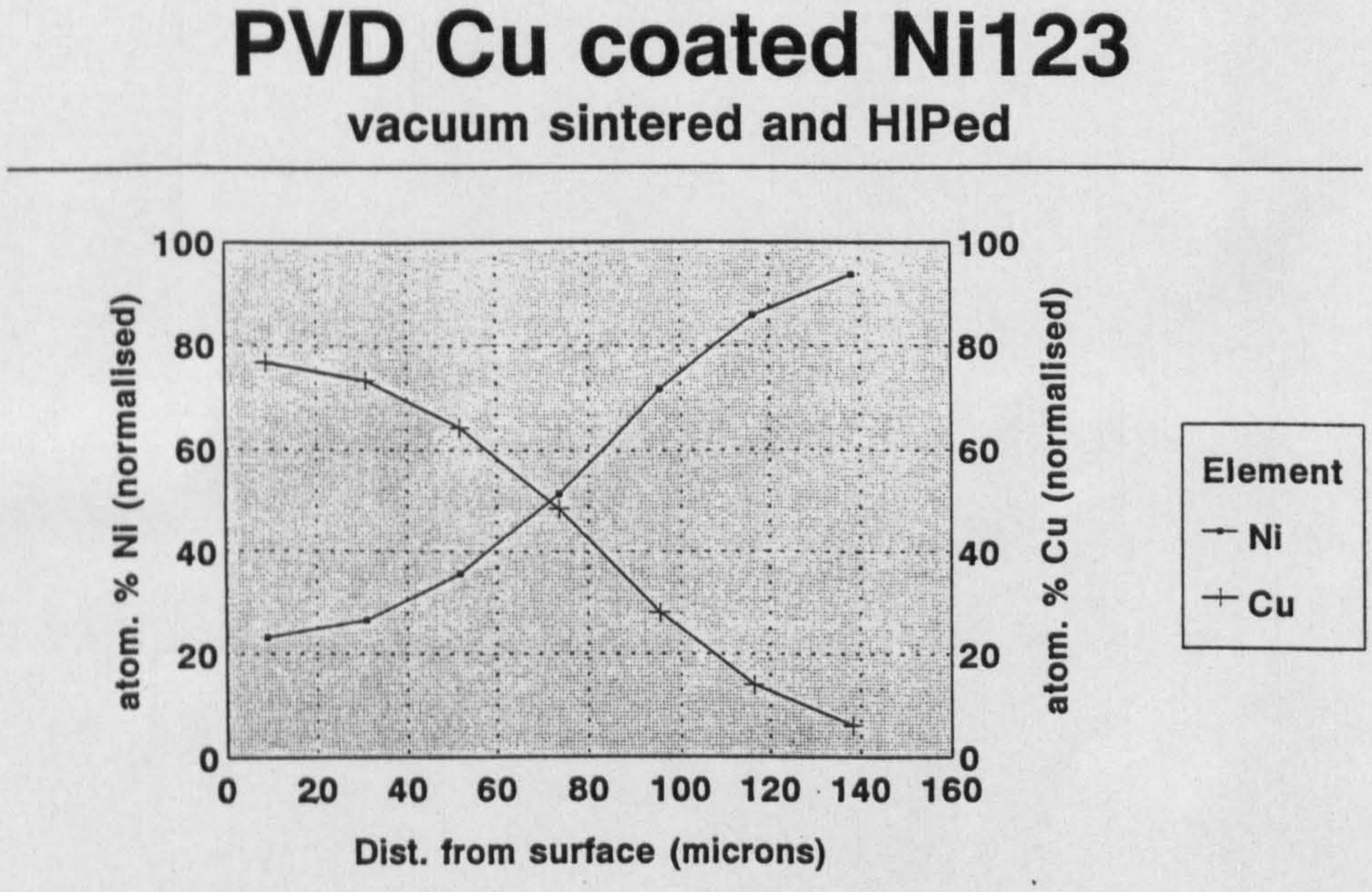

Figure 91. (c) SEM Digipoint Analysis for Sinter-HIP'ed Cu-Coated Ni Powder Substrate.